Analysis of thermohydraulic spalling in low-clinker blended cement concrete

Zur Erlangung des akademischen Grades eines

Doktors der Ingenieurwissenschaften (Dr.-Ing.)

von der KIT-Fakultät für Bauingenieur, Geo-und Umweltwissenschaften
des Karlsruher Instituts für Technologie (KIT)

genehmigte

Dissertation

von

Tim Pittrich

Tag der mündlichen Prüfung: 30.10. 2026
Erster Gutachter: Prof. Dr.-Ing. Frank Dehn
Zweiter Gutachter: Prof. Dr. techn. Günther Meschke



Mit Ausnahme des Tagungsbeitrags „*Fire-Induced Spalling of Normal Strength Concrete with Different Types of Blended Portland Cement*“, veröffentlicht in *Proceedings of the 13th International Conference on Structures in Fire (SiF 2024)*, ist dieses Werk lizenziert unter einer Creative Commons Namensnennung 4.0 International Lizenz (CC BY 4.0): https://creativecommons.org/licenses/by/4.0/deed.de

Abstract

Concrete exposed to fire, particularly in confined environments such as tunnels, can experience explosive spalling. This phenomenon reduces the load-bearing cross-section and exposes the reinforcement layer, thereby compromising the structural integrity of the building. At the same time, the cement industry is striving to reduce the high CO_2 emissions associated with Portland cement production by introducing blended cements. These cements partially replace clinker with supplementary cementitious materials, significantly lowering the overall carbon footprint. However, as the use of blended cements becomes more widespread, concerns about their behavior under fire exposure are growing. Spalling is primarily driven by thermomechanical and thermohydraulic mechanisms. Cement composition affects the microstructure, moisture content, and dehydration behavior, all of which are impacting thermohydraulic processes.

Therefore, this thesis presents a comprehensive analysis of the spalling behavior of concrete made with blended cements, focusing on the underlying thermohydraulic properties. The goal was to assess how different blended cements influence spalling susceptibility and to identify the material characteristics responsible for this behavior. The key areas of investigation included moisture transport properties as well as the dehydration behavior of the cementitious matrix.

A review of existing literature revealed significant knowledge gaps. Specifically, no clear relationship could be established between cement type and spalling susceptibility, nor are the underlying mechanisms well understood. To address this, spalling experiments were conducted on ring-restrained specimens made with four cement types: CEM I, CEM II/A-LL, CEM III/A, and CEM II/B-Q. The fire tests showed a marked increase in spalling susceptibility in concrete made with blended cements. While the CEM I reference concrete exhibited only minor spalling (up to 1.5 cm), blended cement concretes suffered severe damage, with spalling depths exceeding 5 cm. To understand the causes of these results, 1H-NMR relaxometry was used to analyze thermally induced moisture transport. Small scale cylindrical specimens were measured before and after heating. The tests showed higher initial moisture content in CEM III/A and CEM II/B-Q concrete, differences in pore-size-specific moisture distribution and overall lower permeability in all blended cement concretes. After heating, variations in the depth of the drying front and the development of the moisture accumulation zone, the so-called moisture clogs, were observed. Interestingly, these results did not correlate directly with the measured permeabilities, suggesting that permeability alone is not the decisive factor in moisture transport during fire exposure. Further analysis of the dehydration and decomposition behavior by XRD and TGA revealed that blended cement pastes exhibit greater thermal resistance. The dehydration behavior was in good agreement with the development of the drying front suggesting that the mineral phase composition has a strong influence on the thermally induced moisture transport and hence the differences in spalling susceptibility.

The findings suggest that the greater amount of available energy in the form of hot water due to higher initial moisture content, lower permeability, and less dehydration up to 200 °C is the main contributor to the increased spalling tendency observed in blended cement concrete. However, the differences between the single blended cement concretes are still not fully understood.

Kurzfassung

Betonbauwerke unter Brandlast, insbesondere Tunnelbauwerke, neigen zu explosionsartigem Abplatzen. Durch das Abplatzen reduziert sich der tragende Querschnitt und die Bewehrungslage kann freigelegt werden, was die Tragwerkssicherheit des Gebäudes erheblich beeinträchtigt. Gleichzeitig versucht die Zementindustrie, die CO_2-Emissionen, die bei der Herstellung von Portlandzementklinker entstehen, durch den Einsatz klinkereffizienter Zemente zu reduzieren. Bei diesen Zementen werden Teile des Klinkers durch Zusatzstoffe ersetzt, wodurch der CO_2-Fußabdruck deutlich verringert werden kann. Die wachsende Popularität löst jedoch Bedenken hinsichtlich des Hochtemperaturverhaltens von Betonen mit diesen Zementen aus. Das Abplatzen basiert auf thermomechanischen und thermohydraulischen Mechanismen. Die Zementart beeinflusst die Mikrostruktur, das Feuchtetransportverhalten sowie das Dehydrationsverhalten der Zementsteinmatrix. All diese Faktoren sind an thermohydraulischen Prozessen beteiligt.

Diese Dissertation beinhaltet eine ganzheitliche Analyse des Abplatzverhaltens von Betonen mit klinkereffizienten Zementen. Ziel war es herauszufinden, wie diese Zemente das Abplatzverhalten beeinflussen und welche Eigenschaften dafür verantwortlich sind. Der Fokus lag auf den Feuchtetransporteigenschaften und dem Dehydrationsverhalten des Zementsteins.

Der aktuelle Stand der Technik zeigte bestehende Wissenslücken auf. Daten aus der Literatur lieferten keinen klaren Zusammenhang zwischen Zementart und Abplatzverhalten sowie den zugrunde liegenden Mechanismen. Zur Schließung dieser Lücke wurden Brandversuche an Betonen mit vier verschiedenen Zementen (CEM I, CEM II/A-LL, CEM III/A, CEM II/B-Q) durchgeführt. Die Ergebnisse zeigten, dass der Einsatz klinkereffizienter Zemente zu einem erhöhten Abplatzrisiko führt. Während CEM I Beton nur Abplatzungen mit Tiefen bis zu 1.5 cm aufwies, wurden in Betonen mit klinkereffizienten Zementen mit über 5 cm deutlich größere Abplatztiefen festgestellt. Zur Analyse der Ursachen wurde der thermisch induzierte Feuchtetransport mittels 1H-NMR Relaxometrie untersucht. Dabei wurden kleinformatige Proben vor und nach einseitiger Erwärmung gemessen. Auffällig war die erhöhte Ausgangsfeuchte in CEM III/A und CEM II/B-Q Betonen sowie verschiedene porengrößenspezifische Feuchteverteilungen. Zusätzlich wurden insgesamt niedrigere Permeabilitäten bei Betonen mit klinkereffizienten Zementen festgestellt. Die Messungen nach der Erwärmung zeigten unterschiedlich stark ausgeprägte Trocknungsfronten und Feuchteakkumulationen. Diese Unterschiede lassen sich jedoch nicht nur durch die Permeabilität erklären. Untersuchungen zum Dehydrationsverhalten der verschiedenen Zementsteine mittels XRD und TGA zeigten, dass klinkereffiziente Zemente zur Ausbildung thermisch stabilerer Hydratphasen neigen. Der Vergleich zwischen Dehydratation- und Trocknungsverhalten zeigt, dass der Feuchtetransport stark vom Phasenbestand abhängt.

Zusammenfassend lässt sich feststellen, dass infolge höherer Ausgangsfeuchten mehr Energie in der Form von heißem Wasser gespeichert werden kann. Dies stellt zusammen mit niedrigeren Permeabilitäten und geringerer Dehydration in einem Temperaturbereich bis zu 200 °C die Hauptfaktoren für die erhöhte Abplatzneigung in Betonen mit klinkereffizienten Zementen dar. Die

Unterschiede zwischen den einzelnen Zementtypen lassen sich mit den präsentierten Daten jedoch nicht vollständig erklären.

Acknowledgements

The dissertation was completed as part of a DFG joint project with Ruhr University Bochum at the Federal Institute for Materials Research and Testing in collaboration with the Karlsruhe Institute of Technology.

First and foremost, I would like to express my sincere gratitude to Prof. Dr.-Ing. Frank Dehn for giving me the opportunity to work under his supervision and for serving as the first examiner. I am also deeply thankful to Prof. Dr. techn. Günther Meschke for kindly agreeing to act as the second examiner. Furthermore, I would like to extend my appreciation to the committee members, Prof. Dr.-Ing. Philipp Dietsch and Prof. Dr.-Ing. Steffen Freitag, for their valuable contributions.

Beyond that, I am profoundly grateful to Dr.-Ing. Frank Weise and Dr.-Ing. Ludwig Stelzner, whose unwavering support and guidance throughout this challenging process have been invaluable. Their encouragement and expertise have significantly shaped this work.

I would like to thank Dr.-Ing. Andreas Rogge and Dr. rer. nat. Birgitt Meng for their support of my dissertation project.

I would also like to thank all my colleagues at BAM, particularly those from Division 5.1, Microstructure Design and Degradation, 6.3 Structural Analytics, 7.1 Building Materials, 7.3 Fire Engineering, and 7.4 Technology of Construction Materials, for their technical support and collaboration. In particular I would like to mention Michaela Buchheim, Dominik Al-Sabbagh, Carsten Prinz, Andre Gardei, Peter Benkendorf and Frank Haamkens. Moreover, I would like to express many thanks to my colleagues Ahmad, Alena, Lucas, Peter, and Tim for the wonderful memories and enjoyable moments we shared both during and after work.

I would also like to thank Dr.-Ing. Simon Peters for the countless fruitful discussions and the harmonic cooperation throughout the time of the DFG Project.

Additionally, I am thankful to Dr. rer. nat. Daniel Jansen for his assistance and for conducting the evaluation of the XRD measurements at the Friedrich-Alexander University of Erlangen.

Finally, I would like to express my heartfelt gratitude to my parents, Gabi and Martin, for instilling in me the importance of education; to my brother, Nicholas, for teaching me the value of hard work; and to my wonderful girlfriend, Glawdis, for her constant encouragement and company throughout this time. Without all of you, I would not be where I am today.

Content

Abstract i

Kurzfassung ii

Acknowledgements iv

Content v

List of Figures vii

List of Tables viii

List of Abbreviations ix

List of Publications xi

1 Introduction 12

1.1 Tunnel fires 12

1.1.1 Tunnel fire characteristics 12

1.1.2 Examples of historic tunnel fires 13

1.1.3 Tunnel fires today 14

1.2 Decarbonation of the cement industry 14

1.2.1 Portland cement production 14

1.2.2 Reduction of the clinker factor: Chances and Challenges 15

2 State of the art (Paper 1) 17

2.1 Blended cements 17

2.1.1 Latent hydraulic SCMs 18

2.1.2 Pozzolanic SCMs 18

2.1.3 Fillers 18

2.2 Fire-induced concrete spalling 19

2.2.1 Mechanisms 19

2.2.2 Influencing parameters 20

2.2.3 Measures against spalling 22

2.3 Impact of blended cements on the fire induced spalling behavior 22

3 Research objectives 25

4 Experimental investigations 27

4.1 Fire tests of blended cement concrete (Conf. paper) 27

4.1.1 Methodology 27

4.1.2 Results 28

4.1.3 Main findings 29

4.2 Thermally induced moisture transport in blended cement concrete (Paper 2) . 30

4.2.1 Methodology 30

4.2.2 Results 31

4.2.3 Main findings 34

4.3 Thermally induced phase decomposition and dehydration behavior of blended cement paste (Paper 3) 35
4.3.1 Methodology 35
4.3.2 Results 35
4.3.3 Main findings 39
4.4 Impact of PP fibers (Conf. Paper & Paper 4) 39
4.4.1 Methodology 39
4.4.2 Results 40
4.4.3 Main findings 42

5 Discussion 43
5.1 Contextualization with respect to data from literature 43
5.2 Contextualization with respect to selected spalling theories 45

6 Conclusion and Outlook 48

Bibliography 51

Paper 1: 57

Conference Paper: 79

Paper 2: 91

Paper 3 112

Paper 4 127

List of Figures

Figure 1 Maximum temperatures in the walls during a) a road tunnel fire and b) an underground railway tunnel fire [5] 12
Figure 2 Damages of the tunnel lining after the fire a) Channel Tunnel, 1996 [10] b) Mont Blanc Tunnel, 1999 [10] and c) Gotthard Tunnel, 2001 (https://www.alptransit-portal.ch/en/media/file/3768) 13
Figure 3 Cement production [20] 15
Figure 4 Ternary diagram of commonly used SCMs [Paper 1 modified] 17
Figure 5 Schematic representation of the thermohydraulic spalling mechanism [Paper 1] 19
Figure 6 Schematic representation of the thermomechanical spalling mechanism [Paper 1] 20
Figure 7 Breakdown of the number of articles evaluated 24
Figure 8 Research structure 26
Figure 9 Spalling depths in the different concretes after HC fire exposure 28
Figure 10 Temperature development in 50 mm depth during the fire test 29
Figure 11 Intrinsic gas permeability of concretes with different blended cements after exposure to 20 ° C, 105 ° C, 150 ° C, 170 ° C and 300 ° C [Paper 2] 31
Figure 12 a) Cumulative porosity and b) incremental porosity of the concretes in the initial state [Paper 2] 32
Figure 13 Moisture distribution before and after heating determined by ^{1}H-NMR [Paper 2] 33
Figure 14 Summarized illustration of the moisture distribution in the different types of concrete after heating showing an increased moisture content for blended cement concretes in the moist zone before the moisture clog. The dashed lines indicate the on-set of the moisture clog for the corresponding concrete [Paper 2 modified] 34
Figure 15 Phase content of the different hardened cement pastes after high temperature exposure to 20 ° C, 105 ° C, 300 ° C and 500 ° C 37
Figure 16 a) TGA and DTG of the hardened cement pastes b) Dehydration behavior of the hardened cement pastes (TGA) and the moisture profiles in concrete after one-sided heating (^{1}H-NMR) show the same sequence of water loss [Paper 4] 38
Figure 17 Spalling depth after HC exposure in PP fiber concrete 40
Figure 18 Temperature development in 50 mm depth for the different PP fiber concretes 41
Figure 19 1D moisture profiles of the concretes after heating a) without PP fibers b) with PP fibers [Paper 4] 41
Figure 20 a) Intrinsic gas permeability b) Incremental pore size distribution obtained by MIP [Paper 4] 42
Figure 21 Coherent representation of the investigations carried out with regard to dehydration behavior, gas permeability, moisture distribution, and temperature distribution normalized over the sample length in different types of concrete a) without PP-fibers, b) with PP-fibers [Paper 4] 47
Figure 22 Recommendations for future work 50

List of Tables

Table 1 System parameters influencing the spalling behavior of concrete (▲ increase ▼ decrease) 21
Table 2 Concrete mixture and properties 28
Table 3 PP fiber concrete mixture and properties 40
Table 4 Maximum spalling depth from fire tests with blended cement concrete from different research groups 45

List of Abbreviations

AFm	Monosulfoaluminate type phases
AFt	Tri-sulfoaluminate (ettringite)
Al_2O_3	Aluminium oxide
Ar	Argon
BFS	Blast furnace slag
C-(A)-S-H	Calcium aluminium silicate hydrate
C-S-H	Calcium silicate hydrate
C_2S	Dicalcium silicate (belite)
C_3A	Tricalcium aluminate
C_3S	Tricalcium silicate (alite)
C_4AF	Tetracalcium aluminoferrite
$Ca(OH)_2$	Calcium hydroxide
$CaCO_3$	Calcium carbonate
CaO	Calcium oxide
CC	Calcined clay
CO_2	Carbon dioxide
CTE	Coefficient of thermal expansion
DTG	Differential thermogravimetric analysis
FA	Fly ash
Fe_2O_3	Iron (III) Oxide
H	Hydrogen
HC	Hydro carbon
HSC	High strength concrete
ITZ	Interfacial transition zone
LC^3	Limestone calcined clay clinker cement
LITS	Load-induced thermal strains
LS	Limestone
MgO	Magnesium oxide
MIP	Mercury intrusion porosimetry
MK	Metakaolin
NMR	Nuclear magnetic resonance
NSC	Normal strength concrete
OPC	Ordinary Portland cement
PP fibers	Polypropylene fibers
RILEM	Réunion Internationale des Laboratoires et Experts des Matériaux, systèmes de construction et ouvrages (French) - International Union of Laboratories and Experts in Construction Materials, Systems and Structures (English)
SP	Superplasticizer
RH	Relative humidity
SCMs	Supplementary cementitious materials
SF	Silica fume

Si	Silicon
SiO_2	Silicon oxide
TGA	Thermo gravimetric analysis
UHPC	Ultra high-performance concrete
XRD	X-ray diffraction

List of Publications

Sections of this dissertation have been published in the following peer-reviewed journal articles:

- Pittrich, T.; Weise, F.; Stelzner, L. The impact of blended cements on the spalling behavior of concrete at elevated temperatures: a review. *Mater Struct 58*, 186: (2025) https://doi.org/10.1617/s11527-025-02713-x
- Pittrich, T.; Peters, S.; Meschke, G.; Weise, F.; Stelzner, L. Thermally induced moisture transport in blended cement concrete studied by ^{1}H-NMR relaxometry. *Mater Struct* 59, 133: (2026) https://doi.org/10.1617/s11527-026-03025-4
- Pittrich, T.; Jansen, D; Weise, F.; Stelzner, L. Dehn, F. Thermal Decomposition in Blended Cement Systems and its Effect on Fire-induced Concrete Spalling: Insights from XRD and TGA. *Case Stud. Constr. Mater.* 24:(2026) https://doi.org/10.1016/j.cscm.2026.e05784
- Pittrich T.; Dehn, F.; Weise, F.; Stelzner, L. Analysis of thermohydraulic spalling in blended cement concrete. *Fire Tech* 62, 158: (2026) https://doi.org/10.1007/s10694-026-01989-x

Additional publications within context of this work are listed below:

Peer-reviewed journal articles:

- Peters, S.; Pittrich, T.; Stelzner, L.; Weise, F.; Meschke, G. Concretes containing blended-cements with reduced carbon-dioxide emissions: A chemo-thermo-hygro-mechanical model for elevated temperatures. *Cem Con Compo* 163: (2025) https://doi.org/10.1016/j.cemconcomp.2025.106163

Conference papers:

- Pittrich, T.; Stelzner, L.; Weise, F. Fire-induced spalling of normal strength concrete with different types of blended Portland cement. *Proceedings of the 13th International Conference on Structures in Fire* (2024), Coimbra, Portugal pp. 451 – 461 https://doi.org/10.30779/cmm_SIF24
- Pittrich, T.; Stelzner, L.; Weise, F. Tunnelbrand – Abplatzverhalten von normalfesten Betonen mit verschiedenen klinkereffizienten Zementen. *11. Jahrestagung des DAfStb mit 63. Forschungskolloquium der BAM Green Intelligent Building* (2024), Berlin, Germany, pp. 253 – 262 https://doi.org/10.26272/opus4-61338
- Stelzner, L.; Kobe, A.; Pittrich, T. Konstruktiver Brandschutz – Abplatzverhalten von Beton - Innovativer Versuchsaufbau und klinkereffiziente Zemente. *Forschung + Praxis, U-Verkehr und unterirdisches Bauen STUVA-Tagung.* 61:(2025), Hamburg, Germany pp. 437 – 444

1 Introduction

1.1 Tunnel fires

The global population continues to grow, driving an increase in both public and industrial traffic. This surge creates a rising demand for safe and efficient transportation systems. A key component of modern infrastructure is the development of tunnels and tunnel networks, which play a vital role in meeting society's transportation needs. All modes of transport carry inherent risks, including the potential for fire, which can be caused by the ignition of fossil fuels or electric car batteries as well as by the transport of highly flammable substances. Fires have long posed a serious threat to tunnel infrastructure. Due to the confined environment of tunnels, fires can escalate rapidly, leading to devastating consequences such as loss of life and extensive structural damage. Numerous incidents around the world have underscored the severity of this risk, highlighting its impact not only on human safety but also on infrastructure integrity and economic stability.

1.1.1 Tunnel fire characteristics

Tunnel fires typically originate from the ignition of vehicles or train wagons within road or railway tunnels. Due to the elongated and confined geometry of tunnels, such fires can rapidly generate extremely high temperatures and facilitate the spread of smoke and toxic gases [1]. The rate of temperature rise and the peak temperatures obtained are largely dependent on the fire load (see Figure 1), which corresponds to the type of vehicle involved (e.g., car, bus, or train wagon) and the composition of its materials (e.g., plastics, aluminum, steel) [2] as well as its cargo. The highest gas temperatures typically develop near the tunnel ceiling, with values up to 1350 °C [3]. This extreme thermal exposure leads to significant degradation of the concrete's mechanical properties, often accompanied by severe spalling. Spalling, and the consequent loss of the concrete cover, poses a critical threat to structural integrity, as it exposes the reinforcement directly to high temperatures. This exposure results in a rapid decline in the load-bearing capacity of the reinforcement [4], thereby compromising the overall stability of the tunnel structure.

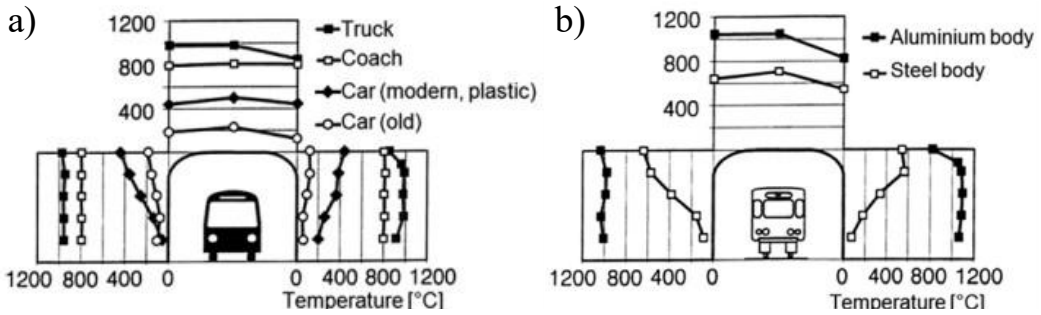


Figure 1 Maximum temperatures in the walls during a) a road tunnel fire and b) an underground railway tunnel fire [5].

1.1.2 Examples of historic tunnel fires

The following examples illustrate the serious consequences of tunnel fires, which include death and destruction. A more detailed list on tunnel fire incidents over the last century can be found in the PhD thesis of Lönnermark [6].

On the 18th November 1996, a vehicle on board of a shuttle wagon caught fire and was carried into the rail road Channel tunnel, which connects the United Kingdom and France. Subsequently, the fire spread on to several wagons and reached temperatures of approximately 1000 °C. Luckily, no fatalities were caused, however, the tunnel lining out of precast reinforcement concrete was heavily damaged (see Figure 2 a)). On the 24th of January 1997, the repair agreement was reached. In total 690 tons of plain shotcrete and 630 tons of fiber reinforced shotcrete were required to replace the linings within 60 days [7].

One of the most devastating tunnel fires in history was the Mont Blanc Tunnel fire, which occurred on March 24, 1999. At the time, the Mont Blanc Tunnel, spanning 11.76 kilometers, was the longest road tunnel in the world, connecting France and Italy. The disaster began when a truck carrying margarine, flour, and diesel caught fire. The blaze burned for 53 hours, reaching temperatures of up to 1000 °C. Unfortunately, 39 people lost their lives, and the tunnel sustained extensive damage (see Figure 2 b)). It took three years of repair and safety enhancement work before the tunnel was reopened in 2002 [8].

Another major tunnel fire that received significant media attention was the Gotthard Road Tunnel fire on October 24, 2001, in the Swiss alps. The incident began with a collision between two trucks, which caused diesel fuel to spill and ignite, likely due to a short circuit in an electrical cable. The resulting fire engulfed both trucks and their cargo. Tragically, eleven people died, and the tunnel sustained severe structural damage over a 230-meter stretch (see Figure 2 c)). In the aftermath, the tunnel was closed for two months, with the total associated costs estimated at around 14 million Swiss francs [9].

a) Channel Tunnel (1996) b) Mont Blanc Tunnel (1999) c) Gotthard Tunnel (2001)



Figure 2 Damages of the tunnel lining after the fire a) Channel Tunnel, 1996 [10] b) Mont Blanc Tunnel, 1999 [10] and c) Gotthard Tunnel, 2001 **(**https://www.alptransit-portal.ch/en/media/file/3768**)**

1.1.3 Tunnel fires today

Today, an increasing number of safety measures are being implemented in tunnels to prevent the worst from happening. However, the number of accidents and incidents continues to rise. This growing risk is primarily driven by increasing traffic volumes, higher vehicle speeds, and the expanding length of modern tunnels [2]. Currently, there are no official global statistics available on tunnel fires. Statistics from highway tunnel fires in China between 2000 and 2016 recorded 161 total incidents, which accounts to 0.8 per month. One quarter of the recorded tunnel fires caused damage to the tunnel structure [11]. In Australia, recent statistics report 8 fires per billion vehicle-kilometers travelled. Between 2000 and 2016, 74 fires were recorded in major roadway tunnels, averaging approximately 0.4 tunnel fires per month [12]. In Europe, the rate is higher, with around 20 fires per billion vehicle-kilometers travelled [13]. Media reports from Switzerland, Germany, and Austria recorded a total of 439 fire incidents in road and railway tunnels between 2012 and 2023. This equates to an average of three incidents per month, with Germany leading the count at an average of 1.6 tunnel fires per month. While a slight decline in railway tunnel fires has been observed, the number of road tunnel fires continues to rise steadily [14]. Although not all these incidents result in severe structural damage, the risk remains significant and must not be underestimated.

1.2 Decarbonation of the cement industry

To meet the growing infrastructure demands driven by growing populations and rapid urbanization, the need for construction materials, particularly concrete, is still increasing. Concrete is already the most widely used man-made material on Earth and is responsible for approximately 6-8% of global carbon dioxide (CO_2) emissions [15, 16]. The majority of these emissions, roughly 5%, come from the production of ordinary Portland cement (OPC) [15] due to the high energy demand and the decomposition of limestone-based raw materials. In light of ongoing climate change, there is an urgent need to pursue sustainable solutions with a reduced carbon footprint. The Paris Climate Agreement commits governments to keep global warming below 2 °C, preferably below 1.5 °C. To achieve this goal, the economy, including the cement and concrete production must be carbon neutral by 2050 [15]. Therefore, developing and adopting solutions is essential for achieving the climate targets that have been set.

1.2.1 Portland cement production

The production of cement clinker begins with the extraction of raw materials, primarily limestone and clay. These materials are mined and transported to the cement manufacturing plant, where they are dried, crushed, and ground. The raw mix is then pre-homogenized to minimize variations in chemical composition, which could affect the quality of the final product [17]. Typically, the raw meal consists out of 75 – 79 wt.-% calcium carbonate $CaCO_3$ and 25 -21 wt.-% Clay [18].

The next phase is pyro-processing, which includes preheating, pre-calcination, and clinker production in rotary kilns. The preheating stage, introduced to improve energy efficiency, reduces the thermal energy required in the main combustion chamber. In this stage, the raw material passes

through a series of cyclones in a preheater tower, where it is heated by hot flue gases rising from below. Following this, the pre-calcination stage occurs, during which $CaCO_3$ decomposes into calcium oxide (CaO) and CO_2 [19]. This reaction is a major contributor to CO_2 emissions in cement production. The raw meal is then fed into a rotary kiln, where it is heated to temperatures of up to 1450 °C to form clinker, the primary component of cement [19]. Fuels such as natural gas, petroleum coke, and coal are used to reach these temperatures, further contributing to CO_2 emissions [17]. Finally, the clinker is air-cooled to approximately 120 °C, where parts of the thermal energy are reused in the preheating and pre-calcination stages. Subsequently, the clinker is transferred to a storage tank [19]. Overall, the calcination process, particularly the decomposition of limestone, is responsible for roughly two-thirds of the CO_2 emissions in cement production, while the operation of the rotary kiln accounts for the remaining third [15, 16]. The average Portland cement clinker consists out of 65 wt.-% C_3S, 13 wt.-% C_2S, 11 wt.-% C_3A, 8.3 wt.-% C_4AF, 1.2 wt.-% CaO and 1.5 wt.-% MgO [18]. Lastly, the clinker is ground while adding the sulphate carriers (typically gypsum) making the production of Portland cement complete. An overview of the production process is given in Figure 3.

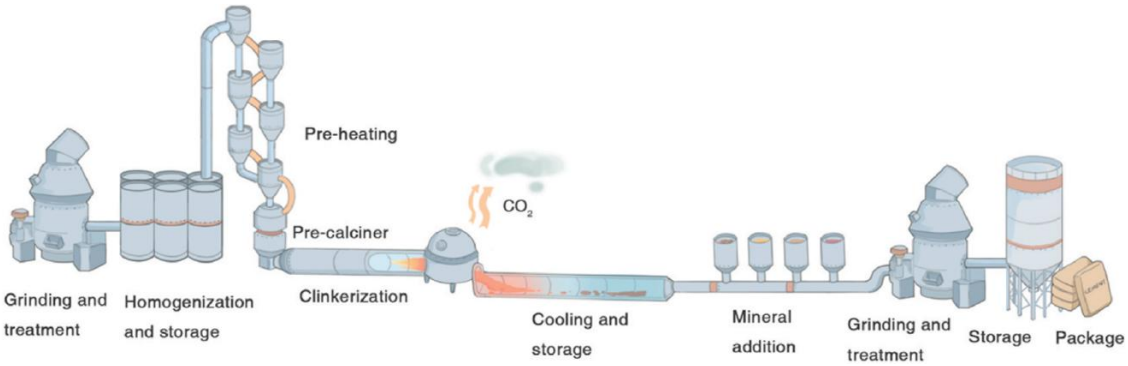


Figure 3 Cement production [20]

1.2.2 Reduction of the clinker factor: Chances and Challenges

Recent developments have revealed several promising strategies to reduce the cement industry's CO_2 footprint. These include improving energy efficiency, adopting alternative fuels, using alternative binding materials, and implementing carbon capture technologies. However, even in technologically optimized cement plants, the chemical decomposition of limestone during clinker production remains unavoidable [16]. Therefore, the reduction of the clinker factor, which describes the clinker to cement ratio, remains by far the most effective way to reduce CO_2 emissions associated with cement production [16]. This is primarily achieved by replacing a portion of Portland cement clinker with supplementary cementitious materials (SCMs) to produce blended cement. Between 1990 and 2022, the global average clinker factor decreased from 0.85 to 0.77 [20], reflecting the growing adoption of this strategy worldwide.

SCMs can originate from natural sources, such as limestone or from industrial byproducts like fly ash (FA) and blast furnace slag (BFS). Consequently, the local substitution rate for Portland

cement clinker is highly dependent on the availability of natural resources and the presence of relevant industries in a given region. While natural materials like limestone are generally unaffected by political or economic decisions, the same cannot be said for industrial byproducts. For instance, in Europe, and particularly in Germany, the energy and steel industries are transitioning toward more sustainable practices. As a result, coal-fired power plants are being phased out, which will soon eliminate the availability of FA [15, 21]. Similarly, the raw iron production is moving toward hydrogen-based reduction processes, casting doubt on the long-term availability and consistent quality of BFS [21].

This growing scarcity underscores the urgent need for alternative SCMs. Among the most promising candidates are activated clays. The activation can be either thermal or mechano-chemical. During thermal activation, also referred to as calcination, the dehydroxylation of the crystal lattice caused by high-temperature treatment (between approx. 600 °C and 900 °C) leads to its amorphization and simultaneously activates the pozzolanic properties of the resulting calcined clays (CCs) [22]. Thermo-mechanical activation also involves dehydroxylation and subsequent amorphization of the structure, but instead of heat, the required energy is supplied through intensive grinding, where mechanical forces from the milling balls are transferred into the material [23]. Until now, most attention has been given to CCs. Although the potential for replacing clinker with CC has been known for decades, it has regained significant interest in the current era due to the increasing focus on sustainability. Thanks to its global abundance and excellent pozzolanic properties, it is expected to play a major role in future cement formulations [24]. The calcination of clay requires significantly lower temperatures than clinker production and involves virtually no limestone decomposition, resulting in substantial CO_2 savings. Looking ahead, ternary cement systems composed of Ordinary Portland Cement (OPC), limestone (LS), and CC are projected to become leading sustainable alternatives. With these new cements often referred to as limestone calcined clay clinker cements (LC^3) achieving clinker factors as low as 0.4 seems possible. However, despite their advantages, these systems also present challenges. The quality of raw clays can vary widely, making the performance of the final calcined clay blended cement highly dependent on the source material. Additionally, calcined clays have a high-water demand, which negatively affects the workability of fresh concrete, while at the same time commonly used superplasticizers show worse effectiveness. Furthermore, there is still limited knowledge regarding the long-term durability and performance of these materials under extreme conditions, such as fire [25].

2 State of the art (Paper 1)

Paper 1 concludes the critical review of the current state of the art, including blended cements, spalling theories and mainly the impact of blended cements on the fire induced spalling behavior of concrete. The paper summarizes the experimental results and highlights the shortcomings and challenges within the current research.

2.1 Blended cements

The practice of partially substituting Portland cement clinker with SCMs has been known for a long time. Historically, this approach was primarily driven by cost savings and economic advantages, as the replacement materials were often industrial byproducts from the iron, steel, or power sectors [26]. In recent years, however, blended cements have regained attention as a more sustainable alternative to OPC. Nevertheless, the incorporation of SCMs into the cementitious system changes the material properties, which affects both the fresh and hardened concrete properties. In general, SCMs needed for blended cements can be classified after their chemical composition and their properties displayed in Figure 4.

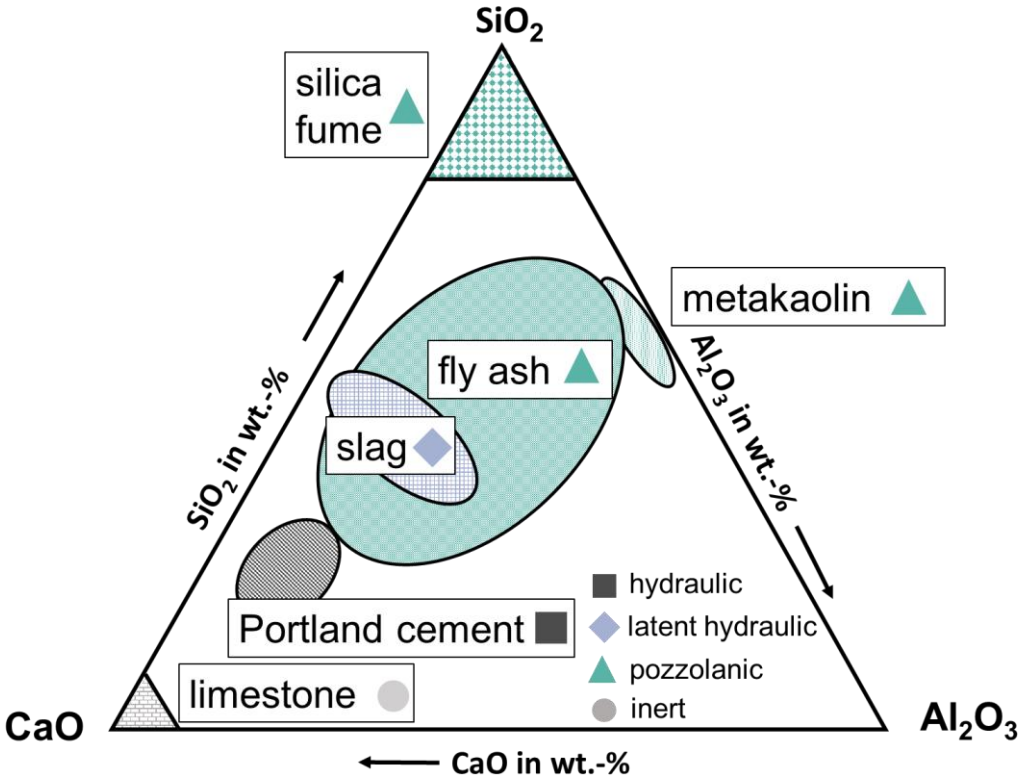


Figure 4 Ternary diagram of commonly used SCMs [Paper 1 modified]

2.1.1 Latent hydraulic SCMs

The most abundant latent hydraulic SCM is BFS. As previously mentioned, it is a byproduct of the pig iron manufacturing process and has been used in cement production since as early as 1865 [27]. BFS is an amorphous material that forms the same primary hydration product as OPC, calcium silicate hydrate (C-S-H), but reacts at a significantly slower rate [28, 29]. Consequently, replacing OPC with BFS typically results in reduced early-age strength, followed by a gradual increase in strength over time [29, 30]. Studies have shown that in slag-based systems, the outer C-S-H product more effectively fills the pore space, minimizing the formation of interconnected capillary pores [31, 32]. Additionally, slag-blended cement systems exhibit improved thermal stability, with reduced pore coarsening when exposed to high temperatures [33].

2.1.2 Pozzolanic SCMs

Natural pozzolanic materials have been used since Roman times, dating back over 3000 years [34]. Today, a wide range of pozzolanic SCMs are available and commonly used in the production of blended cements. FA has historically been the most widely used pozzolanic material; however, due to concerns about its long-term availability [15], interest in CCs is growing. In general, pozzolanic SCMs have a chemical composition like that of OPC, consisting primarily of silicates or aluminosilicates in combination with lower amounts of calcium oxide. During the later stages of cement hydration, the pozzolanic reaction occurs, where the pozzolan reacts with Portlandite ($Ca(OH)_2$) in the presence of water to form C-S-H or calcium aluminum silicate hydrate C-(A)-S-H respectively [35]. The impact of pozzolanic SCMs on concrete properties depends heavily on the type and dosage used, making their effects complex and variable. However, for commonly used materials such as FA, silica fume (SF), and metakaolin (MK), compressive strength tends to increase with replacement levels up to approximately 30%. This strength gain is typically accompanied by reduced porosity and permeability. At higher replacement levels, however, the opposite effect seems to occur [36].

2.1.3 Fillers

In addition to reactive replacement materials, inert fillers can also serve as SCMs. Although they do not contribute to the formation of strength-giving hydration products, fillers are considered more sustainable since they typically require minimal processing beyond grinding. Limestone is the most commonly used filler, but other mineral materials such as quartz are also utilized [37]. While fillers do not directly participate in hydration reactions, they can still enhance concrete strength by providing additional nucleation sites, which accelerate the hydration of the cementitious components. Moreover, they help fill interstitial voids between cement paste and aggregates, thereby densifying the concrete [37]. It is important to note that fillers are not entirely inert. For example, limestone has been shown to react with aluminate phases in cement to form monocarboaluminate hydrates [35, 38]. Similarly, quartz fillers have demonstrated pozzolanic activity over extended periods [37]. Regarding replacement levels, studies have shown that substituting more than 10% of cement with limestone can lead to a reduction in compressive strength, although this does not necessarily correlate with increased porosity [36].

2.2 Fire-induced concrete spalling

Concrete exposed to fire can experience different types of spalling including aggregate spalling, corner spalling, surface spalling and explosive spalling. Explosive concrete spalling is a particularly critical phenomenon in concrete structures, referring to the violent ejection of concrete fragments within the first few minutes of fire exposure [39]. A wide range of interacting parameters influence whether spalling occurs and how severe it becomes. Thermo-mechanical and thermo-hydraulic mechanisms have been identified as the primary driving forces behind explosive spalling. However, due to the complexity of the phenomenon, the exact working of these mechanisms is still not fully understood. In the following section the main mechanisms and the main influencing parameters are briefly described.

2.2.1 Mechanisms

The **thermohydraulic mechanism** was first introduced by Shorter and Harmathy [40] and later refined by Harmathy [41] into what is known as the "moisture clog" theory. This theory describes the buildup of steam pressure within the pore structure of concrete when exposed to elevated temperatures. As the temperature rises, pressure-driven moisture transport occurs, pushing water vapor both outward to the concrete surface and inward toward the cooler core. In the cooler regions, the vapor condenses, gradually forming a fully saturated layer. This saturated zone, referred to as the moisture clog, impedes further vapor escape, resulting in a rapid increase in pore pressure. If this pressure exceeds the tensile strength of the concrete, spalling occurs. However, the theory was never completely verified experimentally due to the challenges associated with measuring pore pressure during fire exposure. Nevertheless, several studies have successfully demonstrated the formation of moisture clogs under such conditions [42-45] . A schematic representation of this mechanism is shown in Figure 5.

A more recent approach was proposed by Felicetti et al. [46], who explained the acceleration of concrete fragments through the vaporization of liquid water and its adiabatic expansion following initial cracking. Over the years, multiple theories addressing thermohydraulic spalling have emerged, and a comprehensive summary of these can be found in the review by McNamee [47].

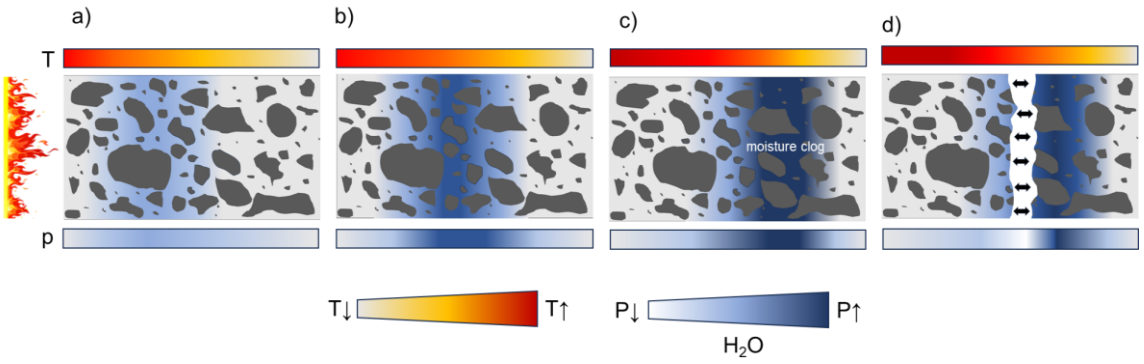


Figure 5 Schematic representation of the thermohydraulic spalling mechanism [Paper 1]

The **thermomechanical mechanism** is governed by two primary factors. The first is the thermal incompatibility between the main components of concrete, the hardened cement paste and the aggregates. When exposed to elevated temperatures, particularly above 150 °C, the aggregates keep expanding, while the hardened cement paste begins to shrink [48]. This mismatch in thermal behavior generates internal stresses and leads to the formation of microcracks, potentially promoting explosive spalling[47]. Simultaneously, the development of cracks causes deterioration of the cementitious matrix, resulting in increased permeability [49]. The higher permeability promotes greater water vapor release, thereby diminishing the effect of thermohydraulic mechanisms.

The second, and likely more dominant factor, is the development of a pronounced temperature gradient within the concrete due to its low thermal diffusivity. During fire exposure, the surface of the concrete heats up rapidly, while the interior remains relatively cool. This temperature differential causes restrained thermal expansion near the heated surface, resulting in high compressive stresses [50]. These compressive stresses, acting in a biaxial manner, are accompanied by tensile stresses perpendicular to the heated surface. When these tensile stresses exceed the tensile strength of the concrete component, spalling occurs [51, 52]. A graphical depiction of this process is provided in Figure 6 below.

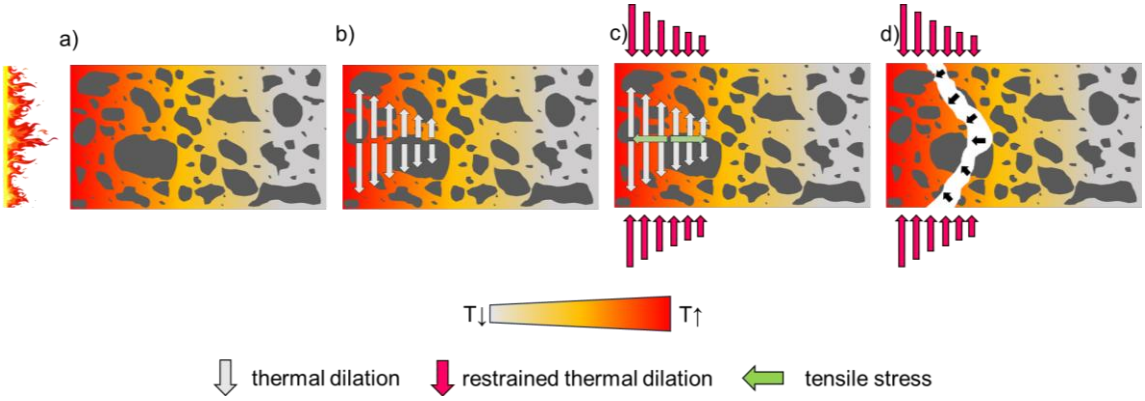


Figure 6 Schematic representation of the thermomechanical spalling mechanism [Paper 1]

2.2.2 Influencing parameters

Explosive spalling in concrete is a complex phenomenon influenced by a multitude of factors, including material, component and loading parameters summarized in Table 1. Among these, the thermal exposure parameters are particularly critical. Elevated heating rates induce steep thermal gradients within the concrete cross-section, resulting in a greater restraint of the thermal expansion and the development of internal stresses that can cause explosive spalling. The absolute temperature reached is also a determining factor, with spalling typically initiating up to 300 °C [53]. Furthermore, the orientation of the heat source and the duration of fire exposure significantly affect the severity and likelihood of spalling.

The concrete strength class plays a pivotal role in spalling susceptibility. While normal-strength concrete (NSC) generally exhibits lower vulnerability, high-strength concrete (HSC) and ultra-

high-performance concrete (UHPC) are markedly more prone to spalling. This increased susceptibility is primarily attributed to their inherently low porosity and permeability [54], which hinder vapor escape and promote pore pressure buildup. These microstructural characteristics also modulate the influence of moisture content. In low-density concretes, moisture contents in the range of 3–4 wt.-% are typically critical [53], whereas in dense concretes, spalling has been observed at moisture levels as low as 1 wt.-% [55].

Aggregate characteristics, specifically size, shape, and mineralogical type, also affect spalling behavior. Smaller [54, 56, 57] and angular aggregates [58] tend to elevate the risk. Further studies have shown that river gravel and flint aggregates are associated with higher spalling susceptibility compared to granitic and basaltic or quarzitic and calcareous aggregates respectively [59, 60]. Particularly the coefficient of thermal expansion (CTE) of the mineral aggregate plays a decisive role. Aggregates with a high silicon (Si) content have been shown to exhibit comparatively higher CTE values [61, 62]. The resulting increase in thermal expansion leads to elevated thermal stresses and, consequently, more pronounced crack formation [62]. These stresses can, on the one hand, promote thermomechanical spalling mechanisms; on the other hand, the associated increase in permeability due to cracking reduces the contribution of thermohydraulic effects. A summary of typical CTE values for different concrete aggregates can be found in the work of Johnson and Parsons [63]

In addition to material properties, component geometry and design parameters display significant influence. Larger concrete members are more susceptible to spalling [57, 64]. Conversely, older concrete elements tend to exhibit reduced spalling risk as a result of progressive drying over time [65, 66]. Lastly, the applied load and surrounding environment play a crucial role for explosive spalling. Studies have shown that mechanical loaded or restrained test specimens experienced a lot more damage in comparison to unloaded counterparts [54, 67].

Table 1 System parameters influencing the spalling behavior of concrete (▲ increase ▼ decrease)

Parameter			**Spalling susceptibility**
Material Parameters	Composition	Cement/SCM type	▲ SF, MK
		Aggregate type	▲ river gravel, flint
		Aggregate size	▼ large ▲ small
		Aggregate shape	▲ angular ▼ round
		w/c ratio	▼ high ▲ low
	Properties	Strength	▲ high ▼ low
		Porosity and Permeability	▲ low ▼ high
		Moisture content	▲ high ▼ low
Component Parameters	Reinforcement	Location	▼ wide ▲ narrow
		Preload	▲ high ▼ low
		Concrete Cover	▲ large ▼ small
	Dimension	Size	▼ small ▲ large
Load Parameters	Fire load	$\Delta\vartheta$/min	▲ high▼ low
		ϑ_{max}	▲ high ▼ low
		Temperature gradient	▲ large ▼ small
	Mechanical load	Compressive load	▲ high ▼ low
		Tensile load	▲ high ▼ low
		Restraint	▲ high ▼ low

2.2.3 Measures against spalling

According to DIN EN 1992-1-2 [68], fire-induced spalling must be taken into account in structural design. So far, the recommended measures only concern high strength concrete. One widely adopted mitigation strategy involves incorporating at least 2 kg/m³ of polypropylene fibers (PP-fibers) into the concrete mix. During a fire, the PP fibers begin to melt at approximately 170 °C, creating expansion space in the form of empty fiber beds, which reduces internal pore pressure and helps prevent explosive spalling. Additionally, the melting of fibers promotes the formation of a network of microcracks, which increases the permeability of concrete and facilitates the release of water vapor [69]. Other effective measures include the use of a reinforcement mesh placed with a nominal concrete cover of 15 mm, which helps maintain structural integrity during spalling events. Furthermore, the application of fire protection materials to the concrete surface can provide an additional layer of defense against high temperatures and thermal degradation [68].

2.3 Impact of blended cements on the fire induced spalling behavior

With the rising popularity of blended cements and the increasing use of SCMs, it is essential to understand their influence on the high-temperature behavior of concrete, particularly regarding fire-induced spalling. To address this, the existing literature on spalling in blended cement concretes was systematically reviewed and evaluated.

A distinction was made between: Standardized blended cements, as defined by regulations such as DIN EN 197-1, and laboratory-blended cements, where OPC was partially replaced with SCMs without considering the broader implications on material properties (e.g. fineness and sulphate content). Furthermore, the studies were categorized based on whether they involved: Dedicated spalling experiments with a structured testing program and evaluation methodology, or just general high-temperature tests, where spalling was only described as a side effect. In total, 66 studies were evaluated (see Figure 7).

The key findings are summarized below:

I) Only a small number of studies conducted in-depth investigations into fire-induced spalling, including comprehensive descriptions of materials, testing procedures, and evaluation criteria. In particular, studies using standardized blended cements often lacked detailed material characterization. This was especially evident in the specification of SCM content. For example, DIN EN 197-1 allows a wide substitution range for certain cement types (e.g., CEM III/A: 35–64 wt.-% blast furnace slag), making it difficult to assess the specific influence of the SCM on spalling behavior without more precise data.

II) The majority of studies focused on the general high-temperature performance of blended cement concretes. Consequently, many employed test setups were unsuitable for assessing spalling. Most results were derived from small-scale specimens tested

at concrete ages below 90 days. This is problematic, as blended cements typically require longer curing times than OPC to achieve comparable hydration and strength development. The use of small specimens also tends to reduce the severity of spalling, potentially masking the true influence of cement type under realistic fire conditions.

III) Moisture content, a critical factor in spalling, was often not reported. This omission makes it difficult to determine whether thermomechanical or thermohydraulic mechanisms were the primary drivers of spalling. Additionally, most tests were conducted without applied load or restraint, which does not reflect real structural conditions.

IV) Several studies concluded that cement type does influence spalling behavior. The responsible parameters identified include moisture content, the definition of the interfacial transition zone (ITZ) and density. However, due to variations in material properties (e.g., strength, aggregate type) and testing conditions (e.g., heating rate, specimen size, applied load), comparisons across studies are limited. This is further complicated by inconsistent spalling evaluation methods, such as counting spalling events, measuring depth, or calculating volume.

V) Based on the reviewed data, SF and MK tend to increase spalling susceptibility due to the formation of a dense microstructure that disables water vapor escape. The effect of FA is more complex. While low replacement levels showed no clear trend, high-volume FA replacements ($\geq$ 25%) appeared to reduce spalling, likely due to a potential accompanied increase in porosity and permeability. No consistent relationships were found between other cement types and spalling susceptibility.

In conclusion, the current state of research reveals significant inconsistencies and contradictions regarding the influence of cement type on fire-induced spalling. Further in-depth studies are urgently needed, especially as new types of blended cements are increasingly adopted in practice. Particular attention should be given to calcined clays, which are expected to play a major role as future SCMs against the background of sustainability.

To improve comparability and reliability of results, testing protocols, such as those recommended by the Réunion Internationale des Laboratoires et Experts des Matériaux, systèmes de construction et ouvrages (RILEM), should be adopted. However, additional considerations are necessary when working with blended cements. It is strongly recommended to provide information beyond the compressive strength of the corresponding concrete, as the incorporation of certain SCMs can significantly influence microstructural properties, such as porosity and permeability, without markedly affecting mechanical performance. Moreover, the standard method of free moisture determination by drying at 105 °C until mass constant, should be re-evaluated. The type of cement used has a substantial influence on the mineral phase composition of the cementitious matrix, which in turn affects its dehydration behavior, where lots of water is removed beyond 105 °C. Therefore, higher drying temperatures, such as 300 °C, may be more appropriate to ensure a more precise determination of the water content. However, care must be taken to avoid temperatures that coincide with the decomposition of specific mineral phases, such as calcium carbonate, to prevent misinterpretation of mass loss data or water content respectively.

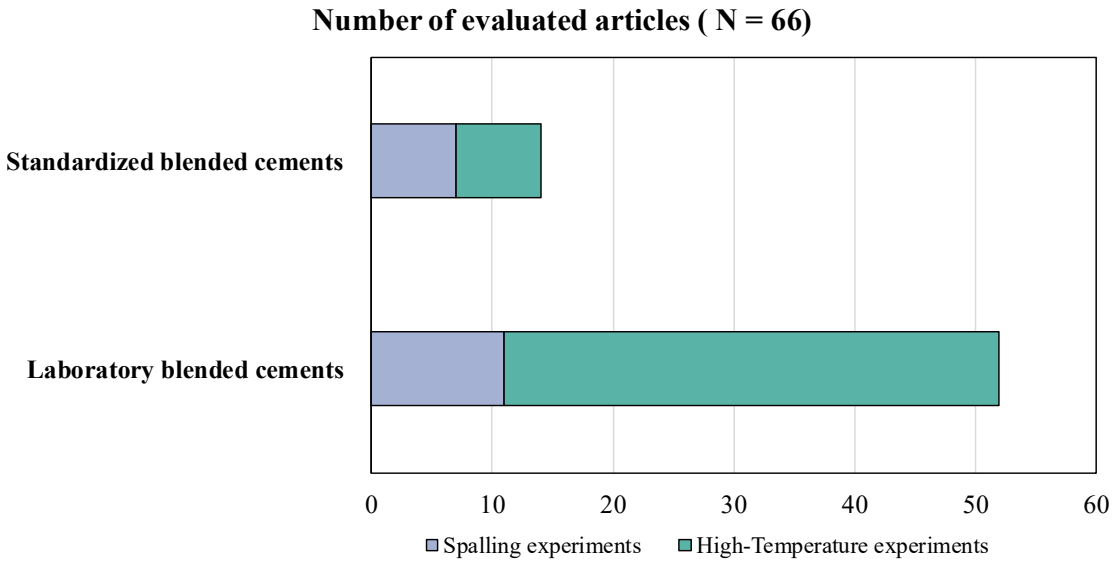


Figure 7 Breakdown of the number of articles evaluated

3 Research objectives

The increasing use of novel blended cements in infrastructure and housing is driven by their lower CO_2 footprint. However, this shift raises concerns regarding the fire resistance of such concretes, particularly their susceptibility to explosive spalling. As highlighted in Chapter 2, the type of cement can significantly influence the spalling behavior of concrete. Nevertheless, current research does not establish a clear correlation between cement type and spalling susceptibility. Furthermore, there is a notable lack of data on the fire performance of concretes incorporating CC, a SCM expected to play a key role in future construction due to the declining availability of commonly used SCMs such as FA and BFS.

In addition to these knowledge gaps, many existing studies suffer from methodological limitations, employing inadequate testing and evaluation procedures. This compromises the reliability and comparability of their findings. To address these shortcomings, the present thesis aims to systematically investigate the spalling behavior of concretes made with various blended cements under fire exposure, with a particular focus on the underlying thermohydraulic mechanisms.

An overview of the research approach is provided in Figure 8.

The first phase of the study involved comprehensive spalling tests on tunnel-grade concrete incorporating four different cement types, subjected to hydrocarbon (HC) fire exposure. Ordinary Portland cement (CEM I) was used as a reference. Two widely used blended cements, CEM II/A-LL (with limestone) and CEM III/A (with blast furnace slag), were selected to represent current practice. A fourth binder, CEM II/B-Q, containing calcined clay, was included to reflect future trends. The testing methodology and evaluation of spalling behavior followed the guidelines of RILEM TC-256-SPF published in [70] and [71].

In the second phase, the focus shifted to analyzing the thermohydraulic mechanisms responsible for explosive spalling. This involved a detailed investigation of the pore structure and transport properties of the different blended cements. Special emphasis was placed on thermally induced moisture transport, studied using ^{1}H-NMR relaxometry. This technique provided insights into pore-size-specific moisture distribution before and after heating, and the associated development of the moisture clog. To correctly interpret these findings, mercury intrusion porosimetry and gas permeability measurements were conducted.

In parallel, the mineralogical characteristics of the cement pastes were examined to understand the effects of decomposition and dehydration at elevated temperatures. X-ray diffraction (XRD) analyses were performed on binder samples exposed to various temperature levels, complemented by thermogravimetric analysis (TGA) and subsequent differential thermogravimetric analysis (DTG) to assess the stability and water release behavior of the hydrate phases.

Lastly, the effectiveness of PP fibers, which are recognized as a proven strategy for mitigating spalling was evaluated for the different concrete types through fire tests, as well as NMR and permeability measurements.

Ultimately, the integration of data on moisture content, transport dynamics, and binder decomposition aims to enhance the understanding of thermohydraulic spalling in concretes made with blended cements. This knowledge is essential for developing more fire-resilient concrete formulations in the context of sustainable construction.

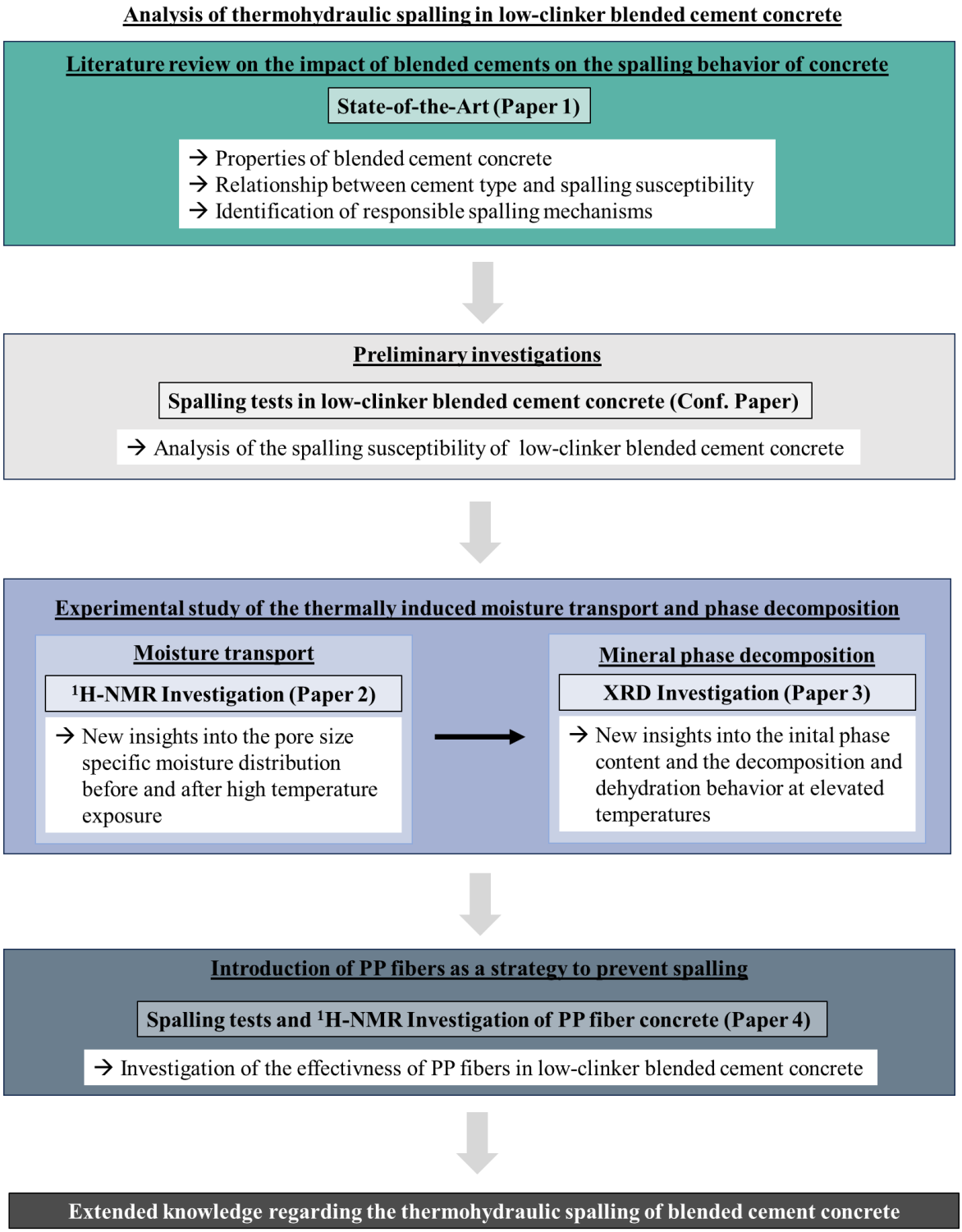


Figure 8 Research structure

4 Experimental investigations

In this chapter, the experimental studies of the thesis are presented.

4.1 Fire tests of blended cement concrete (Conf. paper)

This chapter presents the summarized results of the fire tests published in the conference proceedings of the 13th International conference on structures in fire.

4.1.1 Methodology

A total of four different normal-strength concretes were tested, produced using CEM I 42.5 N, CEM II/A-LL 42.5 N, CEM III/A 42.5 N, and CEM II/B-Q 42.5 N cements. Two specimens of each concrete were cast in cylindrical form (d = 48; h = 30 cm) with a water-to-cement ratio of 0.47. For CEM II/B-Q concrete a polycarboxylate-ether based superplasticizer (SP) was needed to ensure comparable workability. Thermocouples Type K were embedded during casting at depths of 5 mm, 10 mm, 20 mm, 30 mm, 50 mm, and 100 mm to the fire exposed surface.

After 24 h, the specimens were demolded and placed in a water bath for an additional six days. Subsequently, they were conditioned at (20 ± 2) °C and (65 ± 5) % relative humidity (RH) until reaching a minimum testing age of 90 days, as recommended by [70]. During conditioning, the lateral surface was sealed to ensure one-dimensional moisture transport, simulating the conditions in a large-scale concrete element.

Prior to testing, the specimens were grouted into a steel ring using an expansive mortar to create a restrained testing environment similar to Klimek et al. [67], following the methodology of Ozawa et al. [72]. Since the steel ring remains insulated from the direct fire exposure, the thermal expansion of the concrete is partially restrained, simulating the thermomechanical conditions of a large-scale concrete member exposed to fire. In addition, the steel ring prevents moisture release via the outer surface of the test specimen. The free moisture content was determined by drying accompanying concrete cylinders (h = 30 cm; d = 10 cm) from the same production batch until mass constant. In addition, the further moisture content—here referred to as the detectable moisture content, including free water, gel pore water and portions of the chemically bound water—was determined in the sample edge zone using ^{1}H-NMR relaxometry on an additional set of cylinders (h = 30 cm, d = 7 cm). The surface topography of the specimens was analyzed before and after testing using a 3D laser scanner. The concrete's composition and properties are given in Table 2.

Table 2 Concrete mixture and properties

	Unit	CEM I 42.5 N	CEM II/A-LL 42.5 N	CEM III/A 42.5 N	CEM II/B-Q 42.5 N
cement	[kg/m³]	420			
water	[kg/m³]	197			
SP	[kg/m³]	0	0	0	2.5
quarzitic aggregates					
0 / 2 mm	[kg/m³]	646	646	646	634
2/ 4 mm	[kg/m³]	153	153	153	150
4/ 8 mm	[kg/m³]	221	221	221	217
8/ 16 mm	[kg/m³]	679	679	679	666
cube compressive strength					
28 d	[MPa]	46	51	57	57
> 90 d	[MPa]	50	55	59	56
Moisture content					
Drying at 105 °C	[wt.-%]	5.43	5.67	5.60	-
^{1}H-NMR	[wt.-%]	3.66	3.93	4.17	4.52

The fire tests were carried out in an oil-burner furnace with a volume of 1 m³, following the HC fire curve for a duration of 1 hour. During the experiment sound and video recordings were performed. The evaluation of the spalled volume was based on 90% of the fire-exposed surface, in accordance with the recommendations outlined in [70], described in the bachelor thesis of Peter Sorge [73].

4.1.2 Results

The results (see Figure 9) revealed an increased spalling susceptibility in concretes made with low-clinker blended cements. Concrete made with CEM I exhibited only minor spalling, with an average volume loss of approximately 1.5%. In contrast, CEM II/A-LL and CEM III/A showed significantly greater damage, with comparable spalling volumes of around 7%. The highest degree of spalling was observed in CEM II/B-Q concrete, which experienced a volume loss exceeding 9%.

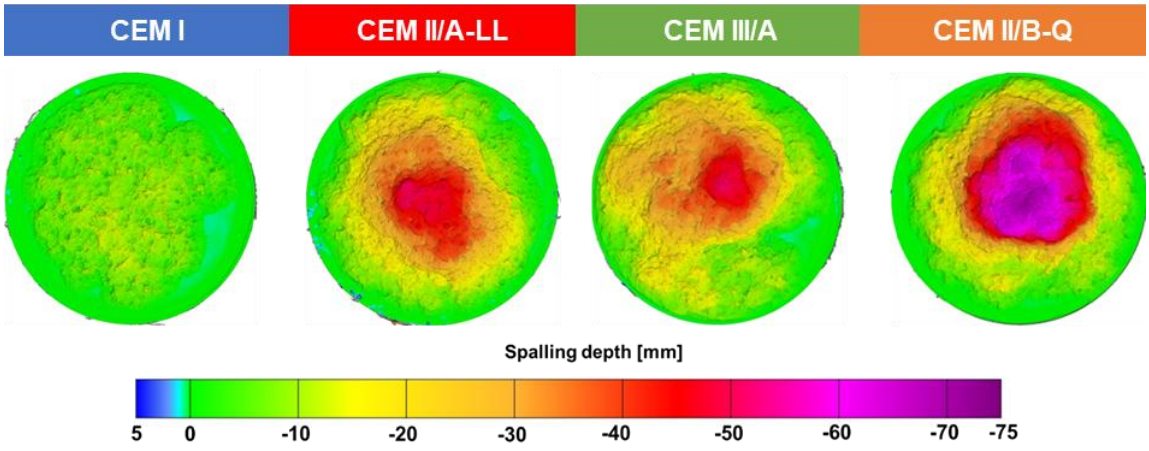


Figure 9 Spalling depths in the different concretes after HC fire exposure

An analysis of the temperature development at a depth of 50 mm (see Figure 10) revealed a rapid temperature rise and final temperatures of roughly 700 °C, 600 °C, and 1000 °C for CEM II/A-LL, CEM III/A, and CEM II/B-Q, respectively. This behavior is attributed to the absence of sufficient concrete cover. This depth is particularly critical, as it corresponds to the typical location of reinforcement layers, which would be severely compromised by direct flame exposure in concrete made with blended cement.

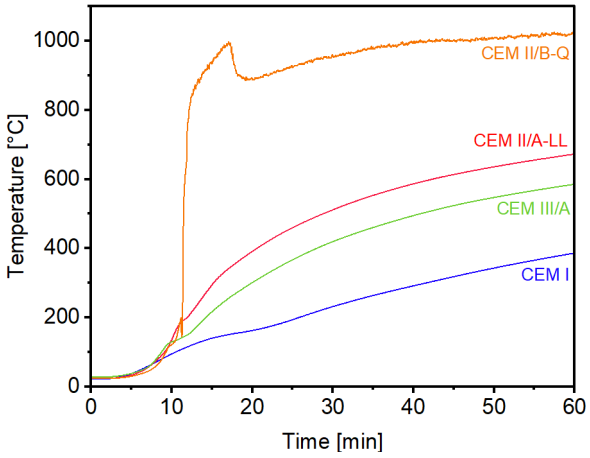


Figure 10 Temperature development in 50 mm depth during the fire test

4.1.3 Main findings

It was demonstrated that the type of cement significantly influences the spalling behavior of normal-strength concrete. The use of low-clinker cements, particularly CEM II/B-Q, leads to a markedly increased tendency for spalling. This results in a reduction of the effective cross-section and exposes the reinforcement directly to fire, potentially compromising the structural integrity of the element. The results indicate that a higher moisture content in blended cement concrete is at least partially responsible for the enhanced spalling risk. Consequently, a thorough understanding of the underlying material properties and mechanisms responsible for spalling is essential in order to develop effective mitigation strategies. This is in particular important as up to now Eurocode 2 is not considering any measures against spalling for normal strength concrete as necessary [74].

4.2 Thermally induced moisture transport in blended cement concrete (Paper 2)

Paper 2 presents the impact of the cement type on the thermally induced moisture transport studied by ^{1}H-NMR relaxometry.

4.2.1 Methodology

To investigate the influence of different cement types on thermally induced moisture transport, ^{1}H-NMR relaxometry studies were conducted before and after high-temperature exposure, following the methodology established by Stelzner et al. [45]. The objective was to identify differences in pore-size-specific moisture distribution, as well as variations in drying behavior and the development of the moisture clog.

Complementary analyses of pore structure and transport properties were performed using mercury intrusion porosimetry (MIP) and gas permeability measurements. Due to the varying Fe_2O_3 contents in the cements, which can distort T_2 relaxation times towards shorter times [75], it was necessary to estimate the surface relaxivity ρ to accurately determine pore sizes. This estimation was achieved by correlating results from fully pressure-saturated samples measured by ^{1}H-NMR with MIP data, as the latter are unaffected by paramagnetic impurities.

The concrete mixture used corresponds to that described in Chapter 4.1.1. Fresh concrete was cast into slightly conical marcor ceramic tubes (h = 10 cm; d = 5 cm) and subjected to the same conditioning regime as the fire test specimens. Additionally, small concrete fragments and drill cores (h = 5 cm, d = 5 cm) extracted from concrete cubes were prepared for MIP and gas permeability measurements. It should be noted that the fresh concrete was sieved to a maximum aggregate size of 8 mm to ensure a suitable ratio between aggregate size and sample diameter for the ^{1}H-NMR relaxometry investigations.

The ^{1}H-NMR relaxometry measurements were performed by an NMR-tomograph from pure devices GmbH. The device operated with a vertical resolution of 2 mm and was fitted with a radio-frequency coil measuring 52 mm in diameter. To reduce the decay of the transverse relaxation time (T_2), a Carr–Purcell–Meiboom–Gill (CPMG) pulse sequence was applied. This sequence featured an echo time of 70 µs, produced 1429 echoes, and included 200 scans per slice (for additional details on the device, see [76]). Signal inversion was performed using NUCLEUS, a MATLAB-based tool developed by Hiller and Costabel [77]. After the initial pore size specific moisture distribution was determined, the specimens were heated at a rate of 10 K/min until a target temperature of 300 °C was reached. This temperature was maintained for 40 minutes, followed by a free cooling phase lasting 120 minutes. Subsequently, the pore size specific moisture distribution was determined again.

The porosity and pore size distribution of the concrete were analyzed in their initial state using MIP on two samples of each concrete type. The porosimeter operated within a pressure range of 0.0007 to 420 MPa, applying a wetting angle of 140° in accordance with ISO 15901-1 [78]. For the purposes of this study, pores are classified as gel pores ($\leq$ 10 nm) and capillary pores

(> 10 nm). Prior to testing, the samples were subjected to vacuum treatment and simultaneously dried at 40 °C for 24 hours.

Gas permeability tests were performed in the initial state and after heating to 105 °C, 150 °C, 170 °C, and 300 °C under Argon (Ar) atmosphere. A moderate heating rate (approx. 1 K/min) was selected to minimize the risk of excessive crack formation due to thermal stresses, which would arise from steep temperature gradients. Afterwards, the intrinsic permeability was determined according to Klinkenberg [79].

4.2.2 Results

Figure 11 displays the permeabilities of the concretes before and after high temperature exposure. CEM I concrete had the highest permeability in comparison to the other concretes. After heating to 105 °C, all concretes showed similar increases of permeability. At higher temperatures (150–300 °C), CEM II/B-Q and CEM III/A samples exhibited stronger permeability growth, while CEM II/A-LL concrete showed the overall weakest increase. By 300 °C, CEM I, CEM III/A, and CEM II/B-Q concrete reached similar final permeability values, while CEM II/A-LL concrete exhibited the lowest permeability.

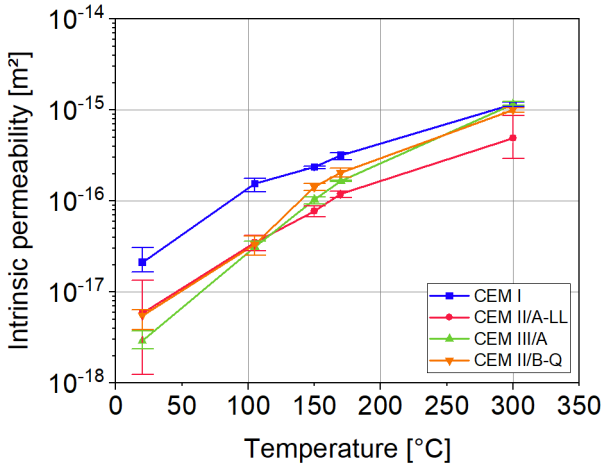


Figure 11 Intrinsic gas permeability of concretes with different blended cements after exposure to 20 °C, 105 °C, 150 °C, 170 °C and 300 °C [Paper 2]

The MIP results provided in Figure 12 show similar total porosity across all concretes: CEM I (13.26 Vol.-%), CEM II/A-LL (13.21 Vol.-%), CEM III/A (13.79 Vol.-%), and CEM II/B-Q (12.87 Vol.-%). CEM I and CEM II/A-LL concrete had similar pore distributions. CEM II/B-Q concrete had fewer capillary pores >10 nm but more gel pores down to 3.6 nm. CEM III/A concrete had the fewest large capillary pores (>30 nm) but the smallest capillary and gel pores. No major differences were found for pore sizes above 200 nm.

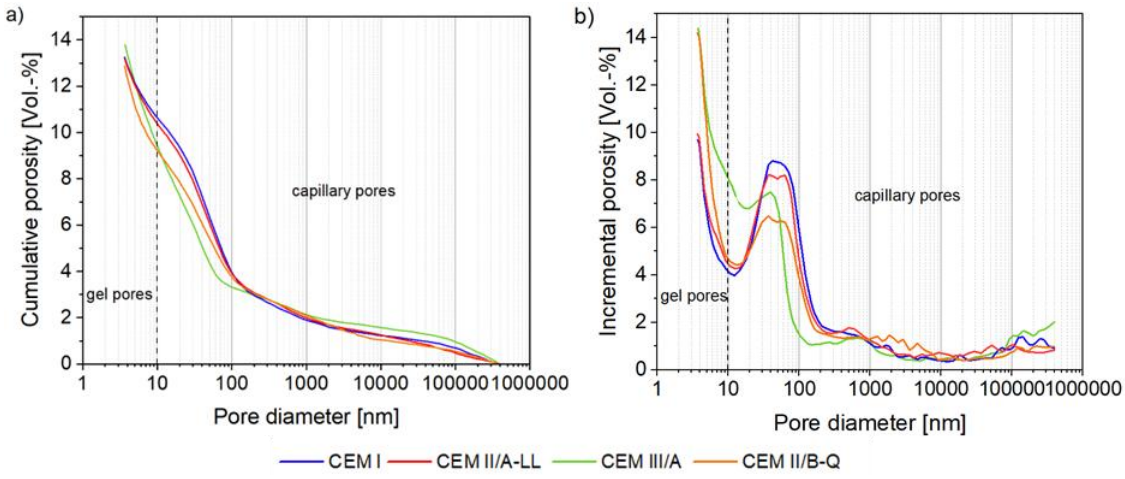


Figure 12 a) Cumulative porosity and b) incremental porosity of the concretes in the initial state [Paper 2]

Figure 13 shows the pore size specific moisture distribution before and after heating. Before heating, CEM I and CEM II/A-LL concrete showed steeper drying gradients than CEM III/A and CEM II/B-Q samples, though all reached similar depths (20–30 mm). CEM I and CEM II/A-LL had slightly lower moisture contents (~12 and 11 Vol.-%) compared to CEM III/A and CEM II/B-Q concrete (>13 Vol.-%). Most water was in gel pores across all types. CEM III/A concrete had the highest capillary pore fraction, while CEM II/B-Q concrete had the most gel pores. After heating, a drying front formed in all samples. CEM II/B-Q sample showed the deepest drying front (~50 mm) and steepest gradient. CEM I and CEM II/A-LL samples developed the strongest moisture clogs, while CEM II/B-Q had the weakest. Moisture shifted from gel to capillary pores in all types, but only in CEM II/B-Q sample did gel pores remain dominant before and after heating.

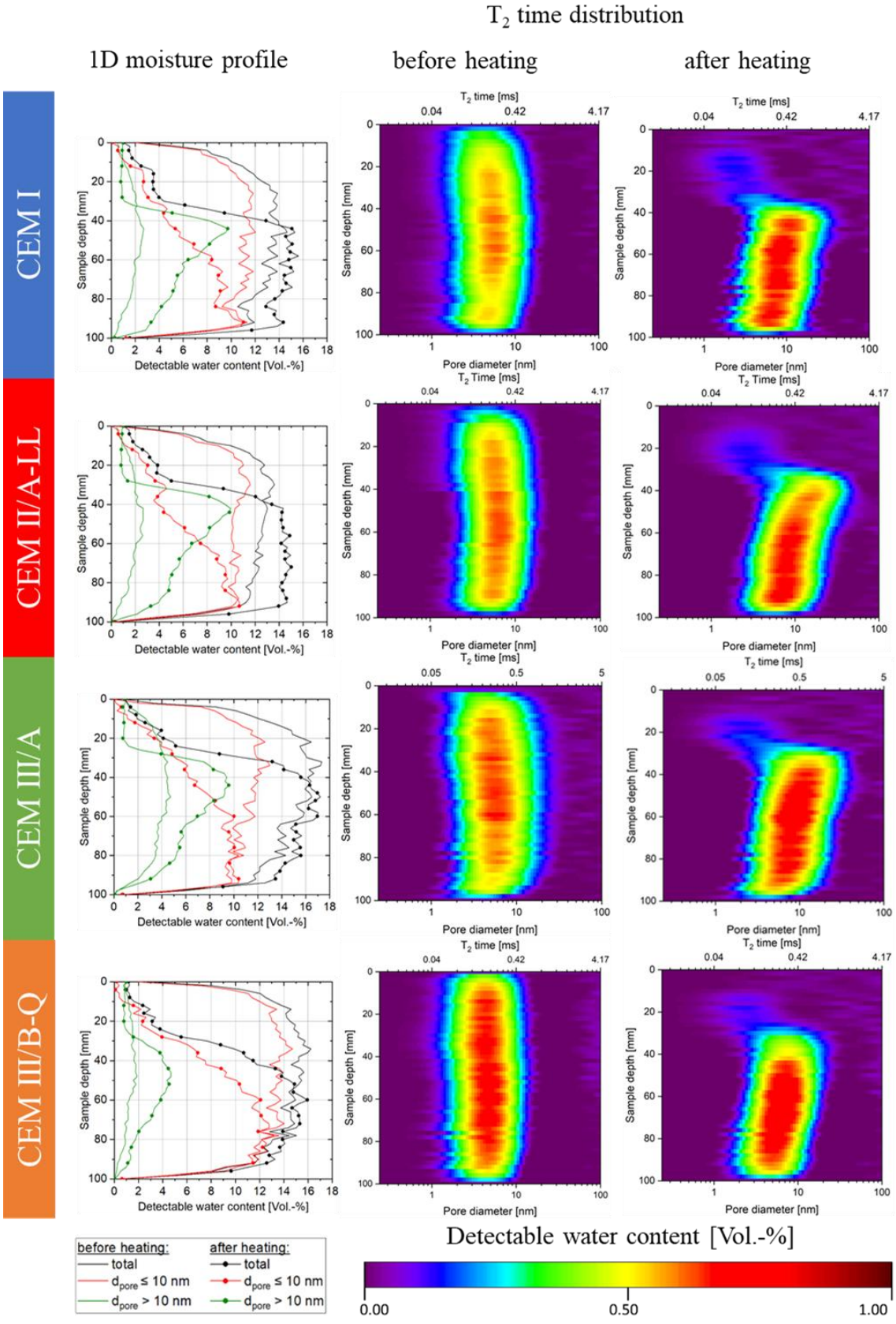


Figure 13 Moisture distribution before and after heating determined by ^{1}H-NMR [Paper 2]

A comparison of the one-dimensional moisture profiles after heating shows that three zones develop (figure 14): a dry layer, a moist region, and a saturated area known as the "moisture clog." The dry zone reaches from the heated surface down to the point where the water content begins to increase noticeably. From there, the moist zone continues until it meets the moisture clog, which is identified as the point where the post-heating moisture curve intersects the initial moisture profile. All blended cement concretes contain more water ahead of the moisture clog. This means they store more thermal energy as hot water heightens the risk of spalling.

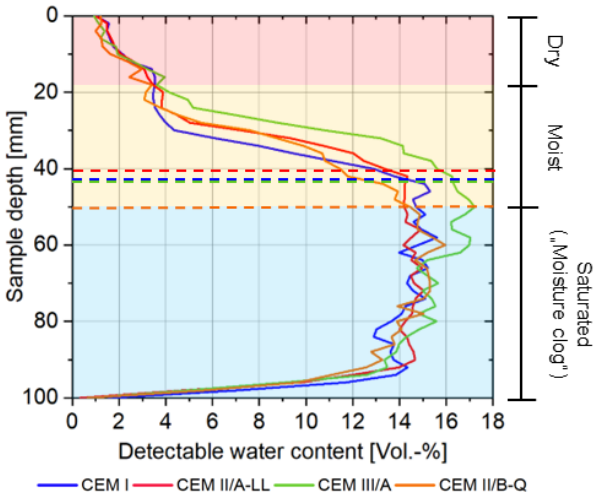


Figure 14 Summarized illustration of the moisture distribution in the different types of concrete after heating showing an increased moisture content for blended cement concretes in the moist zone before the moisture clog. The dashed lines indicate the on-set of the moisture clog for the corresponding concrete [**Paper 2** modified]

4.2.3 Main findings

The investigation into thermally induced moisture transport in concretes made with different blended cements revealed several key findings.

I) Initial permeability and porosity were found to be dependent on the cement type, with CEM I concrete exhibiting the highest initial permeability. However, these differences diminished with increasing temperature, resulting in similar final permeability values for CEM I as well as CEM III/A and CEM II/B-Q concretes after exposure to 300 °C.

II) CEM III/A and CEM II/B-Q concretes showed higher initial moisture contents and distinct pore-size-specific moisture distributions. While CEM III/A contained a greater proportion of capillary pore water, CEM II/B-Q was characterized by a higher content of gel pore water. The high amount of gel pore water might increase pore pressure, as with decreasing pore size, pore pressure increases reported by Jiang et al. [80]. All specimens exhibited the formation of a drying front and moisture clog after thermal exposure, accompanied by pore coarsening. However, the extent and depth of these features varied significantly between cement types and could not be explained by permeability alone.

III) Blended cement concretes contain more water and lower permeabilities in the area before the moisture clog, which corresponds to more available energy for explosive concrete spalling.

4.3 Thermally induced phase decomposition and dehydration behavior of blended cement paste (Paper 3)

Paper 3 the thermal decomposition and dehydration in blended cement paste systems studied by XRD and TGA.

4.3.1 Methodology

For the XRD analysis cubic samples out of hardened cement paste (ca. 4 x 4 x 4 cm^3) of each cement type were exposed to 20, 105, 300 and 500 °C for 72 h. Afterwards, the samples were sealed in plastic foil and stored in a desiccator to avoid any rehydration. In the next step the samples were crushed, immersed into anhydrous isopropanol and further ground in a McCrone mill. Thereafter, the measurements were carried out with a Bruker D8 DaVinci Diffractometer equipped with an energy dispersive LynxEye detector. The measurement was executed in a 2θ range of 5° - 80 ° with a step width of 0.011° per 0.5 seconds. Subsequently, the Rietveld analysis was conducted in TOPAS V7.0.

The TGA analysis was performed on residual powder of the XRD samples which did not experience high temperature exposure. A Mettler Toledo TGA/DSC 3 was used. The measurements were carried out under nitrogen (N_2) atmosphere with a temperature increase of 10 K/min from 25 to 1000 °C.

4.3.2 Results

The results of the XRD-Rietveld analysis are presented in Figure 15. Notable differences in phase composition were observed in the initial state at 20 °C. Calcite was detected in all cement paste specimens, with the highest concentrations found in CEM II/A-LL, where it serves either as a secondary component or as the primary clinker replacement material. In addition to calcite, vaterite was also identified, likely due to carbonation of the samples. Particularly high vaterite contents were observed in CEM III/A and CEM II/B-Q, indicating more extensive carbonation, which is typical for systems containing slag or calcined clay [81, 82]. A significant quartz content, exceeding 12 wt.-%, was measured in the CEM II/B-Q sample. This is attributed to the presence of quartz as a byproduct of calcined clay.

Regarding the hydrate phases, lower amounts of AFt and AFm phases were recorded in the blended cement pastes (ranging from 8.5 to 9 wt.-%) compared to the CEM I paste (11.6 wt.-%). Upon exposure to 105 °C, ettringite was completely dehydrated and no longer detectable in the XRD patterns. Further heating to 300 °C led to the decomposition of AFm phases across all

cement types. Additionally, lower quantities of C-(A)-S-H were found in the CEM III/A and CEM II/B-Q pastes, with values around 22 and 23 wt.-%, respectively. In contrast, CEM I and CEM II/A-LL showed significantly higher contents of approximately 30 wt.-%. Despite these initial differences, a pronounced reduction in C-S-H content was observed in CEM I and CEM II/A-LL after exposure to 300 °C, whereas the C-(A)-S-H content in CEM III/A and CEM II/B-Q remained relatively stable. This suggests enhanced thermal resistance of C-(A)-S-H in the cement types with reactive SCMs. Responsible for this increased thermal stability might be the denser foil like structure leading to an incorporation of more non evaporable water in C-(A)-S-H of slag containing systems [33, 83]. Furthermore, carbonation in blended cement pastes can lead to the formation of a calcium-carbonate modified silica gel with improved thermal properties [84]. At 500 °C, the C-(A)-S-H content decreased in all samples, accompanied by a marked increase in the amorphous phase content. In addition to changes in C-(A)-S-H, differences in portlandite content were also observed. Initially, CEM I and CEM II/A-LL contained higher amounts of portlandite (10 and 8 wt.-%, respectively), while CEM III/A and CEM II/B-Q showed lower levels (around 5 wt.-%), reflecting their lower clinker content and pozzolanic nature. Even after exposure to 500 °C, portlandite remained detectable in all samples. However, the corresponding XRD peaks exhibited reduced intensity and increased broadening, indicating a loss of crystallinity rather than complete structural degradation. Similar findings have been reported by Song et al. [85].

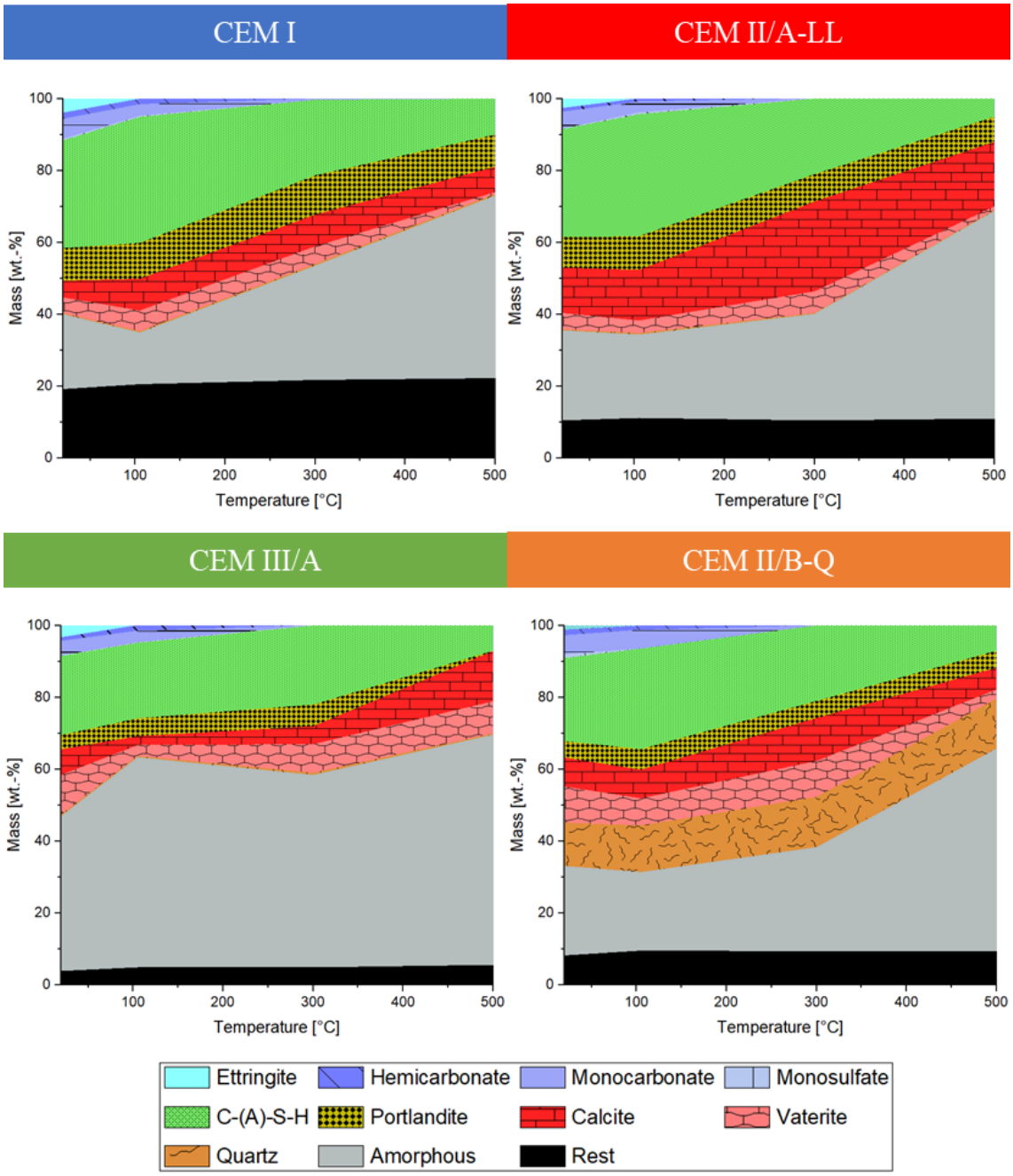


Figure 15 Phase content of the different hardened cement pastes after high temperature exposure to 20 °C, 105 °C, 300 °C and 500 °C

The TGA results are shown in Figure 16. Due to solvent exchange during sample preparation, no free evaporable water remained in the samples. The mass loss observed up to approximately 200 °C is primarily attributed to the dehydration of AFt and AFm phases. This effect was most pronounced in the CEM I cement paste. However, CEM II/B-Q also exhibited a significant mass loss between 140 °C and 200 °C, particularly due to the decomposition of AFm phases, most likely monocarboaluminate. Notably, the CEM III/A paste showed the lowest overall mass loss up to 500 °C, supporting the hypothesis of a thermally more stable C-(A)-S-H phase, as also indicated by the XRD results. The mass loss between 400 °C and 500 °C corresponds to the

dehydration of portlandite and was more prominent in the CEM I and CEM II/A-LL samples compared to CEM III/A and CEM II/B-Q. Above 500 °C, up to around 760 °C, the decomposition of calcium carbonate phases becomes evident. A more detailed analysis of the DTG curve reveals that this process occurs in two distinct stages: the first corresponds to the decomposition of amorphous and low-crystalline vaterite, while the second is associated with the breakdown of calcite [84]. As expected, CEM II/A-LL exhibited the highest mass loss due to its high carbonate content, followed by CEM III/A and CEM II/B-Q, which also showed elevated losses due to increased carbonation. These findings are consistent with the XRD data. In conclusion, CEM I experienced the highest mass loss primarily due to dehydration processes, whereas CEM II/A-LL showed the greatest total mass loss, largely resulting from the high calcite content in its raw materials.

Furthermore, the comparison between the TGA and ^{1}H-NMR results revealed that thermally induced moisture transport is strongly influenced by the dehydration behavior of the cementitious matrix. This is illustrated in Figure 16 b), where the sequence of mass loss closely corresponds to the progression of the drying front. Therefore, it can be concluded that permeability alone is not the decisive factor governing moisture distribution during heating. Additionally, the observed changes in permeability with increasing temperature appear to be of minor relevance, as the majority of water is released below 200 °C.

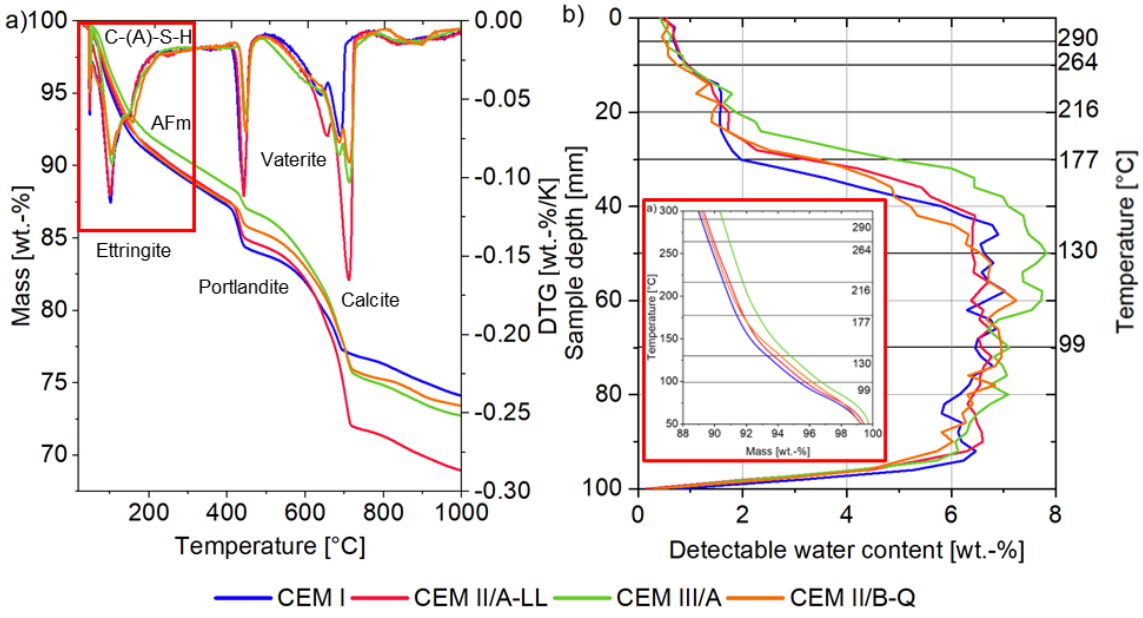


Figure 16 a) TGA and DTG of the hardened cement pastes b) Dehydration behavior of the hardened cement pastes (TGA) and the moisture profiles in concrete after one-sided heating (^{1}H-NMR) show the same sequence of water loss [Paper 4]

4.3.3 Main findings

The characterization of the mineral phase composition and decomposition at elevated temperatures revealed significant differences between the various cement pastes. In relation to the phenomenon of explosive spalling in concrete, the following insights were derived:

I. Blended cement pastes generally exhibited lower quantities of early-dehydrating AFt and AFm phases than the CEM I paste, as shown in XRD analyses. TGA supported this trend, indicating slightly higher water loss in CEM I. This suggests that blended cement concretes may retain more moisture at elevated temperatures, potentially increasing the risk of explosive spalling in concrete made with this type of cement.
II. The C-(A)-S-H phases in blended cements, with latent hydraulic or pozzolanic components, demonstrated superior resistance to thermal degradation. This was particularly evident in CEM III/A paste, which showed minimal decomposition as temperatures rose. This enhanced stability may be attributed to the denser microstructure of the C-(A)-S-H gels and their increased carbonation, which leads to the formation of calcium-modified silica gels with better thermal performance.
III. It was shown that the thermally induced moisture transport and the movement of the drying front described in chapter 4.2 is strongly dependent upon the dehydration behavior of the cementitious matrix. The development of permeability, particularly the steep increase in CEM III/A and CEM II/B-Q concrete, seems to have only a minor impact, as most of the water is already released below 200 °C. Instead, the initial permeability of the concrete plays a more significant role in assessing its vulnerability to explosive spalling.

4.4 Impact of PP fibers (Conf. Paper & Paper 4)

This chapter presents the summarized results of the fire tests of concrete with PP fibers and the impact on the thermally induced moisture transport published in the conference proceedings of the 13th International conference on structures in fire and **Paper 4.**

4.4.1 Methodology

The fire tests and the investigation of thermally induced moisture transport in concrete with PP fibers were conducted following the same methodology described in Chapters 4.1.1 and 4.2.1, respectively. The composition and properties of the PP fiber-reinforced concrete are presented in Table 3.

According to Eurocode 2, no mitigation strategies are specified for NSC. However, since spalling was observed in NSC, a dosage of 2 kg/m³ PP fibers as recommended for HSC was applied. The fibers, supplied by Baumhueter Extrusion GmbH, had a length of 6 mm and a diameter of 15.4 µm. To ensure comparable workability, varying amounts of superplasticizer were used for each concrete formulation, since the addition of PP fibers noticeably compromised the concrete's workability, this was most pronounced in the mixture containing calcined clays.

Table 3 PP fiber concrete mixture and properties

	Unit	CEM I 42.5 N	CEM II/A-LL 42.5 N	CEM III/A 42.5 N	CEM II/B-Q 42.5 N
cement	[kg/m³]	420			
water	[kg/m³]	197			
PP fibers	[kg/m³]	2	2	2	2
SP	[kg/m³]	1.5	3.4	2.1	5
quarzitic aggregates					
0 / 2 mm	[kg/m³]	640	634	637	628
2 / 4 mm	[kg/m³]	152	150	151	149
4 / 8 mm	[kg/m³]	219	217	218	215
8 / 16 mm	[kg/m³]	675	668	669	661
cube compressive strength					
28 d	[MPa]	46	54	65	60
> 90 d	[MPa]	52	61	73	62
Moisture content					
Drying at 105 °C	[wt.-%]	5.66	5.46	5.44	6.08
^{1}H-NMR	[wt.-%]	3.77	3.89	4.02	4.72

4.4.2 Results

After exposure to the HC-fire for 1 h, none of the specimens exhibited spalling (Figure 17). Only crack formation and a slight outward deformation of the surface were observed. This clearly demonstrates that the PP fibers performed effectively, regardless of the cement type used.

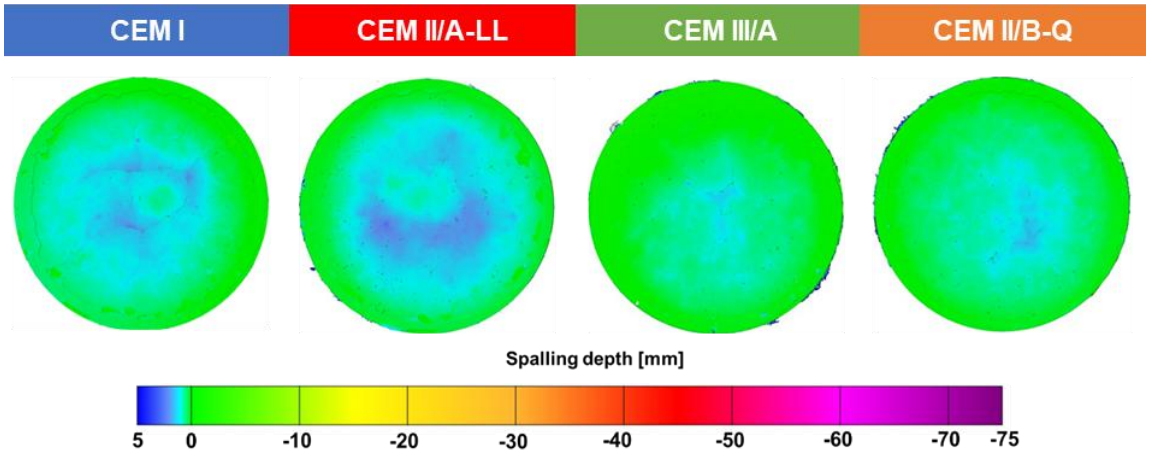


Figure 17 Spalling depth after HC exposure in PP fiber concrete

Additionally, it is worth noting that the temperature measured at a depth of 50 mm was comparable across all concrete types, reaching approximately 200 °C (see Figure 18). This suggests that a potential reinforcement layer at this depth would be shielded from direct flame contact, thereby reducing the risk of significant strength loss.

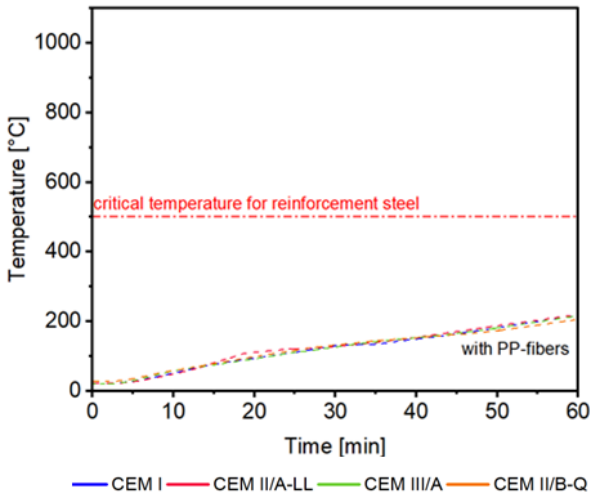


Figure 18 Temperature development in 50 mm depth for the different PP fiber concretes

The influence of PP fibers was evident in the measurements of thermally induced moisture transport, as illustrated in Figure 19. The ^{1}H-NMR results revealed a slightly lower initial moisture content in the mixes containing PP fibers. After one-sided heating, all concrete types exhibited a more pronounced drying front with similar drying gradients. Despite the presence of fibers, a moisture clog was still observed in all samples. This suggests that, at elevated temperatures, the addition of fibers equalized the transport properties across different concrete types, effectively eliminating microstructure specific differences. This observation is further supported by permeability measurements, which show a sudden increase in permeability beyond 105 °C, reaching similar levels across concretes. Interestingly, the most significant rise occurs at temperatures below the fiber melting point, around 150 °C, a trend also reported in previous studies [86, 87]. This behavior is likely caused by cracking induced by the expansion forces of the heated fibers. MIP results for PP fiber mixes revealed a slight increase in porosity and an overall pore coarsening effect in the initial state. However, this coarsening did not lead to a higher initial permeability in PP-fiber concrete. The measured permeability and porosity are presented in Figure 20.

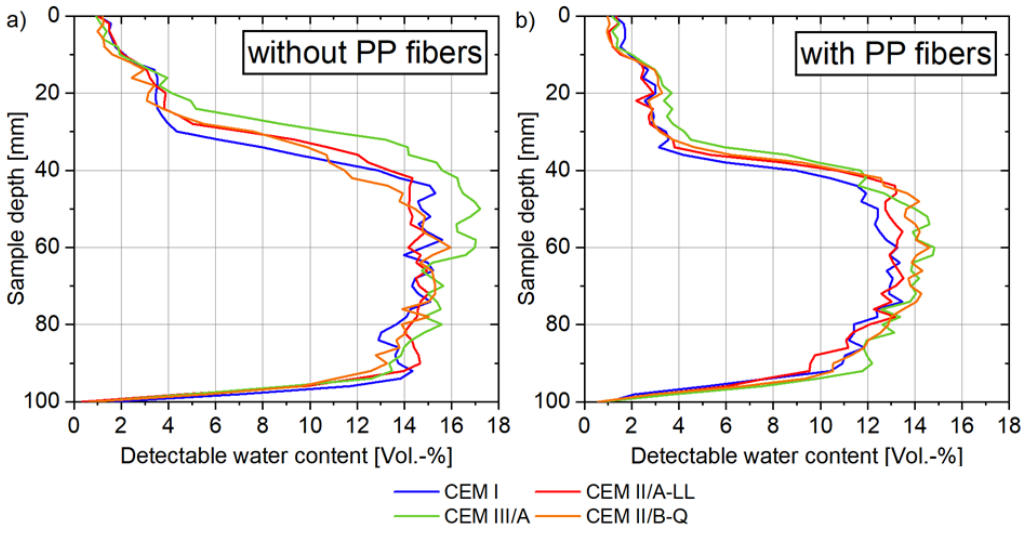


Figure 19 1D moisture profiles of the concretes after heating a) without PP fibers b) with PP fibers [Paper 4]

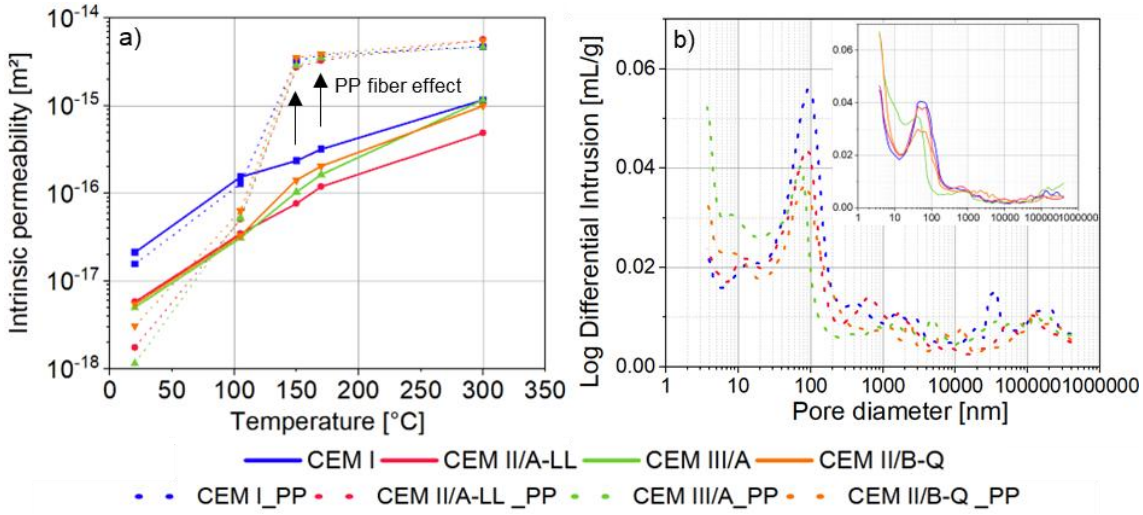


Figure 20 a) Intrinsic gas permeability b) Incremental pore size distribution obtained by MIP [Paper 4]

4.4.3 Main findings

The addition of PP fibers to concrete with low-clinker cement led to the following conclusion:

I. The incorporation of PP fibers negatively affects concrete workability. This effect is particularly pronounced in mixes containing calcined clays, where high amounts of superplasticizer were required to achieve adequate workability. Therefore, further investigation is needed to determine whether lower fiber dosages could be sufficient. Alternatively, the use of altered PP fibers which demonstrate higher effectiveness [88] might be a viable solution.

II. Fire-induced spalling was successfully prevented regardless of the cement type used. Consequently, PP fibers remain an effective strategy for mitigating spalling, even in more sustainable concrete compositions with low-clinker cements.

III. The addition of PP fibers resulted in a significant and uniform increase in permeability across all concrete types at 150 °C. This reduced the influence of binder-specific properties and enabled consistent moisture release. As a result, less hot water was available before moisture clogging occurred, thereby minimizing the risk of spalling.

5 Discussion

5.1 Contextualization with respect to data from literature

In this section, the findings of this study are compared with selected results from the literature. As previously mentioned, comparing spalling data is inherently limited due to the complexity of the phenomenon, which involves numerous interacting factors. The comparison between the obtained data and literature reveals both consistencies and contradictions. An overview of the maximum recorded spalling depth of the selected data is given in Table 4.

The results presented in this thesis align well with those reported by Kirnbauer and Schneider [58]. In their study, NSC made with CEM I 42.5 N and CEM II/A-L 42.5 R was tested under ISO 834 fire exposure. They observed that the use of CEM II/A-L increased the susceptibility to spalling, despite similar free moisture contents obtained by drying at 105 °C until mass constant. Similar observations were made in this thesis. This suggests that moisture content alone is not the decisive factor in determining spalling proneness. Unfortunately, no further data on porosity or permeability were provided, making it unclear whether a denser microstructure inhibited water release or if other factors, such as thermomechanical effects, played a role. Additionally, the lack of information on cement composition limits the comparability with the cements used in this study.

A similar spalling tendency between CEM II/A-LL 42.5 R (85 wt.-% clinker, 12 wt.-% LS, 3 wt.-% BFS) and CEM III/A 42.5 N (54 wt.-% clinker, 3 wt.-% LS, 43 wt.-% BFS) was also reported by Miah [89], who tested NSC slabs under various biaxial loading conditions and ISO 834 exposure. The cement compositions, concrete strengths, and moisture contents were comparable to those in this study. While the permeability values were also within a similar range, Miah noted larger initial differences in permeability between CEM II/A-LL and CEM II/A concretes. In contrast, this thesis found the initial permeabilities of the different blended cement concretes to be nearly equal. This suggests that comparable clinker replacement levels in blended cements may lead to similar microstructures and, consequently, similar spalling behavior. Tests conducted on uniaxial load small scale cubes revealed an increased spalling susceptibility for CEM II/A-LL concrete. However, partially large fluctuations were reported in the results and the small sample size might have blurred the actual effect of the cement type on the spalling susceptibility of concrete.

Reiners [90] investigated the spalling behavior of concrete with CEM I 42.5 N, CEM II/A-LL 42.5 N, and CEM III/A 42.5 N under both restrained and unrestrained ISO 834 exposure. An increased spalling tendency in CEM III/A concrete compared to CEM I concrete was observed, which is consistent with the findings of this thesis. Reiners attributed this to a denser microstructure and higher moisture content, leading to so called “moisture weakening”, which was described as the observed decrease of tensile/flexural strength in high saturated concrete. Thus, making it easier to overcome the stress needed to violently eject concrete pieces in the form of explosive

spalling. This type of explanation would also apply to the findings of the presented work as the blended cement concretes with increased moisture content showed increased spalling susceptibility. However, Reiners also reported a similarly low spalling tendency between CEM I and CEM II/A-LL concrete, which contradicts this thesis findings. Here, CEM II/A-LL concrete showed a significantly higher spalling tendency than CEM I concrete. One possible explanation lies in differences in microstructure and porosity. Reiners observed a significant increase in capillary porosity for CEM II/A-LL concrete, along with a roughly 10 MPa lower compressive strength. Although no permeability measurements were provided, the higher porosity and lower strength might suggest increased permeability. In contrast, this study found similar strength and porosity between CEM I and CEM II/A-LL concrete, but significantly lower permeability in the latter, which may have contributed to the higher spalling risk. Again, the absence of cement composition data complicates further interpretation. The clinker replacement ratio in CEM II cements (6–20 wt.%) is crucial for microstructure development. Panesar et al. [36] concluded that limestone replacement above 10% leads to a gradual strength reduction, indicating that raw cement composition can significantly influence microstructure and therefore the spalling behavior. This highlights the importance of comprehensive material characterization.

Hager et al. [59] studied the spalling behavior of HSC made with CEM I 42.5 R and CEM III/A 42.5 N under unloaded ISO 834 exposure. Regardless of the aggregate type (basaltic or granitic), CEM I concrete exhibited slightly more spalling, despite lower permeability in CEM III/A. These results contradict the findings of this study and the general consensus. The authors argued that initial permeability and general material properties are not decisive for the spalling behavior in HSC. Instead, they emphasized the role of structural factors such as the cold rim. However, the promotion of thermomechanical effects trough the cold rim might only be small in a setup without applied external restraint [67]. In addition, no detailed cement composition data were provided. In CEM III/A, 36–64 wt.-% of clinker can be replaced by blast furnace slag, a wide range that significantly affects hydrate phase composition. Whittaker et al. [91] demonstrated that chemistry and particularly the replacement amounts of clinker with slag strongly influence the hydrate mineral phase composition: Increasing replacement rates led to decreasing amounts of AFt and Portlandite and increasing amounts of AFm and C-S-H. Moreover, it was revealed that SO^{3-} contents above 4 wt.-% increased the formation of ettringite, which promoted explosive spalling in high volume slag cement concrete [92]. In this study, it was shown that phase composition and associated dehydration behavior significantly affect moisture transport during heating, which in turn impacts explosive spalling. Therefore, material properties once more should not be underestimated.

To date, no in-depth studies have addressed the spalling behavior of concrete with calcined clays and in particular not in standardized cements such as the here presented CEM II/B-Q. Preliminary fire and high-temperature tests on small-scale specimens with MK indicate an increased spalling risk due to a denser microstructure and the associated restriction of water vapor release [93-95]. These findings provide initial confirmation of the results presented here. However, it must be noted that in practice, various types of calcined clays will be used, each potentially affecting concrete properties differently. Given that calcined clay is expected to become the most widely used SCM in the long term, further investigation into its fire-induced spalling behavior is essential.

Table 4 Maximum spalling depth from fire tests with blended cement concrete from different research groups

Fire curve	Reference	Maximum spalling depth [mm]			
		CEM I	CEM II/A-L(L)	CEM III/A	CEM II/B-Q
ISO 834	Kirnbauer & Schneider	0[a)c)h)]	45[a)c)h)]	-	-
		22[b)c)h)]	35[b)c)h)]	-	-
	Hager et al.	45[d)h)]	-	40[d)h)]	-
		65[e)h)]	-	50[d)h)]	-
	Miah	-	0[c)h)]	0[c)h)]	-
		-	61[c)i)]	58[c)i)]	-
	Reiners	0[f)h)]	0[f)h)]	25[f)g)]	-
		10[f)j)]	10[f)j)]	30[f)i)]	-
HC	Pittrich	15[b)g)j)]	53[b)g)j)]	52[b)g)j)]	72[b)g)j)]

a) moisture content 5%; b) moisture content 6%, c) calcareous; d) basalt; e) granite; f) Rhine gravel; g) siliceous
h) unloaded; i) 5 MPa biaxial; j) restraint

5.2 Contextualization with respect to selected spalling theories

In this thesis high moisture contents, low permeabilities and thermally more stable hydrate phases have been identified as the main factors responsible for the increased spalling susceptibility in blended cement concrete. But how would those parameters interact within the framework of popular spalling theories? In the following section, the experimentally obtained results will be discussed in regard to selected spalling theories.

The earliest and well-known ''moisture clog'' theory claims that with the formation of the moisture clog the inward transport of further water vapor is restricted leading to an increase in pore pressure and finally to explosive concrete spalling [40, 41]. Therefore, higher moisture contents and denser microstructures lead to an increased spalling susceptibility. From a general point of view this applies to the observations made in this thesis as the existence of the moisture clog was validated in every sample and the blended cement concretes with lower permeabilities and higher moisture contents showed increased spalling proneness. However, pore pressure measurements in NSC and HSC exhibited values below the tensile strength of the material in a temperature range of 220 – 300 °C [96]. Hence, pore pressure alone cannot be responsible for explosive concrete spalling. More recent advances by Felicetti et al. [46] and Yarmohaamdian and Felicetti [97] propose a two-stage process causing the violent ejection of concrete fragments. The first stage describes the crack initiation by exceeding the tensile strength of concrete through the combined effects of pore pressure and thermal stresses. This is in alignment with experimental results, where it was shown that dry as well as non-restraint or loaded specimens show lower spalling tendencies in comparison to moist and restraint or loaded samples respectively [53, 54, 67]. The second stage describes crack instability and propagation, which appears when the internal pressure exceeds the remaining strength of the concrete cross-section. Thereafter, sudden pressure drop leads to flash evaporation of the superheated water, whereas the adiabatic expansion ignites the acceleration of the concrete fragments known as spalling. The researchers in particular highlight the crack initiation timing paired with sufficient thermal energy and water as decisive for the spalling severity.

The experimental results showed increased initial water contents for CEM III/A and CEM II/B-Q as well as lower permeabilities especially emphasized in temperature ranges (50 – 170 °C) where most of the water is released during heating in CEM II/A-LL, CEM III/A and CEM II/B-Q concrete. This is shown in the consolidated overview of the performed investigations, normalized across the depth of the one-sided heated cylinders from section 4.2 in Figure 21. Three distinct regions were assigned: a dry zone, a moist zone, and a saturated zone ("moisture clog"). The dry zone describes the area up to the point where the moisture content begins to increase significantly, marking the transition into the moist zone. This moist zone continues until the formation of the moisture clog, which is defined as the point where the post-heating water content intersects with the initial, unheated moisture profile. Due to reduced dehydration and lower permeability, blended cement concretes retain more water in the moist zone prior to the beginning of the moisture clog at a temperature range between 150 – 230 °C. This corresponds well to the temperature range of 170 – 240 °C, where spalling was observed during the fire tests. Hence, it can be concluded that the greater amount of available thermal energy in the form of hot water significantly increases the risk of explosive spalling in concrete made with blended cements. Thereby supporting the idea of the proposed mechanism. The addition of PP fibers, which is combined with a significant increase in permeability at elevated temperatures, accelerates the drying process. This results in a more pronounced dry zone extending to greater depths, followed by a much thinner moist zone with lower but uniformly distributed water content across all concrete types. The reduced moisture availability in regions with lower temperatures (ca. 125 – 175 °C) means that insufficient thermal energy is present to cause explosive spalling. Nevertheless, despite similar material properties, noticeable differences between the spalling susceptibility between the different blended cement concretes appear which cannot solely be explained by the current state of the art of thermohydraulic approaches. This raises the question of whether differences in the mineral phase composition also influence the thermomechanical modes of action, such as initial crack formation and propagation.

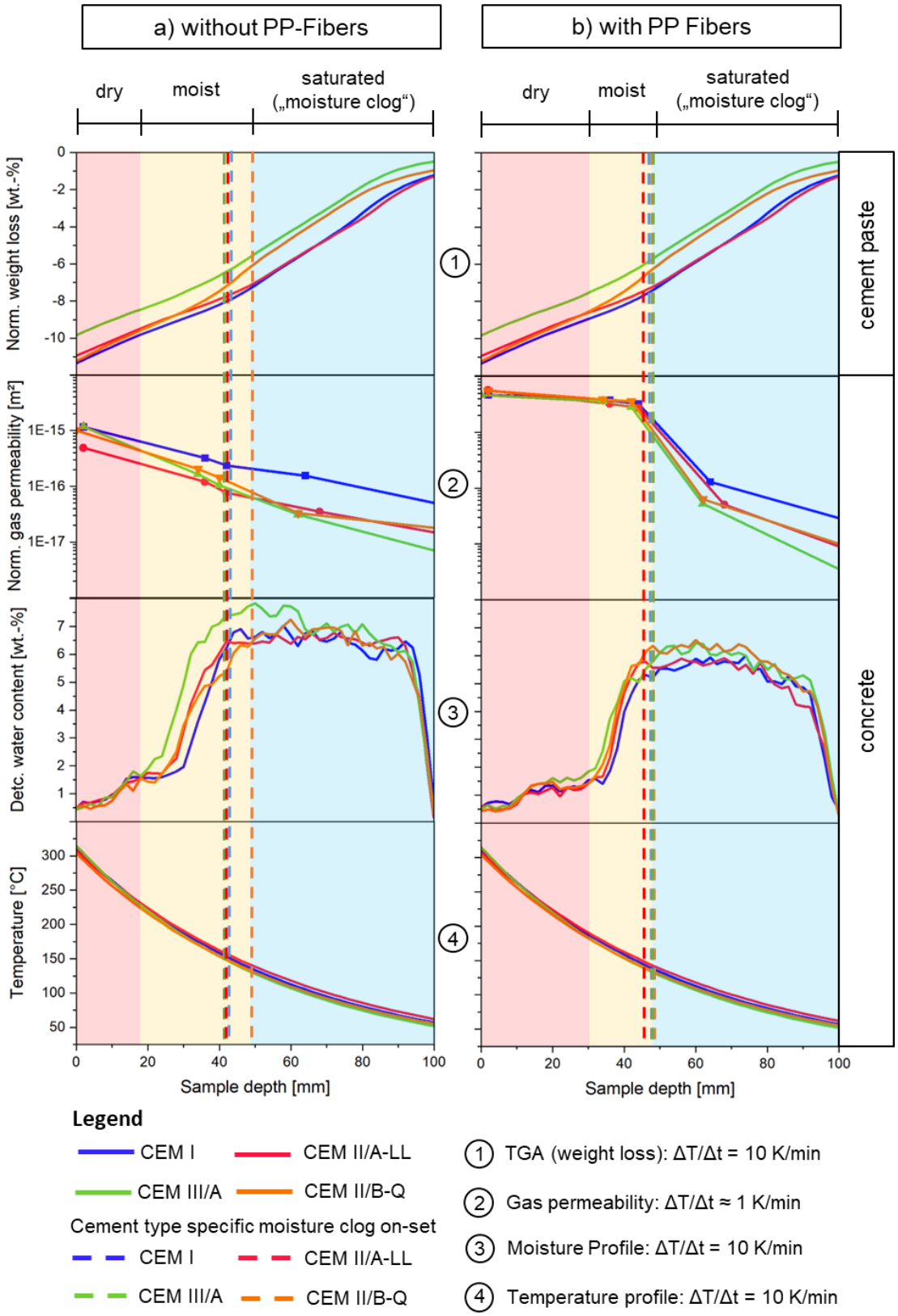


Figure 21 Coherent representation of the investigations carried out with regard to dehydration behavior, gas permeability, moisture distribution, and temperature distribution normalized over the sample length in different types of concrete a) without PP-fibers, b) with PP-fibers [Paper 4]

6 Conclusion and Outlook

The present thesis investigated the impact of low-clinker blended cements on the fire spalling behavior of concrete in combination with a comprehensive study of the underlying thermohydraulic properties. It was shown that the utilization of CEM II/A-LL, CEM III/A and CEM II/B-Q significantly increases the spalling vulnerability of concrete. Above all, the addition of calcined clays shown in CEM II/B-Q appears to greatly increase the tendency to spalling, for which widespread use is predicted in the near future. Furthermore, it should be emphasized that the use of blended cements causes NSC to spall so severely that a potential reinforcement layer is endangered due to direct flame exposure. However, up to now, according to Eurocode 2, no prevention strategies are considered necessary in NSC. Both of those aspects should be considered in the sense of sustainable construction in the future.

The determination of the pore size-specific moisture distribution before and after high temperature exposure showed clear differences in dependency of the cement type. Here, CEM III/A and CEM II/B-Q exhibited a higher initial moisture content already indicative for the more severe spalling observed. Moreover, permeability measurements showed noticeable lower values for all types of blended cement concrete further promoting the spalling risk. However, a comparison between the permeabilities and the obtained drying fronts showed that this cannot be the only influencing factor. XRD and TGA analyses revealed that the decomposition and dehydration behavior of the cementitious matrix is one main driver of moisture transport during high-temperature exposure. It was shown that the sequence of mass loss in the hardened cement paste corresponds to the sequence of drying observed in the concrete samples. The reasons for this appearance are less AFt and AFm phases in blended cement pastes and additionally a more temperature resistant C-(A)-S-H phase in CEM III/A and CEM II/B-Q samples. Both the lower permeabilities and the increased thermal stability of the cement pastes lead to higher water retention in a temperature range critical for explosive spalling. With the addition of 2 kg/m³ of PP fibers, binder-specific influences on the microstructure were largely eliminated at elevated temperatures, resulting in a uniform increase in permeability and, consequently, a consistent moisture release. This enhanced drying process ensures that significantly more water is expelled, leaving insufficient thermal energy to cause explosive spalling. Therefore, PP fibers remain an effective mitigation strategy, even for more sustainable concrete compositions incorporating blended cements. However, PP fibers strongly affect the workability of fresh concrete. It is therefore necessary to investigate whether lower fiber dosages could achieve similar performance or whether the introduction of altered PP fibers with improved efficiency is required to ensure practical, problem-free application.

The findings presented here offer a solid explanation for the general differences in spalling behavior between Portland cement and blended cement concrete. However, the variations observed among individual blended systems are not fully understood. Notably, the increased spalling tendency in CEM II/A-LL, despite having similar moisture content and dehydration characteristics to CEM I and the even greater spalling observed in CEM II/B-Q in comparison to the other blended cements suggest that additional mechanisms must be influential.

Based on the insights gained, several directions for future research can be proposed (see figure 22). From a thermohydraulic standpoint, the moisture distribution across different pore sizes needs closer examination. In particular, the elevated presence of gel pore water, which appears to be unique to CEM II/B-Q concrete, should be investigated further. Results in literature indicate that as pore size decreases, pore pressure in unsaturated pores tends to increase [80]. While pore pressure alone may not be the primary driver of explosive spalling, it could still contribute to the overall process, potentially playing a more significant role in CEM II/B-Q concrete, where the most severe damage was observed. From a thermomechanical perspective, differences in mineral phase composition may also be critical. The enhanced thermal stability of C-(A)-S-H in CEM II/B-Q and CEM III/A cements could influence the thermomechanical response of concrete, particularly with respect to load-induced thermal strains (LITS). In structures where thermal expansion is constrained, LITS potentially have a mitigating effect by developing in the direction of the applied load, thereby reducing compressive stresses caused by restrained thermal dilation [98]. This stress relaxation may help lower the risk of explosive spalling. LITS are primarily driven by thermal transient creep and drying creep, both of which are closely linked to the decomposition of hydration phases and the movement of water within the cement matrix [99, 100]. Peters et al. [101] observed that the progression of C-S-H dehydration closely follows the development of LITS, which is attributed to creep-like sliding of C-S-H under compressive stress. However, in cement systems such as CEM II/B-Q and CEM III/A, the presence of thermally stable C-(A)-S-H may inhibit this sliding mechanism. As a result, LITS may be reduced, leading to lower stress relaxation and potentially increasing the material's susceptibility to spalling under elevated temperatures. Another important factor contributing to explosive spalling is the thermal mismatch between the cement paste and the aggregates. At temperatures around 150 °C, the cement paste tends to shrink while the aggregates expand, generating internal stresses that might contribute to spalling. In blended cement systems, the composition of residual non-hydrated phases varies significantly and must be considered. For example, the CEM II/B-Q cement analyzed in this study contains a high proportion of quartz, which acts as micro-aggregates and introduces thermal incompatibility even within the binder matrix. Quartz aggregates are known for their pronounced thermal mismatch, but similar behavior is also observed with limestone and slag aggregates [48]. These incompatibilities are key contributors to spalling behavior and should be carefully evaluated when assessing the influence of cement type on fire resistance and thermal performance.

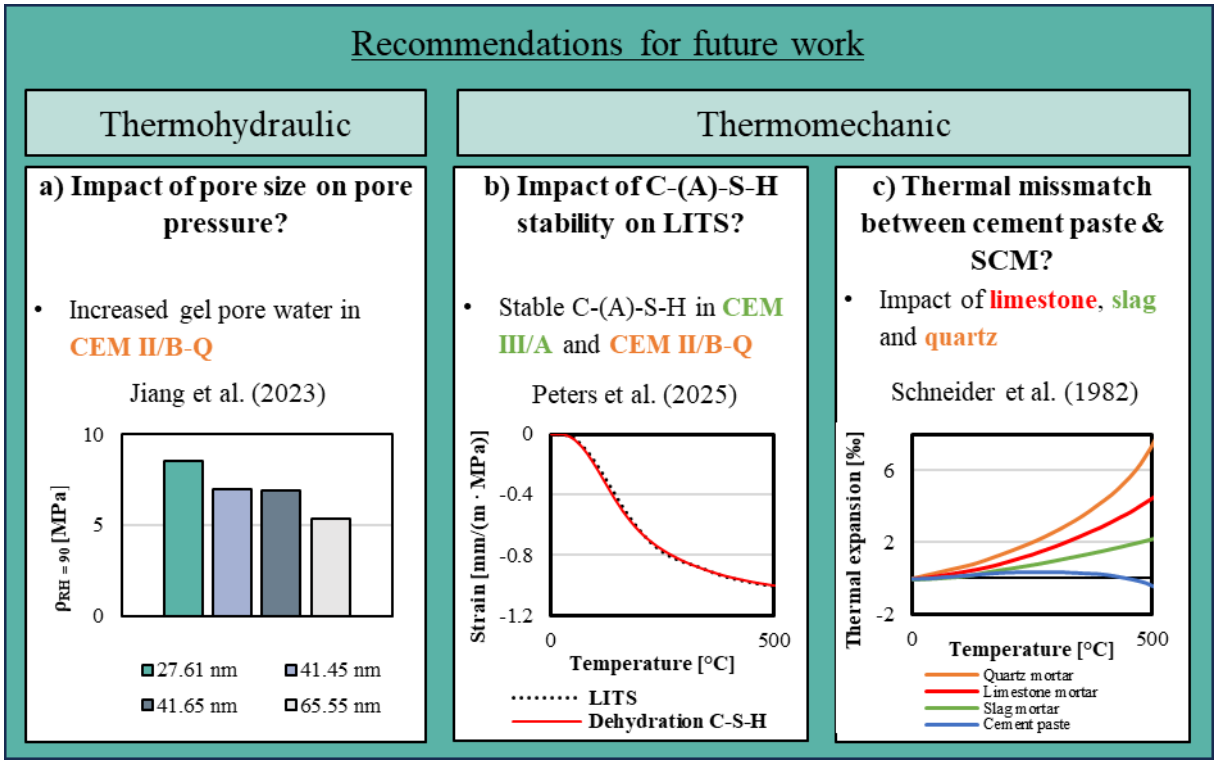


Figure 22 Recommendations for future work

Bibliography

1. Yao Y (2019) Fire Behaviors and smoke transportation law of tunnel fires under confined portal boundaries. University of Science and Technology of China
2. Fehérvári S (2008) Characteristics of Tunnel fires. Concrete Structures 56-60.
3. Li Y Z and Ingason H (2012) The maximum ceiling gas temperature in a large tunnel fire. Fire Safety Journal 48:38-48. https://doi.org/10.1016/j.firesaf.2011.12.011
4. Topcu I B and Karakurt C (2008) Properties of Reinforced Concrete Steel Rebars Exposed to High Temperatures. Advances in Materials Science and Engineering https://doi.org/10.1155/2008/814137
5. Richter E (1993) Heißgasentwicklung bei Tunnelbränden mit Straßen- und Schienenfahrzeugen – Vergleich gemessener und in Vorschriften enthaltener Temperatur-Zeit-Verläufe. STUVA Tagung '93 in Hamburg: Cologne, Germany 131-137.
6. Lönnermark A (2005) On the Characteristics of Fires in Tunnels Lund University
7. Kirkland C J (2002) The fire in the Channel Tunnel. Tunnelling and Underground Space Technology 17:129-132.
8. Catmur J, King K, Parsons M et al (2023) A Service Analysis of the Mont Blanc Tunnel Fire. Safety Critical Systems Symposium:113-145.
9. Pospisil P (2021) The Gotthard Road Tunnel Fire: 20 Years On. Tunnelling Journal 14-19.
10. Haack A (2003) Catastrophic Tunnel Fires – What have we learnt? International Symposium on Catastrophic Tunnel Fires (CTF): Boras, Sweden 7-17.
11. Ren R, Zhou H, Hu Z et al (2019) Statistical analysis of fire accidents in Chinese highway tunnels 2000–2016. Tunnelling and Underground Space Technology 83:https://doi.org/10.1016/j.tust.2018.10.008
12. Casey N (2020) Fire incident data for Australian road tunnels Fire Safety Journal 111:https://doi.org/10.1016/j.firesaf.2019.102909
13. Nævestad T-O and Meyer S (2014) A survey of vehicle fires in Norwegian road tunnels 2008–2011. Tunnelling and Underground Space Technology 41:104-112. http://dx.doi.org/10.1016/j.tust.2013.12.001
14. Tunnel fires from 2012 to 2023: Statistics from media reports (2024) https://www.ifa-swiss.ch/en/magazine/detail/tunnel-fires-from-2012-to-2023-statistics-from-media-reports (access date: 07/15/2025)
15. Favier A, De Wolf C, Scrivener K et al (2018) A sustainable future for the European Cement and Concrete Industry - Technology assessment for full decarbonisation of the industry by 2050. ETH Zurich, Zurich
16. Schneider M (2019) The cement industry on the way to a low-carbon future. Cem Concr Res 124:https://doi.org/10.1016/j.cemconres.2019.105792
17. Ige O E, Olanrewaju O A, Duffy K J et al (2021) A review of the effectiveness of Life Cycle Assessment for gauging environmental impacts from cement production. Journal of Cleaner Production 324:https://doi.org/10.1016/j.jclepro.2021.129213
18. Locher F W (2000) Zement - Grundlagen der Herstellung und Verwendung. Verlag Bau + Technik GmbH, Düsseldorf
19. Gao T, Shen L, Shen M et al (2016) Analysis of material flow and consumption in cement production process. Journal of Cleaner Production 112:553-565. http://dx.doi.org/10.1016/j.jclepro.2015.08.054
20. Chen H, Li N, Unluer C et al (2025) 200 years of Portland cement: Technological advancements and sustainability challenges. Journal of Cleaner Production 486:https://doi.org/10.1016/j.jclepro.2024.144500

21. (2022) Hrsg. Ressourcen der Zukunft für Zement und Beton – Potenziale und Handlungsstrategien. Verein Deutscher Zementwerke, VDZ, Düsseldorf
22. Hanein T, Thienel K-C, Zunino F et al (2022) Clay calcination technology: state-of-the-art review by the RILEM TC 282-CCL. Mater Struct 55:https://doi.org/10.1617/s11527-021-01807-6
23. Tole I, Habermehl-Cwirzen K and Cwirzen A (2019) Mechanochemical activation of natural clay minerals: an alternative to produce sustainable cementitious binders – review. Mineralogy and Petrology 113:449-462. https://doi.org/10.1007/s00710-019-00666-y
24. Scrivener K L, Vanderley J M and Gartner E M (2018) Eco-efficient cements: Potential economically viable solutions for a low-CO2 cement-based materials industry. Cem Concr Res 114:2-26. https://doi.org/10.1016/j.cemconres.2018.03.015
25. Sharma M, Bishnoi S, Martirena F et al (2021) Limestone calcined clay cement and concrete: A state-of-the-art review. Cem Concr Res 149:
26. Juenger M C C and Siddique R (2015) Recent advances in understanding the role of supplementary cementitious materials in concrete. Cem Concr Res 78:71-80. https://doi.org/10.1016/j.cemconres.2015.03.018
27. Trout E A R (2019) Lea's chemistry of cement and concrete.
28. Pal S C, Mukherjee A and Pathak S R (2003) Investigation of hydraulic activity of ground granulated blast furnace slag in concrete. Cem Concr Res 33:1481-1486. https://doi.org/10.1016/S0008-8846(03)00062-0
29. Vaclavik V, Dirner V, Dvorsky T et al (2012) The use of Blast Furnace Slag. Metalurgija 51:461-464.
30. Ahmed M S, Kayali O and Anderson W (2008) Chloride penetration in binary and ternary blended cement concretes as measured by two different rapid methods. Cem Concr Compos 30:576-585. https://doi.org/10.1016/j.cemconcomp.2008.02.005
31. Richardson I G and Groves G W (1992) Microstructure and microanalysis of hardened cement pastes involving ground granulated blast-furnace slag Journal of Material Science 27:6204-6212.
32. Richardson I G (1999) The nature of C-S-H in hardened cements. Cem Concr Res 29:1131-1147.
33. Jia Z, Chen C, Shi J et al (2019) The microstructural change of C-S-H at elevated temperature in Portland cement/GGBFS blended system. Cem Concr Res https://doi.org/10.1016/j.cemconres.2019.05.018
34. Dedeloudis C, Zervaki M, Sideris K et al (2018) Properties of Fresh and Hardened Concrete Containing Supplementary Cementitious Materials: State-of-the-Art Report of the RILEM Technical Committee 238-SCM, Working Group 4 181-231.
35. Skibsted J and Snellings R (2019) Reactivity of supplementary cementitious materials (SCMs) in cement blends. Cem Concr Res 124:https://doi.org/10.1016/j.cemconres.2019.105799
36. Panesar D K and Zhang R (2020) Performance comparison of cement replacing materials in concrete: Limestone fillers and supplementary cementing materials – A review. Constr Build Mater 251:https://doi.org/10.1016/j.conbuildmat.2020.118866
37. Moosberg-Bustnes H, Lagerblad B and Forssberg E (2004) The function of fillers in concrete. Mater Struct 37:74-81. https://doi.org/10.1007/BF02486602
38. Lothenbach B, Le Saout G, Gallucci E et al (2008) Influence of limestone on the hydration of Portland cements. Cem Concr Res 38:848-860. https://doi.org/10.1016/j.cemconres.2008.01.002
39. Meyer-Ottens C (1972) Zur Frage der Abplatzungen an Betonbauteilen aus Normalbeton bei Brandbeanspruchung. Technischen Universität Carolo - Wilhelmina zu Braunschweig

40. Shorter G W and Harmathy T Z (1961) Discussion on the Fire-resistance of prestressed concrete beams. 313-315
41. Harmathy T Z (1965) Effect of moisture on the fire endurance of building elements. ASTM Special Technical Publication No. 385:
42. Dauti D, Tengattini A, Dal Pont S et al (2018) Analysis of moisture migration in concrete at high temperature through in situ neutron tomography. Cem Concr Res 111:41-55. https://doi.org/10.1016/j.cemconres.2018.06.010
43. Van der Heijden G H A, Pel L and Adan O C G (2012) Fire spalling of concrete, as studied by NMR. Cem Concr Res 42:265-271. https://doi.org/10.1016/j.cemconres.2011.09.014
44. Chen X-T, Rougelot T, Davy C A et al (2009) Experimental evidence of a moisture clog effect in cement-based materials under temperature. Cem Concr Res 39:1139-1148. http://dx.doi.org/10.1016/j.cemconres.2009.07.015
45. Stelzner L, Powierza B, Oesch T et al (2019) Thermally-induced moisture transport in high-performance concrete studied by X-ray-CT and 1H-NMR. Constr Build Mater 224:600-609. https://doi.org/10.1016/j.conbuildmat.2019.07.065
46. Felicetti R, Yarmohammadian R, Dal Pont S et al (2024) Fast vapour migration next to a depressurizing interface: A possible driving mechanism of explosive spalling revealed by neutron imaging. Cem Concr Res 180:https://doi.org/10.1016/j.cemconres.2024.107508
47. McNamee R (2019) Fire Spalling Theories - Realistic and More Exotic Ones. 6th International Workshop on Concrete Spalling due to fire exposure: Sheffield, England
48. Schneider U (1982) Behaviour of Concrete at High Temperatures Deutscher Ausschuss für Stahlbeton 1-110.
49. Mindeguia J-C, Pimienta P, Carre H et al (2012) On the influence of aggregate nature on concrete behaviour at high temperature. European Journal of Environmental and Civil Engineering 16:236-253. https://doi.org/10.1080/19648189.2012.667682
50. Fu Y and Li L (2011) Study on mechanism of thermal spalling in concrete exposed to elevated temperatures. Mater Struct 44:361-376. https://doi.org/10.1617/s11527-010-9632-6
51. Bažant Z P (1997) Analysis of Pore Pressure, thermal Stredd and Fracture in Rapidly Heated Concrete. International Workshop on fire Performance of High-Strength Concrete: Gaithersburg
52. Ulm F J, Coussy O and Bazant Z P (1999) The ‘‘Chunnel’’ fire I: chemoplastic softening in rapidly heated concrete. Journal of Engineering Mechanics 125:272-282. https://doi.org/10.1061/(ASCE)0733-9399(1999)125:3(272)
53. Hertz K (2003) Limits of spalling of fire-exposed concrete. Fire Safety Journal 38:103-116. https://doi.org/10.1016/S0379-7112(02)00051-6
54. Khaled al-Bashiti M and Naser M Z (2023) What can we learn from over 1000 tests on fire-induced spalling of concrete? A statistical investigation of critical factors and unexplored research space. Constr Build Mater 403:https://doi.org/10.1016/j.conbuildmat.2023.133200
55. Hertz K (1984) Heat-induced Explosion of Dense Concretes. Technical University of Denmark, Department of Civil Engineering,
56. Pan Z, Sanjayan J G and DKong D L Y (2012) Effect of aggregate size on spalling of geopolymer and Portland cement concretes subjected to elevated temperatures. Constr Build Mater 36:365-372. https://doi.org/10.1016/j.conbuildmat.2012.04.120
57. Mohd Ali A Z, Sanjayan J and Guerrieri M (2017) Specimens size, aggregate size, and aggregate type effect on spalling of concrete in fire. Fire Mater 42:59-68. https://doi.org/10.1002/fam.2457
58. Kirnbauer J and Schneider U (2011) Influence of cement type and aggregate shape on explosive concrete spalling. 2nd International RILEM Workshop on Concrete Spalling due to Fire Exposure: Delft, The Netherlands 432-439.

59. Hager I, Mróz K and Tracz T (2018) Concrete propensity to fire spalling: Testing and observations. MATEC Web of Conf. 163:https://doi.org/10.1051/matecconf/201816302004
60. Xing Z, Beaucour A-L, Hebert R et al (2011) Influence of the nature of aggregates on the behaviour of concrete subjected to elevated temperature. Cem Concr Res 41:392-402. https://doi.org/10.1016/j.cemconres.2011.01.005
61. Naik T R, Kraus R N and Kumar R (2011) Influence of Types of Coarse Aggregates on the Coefficient of Thermal Expansion of Concrete. Journal of Materials in Civil Engineering 23:https://doi.org/10.1061/(ASCE)MT.1943-5533.0000198
62. An J, Kim S S, Nam B H et al (2017) Effect of Aggregate Mineralogy and Concrete Microstructure on Thermal Expansion and Strength Properties of Concrete. Applied Sciences 7:https://doi.org/10.3390/app7121307
63. Johnson W H and Parsons W H (1944) Thermal expansion of concrete aggregates and materials. J. Res. Nat. Bureau Stand. 32:https://doi.org/10.6028/jres.032.002
64. Klimek A, Stelzner L, Hothan S et al (2022) Fire induced concrete spalling in combination with size effects. Mater Struct 55:https://doi.org/10.1617/s11527-022-02051-2
65. Lenglet C (2011) Evolution of Spalling with time and age. 2nd International RILEM Workshop on Concrete Spalling due to Fire Exposure: Delft, The Netherlands
66. Boström L and Jansson R (2011) The Age Effect on Fire Spalling of Concrete. 2nd International RILEM Workshop on Concrete Spalling due to Fire Exposure: Delft, The Netherlands
67. Klimek A, Stelzner L, Hothan S et al (2024) Influence of thermal strain on concrete spalling. Mater Struct 57:https://doi.org/10.1617/s11527-023-02274-x
68. DIN EN 1992-2 - Teil 2: Betonbrücken - Bemessungs- und Konstruktionsregeln Beuth Verlag GmbH, Berlin, 2010
69. Pistol K, Weise F, Meng B et al (2011) The mode of action of polypropylene fibres in high performance concrete at high temperatures. 2nd International RILEM Workshop on Concrete Spalling due to Fire Exposure: Delft, The Netherlands 289-296.
70. Pimienta P, McNamee R, Hager I et al (2023) Recommendation of RILEM TC 256-SPF on the method of testing concrete spalling due to fire: material screening test. Mater Struct 56:https://doi.org/10.1617/s11527-023-02202-z
71. Pimienta P, McNamee R, Robert F et al (2024) Recommendation of RILEM TC 256-SPF on fire spalling assessment during standardised fire resistance tests: complementary guidance and requirements. Mater Struct 57:https://doi.org/10.1617/s11527-023-02248-z
72. Ozawa M, Tanibe T, Kamata R et al (2018) Behavior of ring-restrained high-performance concrete under extreme heating and development of screening test. Constr Build Mater 162:215-228. https://doi.org/10.1016/j.conbuildmat.2017.11.144
73. Sorge P (2024) Charakterisierung des Abplatzverhaltens von Betonen mit Portlandpuzzolanzement im Brandversuch unter Verwendung einer Tunnelbrandkurve. Bachelor thesis, Fachhochschule Potsdam
74. Eurocode 2: Design of concrete structures - Part 1-2: General rules - Structural fire design; German version EN 1992-1-2:2004 + AC:2008, Beuth Verlag GmbH, Berlin, 2010
75. Schulte Holthausen R and Raupach M (2018) Determination of porosity and pore size distribution in concrete by single-sided ^{1}H NMR - From white cement pastes to grey cement mortars. IBAUSIL: Weimar, Germany 595-603.
76. Nagel S M, Strangfeld C and Kruschwitz S (2020) Application of ^{1}H Proton NMR Relaxometry on Building Materials - A Review-. Journal of Magnetic Resonance
77. Hiller T and Costabel S (2025) NUCLEUS – A Matlab-based graphical user interface for forward and inverse modelling of NMR relaxometry data. SoftwareX 32:https://doi.org/10.1016/j.softx.2025.102447

78. International Organization for Standardization (2016) Evaluation of pore size distribution and porosity of solid materials by mercury porosimetry and gas adsorption— Part 1: Mercury Porosimetry (ISO Standard No. 15901-1)
79. Klinkenberg L J (1941) The Permeability of Porous Media to Liquids and Gases. Production Practice: 200-213.
80. Jiang W, Zhang D, Zheng X et al (2023) Development of Pore Pressure in Cementitious Materials under Low Thermal Effects: Evidence from Optimization of Pore Structure by Incorporation of Fly Ash. Mater 16:https://doi.org/10.3390/ma16124214
81. Lollini F and Redaelli E (2021) Carbonation of blended cement concretes after 12 years of natural exposure. Constr Build Mater 276:https://doi.org/10.1016/j.conbuildmat.2020.122122
82. Bucher R, Diedrich P, Escadeillas G et al (2017) Service life of metakaolin-based concrete exposed to carbonation Comparison with blended cement containing fly ash, blast furnace slag and limestone filler. Cem Concr Res 99:18-29. https://doi.org/10.1016/j.cemconres.2017.04.013
83. Kapeluszna E, Kotwica Ł, Rózycka A et al (2017) Incorporation of Al in C-A-S-H gels with various Ca/Si and Al/Si ratio: Microstructural and structural characteristics with DTA/TG, XRD, FTIR and TEM analysis. Constr Build Mater 155:643-653. http://dx.doi.org/10.1016/j.conbuildmat.2017.08.091
84. Li Y, Mi T, Liu W et al (2021) Chemical and mineralogical characteristics of carbonated and uncarbonated cement pastes subjected to high temperatures. Composites Part B 216:https://doi.org/10.1016/j.compositesb.2021.108861
85. Song H, Jeong Y, Bae S et al (2018) A study of thermal decomposition of phases in cementitious systems using HT-XRD and TG. Constr Build Mater 169:https://doi.org/10.1016/j.conbuildmat.2018.03.001
86. Muhammed A, Carre H, La Borderie C et al (2025) Influence of Polypropylene Fibers on Thermal-Induced Permeability Changes in Concrete. 12th International Conference on Fracture Mechanics of Concrete and Concrete Structures Vienna, Austria https://doi.org/10.21012/FC12.1244
87. Bošnjak J, Ožbolt J and Hahn R (2013) Permeability measurement on high strength concrete without and with polypropylene fibers at elevated temperatures using a new test setup. Cem Concr Res 53:104-111. http://dx.doi.org/10.1016/j.cemconres.2013.06.005
88. Weise F, Stelzner L, Weinberger J et al (2017) Influence of the pre-treatment of PP-fibres by means of electron irradiation on the spalling behaviour of High-Strength Concrete. 5th International Workshop on Concrete Spalling: Boras, Sweden 345-358.
89. Miah M J (2017) The Effect of Compressive Loading and Cement Type on the Fire Spalling Behaviour of Concrete. Université de Pau et des Pays de l'Adour-Laboratoire SIAME
90. Reiners J (2023) The Influence of the Physical and Chemical Properties of Hardened Cement Paste on the Fire-Induced Spalling of Concrete. PhD Thesis, Technische Universität Carolo-Wilhelmina zu Braunschweig
91. Whittaker M, Zajac M, Ben Haha M et al (2014) The role of the alumina content of slag, plus the presence of additional sulfate on the hydration and microstructure of Portland cement-slag blends. Cem Concr Res 66:91-101. http://dx.doi.org/10.1016/j.cemconres.2014.07.018
92. Tsuji D, Kojima M, Ohtsuka Y et al (2019) Influence of SO3 Amount in High Volume Blast Furnace Slag Cement On Fire-Induced Explosive Spalling Resistance. Journal of Structural and Construction Engineering 84:119-127. https://doi.org/10.3130/aijs.84.119
93. Poon C-S, Azhar S, Anson M et al (2003) Performance of metakaolin concrete at elevated temperatures. Cem Concr Compos 25:83-89. https://doi.org/10.1016/S0958-9465(01)00061-0

94. Viswanadha Varma D, Rama Rao G V and Sindhu J (2014) Effect of Temperature on Metakaolin Blended High Strength Concrete. International Journal of Engineering Research and Development 10:57-67.
95. Amrutha, Nayak G, Narasimhan M C et al (2011) High Temperature Performance of Self-Compacting High-Volume Fly Ash Concrete Mixes. Journal of Structural Fire Engineering 2:81-90. http://dx.doi.org/10.1260/2040-2317.2.2.81
96. Lo Monte F, Felicetti R and Miah M J (2019) The influence of pore pressure on fracture behaviour of Normal-Strength and High-Performance Concretes at high temperature. Cement and Concrete Composites 104:https://doi.org/10.1016/j.cemconcomp.2019.103388
97. Yarmohammadian R and Felicetti R (2025) From Crack Initiation To Instability At High Temperature: A Two Stage Mechanism For Fire-Induced Spalling in Concrete. 12th International Conference on Fracture Mechanics of Concrete and Concrete Structures: Vienna, Austria
98. Torelli G, Mandal P, Gillie M et al (2016) Concrete strains under transient thermal conditions: A state-of-the-art review. Eng Struct 127:172-188. http://dx.doi.org/10.1016/j.engstruct.2016.08.021
99. Schneider U (1988) Concrete at High Temperatures -- A General Review. Fire Safety Journal 13:55-68. https://doi.org/10.1016/0379-7112(88)90033-1
100. Bazant Z P and Xi Y (1994) Drying creep of concrete: constitutive model and new experiments separating its mechanisms Mater Struct 27:3-14.
101. Peters S, Vu G and Meschke G (2025) A multiscale model for predicting the Young's modulus and the thermal-expansion coefficient of concrete at high temperatures. Constr Build Mater 479:https://doi.org/10.1016/j.conbuildmat.2025.141259

Paper 1:

The impact of blended cements on the spalling behavior of concrete at elevated temperatures: a review

Publisher's version

Published in *Materials and Structures*

Volume 58, 2025

DOI: https://doi.org/10.1617/s11527-025-02713-x

Authors: Tim Pittrich, Frank Weise, Ludwig Stelzner

Materials and Structures (2025) 58:186
https://doi.org/10.1617/s11527-025-02713-x

ORIGINAL ARTICLE

The impact of blended cements on the spalling behavior of concrete at elevated temperatures: a review

Tim Pittrich · Frank Weise · Ludwig Stelzner

Received: 10 January 2025 / Accepted: 5 June 2025
© The Author(s) 2025

Abstract The cement and concrete industries are striving to reduce the CO_2 emissions caused by the production of Portland cement. An effective way to achieve this is to replace Portland cement clinker with more environmentally friendly supplementary cementitious materials (SCMs) to produce blended cements. A variety of different SCMs are used today, from fly ash to more exotic options such as rice husk ash or waste glass powder. Depending on its material properties, concrete exposed to fire may experience spalling caused by thermomechanical and thermohydraulic mechanisms. Severe spalling leads to a reduction in the cross-section and exposure of the reinforcement, jeopardizing the load-bearing capacity of the concrete element. The use of blended cements changes the concrete properties which can affect spalling behavior at high temperatures. The link between high temperature and spalling behavior of concrete with blended cements has been investigated in several studies. A review of the existing literature led to the conclusion that the cement type influences the spalling behavior of concrete. However, the relationship does not appear to be clear, as there are contradictions and inconsistencies between the evaluated results. Therefore, further in-depth studies will help to gain a more precise understanding of the effects of blended cements on the spalling behavior of concrete at elevated temperatures.

Keywords Fire-induced spalling · Concrete · High temperatures · Blended cements · SCM · Filler

1 Introduction

In blended cements, part of the Portland cement clinker is replaced by another material. Originally, the replacement was motivated by lower costs and economic benefits, as the substitute materials were usually byproducts from other industries such as the iron, steel or power industries [1]. For example, slag cements were already utilized in the 1920s for massive concrete structures such as dams [2]. Next to the economic benefits, blended cements provide additional ecological advantages, now attracting renewed attention as a sustainable alternative to ordinary Portland cement (OPC). Cement clinker production is associated with high CO_2 emissions caused by the use of fossil fuels and the decomposition of limestone during the sintering process. One ton of cement clinker is responsible for roughly 0.87 t of CO_2 [3]. Therefore, large quantities of cements with high replacement rates of supplementary cementitious

T. Pittrich (✉) · F. Weise · L. Stelzner
Bundesanstalt für Materialforschung und-prüfung, Berlin, Germany
e-mail: tim.pittrich@bam.de

F. Weise
e-mail: frank.weise@bam.de

L. Stelzner
e-mail: ludwig.stelzner@bam.de

Published online: 25 June 2025

materials (SCMs) leading to a low clinker factor are desirable [4, 5]. However, the long-term availability of typically used SCMs such as fly ash and blast furnace slag is questionable [4, 6], which leads to rising demands for alternatives. In addition, the different cements affect the concrete's mechanical properties, durability and more even at ambient conditions [7]. Therefore, it can be assumed that the properties under fire load also differ. The increasing availability of blended cements leads to an increasing use of those cements for housing and infrastructure construction, highlighting the need for a profound understanding of the fire behavior of blended cement concrete.

Although concrete does not burn, it undergoes certain chemical and physical changes at elevated temperatures, one of them being explosive spalling. Explosive spalling is particularly critical as it occurs early on during the fire: usually in the first 20 min [8]. Those spalling events are caused by thermohydraulic and thermomechanical mechanisms related to various factors such as moisture content, age, strength, microstructure, etc. During the spalling event, small concrete fragments are dislodged from the concrete surface and accelerated to high speeds. Intensive spalling can lead both to reduction of the cross-section of the load bearing member and to the uncovering of the reinforcement, reducing the structure's overall stability. As well as the structural damage, flying concrete pieces can become an additional danger for humans. The subsequent repair of the building parts after a fire costs a great deal of time and money. The most well-established strategy to minimize or even avoid fire spalling is the addition of polypropylene fibers (PP-fibers) to the concrete mixture [9].

Subsequently, the question arises whether different types of blended cements with different SCMs influence the fire spalling susceptibility of concrete. In this review, the available literature on the spalling behavior of concrete with blended cements was examined to identify a possible relationship between cement type and spalling behavior of concrete.

2 Blended cements

In order to understand and evaluate the spalling behavior of blended concrete, the differences between the various cement types must first be explained.

Blended cements can include different types of SCMs or fillers, distinguished by their chemical composition with latent hydraulic, pozzolanic or inert properties (see Fig. 1). The most common substitute materials are ground blast furnace slag, fly-ash, and limestone but materials such as silica fume or glass powder are also utilized. In the future, reduced availability of slag and fly-ash is forecast for Europe, leading to an increasing demand for alternative SCMs such as calcined clays [6]. SCMs decisively influence the reaction kinetics and therefore the amount, type, and structure of the hydrated phases [10]. The type, number, and dosage of the substitutes determine the cement type in national or international regulations such as DIN or EN e.g., DIN EN 197–1.

2.1 Latent hydraulic SCMs

The most common latent hydraulic SCM is blast furnace slag (BF). Its latent hydraulic properties were already discovered in 1862 [11] and the first slag cements appeared in 1865 [12]. BF is a byproduct of the pig iron manufacturing process. The reactivity of slag is determined by its chemical and mineralogical composition as well as its glass content and fineness. In cementitious composites, BF reacts with water to the same hydration products as OPC in the form of C-S–H [13, 14]. The replacement of Portland cement clinker with slag leads to a decrease in early age strength followed by a delayed increase in strength [14, 15]. The outer product C-S–H in slag systems

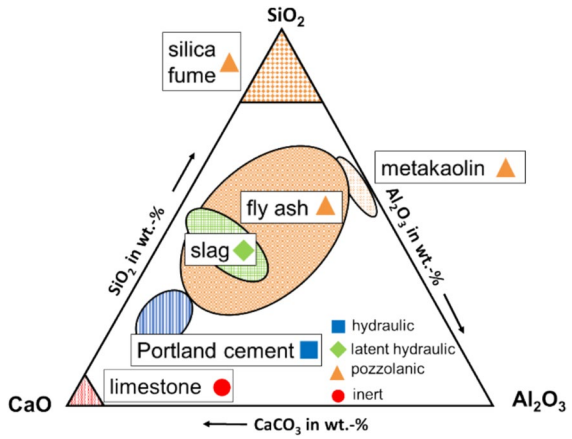


Fig. 1 Ternary diagram of typical cements and SCM adapted from [7]

more effectively fills pore space without forming large interconnected capillary pores [16, 17]. Moreover, the thermal stability of binder containing slag seems to increase as with increasing temperature, less pronounced pore coarsening takes place [18].

2.2 Pozzolanic SCMs

The first utilization of pozzolans for construction purposes dates back to the Romans 3000 years ago [19]. Today, there are a variety of pozzolanic SCMs available which are used in blended cements. A few examples are fly-ash (FA), silica fume (SF), volcanic ash (VA) and metakaolin (MK). Up to now the most frequently used SCM in blended cements was FA. However, the further availability of FA is uncertain since the quantity available is decreasing due to the shutdown of coal-fired power plants [6, 20]. Therefore, the demand for alternatives is rising. Big potential is seen in calcined clays (CC), as they offer good pozzolanic properties and sufficient availability all around the globe [4]. What all pozzolanic SCMs have in common is a similar chemical composition to Portland cement in the form of silicates or aluminasilicates. Under the presence of portlandite $Ca(OH)_2$ and water, they react to form C–S–H or more likely C–A–S–H (depending on the amount of alumina) [20]. However, the influence of pozzolanic SCMs on the microstructure is highly dependent on the type and amount of material used and therefore not consistent. The compressive strength tends to increase up to a replacement rate of 30% while at the same time porosity and permeability decrease for SF, FA and MK. Higher replacement rates lead to the opposite effect [7].

2.3 Fillers

Alongside the abovementioned reactive SCMs, so-called inert fillers are also used to produce blended cements. Since fillers usually need no treatment besides grinding, they are favored in terms of low CO_2-emissions and costs. The most common filler used is limestone, but other types of mineral fillers are also utilized, e.g., quartz [21]. The filler effect describes the filling of intergranular voids between cement paste and aggregates, densifying the concrete. Additionally, fillers can provide nucleation sites, promoting the hydration of the cement paste [21]. It should be mentioned that fillers are not completely inert and may show some kind of chemical reactivity. For example, limestone fillers react with the alumina phases of cement to form monocarboaluminate hydrate [20] [22] and quartz fillers can exhibit pozzolanic properties over a long period of time [21]. It was reported that substitution rates of limestone powder fillers above 10% primarily lead to a reduction in strength but not necessarily to a reduction in porosity [7].

3 Concrete spalling

Heat-induced concrete spalling does not occur during every fire scenario and is dependent on numerous factors. The most influential are the fire conditions but material and specimen properties also have great impact. Furthermore, different types of spalling exist, namely corner spalling, surface spalling, and explosive spalling [23]. An overview of the influencing factors and common fire curves is given in Fig. 2.

The heating or fire conditions are most decisive for the occurrence and severity of spalling. High heating rates induce a stronger thermal gradient inside the structure, resulting in restrained thermal dilations which usually promote spalling. Obviously, the absolute temperature reached is also important since spalling usually starts to happen at around 300 °C [22]. Other factors related to the appearance of spalling are the direction of the flame and duration of the fire with the associated temperature gradient.

In general, concrete with high compressive strength, which is mostly associated with low porosity and low permeability, shows correspondingly high spalling susceptibility [24]. Conversely, normal strength concrete (NSC) is usually less prone to spalling than high strength concrete (HSC) or ultra-high-performance concrete (UHPC). Nevertheless, moisture content must be considered. It was concluded that the spalling risk is relatively low for moisture contents below 3–4 wt% in traditional concrete with comparatively low densities [25]. This is not applicable for dense concrete, where it was shown that spalling took place despite a very low moisture content of 1 wt% [26]. Another factor is aggregate size. Several studies concluded that smaller aggregates lead to heavier spalling [24, 27, 28]. Moreover, it has been observed that the aggregate shape might

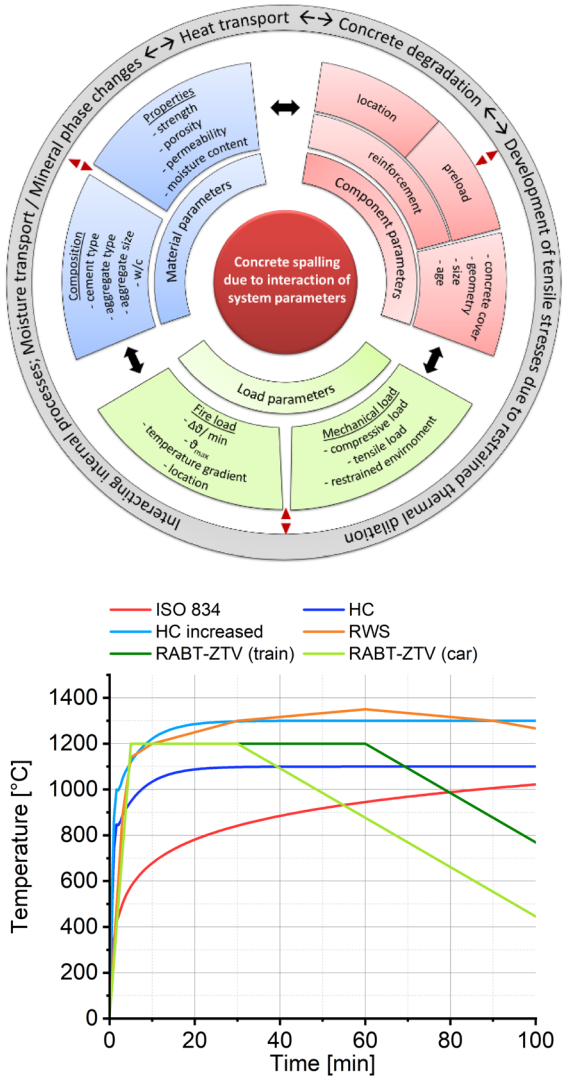


Fig. 2 System parameters influencing heat-induced spalling (top) and commonly used fire curves (bottom)

also affect spalling behavior, as roundish aggregates led to less intense spalling compared to crushed angular aggregates in [29]. Lastly, the aggregate type is also decisive. For example, results of [30] show higher spalling susceptibility for river bed gravel specimens in comparison with granitic or basaltic aggregates and investigations by [31] found more severe damage including spalling in specimens with flint aggregates compared to specimens with quarzitic or calcareous aggregates. Furthermore, the cement type or the addition of SCMs influences the spalling behavior of concrete in certain ways; however, this will be addressed in detail in the main body of this paper.

Alongside material properties, component properties also influence spalling behavior. In particular, the size of the specimen plays an important role as with increasing size increasing spalling can be expected [28, 32]. The spalling risk tends to decrease with increasing concrete age due to the continuous drying of the material [33, 34]. Another strong impact results from the applied load. In many studies, loaded and restrained specimens experienced a lot more damage than unloaded specimens [24, 35].

3.1 Thermohydraulic spalling mechanisms

The initial suggestion that thermohydraulic mechanisms influence the spalling behavior of concrete was made by Shorter and Harmathy [36] and was further developed by Harmathy [37]. The “moisture clog” theory describes the increase of steam pressure inside concrete pores during a fire. Subsequently, the steam begins to move towards the heated external surface of the concrete but also towards the concrete interior where overall colder temperatures are present. The water vapor starts to condense in the colder areas and over time a fully saturated zone develops. This moisture clog prevents any further transversal water vapor escape, resulting in rapidly rising pore pressure. If this pressure exceeds the transversal tensile strength of the specimen, the concrete starts to spall. According to [38], the acceleration of concrete fragments is caused by the vaporization of liquid water and its adiabatic expansion after initial cracking. However, the measurement of pore pressure during fire tests turned out to be quite difficult, as pore pressure drops immediately as soon as thermally induced cracks start to form around the probe. Heat-induced moisture transport and the appearance of the moisture clog were confirmed experimentally in different studies [39–41]. A brief schematic display of the process is given in Fig. 3.

Several more theories deal with moisture influence on concrete spalling, including the frictional forces from vapor flow theory [8, 42], the boiling liquid expanding vapor explosion (BLEVE) theory [43] or the fully saturated pore pressure theory [44, 45]. No fundamental experimental proof exists for those theories. An overview of a variety of different

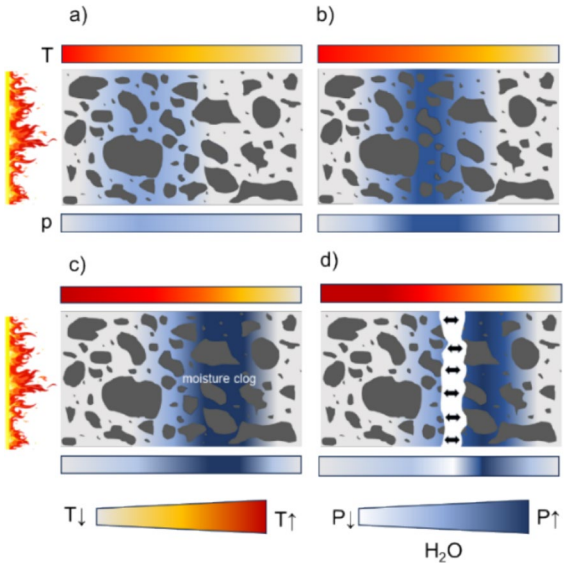


Fig. 3 Schematic representation of thermohydraulic spalling adapted from [40]

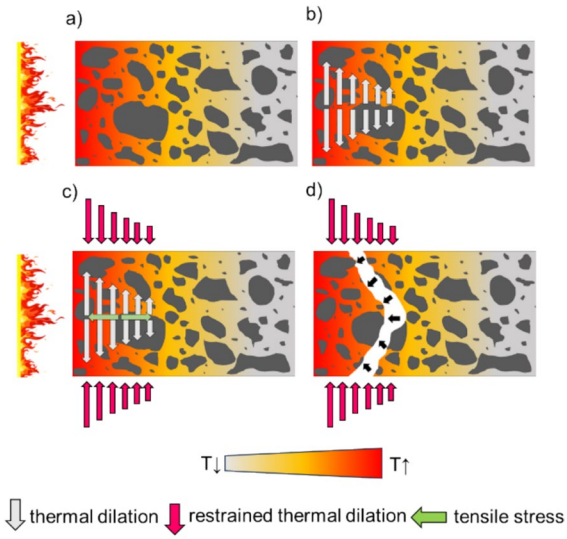


Fig. 4 Schematic representation of thermomechanical spalling adapted from [50]

thermohydraulic spalling mechanism theories and how they work can be found in McNamee's review [46].

3.2 Thermomechanical spalling mechanisms

Two main factors have been identified as responsible for the thermomechanical spalling of concrete. The first is the thermal incompatibility between concrete's main components, hardened cement paste and aggregates, at high temperatures. While hardened cement paste shrinks above temperatures of roughly 150 °C, aggregates dilate [47]. This mismatch leads to thermally induced stresses, resulting in microcracks that promote spalling [46]. The second factor is the development of a temperature gradient inside the concrete due to the material's low thermal diffusivity, resulting in a hot fire-exposed side and a cold interior. The emerging temperature differences subsequently cause restrained thermal dilations, creating high compressive stresses close to the fire exposed surface [23]. The compressive biaxial thermal stress parallel to the heated surface are accompanied by tensile stress perpendicular to the heated surface. If the tensile strength of the concrete is exceeded by those forces, concrete spalls [48, 49]. A representation of mechanically induced spalling is displayed in Fig. 4.

3.3 Measures against spalling

Fire-induced spalling must be considered in normal and high strength concrete according to DIN-EN 1992-1-2 [51]. For high strength concrete, different measures against spalling are recommended. One successful strategy to minimize or even prevent fire spalling is the addition of polypropylene fibers (PP-fibers) to the concrete mix. During a fire event, the fibers start to melt at around 170 °C. The steam pressure is subsequently lowered as there is now expansion space available in the form of empty fiber beds. In addition, an induced network of microcracks is formed which allows the escape of water vapor to the outside [52]. The effectiveness of PP-fibers is strongly dependent on the dosage and geometry [53] and can be further improved by electron radiation pre-treatment [9]. It is recommended to add at least 2 kg/m^3 PP-fibers. Investigations by [9] showed that the amount of fibers can be halved when altered fibers are used. Further measures against spalling include the use of a reinforcement mesh with a nominal concrete cover of 15 mm or the application of fire protection materials according to DIN EN-1992-1-2 [51].

4 Spalling of blended cement concrete

A variety of studies deal with the spalling behavior of Portland cement clinkers mixed with supplementary cementitious materials (SCMs). However, a distinction should be made between standardized cements according to DIN EN 197–1 or ASTM C595/C595M-21 regulations and research where a certain amount of clinker was simply replaced by one or several SCMs. In standardized cements, parameters like fineness and sulphate content are adjusted to guarantee equal strength of the cements, whereas when Portland cement is simply replaced by an SCM, the resulting effects on hydration, strength development, and workability are usually neglected. In addition, this review only considered articles where replacement took place in the cement fraction and not in the aggregate fraction. Therefore, these two types of blended cements are referred to in separate sections in this paper as standardized blended cements and laboratory blended cements. Moreover, the temperatures stated in the article always refer to furnace temperatures, to ensure the greatest possible comparability. The moisture content given always refers to the determination of mass loss after drying to 105 °C until mass constant.

It should be noted that recently published recommendations by RILEM TC 256 SPF provide a guideline for fire spalling tests [54, 55]. The recommendations describe which material, specimen and testing parameters should be determined and chosen to get the best results out of a fire spalling experiment. They also state how to evaluate the recorded data in a meaningful way. Hence, the documents can serve as a unified basis to compare studies from different research groups that followed the recommendations.

4.1 Standardized blended cements

This section summarizes spalling observed in concrete containing blended cements standardized according to DIN EN-197 [56].

4.1.1 Spalling experiments

Studies on the spalling behavior of blended cements were conducted by [29, 30, 57–60]. Table 1 gives an overview of the experiments conducted, including the most relevant material and testing parameters as well as the heating conditions. Under ISO 834 fire exposure, larger spalled volumes and maximum spalling depths were recorded for high strength concrete with CEM I 42.5 R compared to CEM III/A 42.5 N, with basalt as well as gravel aggregates, showing comparable moisture content (2.4–2.8 wt%). This is particularly interesting since higher compressive strength and lower permeability were measured for CEM III/A specimens [30]. The findings contradict the results of Reiners and Müller [57] and Reiners et al. [58]. The former study investigated the spalling behavior of normal strength concrete containing CEM I, CEM II/B-S, CEM II/A-LL, CEM II/B-V and CEM III/A with radiant panel pore pressure–temperature–mass loss (PTM) tests according to Kalifa [61]. The results show that CEM III/A concrete experienced the heaviest spalling followed by CEM II/B-V concrete; the use of other cements led to no spalling. In addition to the PTM tests, spalling experiments with the ISO 834 fire curve on concrete with and without lateral restrain were conducted. Specimens with lateral restraint showed the largest amount of spalling for CEM III/A concrete followed by CEM II/B-V concrete. CEM I and CEM II/A-LL concretes exhibited no spalling. Equal experiments with lateral restraint showed slightly deeper spalling for CEM III/A and CEM II/B-V cement concretes and comparatively low spalling for CEM I and CEM II/A-LL specimens [58]. According to the authors, both the higher moisture content and a weaker defined interfacial transition zone (ITZ) in concretes with reactive SCMs was responsible for the worse spalling behavior. However, the abovementioned statements regarding the spalling propensity of ordinary Portland cement and limestone cement concrete are once more in contradiction to the studies of Kirnbauer and Schneider [29]. The researchers carried out spalling experiments on normal strength concrete with CEM I 42.5 N, CEM II/A-L 42.5 R and sulphate slag cement (Slagstar®) under ISO 834 fire exposure. The study revealed that concrete with CEM II/A-L experienced much more spalling than CEM I-containing concrete for two different moisture states of around 5 and 6 wt% for both types of concrete. The highest amount of spalling was recorded in concrete with sulphate slag cement in all cases. The work of Miah et al. [59] compared the spalling behavior of CEM II/A-LL 42.5 R cement concrete and CEM III/A 42.5 N cement concrete under unloaded conditions and biaxial compressive

Table 1 Material properties and testing conditions of spalling experiments with standardized blended cements

Refs	Specimen					Testing	Result
	Cement type	Coarse aggregate	Geometry	Load/re-straint	Age (≥)	Exposure/furnace type	Spalling
[29]	CEM I 42.5 N CEM II/A-L 42.5 R Sulphate slag cem	calcareous	slab (30×25×10 cm^3)	no/no	28 d	ISO 834 gas burner	▼ ► ▲
[30]	CEM I 42.5 R CEM III/A 42.5 N	basalt granite	slab (120×100 x 30 cm^3)	no/no	90 d	ISO 834 gas burner	▲ ▼
[57]	CEM I 42.5 R CEM II/B-S 42.5 N CEM II/A-LL 42.5 N CEM II/B-V 42.5 R CEM III/A 42.5 N	Rhine gravel	slab (30×30×12 cm^3)	yes/no	1 a	20 °K/min 750 °C radiant panel	▼ ▼ ▼ ► ▲
[58]	CEM I 42.5 N CEM II/A-LL 42.5 N CEM II/B-V 42.5 R CEM III/A 42.5 N	Rhine gravel	slab	no/yes[a)]	1.5 a	ISO 834	▼ ▼ ► ▲
[59]	CEM II/A-LL 42.5 R CEM III/A 42.5 N	calcareous	slab (80×80×10 cm^3)	yes[a)]/no	90 d	ISO 834 gas burner	► ►
[60]	CEM I 42.5 N CEM II/A-LL 42.5 N CEM III/A 42.5 N CEM II/B-Q 42.5 N	quarzitic	cylinder (30×50 cm)	no/yes	90 d	HC oil burner	▼ ► ► ▲
[62]	CEM I 52.5 N CEM II/B-LL 42.5 N CEM II/A-LL 42.5 R CEM III/B 42.5 N	–	slab (142.5×125.0 x≥800 cm^3)	no/no	87 d	HC increased	–

▲ = high spalling susceptibility; ► = medium spalling susceptibility, ▼ = low spalling susceptibility

a) samples were tested with and without load or restraint respectively

stress using ISO 834 fire exposure. Unloaded specimens did not spall, regardless of the cement type used. Applied stress of 0.5 MPa led to spalling in CEM III/A concrete, while the CEM II/A-LL specimen remained unharmed. At higher stress levels (up to 10 MPa) both concretes showed similar spalling behavior and no clear distinguishable differences in spalling depth were observed. The maximum spalling depths of the abovementioned spalling experiments are summarized in Table 2. Investigations by Pittrich et al. [60] examined the spalling behavior of restrained normal strength concrete with CEM I

Table 2 Maximum concrete spalling depth of spalling experiments with blended cements after ISO 834 exposure

Refs	Maximum spalling depth [mm]			
	CEM I	CEM II/A-LL	CEM III/A	CEM II/B-V
Kirnbauer & Schneider [29]	0[a)c)g)]	45[a)c)g)]	–	–
	22[b)c)g)]	35[b)c)g)]	–	–
Hager et al. [30]	45[d)g)]	–	40[d)g)]	–
	65[e)g)]	–	50[e)g)]	–
Miah et al. [59]	–	0[c)g)]	0[c)g)]	–
	–	61[c)h)]	58[c)h)]	–
Reiners et al. [58]	0[f)g)]	0[f)g)]	25[f)g)]	15[f)g)]
	10[f)i)]	10[f)i)]	30[f)i)]	20[f)i)]

a) moisture content 5%; b) moisture content 6%; c) calcareous d) basalt; e) granite; f) Rhine gravel; g) unloaded; h) 5 MPa biaxial stress; i) restraint

42.5 N, CEM II/A-LL 42.5 N, CEM III/A 42.5 N and CEM II/B-Q 42.5 N exposed to HC fire. The results showed only slight surface spalling in CEM I concrete (ca. 1.5 vol%) while the utilization of blended cement caused a significant increase in damage. CEM II/A-LL and CEM III/A experienced comparable spalling, leading to similar spalled volumes (ca. 7 vol%). CEM II/B-Q concrete showed the greatest amount of damage in the form of the deepest recorded spalling depth and largest loss of volume (ca. 9 Vol%). The higher spalling susceptibility of the blended concretes might be related to slightly higher moisture contents of around 5.7, 5.6 and 6.0 wt% in CEM II/A-LL, CEM III/A and CEM II/B-Q in comparison to 5.4 wt% in CEM I. In addition, equal mixtures with PP-fibers were tested. Here it was shown that the fibers prevent explosive concrete spalling regardless of the cement used.

Spalling experiments on large scale cut outs of existing tunnels with different compositions incorporating CEM I, CEM II/A-LL, CEM II/B-LL, and CEM III/B exposed to the HC increased fire curve led to the conclusion that no relation between cement type and spalling behavior could be identified as not enough data and insights on the concrete properties were available [62].

4.1.2 High temperature experiments

Several studies laid their focus on the high temperature behavior of concrete regarding their mechanical performance and microstructural changes on small scale specimens. However, the authors also observed spalling during their experiments [63–69]. The material and testing conditions can be found in Table 3.

Investigations on hardened cement paste and mortars of CEM I and CEM III/A were conducted by [63]. The authors reported that CEM III/A showed better heat resistance and spalling was only noticed in CEM I-containing cement paste specimens around 650 °C (1 K/min). In the studies by Balazs [64] and Lubloy [65] the corners of CEM I-containing concrete spalled after being heated to 500 °C with a rate similar to ISO 834 and

Table 3 Material properties and testing conditions of high temp. experiments with standardized blended cements

Refs	Specimen					Testing	Result
	Cement type	Coarse Aggregate	Geometry	Load/re-straint	Age (≥)	Exposure/ Furnace type	Spalling
[63]	CEM I 52.5 CEM III/A 52.5	none	prism	no/no	104 d	1 K/min 60–650 °C electric	▶ ▼
[64]	CEM I 42.5 R CEM II/A-V 42.5 R CEM II/A-P 42.5 N CEM II/A-S 42.5 N CEM I 42.5 N + SF CEM I 42.5 N + MK	quarzitic	cube (a = 15 cm)	no/no	28 d	ISO 834	▶ ▼ ▼ ▼ ▼ ▼
[65]	CEM I 42.5 R CEM II/A-P 42.5 N CEM II/A-V 42.5 R	quarzitic	cube (a = 15 cm)	no/no	28 d	40 K/min 50 – 800 °C electric	▶ ▼ ▼
[66]	CEM II/A-LL 42.5 R CEM II/B-P 42.5 N	calcareous	cube (a = 15 cm)	no/no	42 d	20 – 600 °C electric	▼ ▼
[67]	CEM I 42.5 N CEM II/A-LL 42.5 N CEM III/B 32.5 N	fire clay	cube (a = 10 cm)	no/no	29 d	ISO 834	▲ ▲ ▼
[68]	CEM I 32.5 R CEM II/A-S 42.5 R CEM III/A 42.5 N	quarzitic calcareous	cube (a = 15 cm)	no/no	28 d	ZTV ING oil burner	▶ ▶ ▶
[69]	CEM I 42. R CEM III/B 32.5 R	granodiorite basalt	cube (a = 10 cm)	no/no	–	HC gas burner	▼ ▼

▲ = high spalling susceptibility; ▶ = medium spalling susceptibility, ▼ = low spalling susceptibility

subsequent holding phase. Concrete with CEM II/A-V, CEM II/A-P, and CEM II/A-S did not show any spalling but visible surface cracks started to develop at 800 °C. Concrete consisting of blended cements showed higher residual compressive strength compared to specimens prepared with ordinary Portland cement and in general exhibited less damage. A possible reason for the different fire resistances is the lower release of water associated with less portlandite in cement pastes made of pozzolanic material. The results of [66] showed only occasional spalling of blended cement concrete with a CEM II/B-P 42.5 N and a CEM II/A-LL 42.5 N. At high temperature loads up to 600 °C (40 K/min), three specimens per concrete were investigated. In total, 18 cubes were tested for both concretes, whereby only one specimen of each mixture spalled around 400 °C. It was assumed that the high thermal gradient inside the specimen was responsible for spalling. Studies by Jocius et al. [67] concluded that CEM I 42.5 N and CEM II/A-LL 42.5 N concrete stayed mostly unharmed, while CEM III/B 32.5 N concrete experienced explosive spalling after both one-sided and volumetric ISO 834 exposure. The researchers assume that the varying thermal dilations and contractions of the different cement pastes as well as the decomposition of certain mineral phases in the slag cement concrete at 700 °C were responsible for the variations in fire resistance. Further small-scale fire tests on concrete with blended cements and fibers were executed by Dehn et al. [68] and Bodnarova et al. [69]. The group of [68] examined the fire behavior of tunnel concrete with CEM I 32.5 R, CEM II/A-S 42.5 R and CEM III/A 42.5 R; in addition, all comparable mixtures contained 20% fly ash (by weight of cement) plus 2 kg/m^3 PP- fibers. The specimens exhibited moisture contents between 4.5 and 5.6 wt%. After exposure to the RABT ZTV-ING fire curve, specimens showed damage in the form of sloughing-off. The results of fire resistance tests on different concrete made of CEM I 42.5 R and CEM III/B 32.5 R with and without polypropylene and steel fibers under HC fire showed no spalling [69]. Apparently, the different moisture contents ranging from 2.9 to 4.4 wt% were not the decisive factor either. It should be noted that the fiber amount and type as well as the aggregate amount and type were not the same in the CEM I and CEM III/B mix. This makes a reasonable comparison rather difficult.

4.2 Laboratory blended cements

This section deals with spalling observed in concrete made with laboratory blended cements.

4.2.1 Spalling experiments

An overview of all the spalling experiments with blended cements is given in Table 4.

Small-scale spalling tests on concrete with different SCMs were performed by [70–72]. The use of 30% FA and BF did not influence the spalling behavior of concrete with 0.05, 0.1 and 0.15 vol% PP fibers as no damage was recorded. If SF was added, spalling could not be prevented regardless of the fiber dosage. Furthermore, a mixture with 10% SF and 20% FA only showed spalling at the lowest fiber dosage of 0.05 vol% and therefore demonstrated reduced spalling tendency compared to SF-only mixes [70]. Results of Nuruudin et al. [71] showed less spalling-induced damage in a ternary blended cement concrete consisting of 80% OPC + 10% FA + 10% RHA in comparison to the pure OPC reference concrete. Both concretes started to spall at the same temperature of 400 °C. In Gedam's study [72] binary mixes without the addition of fibers showed increased spalling in SCM-containing concrete. The researcher concluded that concrete with only OPC did not exhibit any spalling while roughly 17% replacement of OPC with either FA, SF or BF led to more spalling in every case for exposure up to 1000 °C. Of the three SCMs used, the heaviest damage was recorded in BF concrete. The addition of PP fibers or steel fibers improved spalling resistance and ultimately inhibited it completely. Intermediate-scaled spalling experiments were carried out by Ki-Seok and Dong-Woo [73], regarding the impact of SF, FA and BF. The mixes, moisture contents and results of this group's more detailed spalling analyses are summarized in Table 5. For the experiments, two different HSC concretes with targeted compressive strengths of 56 and 70 MPa after 90 d were examined after ISO 834 fire exposure. In the 56 MPa series, specimens with 50% BF showed the least amount of spalling while specimens with ternary binder mixes with SF and BF exhibited the most damage. In the 70 MPa series, the least spalling was recorded in concrete containing SF while all other specimens with ternary binder mixtures displayed heavy damage caused by explosive

Table 4 Material properties and testing conditions of spalling experiments with laboratory blended cements

Refs		Specimen				Testing	Result
	Binder type	Coarse aggregate	Geometry	Load/re-straint	Age (≥)	Exposure/ Furnace type	Spalling
[70]	OPC, FA, SF, BF	–	cylinder (20×10 cm^3)	no/no	28 d	ISO 834	► OPC, FA, BF ▲ SF
[71]	OPC, FA + RHA	–	cube (a = 10 cm^3)	no/no	28 d	200–1200 °C gas	▲ OPC ► FA + RHA
[72]	OPC, FA, SF, BF	–	cylinder (10×20 cm^3)	no/no	28 d	1000 °C electric	▼ OPC ► FA, SF ▲ BF
[73]	OPC, SF, FA, BF	gravel	slab ($50\times50\times15$ cm^3)	no/no	91 d	ISO 834	► OPC, SF, FA, BF ▲ BF + SF
[74]	OPC, SF, FA	calcareous siliceous	column ($381\times41\times41$ cm^3)	yes/no	1 a	ASTM E119-88	▼ OPC, FA ▲ SF
[75]	OPC, FA + NS	granite	slab ($185\times170\times20$ cm^3)	no/no	-	ISO 834	▲ OPC ► FA + NS
[76] [77]	OPC, FA, SF, BF	calcareous	column ($330\times20\times20$ cm^3)	yes/no	210 d	4.16 K/min 8 K/min	▲ OPC ► FA
[78] [79] [80]	OPC + FA	–	slab ($200\times100\times25$ cm^3) slab ($300\times150\times25$ cm^3)	no/no	-	RWS gas	▲OPC ► FA

▲ = high spalling susceptibility; ► = medium spalling susceptibility, ▼ = low spalling susceptibility

Table 5 Summarized results of Ki-Seok and Woo-Dong [73]

Series	Composition	Moisture [wt%]	Spalled area [%]	Avg.depth [mm]	Max.depth [mm]
56 MPa	5% SF	4.0	99.46	19.1	42.9
	25% FA	4.0	92.98	18.0	27.2
	50% BF	3.9	75.05	6.5	16.2
	5% SF + 65% BF	3.3	97.51	59.9	142.9
70 MPa (reinforced)	5% SF	3.4	100	22.5	40.3
	5% SF + 25% FA	2.7	98.07	65.5	112.2
	5% SF + 45% BF	3.1	94.29	77.9	142.2
	5% SF + 65% BF	3.2	98.53	82.2	120.1

spalling. The mixes with OPC, SF and BF turned out to be most prone to spalling in both concrete strength classes. Despite compressive strength differences of 10 MPa no significant differences in spalling behavior between the 5% SF specimens were observed [73]. Kodur and McGrath [74] described heavier spalling with the addition of 13.3% SF on high strength concrete columns under concentrical load and ASTM E119-88 fire exposure [74]. However, several other parameters were changed in the mix design, including the replacement of calcareous by siliceous aggregates. This change most likely increased the spalling as well and therefore the true influence of SF on the spalling behavior of these columns remains rather unclear. Medium-scale spalling investigations on High-Volume FA (ca. 50%) reinforced slabs containing small amounts of nano silica (NS) (5%) were conducted by Mussa et al. [75]. Summarized, the results showed a deeper maximum spalling depth of 19 mm in OPC reference slabs at lower temperatures (480–700 °C) compared to the high-volume FA specimens with 11 mm at higher temperatures (680–840 °C) after

ISO 834 exposure. Seemingly, the higher moisture content of 5.97 wt% in the FA samples compared to 4.95 wt% in the OPC samples was not the crucial factor. Experiments on high-volume FA HSC columns with 10% SF, 10% BF and 25% FA showed a spalled volume of only 17% compared to a spalled volume of 41% in regular HSC [76]. The authors explain the better spalling resistance of high-volume FA concrete by its higher tensile strength at elevated temperatures (up to 20%). Interestingly, despite the more severe spalling in regular HSC columns, only the FA HSC column failed after 165 min. The addition of PP fibers stopped spalling in both cases. It should be noted that the results of the regular HSC columns came from experiments by [77], where the heating rate was almost twice as high; this might have contributed to the more severe spalling recorded and must be viewed critically when comparing the two results. The aforementioned results on the spalling behavior of high-volume FA concrete also align with the research series of [78–80], where the authors recorded less spalling with increasing FA content from 30 to 60% and 70% in reinforced concrete after RWS fire load. The addition of PP fibers to those mixtures reduced spalling but could not prevent it from happening.

4.2.2 High temperature experiments

High temperature experiments where spalling was observed in laboratory blended cement concrete are given in Table 6 below.

In [81–86], spalling was observed in hardened blended cement pastes and mortars. The replacement of 20% OPC with either fly ash, natural pozzolana, limestone (LS) or slag or 10% of OPC with metakaolin showed that only specimens with additional limestone started to spall at a thermal load of 800 °C, while pure OPC specimens started spalling at a temperature of 1000 °C [81]. Investigations by Wang [82] only recorded spalling in no or low-level slag-containing cements (0 and 5 wt%) exposed to a temperature of 1050 °C. Results presented by [83] showed no spalling for pure OPC cement paste exposed to high temperatures up to 800 °C (20 K/min), while studies by [85] only showed spalling in OPC cement paste specimens. Regarding the replacement of OPC by FA, MK or silica fume, only the latter spalled at 800 °C when a replacement of 12 or 15 wt% took place. The higher spalling tendency of SF specimens was caused by their lower porosity [83]. Binary and ternary blended mortars consisting of OPC and MK or OPC, MK and NS showed increased spalling susceptibility compared to the OPC control mix up to 650 °C (10 K/min). However, the recorded spalling frequency varied and no clear relation between replacement rate and spalling tendency was made. The authors propose that the denser pore structure of the MK and NS mortars is responsible for the differences [86]. The available literature shows that spalling susceptibility already varies at the binder level where thermomechanical effects of loading and mismatch between aggregates and cement paste do not exist.

Spalling of blended cement concrete specimens was also noted in several studies dealing with the material properties at elevated temperatures.

Concrete with silica fume in general shows more severe spalling, often happening at lower temperatures compared to concrete with none or other SCMs [26, 70, 87–93]. This phenomenon was first noted and described by Hertz [26] who recorded heavy explosive spalling in SF concrete with an approximate moisture content of 1.2 wt%, exposed to a maximum temperature of 650 °C (1 K/min). Lai et al. [87] concluded that of all tested concretes with various SCMs, explosive spalling only occurred on concrete cubes with an SF replacement ratio of $\geq 10\%$ starting at temperatures of 600 °C. Not only can the amount of spalled material change with the addition of SF but also the spalling type changes from large pieces to small, pulverized particles with increasing SF content [88]. Even when ground to the nano scale, the spalling susceptibility increased when SF is used in comparison to OPC, FA or MK [89]. Responsible for the increased spalling susceptibility is the development of a very dense microstructure caused by the pozzolanic effect and improved packing density of the fine particles, making it impossible for water vapor to escape. However, further results of Poon et al. [90] on NSC and HSC with pure OPC as well as FA, BF and FA + SF showed only occasional spalling in OPC-HSC specimens between 400 and 600 °C (2.5 K/min) and no spalling for the other SCM-containing concretes independently of type, dosage and strength class. Based on their experimental investigations, Phan and Carino concluded that no clear tendency between silica fume and increased spalling susceptibility is given for different concrete mixtures with

Table 6 Material properties and testing conditions of high temp. experiments with laboratory blended cements

Refs		Specimen				Testing	Result
	Binder type	Coarse aggregate	Geometry	Load/re-straint	Age (≥)	Exposure/ furnace type	Spalling
[81]	OPC, FA, LS, BF, MK	none	cube	no/no	90 d	200–1000 °C electric	▶ OPC, ▲LS ▼ FA, BF, MK
[82]	OPC, BF	none	cylinder (2×4 cm^3)	no/no	29 d	25–1050 °C	▲OPC ▼ BF
[83]	OPC, SF, FA, MK	none	prism ($4\times4\times16$ cm^3)	no/no	90 d	ISO 834 electric	▼ OPC, FA, MK ▲ SF
[84]	OPC, LS, SF, NS	none	cube ($a=5$ cm^3)	no/no	3 d 7 d 28 d	20 K/min 20–800 °C electric	▼ OPC, LS, NS ▲ SF
[85]	OPC, SF, FA	none	cube	no/no	30 d	3 K/min 250–800 °C electric	▲ OPC ▼ SF, FA
[86]	OPC, MK, NS	none	cube ($a=7.6$ cm^3)	no/no	56 d	10 K/min 200–650 °C electric	▼ OPC ▲ MK, NS
[26]	OPC + SF	diabase	cylinder (20×10 cm^3)	no/no	80 d	1 K/min 350 – 650 °C electric	▼ OPC ▲ SF
[87]	OPC, BF, FA, SF	-	cube ($a=10$ cm^3)	no/no	28 d	400–1000 °C electric	▼ OPC, BF, FA ▲ SF
[88]	OPC, SF	-	cube ($a=10$ cm^3)	no/no	5 d	5 K/min 500 °C	▼ OPC ▲ SF
[89]	OPC, SF, FA, MK	-	cylinder (6.4×15 cm^3)	no/no	-	250–1000 °C electric	▼ OPC, FA, MK; ▲ SF
[90]	OPC, SF, FA, BF	granite	cube ($a=10$ cm^3)	no/no	60 d	2.5 K/min 200–800 °C electric	▼ OPC ▲ SF, FA, BF
[91]	OPC, FA, SF, BF	siliceous	cylinder (15×45 cm^3)	yes/no	84 d	5 K/min 200–800 °C electric	▼ OPC ▶ FA, BF ▲ SF
[92]	OPC, SF, WGP	-	cylinder (20×10 cm^3)	no/no	35 d	13.33 K/min 25–800 °C electric	▶ WGP ▲ SF
[93]	OPC, SF	-	cylinder	no/no	28 d	20 K/min 800 °C	▶ OPC ▲ SF
[94]	OPC, SF	calcareous	cylinder (10×20 cm^3)	yes[a)]/no	400 d	5 K/min 600 °C electric	▶ OPC ▶ SF
[95]	CEM IIA-LL, BF	calcareous	slab (y x y $\times3.5$ cm^3)	no/no	-	3000 °C	▶ CEM II/A-LL ▼ BF
[96]	OPC, BF	-	cube ($a=10$ cm^3)	no/no	14 d 28 d	27–800 °C electric	▶ OPC ▼ BF
[97]	OPC, BF	granite	cube ($a=15$ cm^3)	no/no	7 d 28 d 56 d	10 K/min ISO 834 200–800 °C gas, electric	▼ OPC; ▶ BF

Table 6 (continued)

Refs		Specimen				Testing	Result
	Binder type	Coarse aggregate	Geometry	Load/re-straint	Age (≥)	Exposure/ furnace type	Spalling
[98]	OPC, BF	granite	cube ($a = 15$ cm^3)	no/no	7 d 28 d 56 d	10 K/min ISO 834 200–800 °C gas, electric	▶ OPC ▲ BF
[99]	OPC, FA, BF	calcareous	cube ($a = 10$ cm^3)	no/no	56 d	1 K/min 200–800 °C electric	▶ OPC, FA, BF
[100]	OPC, FA, BF	calcareous	cylinder (10×20 cm^3)	no/no	60 d	30 K/min 200–800 °C electric	▲ OPC, BF ▲ FA
[101]	OPC, FA, SF, BF, MK, RHA	granite	cylinder (20×10 cm^3)	no/no	28 d	200–800 °C electric	▲ OPC, FA, BF, SF ▶ RHA ▲ MK
[102]	OPC, SF, MK, FA	granite	cube	no/no	60 d	2.5 K/min 200–800 °C	▼ OPC, FA ▶ SF ▲ MK
[103]	CEM II/B-L, MK	-	cube	-	57 d	200–800 °C	▼ CEM II/B-L ▲ MK
[104]	OPC, MK	-	cube ($a = 10$ cm^3)	no/no	28 d 91 d	100–500 °C	▲ OPC ▲ MK
[105]	OPC, FA, SF, MK	-	cube ($a = 15$ cm^3) cylinder (15×30 cm) beam ($50 \times 10 \times 10$ cm^3)	no/no	28 d	27–900 °C electric	▼ OPC, FA, SF ▲ MK
[106]	HL, MK	calcareous siliceous	cube ($a = 10$ cm^3)	no/no	90 d	ISO 834 200–834 °C	▶ HL ▶ MK
[107]	OPC, LC^3	-	cube ($a = 10$ cm^3)	no/no	84 d	10 K/min 200–800 °C electric	▼ OPC ▶ LC^3
[108]	OPC, FA, MK, NS	granite	cube ($a = 15$ cm^3)	no/no	28 d	200–1000 °C electric	▲OPC ▲ FA, MK, NS
[109]	OPC, LS	calcareous	cube ($a = 10$ cm^3)	no/no	28 d	200–600 °C electric	▶ OPC ▲ LS
[110]	OPC, LS	siliceous	cube ($a = 15$ cm^3)	no/no	28 d	20–700 °C electric	▶ OPC ▼ LS
[111]	OPC, CRD	-	cube ($a = 10$ cm^3)	yes/no	35 d	10 K/min 200–800 °C electric	▶ OPC ▶ CRD
[112]	OPC, VA	calcareous	cube ($a = 10$ cm^3)	no/no	56 d	2.5 K/min 200–800 °C electric	▶ OPC ▼ VA
[113]	OPC, BA, MK	granite	cube	no/no	91 d	10 K/min 200–800 °C	▶ OPC, BA ▲ MK
[114]	OPC, VA, FAS	-	cylinder (10×20 cm^3)	no/no	91 d	200–800 °C electric	▶ OPC, VA, FAS
[115]	OPC, RHA, BHSC	calcareous	cylinder (10×20 cm^3)	no/no	90 d	3 K/min 200–1000 °C electric	▼ OPC, RHA ▶ BHSC

Table 6 (continued)

Refs		Specimen				Testing	Result
	Binder type	Coarse aggregate	Geometry	Load/re-straint	Age (≥)	Exposure/ furnace type	Spalling
[116]	OPC, NSHA	-	cube (a = cm^3)	no/no	28 d	10 K/min 200–800 °C electric	► OPC ► NSHA
[117]	OPC, RHA	-	cube (a = 10 cm^3)	no/no	28 d 56 d 90 d	23–1000 °C	► OPC ► RHA
[118]	OPC, SF, FA, BF, AASA, POFA	granite	cube (a = 10 cm^3)	no/no	56 d	5 K/min 400–800 °C electric	► OPC, SF, FA, BS, AASA, POFA
[119]	OPC, BC	calcareous	cube	no/no	7 d 28 d	10 K/min 300–700 °C electric	▼ OPC, BC
[120]	CEM II/A-M, LF, GP, BF	granite calcareous	cube (a = 10 cm^3) cylinder (15 × 30 cm^3)	no/no	180 d	10 K/min 300–600 °C electric	▲ CEM II/A-M, LF, GP, BS

▲ = high spalling susceptibility; ► = medium spalling susceptibility, ▼ = low spalling susceptibility

a) samples were tested with and without load or restraint respectively

moisture contents between 5 and 7.3 wt% exposed up to 600 °C (5 K/min) [94].

According to [95], the replacement of limestone cement with 10% or 20% slag leads to lower concrete surface temperatures and therefore to lower thermal gradients inside the structure, resulting in less spalling. Improved fire spalling resistance by the replacement of OPC with ultra fine slag was also described in [96]; however no supporting data was available in this study. High volume slag cement concrete with a BF content of 30, 50 and 70% were examined by [97]. Only the 50 and 70% BF specimens experienced spalling of the tested cube edges at temperatures of 600 and 800 °C in [99]. In addition, another paper by the same authors [98] described the behavior of a 0% slag reference. In this paper all specimens, irrespective of the replacement percentage, showed spalling at 800 °C (ISO 834 up to 1.5 min., afterwards 10 K/min). However, this paper reported that spalling of pure OPC concrete was the lowest. Similar spalling behavior of cube edges was seen for OPC, OPC-FA and OPC-BF concrete at the same temperature range but with a much lower heating rate of 1 K/min by [99]. In [100], only OPC-FA concrete experienced spalling in comparison to OPC and OPC-BF concrete after exposure to 800 °C (30 K/min). NSC made with high volume FA cements (60% FA) on the other hand only showed explosive spalling in combination with 12% MK or 7% rice husk ash at temperature loads > 600 °C [101].

Information on the impact of MK on the spalling susceptibility of concrete can be found in [102–106]. Increasing MK replacement rates increases the spalling susceptibility [102–104]. In NSC concrete, 5% of the specimens with 10% MK and 16% of the specimens with 20% MK replacement spalled. Regarding HSC concrete, roughly one third of the specimens with 10% MK and half of the specimens with 20% MK replacement spalled as well as 5% of the reference OPC concrete. A replacement of 5% MK caused no spalling in NSC or HSC specimens. In both cases, most of the spalling occurred between 450 and 500 °C (2.5 K/min) [102]. The damage to the specimens was not further investigated. Labiran et al. [103] claimed to record similar results of an increasing spalling proneness with increasing MK content from 0 to 10% between 400 and 800 °C [103]. However, the authors show neither any data related to spalling nor any pictures of damaged specimens. Finally, [105] summarized that only MK-containing concrete spalled in comparison to FA or SF specimens; again no supporting data was given and the

SF concrete mix designs exhibited much lower initial compressive strength which might have led to this finding. Spalling results of concrete with hydraulic lime (HL) as the main binder and replacements of 20 and 30% MK showed no distinguishable influence of MK on the spalling behavior. Spalling began at a temperature load of 400 °C and increased with increasing temperatures up to 800 °C for all test specimens [106]. It should be noted that the test specimens were pre-dried and therefore the recorded spalling behavior might not apply for untreated concrete of the same kind. In mixes where OPC was replaced with 10%, 20% and 30% limestone calcined clay cement (LC^3), corner spalling started to happen at 600 °C and explosive spalling was once noted in a specimen with 20% replacement at 800 °C (10 K/min) [107]. The specimens were dried prior to testing and in conclusion, no meaningful relation between replacement rate and spalling behavior was drawn. Results of a quaternary concrete mix out of OPC, FA, MK and NS compared to an OPC control mix by [108] showed excessive spalling for both types of concrete when heated up to 1000 °C. Some authors explain the increased spalling susceptibility of MK with the development of a denser microstructure promoting the development of higher pore pressures [102, 103].

Explosive spalling in laboratory limestone cement blends were observed by [109, 110]. [109] suggests slightly less spalling for limestone-incorporating concrete as they experienced a lower mass loss at every tested temperature from 200 to 600 °C.

Moreover, heat-induced spalling in concrete with rather non-traditional SCMs or fillers were observed by [92, 111–120]. Spalling in HSC with 25% inert waste glass powder (GP) usually occurred at higher temperatures of 500 °C, whereas HSC with 25% SF showed more destruction already happening at 400 °C for a heating rate of 13.33 K/min in both cases. The greater spalling susceptibility of the HSC-SF specimens can be explained by their higher compressive strength of 142 MPa compared to 81 MPa of HSC-GP specimens [92]. The replacement of Portland cement with up to 40% crushed rock dust (CRD) led to no clear change in the spalling behavior of HSC heated to 800 °C (10 K/min) [111]. The work of Anwar Hossain [112] provided first insights into the spalling behavior of HSC concrete with volcanic ash (VA). The author replaced 5%,10%,15% and 20% of the cement with natural pozzolan. In total, 8% of the control specimens without VA spalled and no HSC with VA spalled throughout the investigations in the range of 200–800 °C (2.5 K/min). Further experiments on the high temperature behavior of concrete with volcanic ash in binary and ternary blends were conducted by [114]. Concrete with pure OPC, 20% VA, 20% FA, 20% VA + 10% furnace arc slag (FAS) and 20% FA + 10% FAS as cement replacements were compared. The results showed clear surface spalling in the OPC control mix and the VA 20% + FAS 10% after exposure to 800 °C. It should be noted that the specimens were already pre-dried to avoid spalling. High temperatures studies on concrete with rice husk ash (RHA) and bagasse ash (BA) were conducted by [115]. The replacement of cement by 10% RHA or 10% BA in general led to better mechanical properties at elevated temperatures; however, the addition of 10% RHA and 10% BA led to more cracking and the latter finally spalled at 672 °C (3 K/min). Spalling was caused by the denser microstructure inhibiting the release of water vapor as well as by the thinner ITZ which provided no cushion for the thermal dilation mismatch of aggregates and cement matrix [115]. It was also reported that with increasing amounts of RHA, the spalling type changes from a surface and aggregate spalling to a softer sloughing-off [117]. In various binary and ternary blended concrete with SF, BF, and FA, thermally activated alum sludge ash (AASA), and palm oil fuel ash (POFA), spalling happened after exposure to 800 °C (5 K/min) in all specimens without any relation to the binder type. The addition of PP fibers reduced or eliminated the risk of explosive spalling in every concrete [118]. With the replacement of 0, 3, 5 and 10% of OPC with biochar (BC), minimal spalling was discovered after 700 °C (3 K/min) exposure for all mixtures except for that with 3% replacement [119]. Anagnostopoulos et al. [120] studied the high temperature behavior of self-compacting concrete (SCC) made from CEM II/A-M 42.5 N plus either additional limestone powder, glass powder or slag with moisture contents between 3.1 and 4.4 wt%. Explosive spalling was observed at 600 °C (10 K/min) in every concrete but according to the authors no influence on the spalling severity related to the different binder blends was identified.

5 Conclusion

The collected data from the published literature on the influence of blended cements on the heat-induced spalling behavior of concrete was analyzed and evaluated. The present review article led to the following conclusions:

1) In total just a few studies focus on in-depth fire spalling studies and deliver a complete picture of the material characteristics. In experiments with standardized blended cements in particular, the initial characteristics of the binder material are often only insufficiently described, meaning that no precise specification regarding the SCM content and composition was given. Information about the proportion of substitution would make it easier to compare different cements from the same classification as these have wide spans of substitution rates defined in the regulations. For example, the specified substitution rate for CEM III/A according to DIN EN-197-1 is between 36 and 65% BF. This large range could also be a possible reason for the differences in spalling behavior of concrete with the same type of cement.
2) Most articles deal with the general high temperature behavior of concrete with blended cements, where spalling often was only noted as a side effect. The majority of those tests were conducted in electric furnaces. This usually led to applied heating rates that are much lower than during an actual fire event. Therefore, the spalling behavior examined in these studies might not correspond to the behavior in practice. Moreover, many results are from small-sized specimens aged less than 90 days. This might blur the spalling differences between the different concretes as smaller test specimens lower the spalling susceptibility, making it harder to distinguish between the impacts of cement type and specimen size. Due to the comparatively young test age, hydration may not yet be complete. This is a particularly important aspect, as different types of cement have different hydration characteristics and blended cements usually undergo longer hydration processes compared to Portland cement. This could mean that the compressive strength of blended concrete is lower than that of Portland cement concrete and that spalling is correspondingly less severe at young testing ages. Therefore, the significance of experiments with small-sized test specimens with an age of less than 90d is very low. In addition, the moisture content was not mentioned in a large number of articles. Due to this lack of information, no conclusion can be drawn as to whether thermo-hydraulic or thermo-mechanical mechanisms are crucial for the differing spalling behaviors. Lastly, most of the conducted experiments were carried out without load or restrained thermal expansion, which is indicative of a scenario that deviates significantly from actuality.
3) The spalling of concrete is influenced by the cement type. This was proven by several studies from different researchers. Factors identified as changing spalling behavior in relation to the cement type were moisture content, definition of ITZ, and density. Since fire-induced concrete spalling is further dependent on additional material properties (strength, aggregate type, etc.) and testing conditions (furnace type, heating rate, load, etc.) a comparison between individual research groups is limited. This is amplified because different research groups use different criteria to evaluate the extent of spalling (frequency, spalling depth, spalled volume, weight loss etc.). Standardized test procedures are therefore urgently needed.
4) In general, the addition of SF or MK tend to increase the spalling risk compared to OPC and cements with other SCMs. This is most likely caused by the development of a very dense microstructure inhibiting the release of water vapor at high temperatures, thus promoting thermohydraulic spalling. The influence of FA on spalling susceptibility is not straightforward. While no clear relation between FA and spalling susceptibility was recorded for low contents, high FA contents ($\geq 25\%$) led to less severe spalling in several studies. This might be attributed to the increase of porosity and permeability caused by the high replacement rates. No further meaningful relation between other cement blends and the influence on spalling susceptibility of concrete could be drawn based on the current data situation.

In view of the inconsistencies and contradictions of the evaluated articles, further in-depth studies on the fire induced spalling behavior of concrete with blended cements must be carried out. Since the

use and variation of blended cements is constantly increasing, a well-founded understanding of their behavior under fire exposure is necessary. In particular, since the addition of MK increases the spalling risk, the influence of other calcined clays must be studied in detail as they are predicted to be the most popular SCMs of the future. To minimize the influence of other factors, the material, testing and evaluation conditions should be strictly defined and follow the guidelines of published recommendations like [54, 55]. Above all, care should always be taken to follow a defined fire curve, as this is the only way to adequately represent the temperature development in the event of a live fire. Furthermore, the tests should be carried out on restrained or loaded specimens of an appropriate size as this is also the closest reflection of reality. For blended cement concrete, a testing age of at least 90 d must definitely be reached, otherwise the differing hydration degrees make a reasonable analysis impossible. While for conventional concrete it might be sufficient to state the typical material parameters like composition, compressive strength and moisture content, this might not be enough for blended cement concrete. Due to the strong influence of the SCMs on the microstructure, it is possible for concrete of similar strength to have very different pore space and permeability, which might not degrade to the same extent at elevated temperatures. It is therefore recommended to further specify the microstructure e.g., through porosity and permeability measurements before and after high temperature exposure. Since different binders lead to different mineral phase compositions, it is also advisable to obtain information about the dehydration behavior of the different cement pastes as these contribute greatly to the release of water during heating. A large fraction of this water is released beyond 105 °C; therefore the typical determination of the moisture content by drying to constant mass at 105 °C is not enough. Hence, the specimen should be dried at higher temperatures, for example at 300 °C, until it is constant in mass. In any case, the selected temperature should not be within the range of other decomposition reactions such as those of calcium carbonate. In addition, a thermogravimetric analysis can be executed if the quantity of water release at different temperature levels is of interest. Lastly, spalling must be conscientiously evaluated during and after temperature load. This means that number, character and point of time of the spalling events as well as the depth and volume must be recorded to guarantee meaningful results.

Acknowledgements We gratefully acknowledge the support and extend our gratitude to the German Research Foundation (DFG) for their financial support throughout the project ‘‘Thermohydraulic spalling mechanisms in concretes with different binders with and without PP fibers under fire exposure: An experimental and numerical analysis’’ (Project Nr. 491928256).

Funding Open Access funding enabled and organized by Projekt DEAL.

Data availability There is no data available for this work.

Declarations

Conflict of interest The authors declare that they have no known competing financial interests, personal relationships or any other affairs that could have appeared to influence the work reported in this paper.

Open Access This article is licensed under a Creative Commons Attribution 4.0 International License, which permits use, sharing, adaptation, distribution and reproduction in any medium or format, as long as you give appropriate credit to the original author(s) and the source, provide a link to the Creative Commons licence, and indicate if changes were made. The images or other third party material in this article are included in the article’s Creative Commons licence, unless indicated otherwise in a credit line to the material. If material is not included in the article’s Creative Commons licence and your intended use is not permitted by statutory regulation or exceeds the permitted use, you will need to obtain permission directly from the copyright holder. To view a copy of this licence, visit http://creativecommons.org/licenses/by/4.0/.

References

1. Juenger MC, Siddique R (2015) Recent advances in understanding the role of supplementary cementitious materials in concrete. Cement Concr Res 78:71–80. https://doi.org/10.1016/j.cemconres.2015.03.018
2. Yasutomo U (2015) History and utilization of portland blast furnace slag cement. Nippon Steel Sumitomo Metal Tech Rep 109:109–113
3. Li C, Gong X, Cui S et al (2011) CO_2 Emissions due to cement manufacture. Materials Science Forum 685. https://doi.org/10.4028/www.scientific.net/MSF.685.181
4. Scrivener KL, John VM, Gartner EM (2018) Eco-efficient cements: Potential economically viable solutions for a low-CO_2 cement-based materials industry. Cement Concr Res 114:2–6
5. Schneider M (2019) The cement industry on the way to a low-carbon future. Cement Concr Res 124:105792. https://doi.org/10.1016/j.cemconres.2019.105792

6. Favier A, De Wolf C, Scrivener K et al (2018) A sustainable future for the European cement and concrete industry–Technology assessment for full decarbonisation of the industry by 2050. ETH Zurich, Zurich
7. Panesar DK, Zhang R (2020) Performance comparison of cement replacing materials in concrete: limestone fillers and supplementary cementing materials–a review. Construct Build Mater 251:118866. https://doi.org/10.1016/j.conbuildmat.2020.118866
8. Meyer-Ottens C (1972) Zur Frage der Abplatzungen an Betonbauteilen aus Normalbeton bei Brandbeanspruchung. Technischen Universität Carolo - Wilhelmina zu Braunschweig
9. Weise F, Stelzner L, Weinberger J et al (2017) Influence of the pre-treatment of PP-fibres by means of electron irradiation on the spalling behaviour of High-Strength Concrete. 5th International Workshop on Concrete Spalling: Boras, Sweden 345–358.
10. Lothenbach B, Scrivener K, Hooton RD (2011) Supplementary cementitious materials. Cement Concr Res 41(12):1244–1256. https://doi.org/10.1016/j.cemconres.2010.12.001
11. Lea FM (1971) The chemistry of cement and concrete. Chemical Publishing Co., New York
12. Trout EAR (2019) Lea's chemistry of cement and concrete.
13. Pal SC, Mukherjee A, Pathak SR (2003) Investigation of hydraulic activity of ground granulated blast furnace slag in concrete. Cement Concr Res 33(9):1481–1486. https://doi.org/10.1016/S0008-8846(03)00062-0
14. Vaclavik V, Dirner V, Dvorsky T et al (2012) The use of Blast Furnace Slag. Metalurgija 51:461–464
15. Ahmed MS, Kayali O, Anderson W (2008) Chloride penetration in binary and ternary blended cement concretes as measured by two different rapid methods. Cement Concr Compos 30(7):576–582. https://doi.org/10.1016/j.cemconcomp.2008.02.005
16. Richardson IG, Groves GW (1992) Microstructure and microanalysis of hardened cement pastes involving ground granulated blast-furnace slag. J Mater Sci 27:6204–6212
17. Richardson IG (1999) The nature of C-S-H in hardened cements. Cem Concr Res 29:1131–1147
18. Jia Z, Chen C, Shi J, Zhang Y, Sun Z, Zhang P (2019) The microstructural change of CSH at elevated temperature in Portland cement/GGBFS blended system. Cement Concr Res 123:105773. https://doi.org/10.1016/j.cemconres.2019.05.018
19. Dedeloudis C, Zervaki M, Sideris K et al (2018) Properties of fresh and hardened concrete containing supplementary cementitious materials: state-of-the-art report of the RILEM technical committee 238-SCM. Working Group 4:181–231
20. Skibsted J, Snellings R (2019) Reactivity of supplementary cementitious materials (SCMs) in cement blends. Cement Concr Res 124:105799. https://doi.org/10.1016/j.cemconres.2019.105799
21. Moosberg-Bustnes H, Lagerblad B, Forssberg E (2004) The function of fillers in concrete. Mater Struct 37:74–81. https://doi.org/10.1007/BF02486602
22. Lothenbach B, Le Saout G, Gallucci E, Scrivener K (2008) Influence of limestone on the hydration of Portland cements. Cement Concr Res 38(6):848–860. https://doi.org/10.1016/j.cemconres.2008.01.002
23. Fu Y, Li L (2011) Study on mechanism of thermal spalling in concrete exposed to elevated temperatures. Mater Struct 44:361–376. https://doi.org/10.1617/s11527-010-9632-6
24. Al-Bashiti MK, Naser MZ (2023) What can we learn from over 1000 tests on fire-induced spalling of concrete? A statistical investigation of critical factors and unexplored research space. Construct Build Mater 403:133200. https://doi.org/10.1016/j.conbuildmat.2023.133200
25. Hertz KD (2003) Limits of spalling of fire-exposed concrete. Fire Safety J 38(2):103–116. https://doi.org/10.1016/S0379-7112(02)00051-6
26. Hertz K (1984) Heat-induced explosion of dense concretes. Technical University of Denmark, Department of Civil Engineering
27. Pan Z, Sanjayan JG, Kong DL (2012) Effect of aggregate size on spalling of geopolymer and Portland cement concretes subjected to elevated temperatures. Construct Build Mater 36:365–372. https://doi.org/10.1016/j.conbuildmat.2012.04.120
28. Mohd Ali AZ, Sanjayan J, Guerrieri M (2018) Specimens size, aggregate size, and aggregate type effect on spalling of concrete in fire. Fire Mater 42(1):59–68. https://doi.org/10.1002/fam.2457
29. Kirnbauer J and Schneider U (2011) Influence of cement type and aggregate shape on explosive concrete spalling. 2nd International RILEM Workshop on Concrete Spalling due to Fire Exposure: Delft, The Netherlands 411–418.
30. Hager I, Mróz K and Tracz T (2018) Concrete propensity to fire spalling: Testing and observations. MATEC Web of Conf. 163. https://doi.org/10.1051/matecconf/201816302004
31. Xing Z, Beaucour AL, Hebert R, Noumowe A, Ledesert B (2011) Influence of the nature of aggregates on the behaviour of concrete subjected to elevated temperature. Cement Concr Res 41(4):392–402. https://doi.org/10.1016/j.cemconres.2011.01.005
32. Klimek A, Stelzner L, Hothan S, Rogge A (2022) Fire induced concrete spalling in combination with size effects. Mater Struct 55(8):216. https://doi.org/10.1617/s11527-022-02051-2
33. Lenglet C (2011) Evolution of Spalling with time and age. 2nd International RILEM Workshop on Concrete Spalling due to Fire Exposure: Delft, The Netherlands 25–32.
34. Boström L and Jansson R (2011) The age effect on fire spalling of concrete. 2nd International RILEM Workshop on Concrete Spalling due to Fire Exposure: Delft, The Netherlands 33–42.
35. Klimek A, Stelzner L, Hothan S, Zehfuß J (2024) Influence of thermal strain on concrete spalling. Mater Struct 57(1):15. https://doi.org/10.1617/s11527-023-02274-x
36. Shorter GW and Harmathy TZ (1961) Discussion on the Fire-resistance of prestressed concrete beams. 313–315
37. Harmathy TZ (1965) Effect of moisture on the fire endurance of building elements. ASTM Special Technical Publication No. 385:

38. Felicetti R, Yarmohammadian R, Dal Pont S, Tengattini A (2024) Fast vapour migration next to a depressurizing interface: a possible driving mechanism of explosive spalling revealed by neutron imaging. Cement Concr Res 180:107508. https://doi.org/10.1016/j.cemconres.2024.107508
39. van der Heijden GHA, van Bijnen RMW, Pel L et al (2007) Moisture transport in heated concrete, as studied by NMR, and its consequences for fire spalling. Cem Concr Res 37:894–901
40. Stelzner L, Powierza B, Oesch T, Dlugosch R, Weise F (2019) Thermally-induced moisture transport in high-performance concrete studied by X-ray-CT and 1H-NMR. Construct Build Mater 224:600–609. https://doi.org/10.1016/j.conbuildmat.2019.07.065
41. Jansson R (2013) Fire spalling of concrete. KTH Royal Institute of Technology
42. Waubke NV and Schneider U (1973) Tensile stress in concrete due to fast vapour flow. Proceedings of the international RILEM symposium "Pore Structure and Properties of Materials": Prauge, Czech Republic
43. Ichikawa Y (2000) Prediction of Pore Pressures, Heat and Moisture Transfer Leading to Spalling of Concrete during Fire. University of London
44. Khoylou N (1997) Modelling of moisture migration and spalling behaviour in non-uniformly heated concrete. University of London
45. Breunese AJ and Fellinger JHH (2004) Spalling of concrete–an overview of ongoing research in the Netherlands. Third International Workshop Structures in Fire SiF. Ottawa, Canada
46. McNamee R (2019) Fire spalling theories–realistic and more exotic ones. Proceedings of the 6th International Workshop on Concrete Spalling due to Fire Exposure: Sheffield, England
47. Schneider U (1982) Behaviour of Concrete at High Temperatures Deutscher Ausschuss für Stahlbeton 1–110.
48. Bazant Z P (1997) Analysis of pore pressure, thermal stresses and fracture in rapidly heated concrete. Int. Workshop on Fire Performance of High-Strength Concrete: Gaithersburg 155–164.
49. Ulm FJ, Coussy O, Bazant ZP (1999) The "'Chunnel"' fire I: chemoplastic softening in rapidly heated concrete. J Eng Mech 125:272–282. https://doi.org/10.1061/(ASCE)0733-9399(1999)125:3(272)
50. Stelzner L (2021) Analyse des thermisch induzierten Feuchtetransports in gefügedichten Beton. Universität Stuttgart
51. Eurocode 2, 1992–1–2: Design of concrete structures-Part 1–2: General rules-Structural fire design, Brussels, Belgium (2011)
52. Pistol K, Weise F, Meng B, Schneider U (2011) The mode of action of polypropylene fibres in high performance concrete at high temperatures. In: 2nd International RILEM Workshop on Concrete Spalling due to fire exposure. RILEM Publications SARL (pp. 289–296).
53. Maluk C, Bisby L, Terrasi GP (2017) Effects of polypropylene fibre type and dose on the propensity for heat-induced concrete spalling. Eng Struct 141:584–595. https://doi.org/10.1016/j.engstruct.2017.03.058
54. Pimienta P, McNamee R, Hager I, Mróz K, Boström L, Mohaine S, Huang SS, Mindeguia JC, Robert F, Davie C, Felicetti R (2023) Recommendation of RILEM TC 256-SPF on the method of testing concrete spalling due to fire: material screening test. Mater Struct 56(9):164. https://doi.org/10.1617/s11527-023-02202-z
55. Pimienta P, McNamee R, Robert F, Boström L, Huang SS, Mróz K, Davie C, Mohaine S, Alonso MC, Bodnarova L, Bosnjak J (2024) Recommendation of RILEM TC 256-SPF on fire spalling assessment during standardised fire resistance tests: complementary guidance and requirements. Mater Struct 57(1):3. https://doi.org/10.1617/s11527-023-02248-z
56. DIN EN 197–1, Cement-Part 1: Composition specifications and conformity for common cements, Beuth Verlag GmbH, Berlin, Germany (2011)
57. Reiners J, Müller C (2017) Einfluss der chemischen und physikalischen Eigenschaften von Zementstein auf das Trocknungsverhalten von Zementestrich und das Abplatzverhalten von Beton im Brandfall, Teil 2. Beton 67:491–499
58. Reiners J, Zehfuß J, Dehn F, Müller C (2024) The influence of the physical and chemical properties of hardened cement paste on the heat-induced explosive spalling of concrete. Civil Eng Design 6(1):4–21. https://doi.org/10.1002/cend.202300020
59. Miah MJ, Monte FL, Felicetti R, Pimienta P, Carré H, La Borderie C (2023) Impact of external biaxial compressive loading on the fire spalling behavior of normal-strength concrete. Construct Build Mater 366:130264. https://doi.org/10.1016/j.conbuildmat.2022.130264
60. Pittrich T, Stelzner L, Weise F (2024) Fire-induced spalling of normal strength concrete with different types of blended Portland cement. In: Proceedings of the 13th International Conference on Structures in Fire (SiF 2024) (Vol. 1, pp. 461–471).
61. Kalifa P, Menneteau FD, Quenard D (2000) Spalling and pore pressure in HPC at high temperatures. Cement Concr Res 30(12):1915–1927. https://doi.org/10.1016/S0008-8846(00)00384-7
62. Taillefer N, Pimienta P, Dhima D (2013) Spalling of concrete: a synthesis of experimental tests on slabs. In: MATEC Web of Conferences 2013 (Vol. 6, p. 01008). EDP Sciences. https://doi.org/10.1051/matecconf/20130601008
63. Zemri C, Bouiadjra MB (2020) Comparison between physical–mechanical properties of mortar made with Portland cement (CEMI) and slag cement (CEMIII) subjected to elevated temperature. Case Stud Construct Mater 12:e00339. https://doi.org/10.1016/j.cscm.2020.e00339
64. Balázs GL, Kopecskó K, Alimrani NS et al (2018) Fire resistance of concretes with blended cements. High Tech Concrete: Where Technol Eng Meet. https://doi.org/10.1007/978-3-319-59471-2_163
65. Lublóy É, Kopecskó K, Balázs GL, Restás Á, Szilágyi IM (2017) Improved fire resistance by using Portland-pozzolana or Portland-fly ash cements. J Ther Anal Calorim 129:925–936. https://doi.org/10.1007/s10973-017-6245-0

66. Nicolella M and Scognamillo C (2015) Performance characterization of the concrete subjected to fire in terms of sustainability. Sostenibilità Ambientale e Produzione Edilizia: Maggioli 193–212.
67. Jocius V, Skripkiunas G and Lipinskas D (2023) Cement Type Influence on Fire Resistance of Concrete. International Review of Chemical Engineering 15. https://doi.org/10.15866/ireche.v15il.24187
68. Dehn F, Nause P, Juknat M et al (2010) Brand- und Abplatzverhalten von Faserbeton in Straßentunneln. Berichte der Bundesanstalt für Strassenwesen - Brücken- und Ingenieurbau B73
69. Bodnarova L, Valek J, Novosad P (2015) Testing of action of direct flame on concrete. Sci World J 2015(1):371913. https://doi.org/10.1155/2015/371913
70. Han CG, Han MC, Heo YS (2008) Spalling properties of high strength concrete mixed with various mineral admixtures subjected to fire. Int J Concr Struct Mater 2(1):41–48. https://doi.org/10.4334/IJCSM.2008.2.1.041
71. Nuruddin MF, Azmee NM, Yung CK (2014) Effect of fire flame exposure on ductile self-compacting concrete (DSCC) blended with MIRHA and fly ash. Constr Build Mater 50:388–393. https://doi.org/10.1016/j.conbuildmat.2013.09.038
72. Gedam BA (2023) Spalling mitigation techniques for high-performance concrete at elevated temperature. Materials Today: Proceedings https://doi.org/10.1016/j.matpr.2023.03.556
73. Kwon KS, Ryu DW (2015) Fire resistance performance test of high strength concrete by type of mineral admixture. J Korea Inst Build Construct 15(6):597–605. https://doi.org/10.5345/JKIBC.2015.15.6.597
74. Kodur VK, McGrath R (2006) Effect of silica fume and lateral confinement on fire endurance of high strength concrete columns. Can J Civil Eng 33(1):93–102. https://doi.org/10.1139/l05-089
75. Mussa MH, Radzi NA, Hamid R, Mutalib AA (2021) Fire resistance of high-volume fly ash RC slab inclusion with nano-silica. Materials 14(12):3311. https://doi.org/10.3390/ma14123311
76. Khaliq W, Kodur V (2013) Behavior of high strength fly ash concrete columns under fire conditions. Mater Struct 46:857–867. https://doi.org/10.1617/s11527-012-9938-7
77. Raut NK, Kodur VKR (2010) Response of high strength concrete columns under design fire exposure. J Struct Eng 137:69–79. https://doi.org/10.1061/(ASCE)ST.1943-541X.0000265
78. Šejnoha M, Brouček M, Novotná E, Sýkora J (2012) Resistance of concrete with fly ash content under the RWS curve fire loading. Engineering mechanics.
79. Šejnoha M, Brouček M (2013) Experimental Investigation of the Fire Resistance of Modified Concrete. Proc Eng. Mech.
80. Sejnoha M, Broucek M (2014) Fire resistance of concrete with fly ash content–experimental analysis. Eng Mech 21:159–165
81. Kakali G, Leventi R, Benekis V, Tsivilis S (2006) Behavior of blended cement pastes at elevated temperature. Chem Ind Chem Eng Quart 12(2):133–136. https://doi.org/10.2298/CICEQ0602133K
82. Wang HY (2008) The effects of elevated temperature on cement paste containing GGBFS. Cement Concr Compos 30(10):992–999. https://doi.org/10.1016/j.cemconcomp.2007.12.003
83. Abdelmelek N, Lubloy E (2022) Flexural strength of silica fume, fly ash, and metakaolin of hardened cement paste after exposure to elevated temperatures. J Ther Anal Calorim 147(13):7159–7169. https://doi.org/10.1007/s10973-021-11035-3
84. Maheswaran S, Iyer NR, Palani GS, Pandi RA, Dikar DD, Kalaiselvam S (2015) Effect of high temperature on the properties of ternary blended cement pastes and mortars. J Ther Anal Calorim 122:775–786. https://doi.org/10.1007/s10973-015-4817-4
85. Heikal M, El-Didamony H, Sokkary TM, Ahmed IA (2013) Behavior of composite cement pastes containing microsilica and fly ash at elevated temperature. Construct Build Mater 38:1180–1190. https://doi.org/10.1016/j.conbuildmat.2012.09.069
86. Pp A, Kumar R, Kumar V, Patel P, Menon V (2024) Thermal impact on superplasticizer-free metakaolin-nano-silica binary and ternary mortars. Mater High Temp 41(3):409–423. https://doi.org/10.1080/09603409.2024.2329429
87. Ju Y, Tian K, Liu H, Reinhardt HW, Wang L (2017) Experimental investigation of the effect of silica fume on the thermal spalling of reactive powder concrete. Construct Build Mater 155:571–583. https://doi.org/10.1016/j.jobe.2022.104117
88. Ju Y, Tian K, Liu H, Reinhardt HW, Wang L (2017) Experimental investigation of the effect of silica fume on the thermal spalling of reactive powder concrete. Construct Build Mater 155:571–583. https://doi.org/10.1016/j.conbuildmat.2017.08.086
89. Kanagaraj B, Nammalvar A, Andrushia AD, Gurupatham BG, Roy K (2023) Influence of Nano composites on the impact resistance of concrete at elevated temperatures. Fire 6(4):135. https://doi.org/10.3390/fire6040135
90. Poon CS, Azhar S, Anson M, Wong YL (2001) Comparison of the strength and durability performance of normal-and high-strength pozzolanic concretes at elevated temperatures. Cement Concr Res 31(9):1291–1300. https://doi.org/10.1016/S0008-8846(01)00580-4
91. Rahim A, Sharma UK, Murugesan K, Arora P (2013) Effect of load on thermal spalling of reinforced concrete containing various mineral admixtures. InMATEC Web of Conferences. EDP Sciences (Vol. 6, p. 01006). https://doi.org/10.1051/matecconf/20130601006
92. Ali MH, Dinkha YZ, Haido JH (2017) Mechanical properties and spalling at elevated temperature of high performance concrete made with reactive and waste inert powders. Eng Sci Technol, Int J 20(2):536–541. https://doi.org/10.1016/j.jestch.2016.12.004
93. Bastami M, Chaboki-Khiabani A, Baghbadrani M et al (2011) Performance of high strength concretes at elevated temperatures. Scientia Iranica A 18:1028–1036. https://doi.org/10.1016/j.scient.2011.09.001
94. Phan LT, Carino NJ (2002) Effects of test conditions and mixture proportions on behavior of high-strength concrete exposed to high temperatures. ACI Mater J 99(1):54–66

95. Pancar EB (2017) Reducing high temperature effect on concrete by changing concrete mixture. Int J Struct Civil Eng Res 6(4):258–262
96. Saurav, Shukla AK, Malaviya P (2020) A comparative study of fire resistance of concrete incorporating ultrafine slag. InAdvances in Industrial Safety: Select Proceedings of HSFEA 2018. Springer, Singapore. (pp. 291–304)
97. Shumuye ED, Zhao J, Wang Z (2019) Effect of fire exposure on physico-mechanical and microstructural properties of concrete containing high volume slag cement. Construct Build Mater 213:447–458. https://doi.org/10.1016/j.conbuildmat.2019.04.079
98. Shumuye ED, Zhao J, Wang Z (2021) Effect of the curing condition and high-temperature exposure on ground-granulated blast-furnace slag cement concrete. Int J Concr Struct Mater 15:1–20. https://doi.org/10.1186/s40069-020-00437-6
99. Uysal M, Yilmaz K, Ipek M (2012) Properties and behavior of self-compacting concrete produced with GBFS and FA additives subjected to high temperatures. Construct Build Mater 28(1):321–326. https://doi.org/10.1016/j.conbuildmat.2011.08.076
100. Ghazy MF, Abd Elaty MA, Zalhaf NM (2022) Mechanical properties of HPC incorporating fly ash and ground granulated blast furnace slag after exposure to high temperatures. Periodica Polytechnica Civil Eng 66(3):761–774. https://doi.org/10.3311/PPci.19751
101. Amrutha, Nayak G, Narasimhan M, Rajeeva S (2011) High temperature performance of self-compacting high-volume fly ash concrete mixes. J Struct Fire Eng 2(2):81–90. https://doi.org/10.1260/2040-2317.2.2.81
102. Poon CS, Azhar S, Anson M, Wong YL (2003) Performance of metakaolin concrete at elevated temperatures. Cement Concr Compos 25(1):83–89. https://doi.org/10.1016/S0958-9465(01)00061-0
103. Labiran JO, Ezea BU, Igba UT, Akinyele JO (2022) Fire performance of metakolin concrete and mortar blends using Nigerian kaolinite clays. InCurrent Perspectives and New Directions in Mechanics, Modelling and Design of Structural Systems. CRC Press, (pp. 1621–1625).
104. Viswanadha Varma D, Rama Rao GV, Sindhu J (2014) Effect of temperature on metakaolin blended high strength concrete. Int J Eng Res Dev 10:57–67
105. Cachim PB, Morais MM, Coroado J, Lopes N, Velosa AL (2012) Behaviour of limecrete under fire conditions. Fire Mater 36(4):288–296. https://doi.org/10.1002/fam.2353
106. Cachim PB, Morais MM, Coroado J, Lopes N, Velosa AL (2012) Behaviour of limecrete under fire conditions. Fire Mater 36(4):288–296. https://doi.org/10.1002/fam.1110
107. Sharma A, AB DR, Bansal PP (2022) Performance of limestone calcined clay cement (LC^3) at high temperatures. In: 7th International Workshop (p. 248)
108. Kumar VK, Rao PS, Sekhar TS (2022) Effect on quaternary blended concrete using fly ash, metakaolin and nano silica subjected to elevated temerpatures. Adv Eng Sci 54:5045–5058
109. El-Kurdi AA, Abdel-Hakam A, El-Gohary MM (2014) Impact of elevated temperature on properties of limestone concrete. Int J Innovative Technol Exploring Eng (IJITEE) 4(4):1–9
110. El-Hawary M, Ahmed M (2017) Properties, sustainability and elevated temperature behavior of concrete containing Portland limestone cement. InAIP Conference Proceedings. Vol. 1885(1). AIP Publishing. https://doi.org/10.1063/1.5002223
111. Kumar NV, Ram KS (2019) Performance of concrete at elevated temperatures made with crushed rock dust as filler material. Mater Today: Proceed 18:2270–2278. https://doi.org/10.1016/j.matpr.2019.07.009
112. Hossain KM (2006) High strength blended cement concrete incorporating volcanic ash: Performance at high temperatures. Cement Concr Compos 28(6):535–545. https://doi.org/10.1016/j.cemconcomp.2006.01.013
113. Mello LC, dos Anjos MA, de Sá MV, de Souza NS, de Farias EC (2020) Effect of high temperatures on self-compacting concrete with high levels of sugarcane bagasse ash and metakaolin. Construct Build Mater 248:118715. https://doi.org/10.1016/j.conbuildmat.2020.118715
114. Amin MN, Khan K (2020) Mechanical performance of high-strength sustainable concrete under fire incorporating locally available volcanic ash in Central Harrat Rahat, Saudi Arabia. Materials 14(1):21. https://doi.org/10.3390/ma14010021
115. Khaliq W, Mujeeb A (2019) Effect of processed pozzolans on residual mechanical properties and macrostructure of high-strength concrete at elevated temperatures. Struct Concr. https://doi.org/10.1002/suco.201800074
116. Mwilongo KP, Machunda RL, Jande YAC (2020) Effect of elevated temperature on compressive strength and physical properties of neem seed husk ash concrete. Materials. https://doi.org/10.3390/ma13051198
117. Job OF, Pam M and Ishaya AA (2017) Physical and thermal properties of rice husk ash blended high strength concrete at elevated temperature. Int J of Modern Trends in Engineering and Research. https://doi.org/10.21884/ijmter.2017.4354.igqdx
118. Owaid HM, Hamid R and Taha MR (2016) Elevated temperature performance of multiple-blended binder concretes. In: Yilmaz, S High Performance Concrete Technology and Applications, IntechOpen, pp 87–112
119. Pang X, Qin Y, Wei P et al (2024) Enhancing fire resistance: Investigating mechanical properties of biochar-infused concrete under elevated temperatures. Constr Build Mater. https://doi.org/10.1016/j.conbuildmat.2024.136813
120. Anagnostopoulos N, Sideris KK, Georgiadis A (2008) Mechanical characteristics of self-compacting concretes with different filler materials, exposed to elevated temperatures. Mater Struct. https://doi.org/10.1617/s11527-008-9459-6

Publisher's Note Springer Nature remains neutral with regard to jurisdictional claims in published maps and institutional affiliations.

Conference Paper:

Fire-induced spalling of normal strength concrete with different types of blended Portland cement

Publisher's version

Originally published in the
Proceedings of the 13th International Conference on Structures in Fire (SiF 2024), published by CMM – Portuguese Steelwork Association.
Reproduced with permission.

1st Edition, 2024

DOI: https://doi.org/10.30779/cmm_SIF24

Authors: Tim Pittrich, Ludwig Stelzner, Frank Weise

SiF 2024– The 13th International Conference on Structures in Fire
University of Coimbra, Portugal, 19 to 21 June 2024

FIRE-INDUCED SPALLING OF NORMAL STRENGTH CONCRETE WITH DIFFERENT TYPES OF BLENDED PORTLAND CEMENT

Tim Pittrich[1], Ludwig Stelzner[2], Frank Weise[3]

ABSTRACT

The cement industry is looking to reduce its overall CO_2 footprint. Greener manufacturing can be achieved by the introduction of more clinker-reduced cements. Concrete exposed to fire tends to show explosive spalling caused by thermomechanical and thermohydraulic processes. It is therefore essential to determine how concretes with clinker-reduced cements behave under fire exposure, especially for concretes containing calcined clays, as these are expected to be the supplementary cementitious material of the future. In this paper, normal strength concretes with four different cements (CEM I, CEM II/A-LL, CEM III/A and CEM II/B-Q) were examined for their fire-induced spalling behaviour. In addition, a mix with PP fibres was investigated for each concrete. The experiments were conducted on ring-restrained cylindrical specimens exposed to the hydrocarbon fire curve. The results showed that the cement type influences spalling behaviour. Samples with CEM I spalled the least, followed by CEM II/A-LL and CEM III/A. Finally, samples with CEM II/B-Q showed the most severe damage. It was found that the spalling behaviour of different concretes correlates with the moisture content before exposure to fire, meaning that higher moisture content leads to higher spalling susceptibility. The use of 2 kg/m³ PP fibres completely inhibited spalling regardless of the cement type used and therefore remains a successful avoidance strategy.

Keywords: Fire-induced concrete spalling; normal strength concrete; blended Portland cement; SCM; PP-fibres

1 INTRODUCTION

Cement is the most used material in the world, and as the world's population grows, so does the demand for more buildings and infrastructure rise [1]. However, cement clinker production is associated with high CO2 emissions that are mainly caused by the decomposition of limestone and the use of fossil fuels for rotary kilns. In total, the cement industry is responsible for approximately 8% of the global CO2 emissions [2]. One strategy for lowering cement's CO2 emissions is to reduce the clinker factor. This is achieved by replacing cement clinker with supplementary cementitious materials (SCMs) such as fly ash (FA), granulated blast furnace slag (GBFS) or calcined clays. The utilisation of calcined clays in particular is expected to increase, as reduced availability of slag and fly ash is forecast for Europe [2]. Therefore, blended cements with a reduced clinker factor will become an increasingly important aspect for the construction industry.

Concrete structures exposed to fire can experience heavy damage due to explosive spalling. This results on the one hand in reducing the load-bearing cross-section and on the other hand in exposing reinforcement [3]. The reasons behind explosive concrete spalling are not yet fully understood. Concrete is a

[1] Bundesanstalt für Materialforschung und -prüfung
e-mail: tim.pittrich@bam.de, ORCID: https://orcid.org/0009-0003-4397-1958
[2] Bundesanstalt für Materialforschung und -prüfung
e-mail: ludwig.stelzner@bam.de, ORCID: https://orcid.org/0009-0007-3955-7841
[3] Bundesanstalt für Materialforschung und -prüfung
e-mail: frank.weise@bam.de, ORCID: https://orcid.org/0000-0001-6441-0058

multicomponent material consisting of cement paste and aggregates; however, the individual components behave in contrasting ways during heating. The aggregates dilate while the hardened cement paste shrinks from a temperature of approx. 150 °C, resulting in stresses and the formation of microcracks. Additionally, concrete's low thermal diffusivity leads to high thermal gradients between the hot, fire-exposed side and the cool interior. This causes restrained thermal dilation, the obstruction of which results in high compressive stresses close to the fire-exposed surface [4]. These compressive biaxial thermal stresses parallel to the heated surface produce tensile stress perpendicular to the heated surface according to [5], [6]. Exceeding the tensile strength causes brittle fracture of the concrete, described as spalling. Another approach to describing concrete spalling originated with the so-called "moisture clog'' theory by Shorter and Harmathy [7], later developed in more depth by [8]. The authors state that pore pressure inside concrete rises when exposed to fire. Subsequently, water vapour moves out of the specimen towards both the heated surface and the concrete's cooler interior. The lower temperatures further inside the specimen lead to the condensation of water vapour. The ongoing accumulation of liquid water continues until an impermeable fully saturated zone has developed. This impermeable layer prevents any further moisture transport, causing a rapid rise in pore pressure. If the pore pressure exceeds the transversal tensile strength of the concrete, the material starts to crack and spall. The measurement of pore pressure at fast heating rates proved to be difficult, as induced cracks lead to a rapid pressure drop [9]. Therefore, the relation between pore pressure and explosive concrete spalling is not yet totally clarified. Another approach is the boiling liquid expanding water explosion theory (BLEVE). The theory states that when water is heated above 100 °C, it remains liquid as long as a certain pressure is present. When the pressure suddenly drops, the liquid water turns into steam, releasing all the stored energy and thus causing an explosion [10]. The heat-induced moisture transport and the existence of the "moisture clog'' were experimentally confirmed in studies by [11-13].

An effective strategy to avoid spalling is the addition of polypropylene fibres (PP fibres) [14, 15]. After the fibres melt at around 170 °C, expansion space is available in the form of empty fibre beds connected through mechanically induced microcracks. This induced network of canals supports the release of water vapour to the outside, reducing the overall moisture content and steam pressure in the system and thus minimizing the spalling risk [14].

The information available in the literature does not provide clear insights into the relation of cement type to the susceptibility to concrete spalling. Hager et al.[16] investigated concretes containing CEM I 42,5 R and CEM III/A 42,5 N under the ISO 834 fire curve. The experiments showed greater spalling for concretes containing CEM I, even though higher permeability and lower compressive strength were measured for those types of concretes [17]. The authors suggested no explanation for these contrary results. Extensive studies by Reiners [18] using the ISO 834 fire curve showed the following results: the most severe spalling was observed for concretes containing CEM III/A 42,5 N, followed by CEM II/B-V 42,5 R. Concretes containing CEM II/A-LL 42,5 N and CEM I 42,5 R exhibited only comparatively low amounts of spalling under restrained conditions. Equal experiments without restraint showed similar results, except that concrete with CEM I or CEM II/A-LL did not spall [18]. Miah [19] investigated the spalling behaviour of concretes containing CEM II/A-LL 42,5 R and CEM III/A 42,5 N under different applied loads using ISO 834 fire exposure. While unloaded specimens did not spall in both cases, uniaxial loaded samples with CEM II/A-LL showed spalling. In the case of biaxal loading, it was not clearly distinguishable which cement type led to more spalling on average [19]. Lublóy et al. [20] studied concretes with CEM I 42,5 N and CEM II/A-P 42,5 N as well as CEM II/A-V 42,5 R. At temperatures of 500°C, spalling of the cube corners was noticed for CEM I concrete. Concretes with other types of cement experienced no spalling. Kirnbauer et al. [21] investigated the spalling behaviour of CEM I 42,5 N, CEM II/A-LL 42,5 R and a sulphate slag cement concrete by applying the ISO 834 curve. Summarized, concretes with sulphate slag cement and CEM II/A-LL led to more intense spalling than concretes with CEM I [21]. Research on the high temperature behaviour of concretes with metakaolin was carried out by Poon et al.[22]. The authors replaced 5%, 10% and 20% by weight of Portland cement in normal and high-strength concrete with metakaolin. The researchers observed more spalling with increasing metakaolin content in both cases when heating the specimens up to 800 °C [22].

This paper presents the results of fire spalling tests of normal strength concretes (NSC) containing different types of blended cement with and without PP fibres. The aim of the research was to identify how different SCMs influence the spalling behaviour of concretes. Of special interest here was cement containing

calcined clays. Up to this point, no in-depth research concerning the spalling behaviour of calcined clay cement concrete has been carried out. Furthermore, the performance of PP fibres in concrete mixes with different binders was also investigated.

2 RAW MATERIALS AND MIX DESIGN

Table 1 displays the chosen cements classified according to DIN EN 197-1 [23] and their composition. All cements contained Portland cement clinker from the same manufacturing batch and only differed in the type and quantity of SCM. The kaolinitic-illitic clay was calcined at 700 °C to generate pozzolanic properties. Quarzitic aggregates with a grain size up to 16 mm were used in all concrete mixtures. The superplasticizer used throughout the work was a polycarboxylate ether-based product. Lastly, PP fibres of l = 6 mm and Ø = 15.4 µm were used.

Table 1. Composition of the cements used

	CEM I 42,5 N	CEM II/A-LL 42,5 N	CEM III/A 42,5 N	CEM II/B-Q 42,5 N
Portland cement clinker [wt.%]	95.7	85.7	55.8	71.6
Limestone [wt.%]	4.3	14.3	3.8	3.4
Blast furnace slag [wt.%]	-	-	40.4	-
Calcined clay [wt.%]	-	-	-	25.0

Eight different mix designs were tested in total: for each cement one mix without and one mix with PP fibres (Table 2). The water to cement ratio (w/c) was kept equal in all formulations at 0.47. Superplasticizer was not needed in the formulations without PP fibres, except for the one with calcined clays. In the further mixes, 2 kg/m³ PP fibres were added, as recommended in the Eurocode (EN 1992-1-2:2004) [24]. The mix designs with PP fibres contained superplasticiser in different amounts to ensure comparable workability in the fresh concrete state. The compressive cube strength was determined after 28 d and on the day of fire testing (at least 90 d).

Table 2. Concrete mix designs and properties [kg/m³]

	CEM I		CEM II/A-LL		CEM III/A		CEM II/B-Q	
	PC	PC_pp	LC	LC_pp	SC	SC_pp	CC	CC_pp
cement	420		420		420		420	
water (w/c)	197 (0.47)		197 (0.47)		197 (0.47)		197 (0.47)	
superplasticiser	0	1.5	0	3.4	0	2.1	2.5	5.0
PP fibres	0	2	0	2	0	2	0	2
quarzitic aggregates								
0 / 2 mm	646	640	646	634	646	637	634	628
2/ 4 mm	153	152	153	150	153	151	150	149
4/ 8 mm	221	219	221	217	221	218	217	215
8/ 16 mm	679	675	679	668	679	669	666	661
compressive cube strength [MPa]								
28 d	46	46	51	54	57	65	57	60
> 90 d	50	52	55	61	59	73	56	62

3 METHODOLOGY

3.1 Sample preparation

For the fire test two cylindrical samples (h = 29 cm; Ø = 47 cm) of each concrete mix were prepared. The samples were demoulded one day after casting and subsequently placed under water for 6 more days. Afterwards, the samples were stored in a climate chamber at (20 ± 2) °C and (65 ± 5) % RH until the day of testing. Additionally, the lateral surface was covered to provide a 1D moisture transport.

To generate restraint testing conditions, the cylindrical specimens were grouted into a steel ring (outer Ø = 51 cm) after Klimek et al. [25], a methodology based on the work of Ozawa et al. [26]. Both the steel ring and the outer boundary of the concrete remain insulated during the fire test. Therefore, the reduced thermal dilation of the steel ring leads to restraint stresses. The restrained set up and the disabled moisture transport were chosen to simulate the conditions in the centre of a large-scale concrete wall.

3.2 Experimental set-up

The fire tests were conducted in an oil burner furnace running the hydrocarbon fire curve for 1 h under unloaded conditions. The fire room had a volume of 1 m³ and the samples were placed at a furnace opening of 0.25 m². The fire exposed area measured 0.14 m², thus the remaining specimen was insulated by a vermiculite board and high temperature mineral wool. The temperature inside the concrete samples was measured with embedded thermocouples Type K, at depths of 5, 15, 30, 50 and 100 mm from the fire-exposed surface. Acoustic signals of spalling events were recorded with a microphone placed outside the furnace. The moisture content was determined according to the recommendation of RILEM TC 256-SPF [23], by drying two cylindrical samples (h = 30 cm; Ø = 10 cm) at (105 ± 5) °C until mass equilibrium. Mass equilibrium was reached when the mass difference between two consecutive weight intervals within 24 h was less than 0.1 %. Moisture distribution and content were additionally determined on equally treated accompanying concrete cylinders (h = 29 cm; Ø = 7 cm) by means of ^{1}H-NMR relaxometry. The technique can detect water content ranging from water bound in gel pores to free water in coarse pores, which distinguishes it from the method above. The topography of the concrete specimens was measured before and after fire exposure with a handheld 3D laser scanner. In addition, the spalled volume was calculated by defining an assessment area equal to 90% of the fire exposed surface and the corresponding spalling depths according to [27]. Figure 1 shows the set-up of the spalling experiments as well as a sketch of the test specimen.

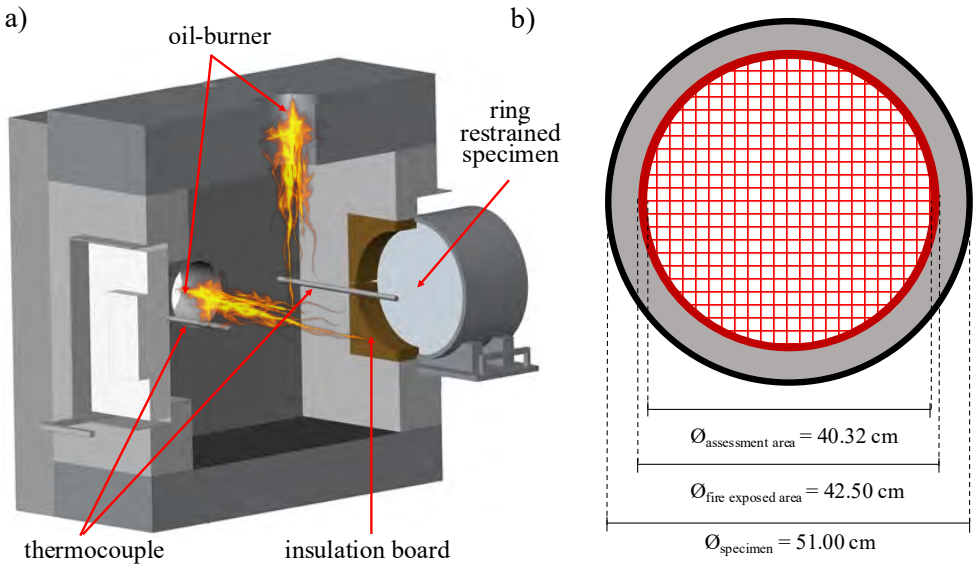


Figure 1. a) Oil-burner furnace with ring restrained concrete specimen b) sketch of clyindrical concrete specimen

4 RESULTS

4.1 Initial moisture content and distribution

Table 3 gives an overview of the moisture content determined by mass loss as stated above. As the addition of PP fibres showed no drastic influence on the initial moisture content, it was assumed that the moisture content of CC and CC_pp was comparable. The captured data showed that PC had the overall lowest moisture content and mix CC_pp the highest.

Table 3. Moisture content

	PC	PC_pp	LC	LC_pp	SC	SC_pp	CC	CC_pp
[wt.%]	5.43	5.66	5.67	5.46	5.60	5.44	-	6.08

Figure 2 presents the initial detectable water content of the concrete cylinders after 90 d up to a depth of 116 mm, measured in 2 mm steps. It shows that all concretes displayed a drying gradient from the concrete centre to the surface. The gradient extended to similar depths in all cases but differed in its absolute moisture content. The mean moisture content for PC was 8.41 Vol.% and for LC 9.05 Vol.%. SC concrete showed slightly higher moisture with an average of 9.59 Vol.%. Concrete mix CC showed the overall highest moisture content with an average value of 10.39 Vol.% The moisture content for the fibre mixes follows the same sequence, as PC_pp presented the lowest amount of water with 8.60 Vol.% followed by LC_pp and SC_pp with 8.98 Vol.% and 9.29 Vol.% respectively. Lastly, CC_pp contained the most water with 10.58 Vol.%. No significant differences between the mixes with and without fibres were observed.

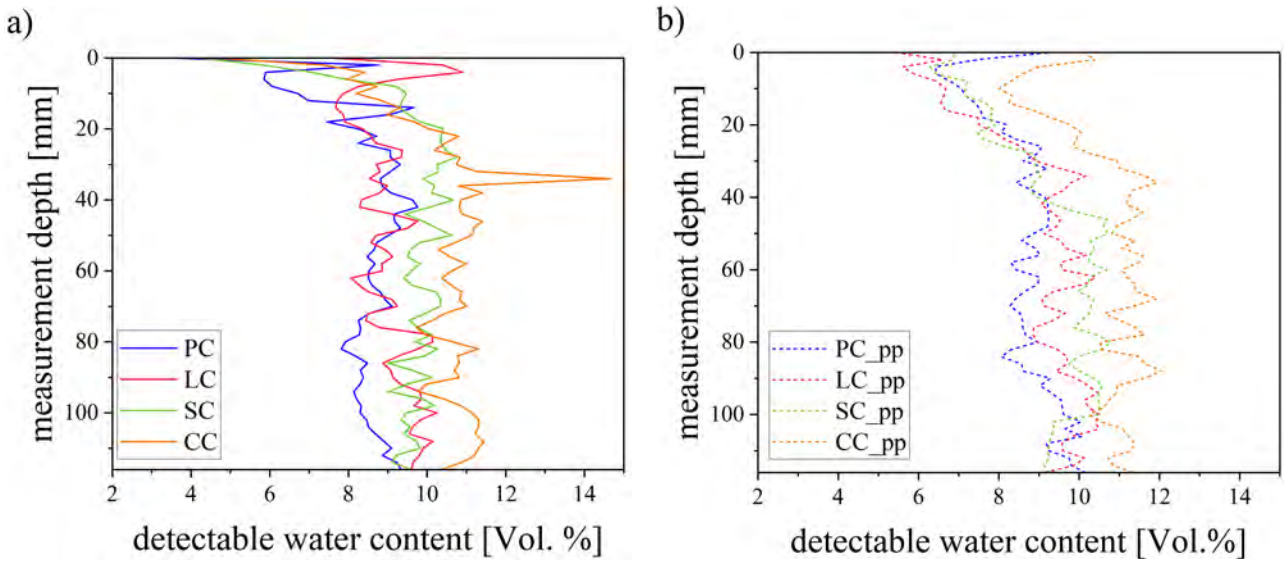


Figure 2. Detectable water content measured by ^{1}H-NMR relaxometry a) mixes without fibres b) mixes with fibres

Both results show that with the same amount of water during preparation, different moisture states occur after 90 days of curing, depending on the binder used.

4.2 Temperature propagation and acoustic registered spalling events

The temperature profiles of the different concretes are shown below in Figures 3 and 4 for one test specimen per cement type. Explosive spalling was observed in each test specimen without PP fibres. The concrete with PC showed a rapid increase in temperature at the depths of 5 and 15 mm around minute 3 after test begin. This increase in temperature is associated with spalling events, uncovering the designated thermocouples, and therefore indicating the approximate depths of spalling. Five spalling events were recorded for each of the specimens tested. Concrete LC exhibited a heavy temperature increase beginning

after 2 mins at the thermocouples embedded at 5, 15 and 30 mm from the fire exposed surface. In total, 70 spalling events for specimen one and 96 for specimen two were counted. Concrete mix SC also showed a rapid temperature rise in minute 3 measured by the first three thermocouples. 88 spalling events were recorded for specimen one and 134 for specimen two. Mix design CC also experienced a high temperature increase after roughly 2 mins. The spalling of the concrete exposed the top four thermocouples. Additionally, 134 and 216 spalling events were counted, respectively. The appearance of temperature plateaus was recorded in all specimens, particularly with the thermocouple located at 100 mm depth. This phenomenon is associated with the evaporation of liquid water, an endothermic process consuming energy. No spalling events were recorded for any sample with PP fibres, leading to a much lower temperature development inside the specimens. Again, temperature plateaus were observed caused by the evaporation of water. It is notable that the plateaus occur at lower temperatures compared to the non-fibre mixes, which indicates lower pressure during phase transition.

Of further interest are the temperatures measured at 50 mm depth, where the reinforcement is usually located. Concrete PC showed a maximum temperature of 400 °C, mix LC and SC showed maximum temperatures of approximately 650 °C and 600 °C, respectively. Mix CC showed a maximum temperature of above 1000 °C. The maximum recorded temperature for PP fibre concretes was around 200 °C, independent of the cement type utilized. The results show that the use of PP fibres would effectively reduce the heating of a potential steel reinforcement.

Furthermore, the temperature of the steel ring was measured at three different locations at a depth of 30 mm for one of each sample. The results always displayed lower temperatures for the steel ring compared to the concrete member (after 30 mins maximum steel temperature 270 °C), confirming the idea of a restraint testing regime by differing thermal dilations. This is consistent with the findings of Klimek et al. who used a similar test setup [25].

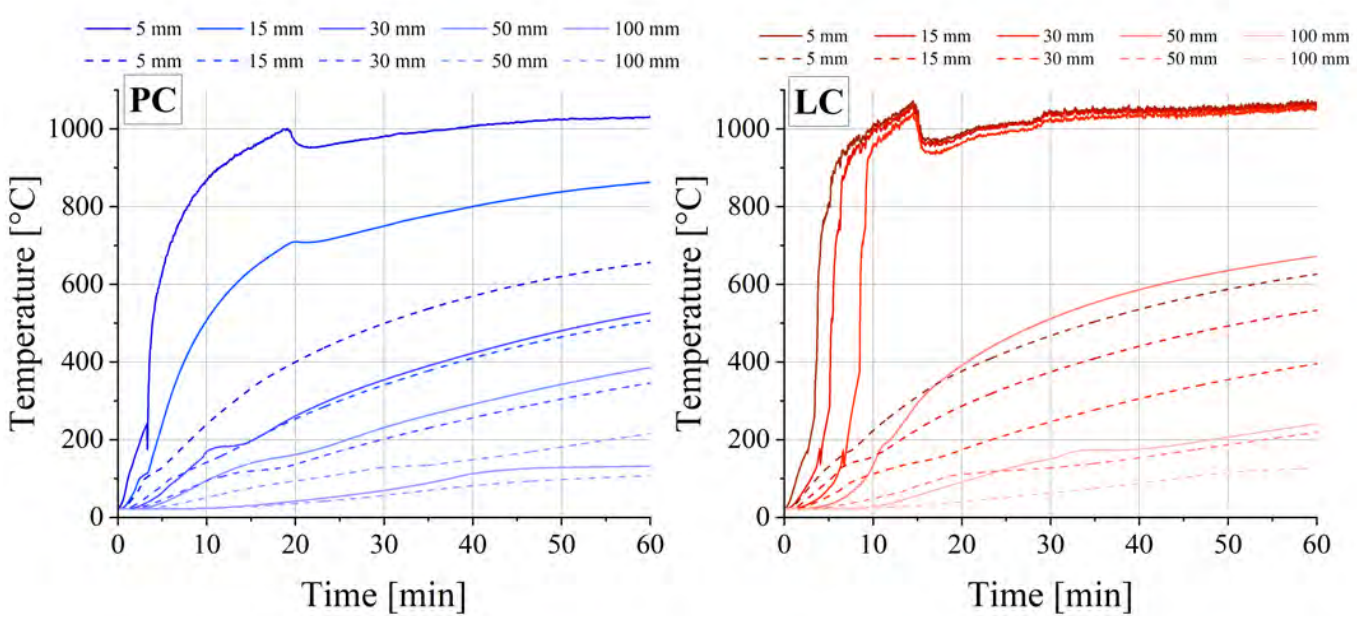


Figure 3. Concrete temperatures of mix PC and LC with applied HC curve (without PP—) (with PP ----)

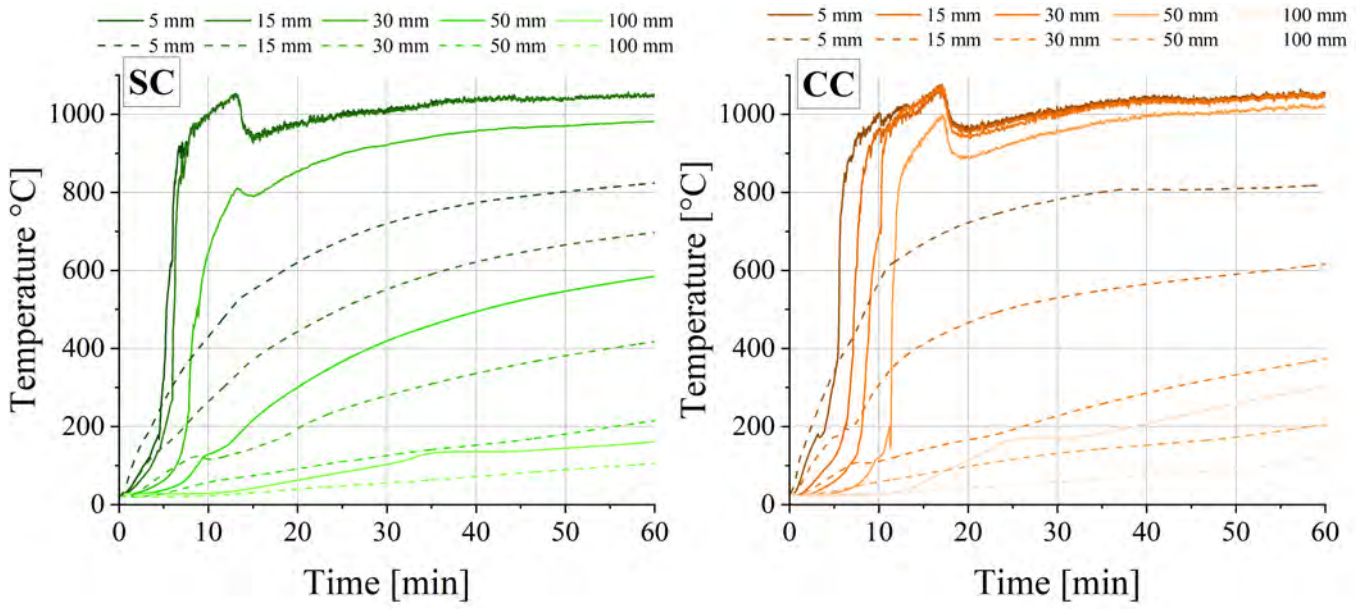


Figure 4. Concrete temperatures of mix SC and CC with applied HC curve (without PP—) (with PP ----)

4.3 3D surface analysis

The results of the 3D surface analysis are summarized in Figure 5 as locally resolved colour coded spalling depths. The different concretes containing various types of cements exhibit different spalling behaviour. PC showed the lowest amount of damage with a spalling volume of 786.83 cm³ and 321.71 cm³. Maximum spalling depths of 15 and 13 mm were recorded. While sample one showed a homogeneous spalled surface, only about half the area of sample two spalled. The residual area showed slight local expansions. Mix LC experienced heavier spalling with a spalled volume of 2385.21 cm³ and 3025.23 cm³. The recorded maximum spalling depth was 46 and 53 mm, respectively. Similar results could be observed for concrete SC. The specimens' entire fire exposed surface spalled and a volume loss of 2302.6 cm³ and 2856.15 cm³ was measured. The maximum spalling depths were 50 and 52 mm, respectively. Samples of mixture CC were most prone to spalling with recorded volumes of 2798.86 cm³ and 4084.07 cm³; their maximum spalling depths sat at 56 and 72 mm. Both the mean spalling depth and the mean spalling volume are given in Table 4 below.

Concretes containing PP fibres did not spall, regardless of the cement type used. Slight damage in the form of cracks and expansions up to 5 mm were determined for every specimen. A change in colour from grey to whitish and reddish colours on the concrete surface was visible. According to Hager [3] the colour change to white is caused by the transformation of $CaCO_3$ to quicklime and the reddish colours appear due to the oxidation of iron-containing mineral composites in the quarzitic aggregates. It should be noted that during the fire test of SC_pp_1 the top oil- burner failed and therefore, the desired HC fire curve was not reached.

Table 4. Mean spalling depth and mean spalling volume of concretes without PP fibres

	PC	LC	SC	CC
$depth_{mean}$ [mm]	4.34	23.54	22.45	26.96
V_{mean} [cm³]	554.27	2705.22	2579.38	3441.47
V_{mean} [Vol. %]	1.49	7.28	6.94	9.26

Concrete specimens	
without PP-fibres	with PP-fibres

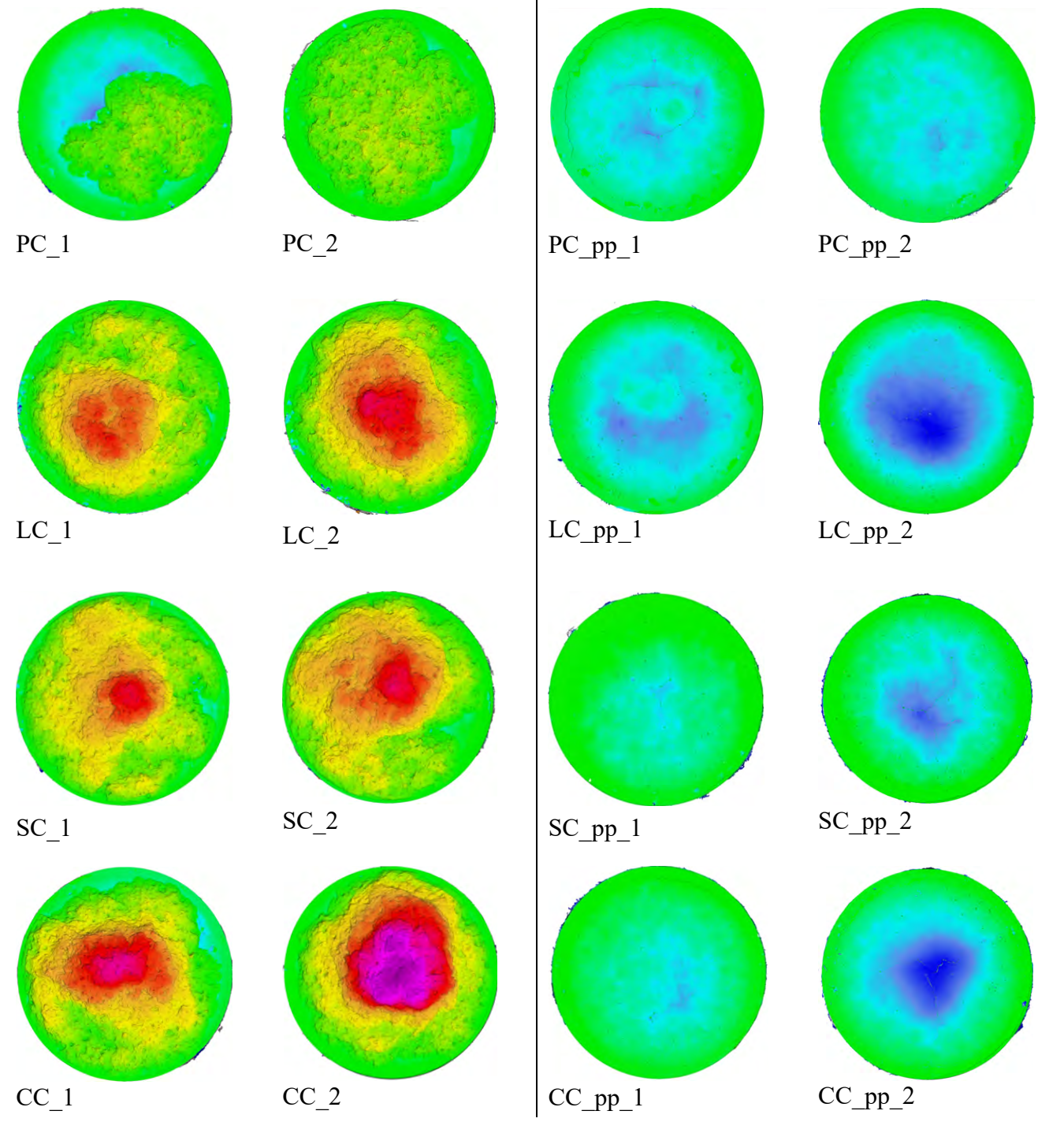


Figure 5. Ring restrained specimens after fire exposure

5 DISCUSSION

Although cements with the same strength class were provided by the same manufacturer and an equal mix design was applied for all concretes, differences in compressive strength appeared. This should be kept in mind when referring to the spalling experiments, since a higher compressive strength leads to more spalling. Also, in this study the concrete mix with CEM I exhibited the lowest strength and the lowest amount of spalling. The problem, however, seems to be unavoidable since an adaption of strength would suggest a change of mix design, most probably affecting the water content. Moreover, the adjustment of the water content to obtain equal compressive strength values would essentially influence the spalling behaviour of the concretes. Furthermore, it is seen that the addition of 2 kg/m³ PP fibres lead to an increase of the compressive strength compared to the mixtures without fibre addition. Mixture SC_pp in particular experienced a heavy strength gain of 24 %. Results in literature show that fluctuations and changes of strength appear dependent on the fibre properties and dosage [28, 29]. The effectiveness of PP fibres was proven in every concrete, as no spalling was observed in any case even though compressive strengths increased. Since the fibres primarily affect internal moisture transport, this further emphasises that thermohydraulic processes are decisive for explosive spalling.

The experiments presented here clearly showed the influence of cement type on the spalling behaviour of NSC. The maximum spalling depths in concretes with blended cements reached values where steel reinforcement could be uncovered and directly exposed by the fire. Direct heat exposure of the steel member can be critical for the residual stability of a building during a fire. The study also shows the relationship between moisture content and spalling intensity, as increasing spalling was observed with increasing moisture content. While all specimens were prepared with the same w/c ratio of 0.47, the water content varied on the day of testing. This is even more emphasised when looking at the ^{1}H-NMR Relaxometry data, which provides insights into the amount of water beyond the free water content. Therefore, the influencing water content must consist of the amount of chemical, physical and free water predetermined by the mineral phase composition of the cements used. For example, an increasing change in the morphology of outer product C-S-H from a fibrillar to a denser foil-like structure is seen in systems containing slag and pozzolana [30]. A denser microstructure with possibly lower permeability would slow the drying process during conditioning as well as disabling the water release at fire exposure. The high availability of water plus the impossibility for it to escape consequently lead to increased explosive spalling of concretes with blended cements. The findings are in agreement with the literature, where it can be found that high moisture content is responsible for heavy spalling [31].

For further understanding of the moisture influence on the fire spalling behaviour of concretes with blended cements, pore size-specific moisture distribution studies will be carried out on specimens before and after heat exposure. In addition, porosity and permeability experiments are planned to finalise the picture.

6 CONCLUSIONS

This paper provides new insights into the spalling behaviour of normal strength concrete containing different types of blended Portland cement. The above-mentioned results of this study can be summed up as follows:

- The cement type influences the explosive spalling susceptibility of NSC. Concretes with CEM I only experienced minimal spalling with an average depth of 4 mm. Concretes containing CEM II/A-LL and CEM III/A already showed deeper spalling with an average depth of 23.5 and 22.5 mm, respectively. The highest average spalling depth was recorded for concrete made with CEM II/B-Q with a value of 27 mm.
- There is a relation between moisture content and spalling amount, as increasing spalling was observed with increasing initial moisture. The respective free water content, determined by drying cylinders at 105 °C, was 5.43 wt.% for CEM I concrete, 5.67 wt.% for CEM II/A-LL concrete, 5.60 wt.% for CEM III/A concrete and 6.08 wt.% for CEM II/B-Q concrete. The results were confirmed by the ^{1}H-NMR relaxometry measurements.

- Spalling occurred between minute 2 and 15 in all concrete mixes without fibre addition. The number of acoustically recorded spalling events correlates with the intensity of damage.
- It was proven that 2 kg/m³ PP fibres inhibit explosive spalling regardless of the cement type in NSC.

Under the given conditions every concrete with a clinker-reduced cement showed worse fire-induced spalling behaviour than concrete with OPC. Above all, concrete with calcined clay-containing binder was damaged the most. This should be taken into consideration when thinking about the utilization of these cements in cases where fire resistance is crucial. However, the problem can be avoided by adding PP-fibres.

ACKNOWLEDGEMENT

We gratefully acknowledge the support and extend our gratitude to the German Research Foundation (DFG) for their financial support, which has been instrumental in conducting the investigations presented in this paper. We also express our sincere appreciation to our colleagues, specifically acknowledging the collaborative efforts of BAM divisions 7.1 “Building Materials”, 7.3 “Fire Engineering”, and 7.4 “Technology of Construction Materials”. Their expertise and resources have significantly enriched the scope and depth of our study.

REFERENCES

1. Schneider,M., The cement industry on the way to a low-carbon future, Cement and Concrete Research 124 (2019).
2. Favier, A., De Wolf, C., Scrivener, K., Habert, G., A sustainable future for the European Cement and Concrete Industry - Technology assessment for full decarbonisation of the industry by 2050, ETH Zurich, Zurich (2018).
3. Hager, I., Behaviour of cement concrete at high temperature, Bulletin of the Polish Academy of Sciences, Technical Sciences 61(1) (2013).
4. Fu, Y., Li, L., Study on mechanism of thermal spalling in concrete exposed to elevated temperatures, Materials and Structures 44 (2011) 361-376.
5. Bazant, Z.P., Analysis of pore pressure, thermal stresses and fracture in rapidly heated concrete, in: Phan, L.T., Carion, N.J., Duthinh, D., Garboczi, E., (Eds.) Int. Workshop on Fire Performance of High-Strength Concrete, National Institute for Standards and Technology, Gaithersburg, (1997) 155-164.
6. Ulm, F.J., Coussy, O., Bazant, Z.P., The ‘‘Chunnel’’ fire I: chemoplastic softening in rapidly heated concrete, Journal of Engineering Mechanics 125(3) (1999) 272-282.
7. Shorter, G.W., Harmathy, T.Z., Discussion on the Fire-resistance of prestressed concrete beams, Institute of Civil Engineers (1961).
8. Harmathy, T.Z., Effect of moisture on the fire endurance of building elements, ASTM Special Technical Publication No. 385 (1965).
9. Stelzner, L., Analyse des thermisch induzierten Feuchtetransports in gefügedichten Beton, Werkstoffe im Bauwesen, Universität Stuttgart (2021).
10. Ichikawa, Y., Prediction of Pore Pressures, Heat and Moisture Transfer Leading to Spalling of Concrete during Fire, Department of Civil and Environmental Engineering, University of London, 2000.
11. van der Heijden, G.H.A., van Bijnen, R.M.W., Pel, L., Huinink, H.P., Moisture transport in heated concrete, as studied by NMR, and its consequences for fire spalling, Cement and Concrete Research 37 (2007) 894-901.
12. Jansson, R., Fire Spalling of Concrete, KTH Architecture and the Built Enviroment, KTH Royal Institute of Technology, Stockholm (2013).
13. Stelzner, L., Powierza, B., Oesch, T., Dlugosch, R., Weise, F., Thermally-induced moisture transport in high-performance concrete studied by X-ray-CT and 1H-NMR, Construction and Building Materials 224 (2019) 600-609.
14. Pistol, K., Weise, F., Meng, B., Schneider, U., The mode of action of polypropylene fibres in high performance concrete at high temperatures, 2nd International RILEM Workshop on Concrete Spalling due to Fire Exposure, (2011), 289-296.

15. Poon, C-S., Shui, ZH., Lam, L., Compressive behaviour of fibre reinforced high-performance concrete subjected to elevated temperatures, Cement and Concrete Research 34 (2004) 2215-2222.
16. Hager, I., Mróz, K., Tracz, T., Concrete propensity to fire spalling: Testing and observations, MATEC Web of Conf. 163 (2018).
17. Hager, I., Tracz, T., Choinska, M., Mróz, K., Effect of Cement Type on the Mechanical Behaviour and Permeability of Concrete Subjected to High Temperatures, Materials 12(18) (2019).
18. Reiners, J., The Influence of the Physical and Chemical Properties of Hardened Cement Paste on the Fire-Induced Spalling of Concrete Technische Universität Carolo-Wilhelmina zu Braunschweig (2023).
19. Miah, M.J., The Effect of Compressive Loading and Cement Type on the Fire Spalling Behaviour of Concrete, Université de Pau et des Pays de l'Adour-Laboratoire SIAME (2017).
20. Lublóy, É., Kopecskó, K., Balázs, G.L., Restás, Á., Szilágyi, I.M., Improved fire resistance by using Portland-pozzolana or Portland-fly ash cements, Journal of Thermal Analysis and Calorimetry 129 (2017) 925-936.
21. Kirnbauer, J., Schneider, U., Influence of cement type and aggregate shape on explosive concrete spalling, 2nd International RILEM Workshop on Concrete Spalling due to Fire Exposure, Delft, (2011), 432-439.
22. Poon, C-S., Azhar, S., Anson, M., Wong, Y-L., Performance of metakaolin concrete at elevated temperatures, Cement & Concrete Composites 25 (2003) 83-89.
23. D.I.f.N. DIN, Cement – Part 1: Composition, specifications and conformity criteria for common cements, Beuth Verlag GmbH, Berlin (2011).
24. D.I.f.N. DIN, Eurocode 2: Design of concrete structures Part 1-2: General rules – Structural fire design, Beuth Verlag GmbH, Berlin, (2010).
25. Klimek, A., Stelzner, L., Hothan, S., Zehfuß, J., Influence of thermal strain on concrete spalling, Materials and Structures 57(15), (2024).
26. Ozawa, M., Tanibe, T., Kamata, R., Uchida, Y., Rokugo, K., Parajuli, S.S., Behaviour of ring-restrained high-performance concrete under extreme heating and development of screening test, Construction and Building Materials 162 (2018) 215-228.
27. Pimienta, P. et al., Recommendation of RILEM TC 256-SPF on the method of testing concrete spalling due to fire: material screening test, Materials and Structures 56(164) (2023).
28. Maluk, C., Bisby, L., Terassi, G.P., Effects of polypropylene fibre type and dose on the propensity for heat-induced concrete spalling, Engineering Structures 141 (2017) 584-595.
29. Mashrei, M.A., Sultan, A.A., Mahdi, A.M., Effects of Polypropylene Fibres on Compressive and Flexural Strength of Concrete Material, International Journal of Civil Engineering and Technology (IJCIET) 9(11) (2018) 2208-2217.
30. Richardson, I.G., The nature of C-S-H in hardened cements, Cement and Concrete Research 29 (1999) 1131-1147.
31. Hertz, K., Limits of spalling of fire-exposed concrete, Fire Safety Journal 38 (2003) 103-116.

Paper 2:

Thermally induced moisture transport in concrete with different types of blended Portland cement studied by ^{1}H-NMR relaxometry

Publisher's version

Published in *Materials and Structures*

Volume 59, 2026

DOI: https://doi.org/10.1617/s11527-026-03025-4

Authors: Tim Pittrich, Simon Peters, Günther Meschke, Frank Weise, Ludwig Stelzner

Materials and Structures (2026) 59:133
https://doi.org/10.1617/s11527-026-03025-4

ORIGINAL ARTICLE

Thermally induced moisture transport in concrete with different types of blended Portland cement studied by ^{1}H-NMR relaxometry

Tim Pittrich · Simon Peters · Günther Meschke · Frank Weise · Ludwig Stelzner

Received: 14 April 2025 / Revised: 21 November 2025 / Accepted: 19 February 2026
© The Author(s) 2026

Abstract Clinker-reduced cements are gaining in popularity as part of efforts to lower the construction industry's CO_2 footprint. Past studies showed that utilization of these cements negatively influences the fire-induced spalling behavior of concrete, which is highly influenced by thermohydraulic damage mechanisms. Therefore, thermally induced moisture transport in normal strength concretes made with different types of blended cements (CEM I, CEM II/A-LL, CEM III/A and CEM II/B-Q) was investigated by means of ^{1}H-NMR relaxometry in combination with supportive side investigations concerning permeability and porosity. In addition, a numerical model was used to analyze in-situ moisture development during high temperature exposure. The results show that the cement type influences both initial moisture content and pore size-specific moisture distribution. This was primarily reflected in an increased water content in CEM III/A and CEM II/B-Q concretes as well as a comparable high gel pore water fraction in CEM II/B-Q concrete before heating. After heating, a similar degree of pore coarsening from gel to capillary pore was observed in all samples. Although the measurements were only conducted after, not during, high temperature exposure, the depth of the drying front and the extent of the moisture clog could be determined. With the additional numerical analysis, it can be assumed that during high temperature load, the drying front is less advanced and the moisture clog even more pronounced. In conclusion, it can be stated that the increased spalling susceptibility in blended cement concrete is caused by the lower initial permeability and increased moisture content.

Keywords Fire concrete spalling · Thermally induced moisture transport · Blended cements · ^{1}H-NMR

T. Pittrich (✉) · F. Weise · L. Stelzner
Bundesanstalt für Materialforschung und -prüfung, Berlin, Germany
e-mail: tim.pittrich@bam.de

F. Weise
e-mail: frank.weise@bam.de

L. Stelzner
e-mail: ludwig.stelzner@bam.de

S. Peters · G. Meschke
Institute for Structural Mechanics, Ruhr-Universität Bochum, Bochum, Germany
e-mail: simon.peters@rub.de

G. Meschke
e-mail: guenther.meschke@rub.de

Published online: 03 March 2026

1 Introduction

To reduce the construction industry's CO_2 emissions, more cements with a reduced clinker factor are finding application in infrastructure and residential construction. Therefore, the risk of low-carbon concretes being exposed to fire rises. Concrete under fire can experience heavy damage caused by explosive

spalling. Results of different research groups showed that the cement type influences spalling behavior; however, no clear relation between cement type and spalling susceptibility has been discovered [1]. Furthermore, there is even less knowledge available on the driving mechanism behind this phenomenon. Fire-induced spalling of concrete is usually caused by thermomechanical and thermohydraulic mechanisms. The thermomechanical spalling mechanism is based on restrained thermal expansion caused by the temperature gradient inside the concrete. The restrained thermal dilation causes high compressive stresses close to the fire-exposed surface, ultimately leading to tensile stress perpendicular to the heated surface, which is responsible for spalling [2, 3]. In addition, the thermal mismatch between expanding aggregates and shrinking cement paste (< 150 °C) [4] leads to the formation of microcracks, which further promote the risk of spalling [5, 6]. The thermohydraulic spalling mechanism was first mentioned by Shorter and Harmathy [7], who described water vapor migration and subsequent accumulation inside the concrete member, known as the moisture clog theory. The moisture clog, a saturated water layer caused by the condensation of water vapor in the concrete's cooler interior, inhibits any further moisture transport. Thus, pore pressure exceeding the tensile strength of concrete rises inside the concrete, causing high stresses which finally lead to explosive concrete spalling. However, the relation between pore pressure and spalling was never clarified and many other possible explanations of thermohydraulic spalling mechanisms have been summarized by McNamee [5]. A common strategy to avoid fire induced concrete spalling is the addition of polypropylene fibers (PP fibers) to the mixture. The PP fibers melt at around 170 °C, creating a network of empty fiber beds and mechanically-induced microcracks which allow water vapor to escape, reducing pore pressure [8].

To understand the impact of moisture on fire-induced spalling of concrete, different experimental studies in recent years have investigated heat-induced moisture transport, confirming the existence of the moisture clog. Neutron radiography studies in high performance cement mortar heated up to 600 °C showed a pronounced drying front as well as an increase in water content in regions where the temperature was close to 100 °C [9]. Further neutron tomography imaging of in-situ heated mortar specimens with superabsorbent polymers (SAP) and SAP in combination with PP fibers was conducted by Toropovs et al. [10]. The researchers investigated mortar slabs (25 × 100 × 100 mm) heated to 550 °C on a copper heating plate and simultaneously measured temperature, pore pressure and moisture content. The sample without PP fibers spalled at a depth correlating to the drying front, while the sample with PP fibers stayed unharmed. A noticeably smoother drying front was recorded for the PP fiber sample, indicating less steep temperature variations and therefore reduced thermal stress and pore pressure, minimizing the risk of spalling. Also, Dauti et al. [11] analyzed in-situ heat-induced moisture transport in high performance concrete (HPC) by means of neutron tomography. Two different mixtures with maximum aggregate sizes of 4 and 8 mm respectively were cast in cylindrical samples (d = 3 cm) and heated up to 300 °C. The drying front started to develop after 10 min at around 170 °C for both samples; however a faster-moving drying front for the sample with bigger aggregates was recorded. This faster drying was attributed to a more well-established crack network induced by the bigger aggregates. Beyond the drying front, water accumulation was visible in both samples at slightly different depths. X-ray tomography studies by Powierza et al. [12] led to similar results. The observations on HPC cylinders (h = 10; d = 4 cm) covered by a Marcor ceramic and aluminum silicate wool casting heated up to 300 °C showed once more the development of a drying front with subsequent appearance of the moisture clog. Van der Heijden et al. [13] used nuclear magnetic resonance (NMR) relaxometry to study the moisture distribution in concrete cylinders equilibrated at different relative humidities (97%, 86%, 75% and 50% RH) heated above 300 °C. The authors concluded that a comparable development of the drying front and condensation happened in all samples. However, only specimens cured at 97% RH and 86% RH reached a fully saturated state described as complete clogging. Furthermore, it was stated that neither the drying front nor condensation influence heat transport in the samples. The work by Stelzner et al. [14] considered heat-induced moisture transport measured by X-ray tomography as well as ^{1}H-NMR relaxometry in HPC cylinders with and without PP fibers equal to [12]. In both methods the development of the drying front and the moisture clog were detected when exposed to temperatures of 300 °C.

The addition of PP fibers led to a faster-moving drying front towards larger depths within the specimen, demonstrating their effectiveness by increasing the material's permeability. While X-ray tomography delivered a three-dimensional in-situ resolution of the moisture transport, NMR results only provided information on water distribution before and after heating. However, with the latter it was possible to quantify the absolute detectable water content as well as recording the reconfiguration processes of water from small to large pores. An overall evolution from fine to coarse pores between 200 and 800 °C was also observed in NMR studies by Guo et al. [15]. Chen et al. [16] investigated the in-situ permeability development of mortar and concrete made with CEM II/B-M (LL-S) and CEM V/A during heating to 60 °C, 105 °C and 200 °C. They concluded that moisture clogging depends on several factors including heating rate, sample scale, degree of saturation, and cement type. The researchers found that height-to-diameter ratios of approx. 2, heating rates between 2.5 and 4.9 K/min, and saturation levels starting at 45% were most critical for clogging. Moreover, it was observed that not only free water but also water released during dehydration of the cementitious matrix contributes to gas retention. Consequently, cement type plays a significant role in the clogging mechanism. Due to the higher thermal stability of CEM V cement paste, dehydration occurred more slowly, leading to a more uniform water release as temperature rises causing weaker gas retention. However, the higher initial saturation found in this type of mortar (exceeding 80%) ultimately also led to severe clogging.

In our previous work, noticeable differences in the spalling behavior of normal strength concrete with different types of blended cements were observed [17]. The spalling susceptibility of the concretes increased in the following order for the used cements CEM I (low), CEM II/A-LL (medium), CEM III/A (medium) and CEM II/B-Q (high) as displayed in Fig. 1. However, no information on the influence of the cement type on thermally induced moisture transport is available as most studies focus on concretes with Portland cement in HSC. Understanding moisture transfer in these concretes is particularly important as it is known that the binder type significantly influences both micro- and pore structure [18, 19] as well as the dehydration behavior of the cementitious matrix [20, 21]. Furthermore, as mentioned above, the utilization of clinker-reduced cements is increasing in practice. Against this background, the aim of this article is to fundamentally investigate the role of thermohydraulic spalling mechanisms in concretes with different types of blended cement. This work also covers the characterization of initial pore size distribution and evolution of the pore structure after heating. Based on the methodology of [14], ^{1}H-NMR relaxometry measurements were carried out on normal strength concretes made with four different types of cement before and after high temperature exposure. A numerical model was applied to simulate the course of the moisture transport during heating and

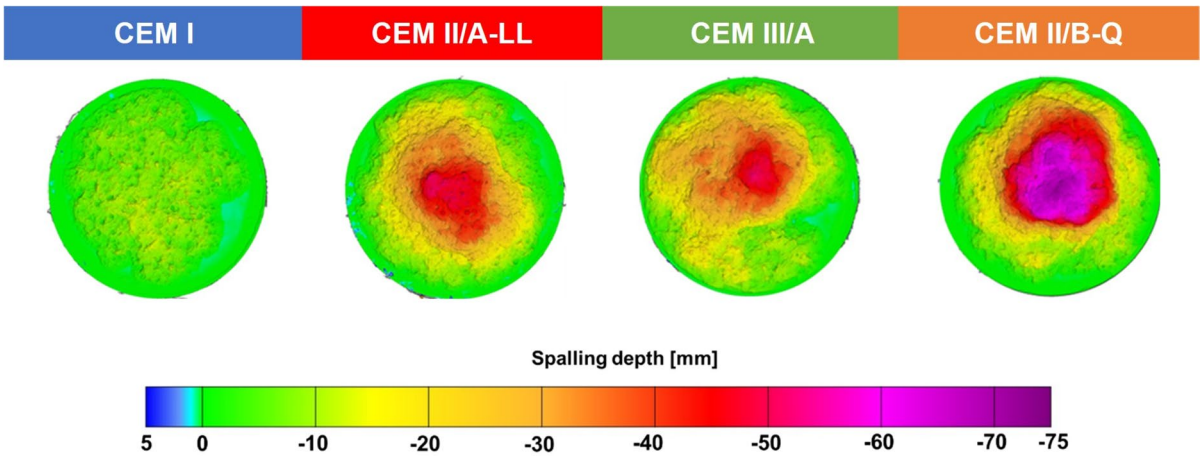


Fig. 1 Spalling depth of blended cement concretes after hydro-carbon fire exposure

Table 1 Main oxide composition of the cements (wt%)

Oxide	CEM I	CEM II/A-LL	CEM III/A	CEM II/B-Q
SiO_2	19.84	18.39	26.44	33.99
Al_2O_3	5.11	4.81	7.29	8.38
Fe_2O_3	2.99	2.66	1.91	3.00
CaO	61.87	60.68	52.47	45.58

Table 2 Blaine values of the cements (cm^2/g)

Cement	CEM I	CEM II/A-LL	CEM III/A	CEM II/B-Q
Blaine value	2900	4650	4890	6050

cooling which was not possible experimentally. In addition, porosity and gas permeability measurements were carried out to provide further information on the pore structure and transport properties.

2 Materials

Four cements, CEM I 42.5 N, CEM II/A-LL 42.5 N, CEM III/A 42.5 N, and CEM II/B-Q 42.5 N in accordance with DIN-EN 197 [22] and quarzitic aggregates were used for the casting of the concrete specimens. All cements contain clinker from the same production batch. A calcined clay with medium reactivity made of a kaolinitic-illitic clay was used for the production of CEM II/B-Q. To ensure a reasonable relation between aggregate size and sample diameter, the original mixture given in [17] with a maximum aggregate size of 16 mm was sieved down to 8 mm. Furthermore, polycarboxylatether-based (PCE) superplasticizer was needed to ensure comparable workability of the concrete with calcined clay cement (CEM II/B-Q) to the rest of the group. All concrete samples were demolded 1 d after casting. Subsequently the samples were stored under water for 6 more days and finally kept in a climate chamber at (20 ± 2) °C and (65 ± 5) % RH according to DIN EN 12390-2 [23] until an age of at least 90 d was reached, as recommended in [24].

The main oxide composition of the cements is given in Table 1, the Blaine values are provided in Table 2. The exact concrete composition and the corresponding fresh and hardened concrete properties of the original 16 mm mixture can be found in Tables 3 and 4. All the different concrete compositions are abbreviated in this paper as PC—Portland cement concrete, LC—limestone cement concrete, SC—slag cement concrete and CC—calcined clay cement concrete.

Table 3 Concrete composition (kg/m^3)

	PC	LC	SC	CC
Cement	420	420	420	420
Water (*w/c*)	197 (0.47)	197 (0.47)	197 (0.47)	197 (0.47)
Superplasticizer	0	0	0	2.5
Quarzitic aggregate				
0/2 mm	646	640	640	634
2/ 4 mm	153	152	152	150
4/ 8 mm	221	219	219	217
(8/16 mm)	(679)	(674)	(674)	(666)

Table 4 Fresh and hardened concrete properties for the concrete composition with 16 mm aggregates

Concrete	Fresh concrete properties	Hardened concrete properties			
	Slump flow (mm)	$f_{c,m}$ (MPa)		Bulk density (kg/m^3)	
		28 d	90 d	28 d	90 d
PC	445	46	50	2300	2300
LC	395	51	55	2330	2313
SC	418	57	59	2290	2310
CC	390	57	56	2317	2307

Three cylinders (drilled cores) with the dimensions h = 5 cm and d = 5 cm were used for gas permeability measurements. The same sample type was also utilized for porosity measurements determined by saturation with the help of the NMR tomograph. Lastly, mercury intrusion porosimetry (MIP) measurements were carried out on small concrete fragments.

To determine the thermally induced moisture transport, two samples of each concrete were prepared and measured by ^{1}H-NMR relaxometry. The fresh concrete was directly filled into slightly conic cylindrical glass–ceramic (Macor) casts and subsequently

densified on a vibrating table. This set-up was chosen to generate a 1D moisture transport, mimicking the conditions of a unilaterally-heated large scale concrete member.

3 Methodology

An overview of the methodology applied is given in Fig. 2. The first part of the main investigation includes analysis of the pore size-specific moisture distribution before and after unilateral heating in blended cement concretes by means of ^{1}H-NMR relaxometry. The second part describes the application of numerical simulations to understand the temporal course of local moisture distribution during heating and cooling. Moreover, supportive side investigations were conducted. Gas permeability measurements at room temperature and after defined high-temperature exposure provide additional information on the transport properties, supporting the interpretation of the moisture analysis by ^{1}H-NMR relaxometry. MIP in combination with ^{1}H-NMR relaxometry of pressure saturated samples was used to eliminate the effect of Fe_2O_3 on the NMR signal by estimating the corresponding surface relaxivity, which allows the conversion of measured transverse relaxation times into pore sizes (explained in detail in Sect. 3.5).

3.1 Gas permeability

The development of gas permeability was analyzed on three specimens of each concrete composition in the initial state and after temperature loading of 105 °C, 150 °C, 170 °C, and 300 °C. A moderate heating rate (approx. 1 K/min) was selected in order to minimize the risk of microcracks due to residual stresses caused by temperature gradients. The gas permeability coefficient was obtained at three different pressure states (3, 4, and 5 bar) using Ar based on the recommendations of RILEM TC 116-PCD [25]. Thereafter, intrinsic permeability, which is defined as apparent permeability extrapolated to infinite pressure, was determined in accordance with Klinkenberg [26].

3.2 Porosity

The concrete's porosity and pore size distribution were investigated by MIP in the initial state for

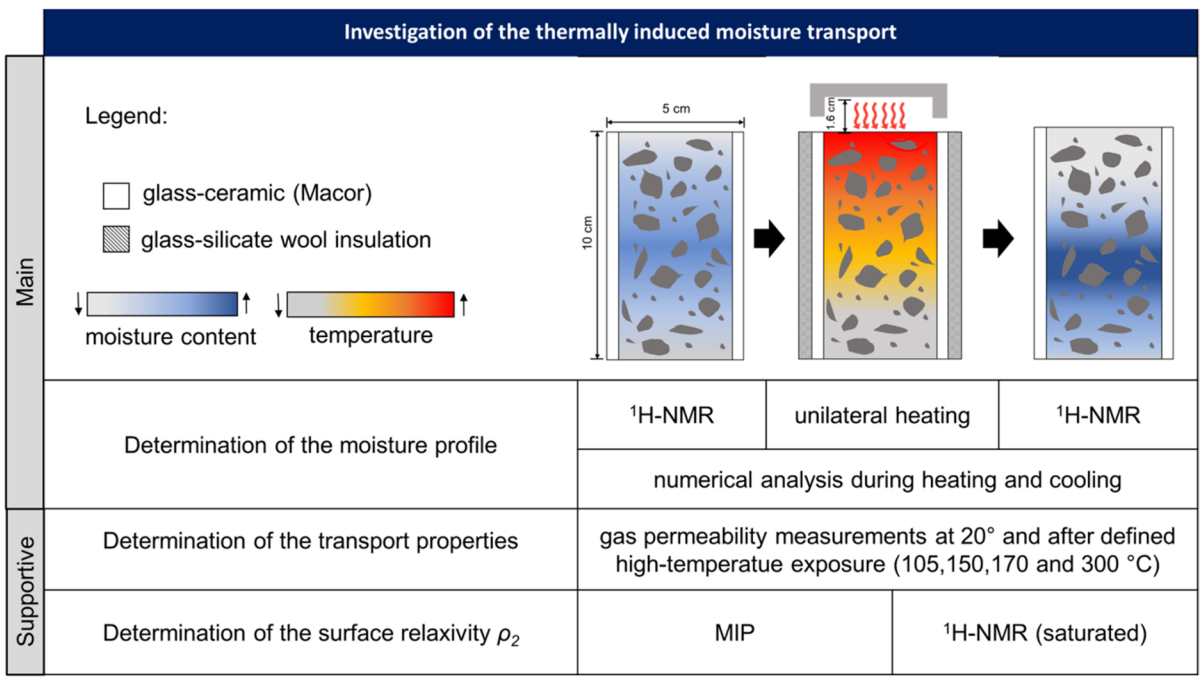


Fig. 2 Investigation program

two samples of each concrete. The porosimeter was operated in a pressure range of 0.0007–420 MPa with a chosen wetting angle of 140° according to ISO 15901-1 [27]. Throughout this paper the pore types are defined as gel pores ≤ 10 nm and capillary pores > 10 nm. Before measurement, the samples were vacuum-pulled and simultaneously dried at 40 °C for 24 h. It should be noted that thermal treatment may alter the pore structure, resulting in an increase of pore size and a higher proportion of capillary pores.

3.3 Unilateral heating

To analyze the thermally-induced moisture transport in the concretes, unilateral heating was applied. Since explosive concrete spalling usually occurs at temperatures around 300 °C, a surface temperature of 300 °C was targeted. This was achieved by using an equal experimental set-up as reported by Stelzner et al. [14], positioning an electrical heating device 1.6 cm above the specimen which was insulated by a glass-silicate wool covering. There was no contact between the sample and the device at any time, which led to heat transfer mainly conveyed by radiation. The heating rate was 10 K/min. Once the target value was reached after roughly 30 min, the temperature was held constant for 40 min. Next, the sample was allowed to cool freely within the room for 120 min. Right after, the sample was placed in the NMR-tomograph for the moisture distribution measurements. The temperature distribution in accompanying test specimens was also recorded.

3.4 Pressure saturation

The pressure saturation was carried out in accordance with [28]. First, the samples were placed under water and subjected to a vacuum with an absolute pressure ranging from 100 to 250 Pa for 3 h. Subsequently, the samples stayed under water at atmospheric pressure for an additional 2 h. Finally, the pressure was increased to 15 MPa, and the samples remained in the chamber for 24 h.

3.5 Experimental analysis of pore size-specific moisture distribution

Moisture content before and after heating was measured by ^{1}H-NMR relaxometry, a technique which allows the quantification of total water content and pore size-specific moisture distribution. An NMR core-analyzing tomograph (8.97 MHz) with a vertical resolution of 2 mm from pure devices GmbH was used; a detailed description of the tomograph and its capabilities can be found in [29]. A radio-frequency coil with a diameter of 52 mm was installed in the instrument. To study the transverse relaxation time (T_2) decay a Carr-Purcell-Meiboom-Gill (CPMG) pulse sequence was applied, where the corresponding echo time was 70 µs and the number of echoes was 1429 with a total of 200 scans per slice. Following the measurement, a multi-component T_2-time fitting was performed. This process is commonly referred to as an inverse Laplace transformation, although it more accurately involves solving a Fredholm integral equation of the first kind, where the measured signal is related to the T_2-time distribution through an exponential kernel [30]. The numerical inversion was performed using the software NucleusInv,[1] which employs lower–upper (LU) decomposition to ensure computational stability. A regularization parameter of $\lambda = 0.1$ (samples before and after heating) and 0.07 (pressure saturated samples) was applied to balance the trade-off between fitting accuracy and the smoothness of the resulting distribution. An exemplary illustration of the data inversion is provided in Fig. 3, including the measured data, the applied fit, and the resulting inversion.

The presence of magnetic impurities such as Fe_2O_3 influences the magnetic signal enhancing the T_2 decay, which causes a shift of the function to smaller T_2 times with increasing Fe_2O_3 content [31]. Hence, the translation of the T_2 time into pore sizes would lead to an overrepresentation of smaller pores. This is of particular importance as different cements with different Fe_2O_3 contents (see Table 1) are compared in this study. One possible way to eliminate this effect is given by estimating the surface relaxivity ρ_2 which describes the strength of the fluid's magnetic interaction with the surrounding pore walls. Thus, Eq. (1)

[1] https://github.com/ThoHiller/nmr-nucleus.

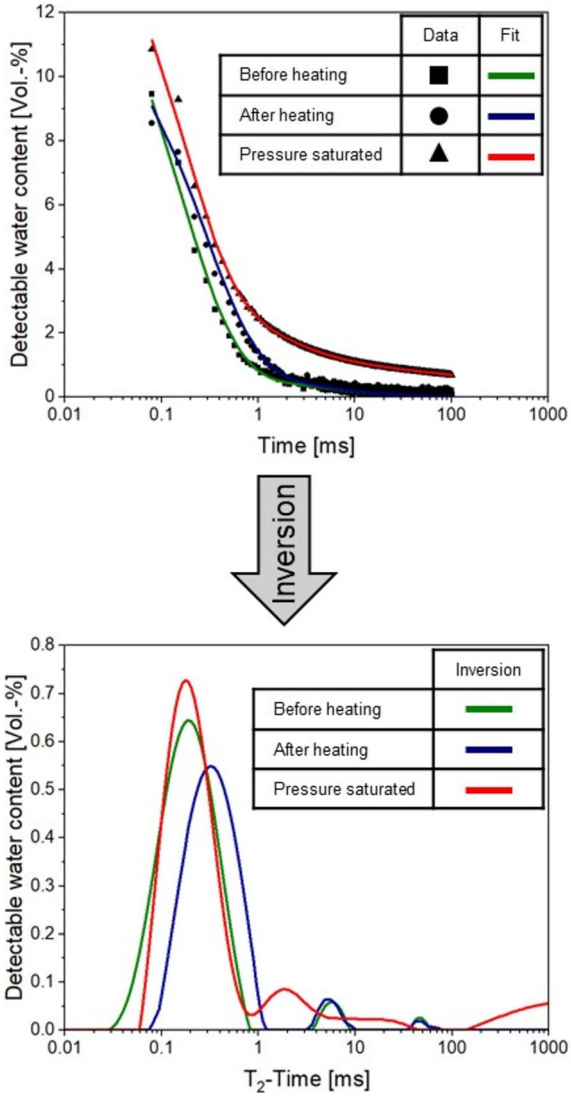


Fig. 3 Data inversion process (example CC)

allows the measured T_2 time to be directly assigned to the corresponding pore radius.

$$\frac{1}{T_2} = \rho_2 \frac{\alpha}{r} \tag{1}$$

where ρ_2 is the surface relaxivity, r is the pore radius, and α is the geometry shape factor. Depending on the pore geometry $\alpha = 1,2$ or 3 for planar, cylindrical or spherical shapes, respectively. To finally determine the surface relaxivity, porosity recorded by measuring vacuum-treated pressure-saturated samples by means of ^{1}H-NMR relaxometry were compared to porosities obtained by MIP. The area selected for curve fitting corresponds to the capillary pore space associated with the interhydrate pores of C-S-H. This region is identifiable as the most prominent capillary pore peak in the MIP curve and was chosen because it demonstrates the highest level of agreement between the measurement methods, as stated by Muller and Scrivener [32]. In this work, pore geometry is assumed to be cylindrical. This assumption arises due to the ink-bottle effect, which causes the MIP to predominantly detect pore throats, particularly in the smaller pore size range that accounts for the majority of the material's porosity. Therefore, the geometry shape factor of $\alpha = 2$ is used, which has also been applied in other studies [33, 34]. Subsequently, the surface relaxivity was chosen as the value leading to the best fit between NMR and MIP results. Once the surface relaxivity is acquired, Eq. 1 can be expressed as follows in Eq. (2), making the calculation of the pore radius in relation to the respective T_2 value possible.

$$r = \rho_2 \cdot a \cdot T_2 = \rho_2 \cdot 2 \cdot T_2 \tag{2}$$

3.6 Multiscale chemo-thermo-hygro-modeling

Due to the challenges associated with in-situ moisture content measurement during heating using NMR, assessments are typically conducted in the cold state. To reconstruct the evolution of the moisture front based on the experimentally obtained data, numerical modeling serves as a valuable tool and will be employed in the following analysis.

The numerical model is based on the hybrid mixture theory proposed by Lewis and Schrefler [35] describing cement-based materials as partially saturated porous media with a solid skeleton and an interconnected pore network containing capillary water, vapor, and dry air. It explicitly accounts for key high-temperature mechanisms, including temperature-dependent material properties, bound water release, phase transitions, and fluid transport. For heat and mass transfer in porous media, the model follows the Thermodynamically Constrained Averaging Theory framework [36], incorporating mass, energy, and momentum conservation at the continuum level. For

detailed formulations and governing equations, see Peters et al. [37, 38] .

The model incorporates four primary state variables: the temperature T, gas pressure p_g, capillary pressure p_c, and displacement field u, consistent with the formulation of Gawin and Pesavento [39] Additionally, five internal variables ξ_i describe the binder-specific dehydration kinetics, while a further internal variable, d, governs the evolution of mechanical damage.

The resulting governing system comprises ten coupled equations: mass balance for liquid water and dry air, an enthalpy balance (energy conservation), a momentum balance (mechanical equilibrium), and six evolution equations to capture the damage and dehydration processes. For completeness, the final form of the governing equations is presented below; a detailed derivation is provided in [40].

The enthalpy balance of the multiphase medium accounts for: (i) heat storage within the material, (ii) conductive heat transfer, (iii) latent heat effects associated with phase transitions, and (iv) heat release or consumption due to dehydration. It is expressed as in Eq. (3):

$$\left(\rho C_p\right)_{eff} \frac{\partial T}{\partial t} - \nabla \cdot \left(\lambda_{\text{eff}} \nabla T\right) = -\dot{m}_{\text{vap}} \Delta H_{\text{vap}} - \dot{m}_{\text{deh}} \Delta H_{\text{deh}} \tag{3}$$

where $(\rho C_p)_{\text{eff}}$ and λ_{eff} is the effective heat capacity of concrete and the effective thermal conductivity, respectively. ΔH_{vap}, ΔH_{deh} and m_{vap} are the enthalpy of evaporation dehydration, and the evaporated water mass, respectively [39].

The evolution of the solid density is governed by the temperature-dependent porosity according to [38] in Eq. (4):

$$\rho_s(T) = \rho_{s,0} \cdot \left(1 - \phi_{p,\text{con}}\right) \tag{4}$$

In the proposed model, the porosity ϕ is not prescribed through an empirical function. Instead, it is directly linked to the dehydration kinetics of the individual hardened cement paste constituents via Eq. 3 The evolution of these constituents is described by five internal variables, each governed by its respective kinetic law, see [41]. Consequently, the cement paste porosity is expressed as in Eq. (5).

$$\phi = \phi_{\text{initial}} + \sum \phi_j \quad \text{with} \ \in \{\text{CH}, \text{AFt}, \text{TCA}, \text{AFm}_c\} \tag{5}$$

The mass balance of dry air accounts for diffusive and advective transport, as well as porosity variations induced by temperature, saturation changes, and density variations of water and air, leading to the following form in Eq. (6):

$$\frac{\partial\left(\phi(1-S)\rho_{\text{ga}}\right)}{\partial t} + \nabla \cdot \boldsymbol{J}_{\text{ga}} = 0 \tag{6}$$

where ρ_{ga} denotes the gas-phase density of air and J_{ga} the corresponding mass flux.

The mass balance of water (liquid and vapor) incorporates diffusive and advective transport of both phases, mass exchange induced by dehydration, and porosity variations arising from temperature changes, saturation evolution, and density variations of liquid water and water vapor. Accordingly, the governing Eq. (7) reads:

$$\frac{\partial\left(\phi(1-S)\rho_{gw} + S\rho_w\right)}{\partial t} + \nabla \cdot \left(\boldsymbol{J}_w + \boldsymbol{J}_b\right) = -\dot{m}_{\text{dehydr}} \tag{7}$$

where ρ_{gw} and ρ_w are the fluid densities and $(J_w + J_b)$ the fluid flux of water in gaseous and liquid state $\dot{m}_{\text{dehydr}}$ characterizes the source term from dehydration.

Fluid transport within the porous medium is governed by pressure-driven flow described by Darcy's law, while gas-phase diffusion and adsorbed water transport are modeled according to Fick's law [38]. These flux formulations enter the mass conservation equations introduced above. The resulting mass fluxes of dry air, water vapor, and liquid water are therefore given by Eq. (8)–(10):

$$\boldsymbol{J}_{\text{ga}} = -\frac{K_{\text{int},g} k_{rg}}{\mu_g} \nabla p_g - \frac{M_a M_w}{M_g^2} D_{\text{eff}} \nabla\left(\frac{p_{\text{ga}}}{p_g}\right) \tag{8}$$

$$\boldsymbol{J}_w = -\frac{K_{\text{int}} k_{rw}}{\mu_w}\left(\nabla p_g - \nabla p_c\right) - \frac{M_a M_w}{M_g^2} D_{\text{eff}} \nabla\left(\frac{p_{gw}}{p_g}\right) \tag{9}$$

$$J_b = -\boldsymbol{D}_b \nabla S_b \tag{10}$$

The multiscale framework of Peters and Meschke [41] is employed to determine binder-specific dehydration behavior and related pore space evolution at elevated temperatures, building on the stoichiometric formulas of each hardened cement paste constituent and the associated dehydration kinetic, governed by

an Arrhenius equation. Subsequently, at each temperature step the actual volume fractions of the constituents are utilized in a micromechanical framework to homogenize the effective macroscopic thermal conductivity; see Peters et al. [37] for further details.

In following numerical analysis, the initial thermal conductivity is calibrated based on the experimentally determined temperature field at depths of 5 mm, 10 mm, 20 mm, 30 mm, 50 mm, and 70 mm. Furthermore, the intrinsic permeability evolution is prescribed by the experiments conducted, see Fig. 4. All input parameters are summarized in Table 6, further material formulations can be found in Peters et al. [37].

4 Results

4.1 Permeability

The average intrinsic gas permeability and the maximum and minimum values determined after conditioning at different high temperature regimes are displayed in Fig. 4. First, it is noted that the PC sample exhibited an initial permeability almost half a magnitude higher than that of the other concretes. After exposure to 105 °C, all samples exhibited a similar increase in permeability. However, a further temperature increase to 150 °C led to a more pronounced permeability rise in CC and SC samples compared to PC and LC specimens. This trend continued for the final temperature steps of 170 and 300 °C and thus the final permeability of CC, SC and PC was equal while the LC showed a slightly lower value. Overall, the results show that with increasing temperature the initial differences in permeability between PC, SC, and CC vanish and ultimately reach the same value after exposure to 300 °C, while LC follows a weaker permeability development, ending at a slightly lower final permeability.

4.2 Porosity

Figure 5 shows the total cumulative porosity obtained by MIP, indicating comparable values for all concretes with 13.26, 13.21, 13.79, and 12.87 Vol.% for PC, LC, SC, and CC, respectively. A closer look into the specific pore sizes shows an equal distribution for PC and LC; the CC sample follows a similar course but exhibits less capillary porosity greater than 10 nm and an increasing number of gel pores down to 3.6 nm. The SC sample shows the lowest number of capillary pores over 30 nm but the highest number of small capillary and gel pores below this size. No significant differences in the pore size distribution above 200 nm were recorded.

4.3 Experimental analysis of pore size-specific moisture distribution

Moisture distribution before and after heating to 300 °C is displayed in Fig. 6. The surface relaxivities obtained were 6 nm/ms for PC, LC, and CC and 5 nm/ms for SC respectively (see Appendix A). In the initial state PC and LC exhibit a steeper drying gradient during conditioning in contrast to SC and CC concrete which finally reach similar depths of 20–30 mm. The absolute water content varied, as PC and LC specimens showed slightly lower total moisture contents of approximately 12 and 11 Vol.% compared to SC and CC which had a total amount of above 13 Vol.% detectable water. Furthermore, differences in the pore size-specific moisture distribution are visible, shown in Table 5. Most of the available water is found in the gel pores in every concrete. However, while PC and LC show comparable fractions of gel and capillary pores, SC shows the highest fraction of capillary pores above 10 nm. CC on the other hand

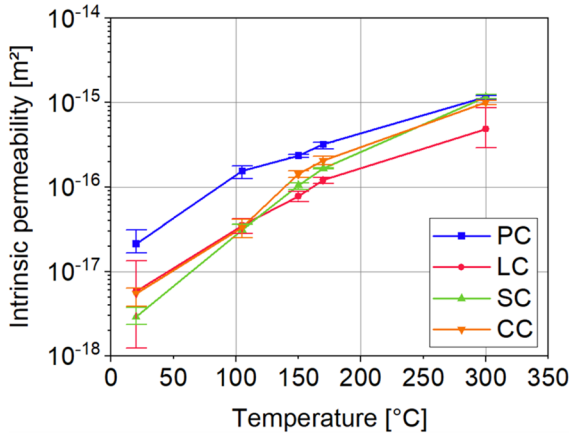


Fig. 4 Average intrinsic gas permeability of the different concretes before and after high-temperature exposure

shows the largest absolute and relative fraction of gel pores.

After heating the surface to 300 °C, a continuous drying front was established, and subsequently the appearance of the moisture clog was detected. Even though all the samples showed similar behavior, notable differences between the concrete types were obtained. Firstly, the drying front of the CC samples reached slightly deeper depths of around 50 mm in comparisons to roughly 40 mm for all other concretes. This corresponded to the steepest drying gradient found in the CC specimen. Furthermore, a more strongly developed moisture clog appeared in PC and LC compared to SC and especially CC. Lastly, moisture reconfiguration from gel pores to capillary pores happened in all specimens. While for the PC, LC, and SC samples, areas close to the beginning of the moisture clog experienced strong reconfiguration leading to more water found in capillary pores than gel pores, this is never the case for CC. Even though reconfiguration takes place, the gel pore fraction always contains the largest amount of water before as well as after high temperature exposure for this type of concrete.

A comparison of the one-dimensional moisture profiles after heating reveals three distinct zones, as shown in Fig. 7: dry, moist, and saturated (‘‘moisture clog’’). The dry zone extends from the top surface down to the point where the water content begins to rise sharply, marking the start of the moist zone. This moist zone ends at the onset of the moisture clog, which is defined here as the intersection between the post-heating water content and the initial water content. It is evident that all types of blended cement concrete exhibit a higher water content before the moisture clog, within a temperature range critical for explosive spalling. In other words, they contain more available thermal energy in the form of hot water in front of the impermeable zone. The lower permeabilities measured in blended cement concrete partly explain this phenomenon. However, the differences between the individual blended cement types cannot be attributed solely to variations in permeability, as those differences are comparatively small.

4.4 Numerical analysis of moisture distribution at elevated temperatures

To investigate the temporal saturation evolution of the different binder systems, the concrete samples have been discretized by 240 elements and analyzed by means of the multiphysics Finite-Element model described in Sect. 3.6. The input parameters are summarized in Appendix B Table 6, with the cement and concrete composition, permeability, and geometry matching experimental measurements. The

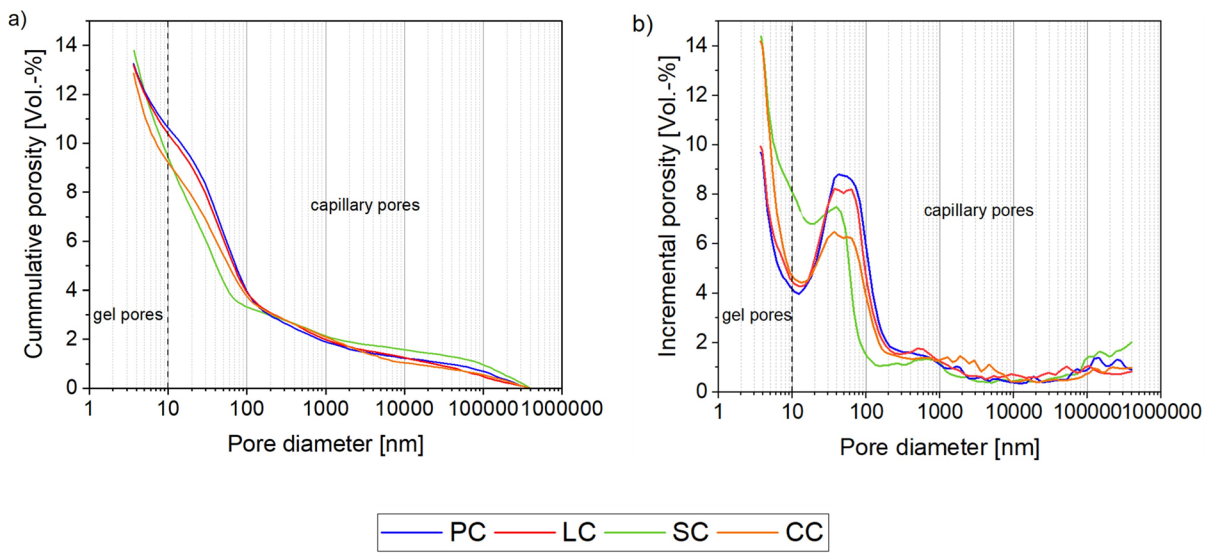


Fig. 5 Average porosity of the different concretes in the initial state **a** cumulative porosity; **b** incremental porosity determined by MIP

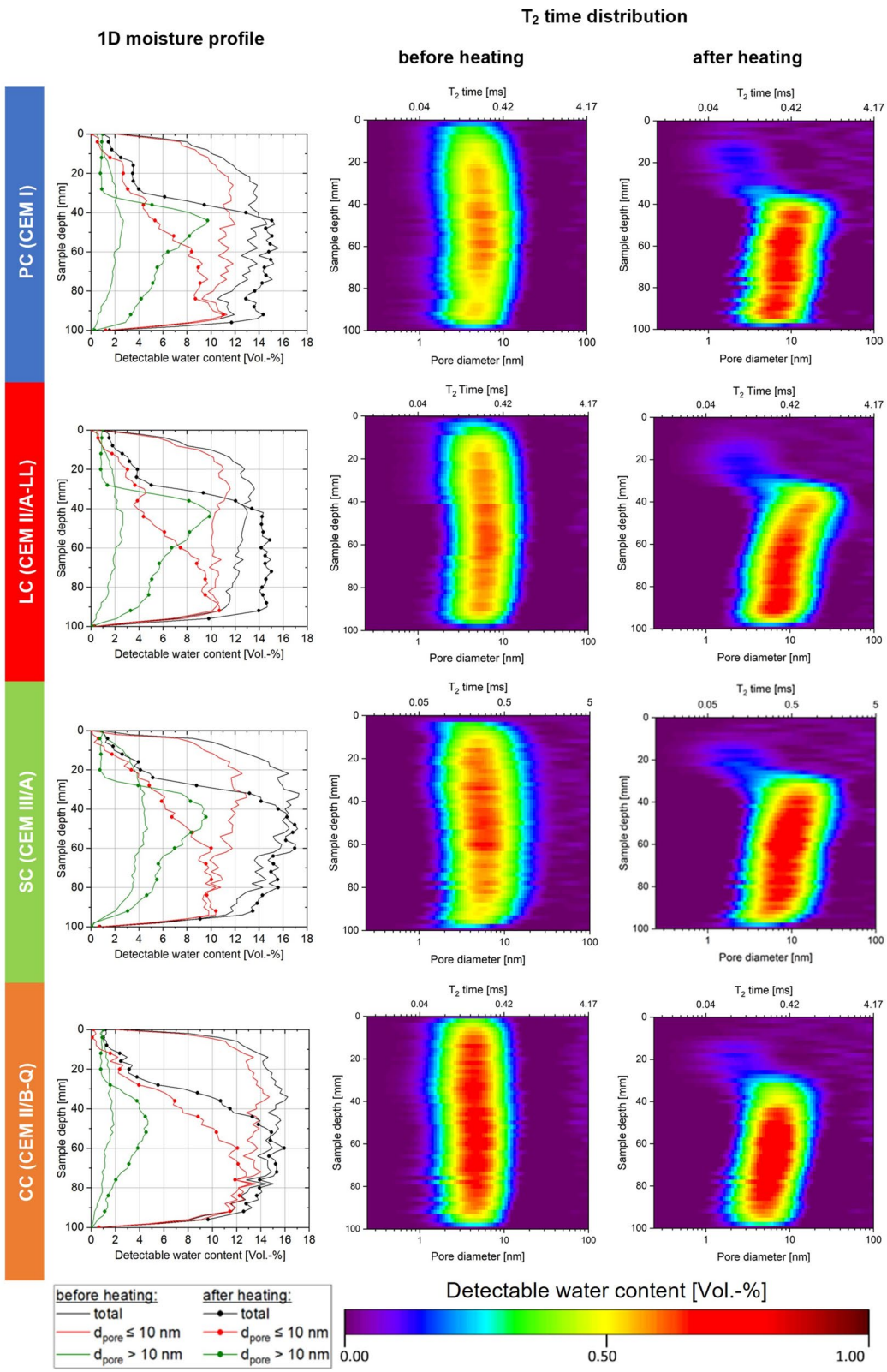
numerically computed temperature profiles at depths of 5 mm, 10 mm, 20 mm, 30 mm, 50 mm, and 70 mm are compared with the experimentally recorded temperatures in Fig. 8a, illustrating good agreement with the experimentally obtained data. The numerically determined moisture profiles represent the experimentally obtained data in Fig. 8 sufficiently, capturing both the individual drying depths and saturation curvatures in the drying zone. Rescaling the numerically determined saturation values into the detectable water content also shows good agreement between the calculated and experimentally determined depths and course of the curves after cooling (Fig. 8 b). This indicates that the qualitative moisture distribution during heating can be illustrated realistically.

Figure 9 contains computational results obtained from re-analyses of the ^{1}H-NMR experiment. It shows the saturation distribution along the depth of the specimen at different points of time during the uniaxial heating procedure protocol. The numerical analysis during the first 30 min of heating yields similar drying behavior for all concretes, see Fig. 9a. After reaching the target surface temperature of 300 °C at 30 min, a faster advancing drying front and lower moisture accumulation in deeper depths is observed for PC and LC as compared to SC and CC in Fig. 9b). On the other hand, the saturation increase behind the drying front remains similar for all concretes. At the start of cooling a more symmetric saturation profile is formed within moist zone for SC and CC as compared to PC and LC, see Fig. 9c. During the cooling phase, all saturation profiles exhibit a flattening effect, characterized by a reduced moisture gradient at the front, decreased saturation in the moist zone, and increased saturation in the previously dried regions, see Fig. 9d. Once again, an increased water content can be observed in front of the moisture clog in blended cement concrete, which is in alignment with the experimental results.

5 Discussion

The results show that the utilization of different blended cements affects concrete's microstructure and transport properties. Blended cement concrete with CEM II/A-LL, CEM III/A or CEM II/B-Q exhibits a lower initial permeability compared to CEM I samples. The increased fineness of the blended cements (Table 2) likely leads to a more densely packed microstructure, attributable to enhanced hydration kinetics and improved space-filling effects [42, 43]. Furthermore, binder-specific characteristics contribute to microstructural differences: in CEM II/A-LL concrete, the filler effect of limestone enhances packing density, while systems incorporating latent hydraulic or pozzolanic binders exhibit reduced portlandite and increased C-S-H contents, which may further densify the material. Moreover, Richardson and Groves [44] and Richardson [45] reported that the foil-like morphology of the outer product C-S-H in slag- or pozzolan-containing systems more efficiently fills space without leaving large interconnected capillary pores. Decreased pore connectivity in blended cement systems containing various types of SCMs has also been reported in other studies [46–49]. In addition, it was found that e.g. pozzolans have only little effect on mechanical properties, but significantly reduce pore connectivity compared to Portland cement [49]. The reduced connectivity limits the release of water vapor during fire exposure, which aligns with the low permeabilities observed in the blended cement concretes presented here. As a result, concrete of the same strength class may exhibit significantly varying spalling behaviors, as stated in this work. However, the permeability differences between CEM I, CEM III/A, and CEM II/B-Q become increasingly smaller above 105 °C and ultimately vanish at 300 °C.

The pore size-specific moisture distribution determined before and after heating by ^{1}H-NMR relaxometry showed that in the initial state, clear differences between the single binder types occur. In particular, the high initial moisture content in CEM III/A and CEM II/B-Q plus the large fraction of gel pore water in CEM II/B-Q, compared to OPC, should be highlighted. Moreover, pore coarsening takes place in all concretes during heating, leading to an increased amount of capillary water in the moisture clog regions after heating. The moisture profiles recorded after high temperature exposure show differences between the single blended concretes regarding the depth and extend of the moisture clog. However, the simulations suggest that these differences become more pronounced during cooling, leading to further movement of the drying front as well as to a decrease in the moisture clog. During heating, comparable depth and extent of the moisture clog are visible in all concretes. This shows that the ^{1}H-NMR measurements in


1D moisture profile
T2 time distribution
before heating
after heating
PC (CEM I)
LC (CEM II/A-LL)
SC (CEM III/A)
CC (CEM II/B-Q)
Sample depth [mm]
Detectable water content [Vol.-%]
T2 time [ms]
Pore diameter [nm]
before heating:
total
dpore ≤ 10 nm
dpore > 10 nm
after heating:
total
dpore ≤ 10 nm
dpore > 10 nm
Detectable water content [Vol.-%]
0.00
0.50
1.00

◂**Fig. 6** Moisture distribution and reconfiguration before and after heating determined by ^{1}H-NMR

the cold state after heating do not provide the moisture distribution which actually occurs during high temperature exposure. Therefore, the applied model turned out to be a valuable tool to close this gap of missing information.

The spalling behavior of the concretes can only be explained to a limited extent with the results presented. Firstly, the existence of the moisture clog was verified in every concrete, which is why a strong contribution of the thermohydraulic mechanism to the spalling can be assumed. However, one should not misinterpret the results by directly linking the depth of the moisture clog to the depth of spalling, since the damage was not caused by a single large spalling event but by many small events over a period of time. The lowest spalling tendency in CEM I concrete is most likely due to its low initial moisture content and comparatively high permeability before and during high-temperature loading leading to the fastest moving drying front. Despite comparable moisture content between CEM I and CEM II/A-LL concretes, the increased tendency to spall could be explained by the overall lowest permeability recorded over the entire temperature range. In CEM III/A concrete, the high initial moisture content appears to be responsible for the increasing spalling intensity. CEM II/B-Q concrete displays a similar high initial moisture content but additionally the highest proportion of gel pore water. Jiang et al. [50] reported that with decreasing pore radius, pore pressure rises inside concrete; this additional effect may lead to the most severe spalling observed in CEM II/B-Q concrete.

In summary, the increased spalling susceptibility of blended cement concrete can be attributed to the greater availability of thermal energy in the form of hot water within the moist zone preceding the moisture clog, which occurs in a temperature range critical for explosive spalling. This finding is supported by both experimental and numerical results. Lower permeabilities and higher initial moisture contents in blended cement systems are partly responsible for this appearance. However, the current data does not fully account for the differences observed among the individual blended concrete types.

The abovementioned findings suggest that the amount and nature of water, which is determined by the mineral phase composition, is decisive for thermohydraulic spalling. The dehydration and decomposition of the cementitious matrix determines the point of time and amount of water released under high temperature exposure. This also explains why CEM I and CEM II/A-LL concretes are quite similar in their pore structure and moisture distribution since they basically have the same mineral phase content. CEM III/A and CEM II/B-Q on the other hand include an additional component (slag or calcined clay) with an additional reaction mechanism (latent hydraulic or pozzolanic) strongly influencing the overall mineral composition in the non-hydrated and hydrated state. For example, it was observed that blended cement pastes with metakaolin or ground blast furnace slag showed larger amounts of C-S-H and calcium aluminate ferrite monosubstituted (AFm) phases but at the same time lower amounts of portlandite and calcium

Table 5 Average pore size specific moisture content (Vol.%)

Condition	Pore type	PC	LC	SC	CC
Before heating	Gel pores	10.09	9.39	10.12	12.04
	Capillary pores	1.62	1.61	3.28	1.15
	Total	**11.71**	**11.00**	**13.40**	**13.19**
After heating	Gel pores	5.75	5.57	6.49	7.52
	Capillary pores	4.08	4.45	4.61	2.23
	Total	**9.83**	**10.02**	**11.10**	**9.75**

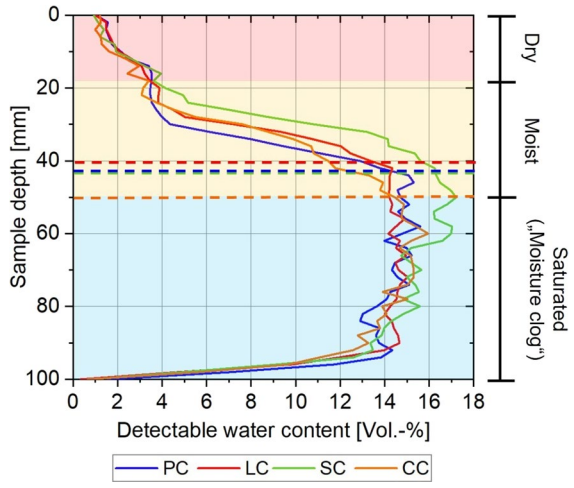


Fig. 7 Summarized illustration of the moisture distribution in the different types of concrete after heating showing an increased moisture content for blended cement concretes in the moist zone before the moisture clog. The dashed lines indicate the on-set of the moisture clog for the corresponding concrete

aluminate ferrite trisubstituted (AFt) phases compared to OPC cement pastes [51]. Furthermore, it has already been proven that low Ca/Si ratios promote Al uptake into C-(A)-S-H and subsequently higher Ca/Si and Al/Si ratios in the C-(A)-S-H phase generally lead to a denser foil like morphology [52]. Moreover, the water uptake increases in the C-(A)-S-H with introduction of Al to the system [52, 53], resulting in large amounts of non-evaporable gel water [52]. In addition to the C-S-H, the amount and type of AFt and AFm phases which are strongly dependent on the chemical composition of the cement [54] must not be neglected. It should be mentioned that these phases already start to decompose at approximately 70 °C and 170 °C, influencing the deterioration and dehydration of the microstructure at comparatively low temperatures. Furthermore, it cannot be ruled out that the different cement pastes have different thermal expansion behavior due to their compositional differences which could possibly lead to differing thermo-mechanical spalling behaviors.

Therefore, further investigations concerning mineral phase composition and their dehydration and decomposition behavior caused by high temperature exposure are planned for a better evaluation of thermally induced moisture transport of concretes with blended cements.

6 Conclusion

The investigations into thermally induced moisture transport in blended cement concrete led to the following conclusions:

- Initial permeability and porosity are influenced by the cement type. CEM I concrete shows the highest initial permeability in comparison to the other concretes made out of CEM II/A-LL, CEM III/A or CEM II/B-Q. The lower initial permeability in blended cement concrete in general appears due to increased fineness and improved hydration kinetics leading to a more efficient filling of the pore space. However, these differences strongly reduce with increasing temperature leading to an equal final permeability after an exposure to 300 °C in CEM III/A and CEM II/B-Q concrete.
- The initial moisture content is increased for CEM III/A and CEM II/B-Q. Additionally, these concretes show different pore size-specific mois-

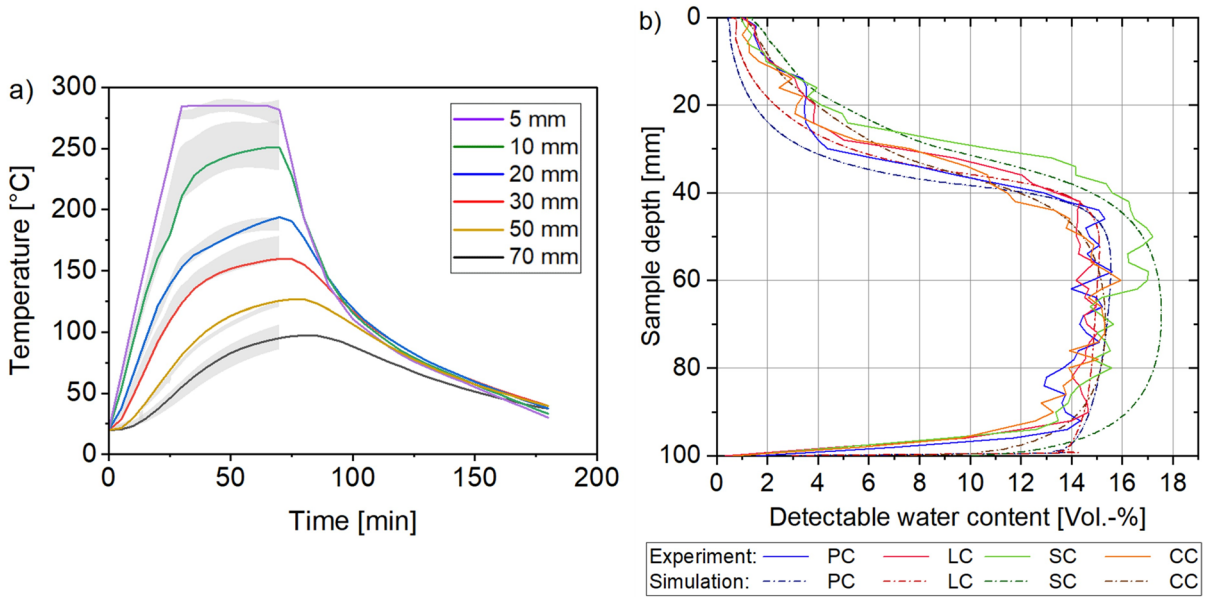


Fig. 8 **a** Numerically determined temperature profiles at depths of 5, 10, 20, 30, 50, and 70 mm for the heating and cooling procedure of 180 min. For comparison, the range of experimentally determined temperatures is included in the grey envelopes in the corresponding depths; **b** Experimental moisture distribution compared to simulated moisture distribution after 70 min of heating and subsequent cooling

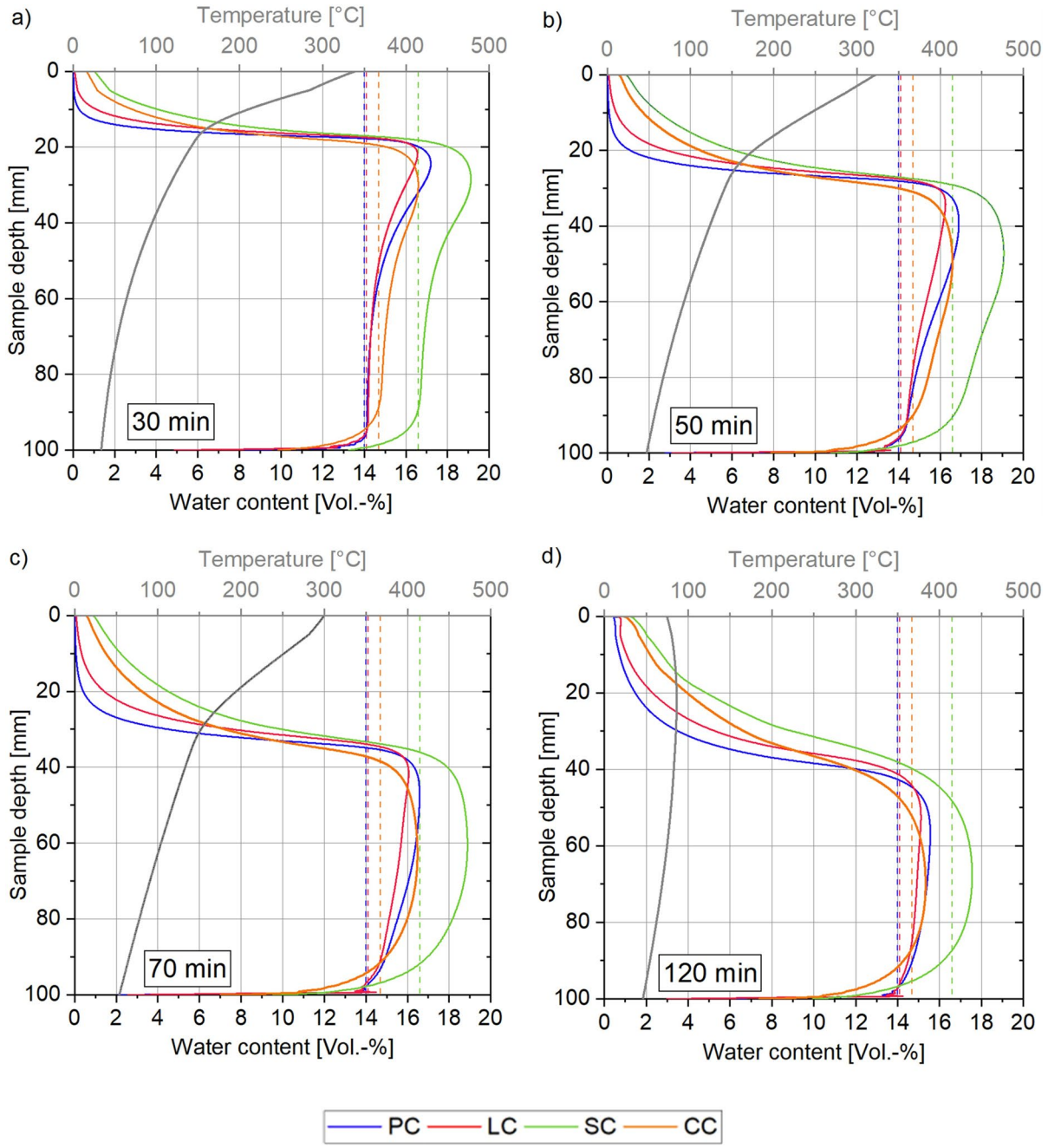


Fig. 9 Time-dependent moisture distribution during heating and cooling obtained by the numerical analysis **a** 30 min; **b** 50 min; **c** 70 min; **d** 120 min. Dashed lines indicate the initial water content of the corresponding concrete composition

ture distributions compared to CEM I and CEM II/A-LL concrete. CEM III/A exhibits the largest amount of capillary pore water while CEM II/B-Q exhibits the largest amount of gel pore water. This could affect the development of pore pressure.

- After temperature exposure, drying front and moisture clog formation in combination with pore coarsening were recorded in all specimens. However, there are clear differences in both the steepness of the drying gradient and the depth

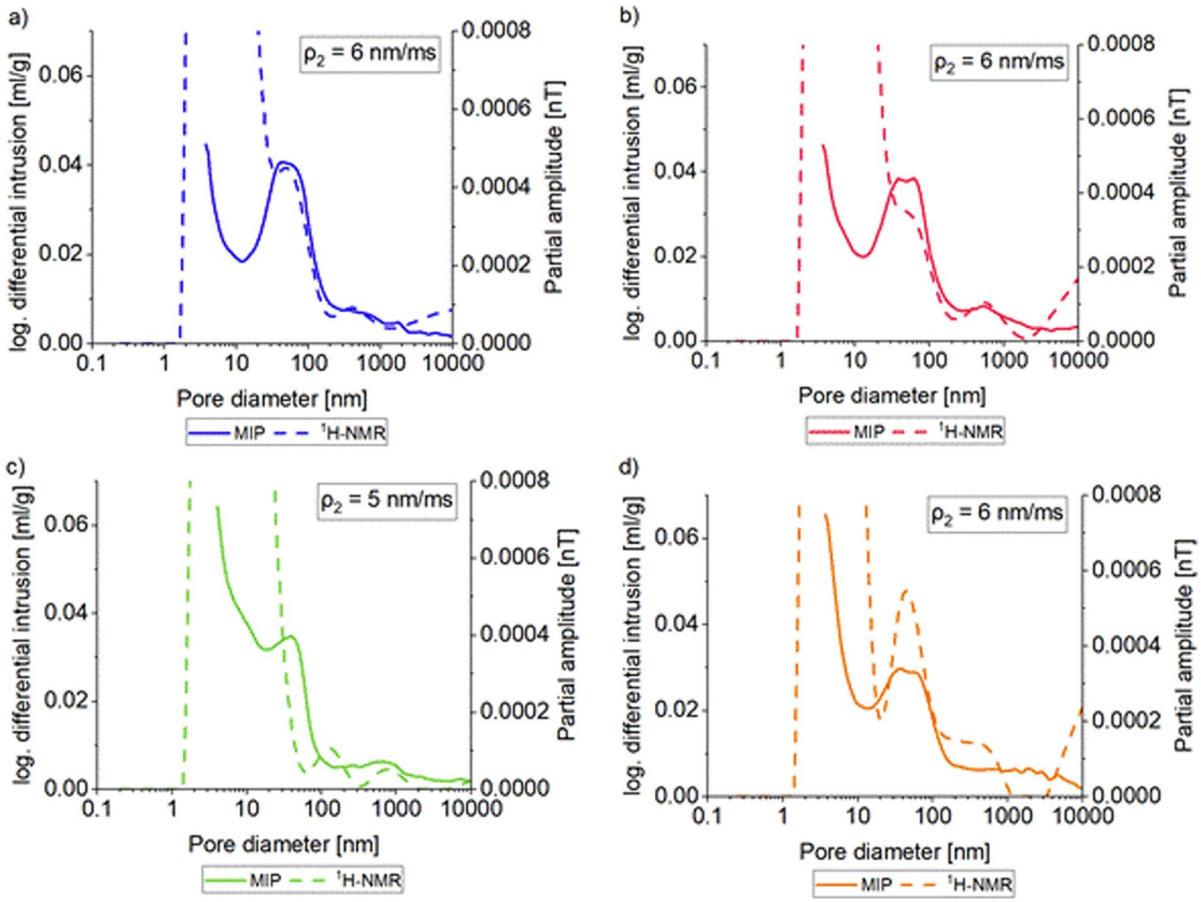


Fig. 10 Estimation of surface relaxivity ρ_2 by matching MIP and ^{1}H-NMR relaxometry results **a** PC; **b** LC; **c** SC; **d** CC

and extent of the moisture clog, which cannot be explained by permeability alone under the given circumstances.

- The simulation model presented shows a good agreement with the experimentally determined values. Additionally, it provides valuable insights into depth-resolved moisture development in the concrete specimen during heating and cooling. From these findings it can be concluded that the ^{1}H-NMR results after cooling are not entirely comparable with the moisture profile at the time of heating as they presented deeper depths of the drying fronts as well as lower water content of the moisture clog. Therefore, it serves as a valuable addition as it compensates for the weaknesses of the non-in situ high temperature measurement of ^{1}H-NMR.
- Blended cement concretes demonstrate higher spalling susceptibility due to the increased availability of hot water in the moist zone before the moisture clog. This relationship was confirmed through both experimental and numerical results. Responsible for this appearance are high initial moisture contents (CEM III/A and CEM II/B-Q concrete) as well as low permeabilities (CEM II/A-LL, CEM III/A and CEM II/B-Q concrete). The differences of spalling proneness between the single concrete types are not yet fully understood.

In the next step, investigations should be carried out at the level of mineral phase composition. Here the focus should be on the dehydration and decomposition behavior of the hardened cement paste after various high temperature loads to evaluate the phase changes, both qualitatively and quantitatively.

Acknowledgements We gratefully acknowledge the support of the German Research Foundation (DFG) and extend our gratitude for their financial support throughout the project

Table 6 Parameters utilized in the numerical analysis

Parameter	PC	LC	SC	CC
Permeability $K_{gas(20\ °C)}$	2.13e-17 (m^2)	5.86e-18 (m^2)	2.93e-18 (m^2)	5.47e-18 (m^2)
Permeability $K_{gas(105\ °C)}$	1.55e-16 (m^2)	3.49e-17 (m^2)	3.10e-17 (m^2)	3.31e-17 (m^2)
Permeability $K_{gas(150\ °C)}$	2.36e-16 (m^2)	7.69e-17 (m^2)	1.04e-16 (m^2)	1.43e-16 (m^2)
Permeability $K_{gas(170\ °C)}$	3.20e-16 (m^2)	1.20e-16 (m^2)	1.65e-16 (m^2)	2.05e-16 (m^2)
Permeability $K_{gas(300\ °C)}$	1.16e-15 (m^2)	4.88e-16 (m^2)	1.17e-15 (m^2)	9.99e-16 (m^2)
Permeability K_{int}	5e-20 (m^2)	5e-20 (m^2)	5e-20 (m^2)	5e-20 (m^2)
Saturation curve	$A_S = 86$ $B_S = 0.59$	$A_S = 86$ $B_S = 0.49$	$A_S = 86$ $B_S = 0.26$	$A_S = 86$ $B_S = 0.29$
$p_{c,initial}$	7.955e7 (Pa)	8.355e7 (Pa)	8.955e7 (Pa)	6.955e7 (Pa)
$p_{g,initial}$	101,325 (Pa)	101,325 (Pa)	101,325 (Pa)	101,325 (Pa)
$T_{initial}$	20 (°C)	20 (°C)	20 (°C)	20 (°C)
pbw	1:1.4:0.6	1:1.4:0.6	1:1.4:06	1:1.4:0.6
w/*c*	0.47	0.47	0.47	0.47
B_{sand}	0.56	0.56	0.56	0.56
$B_{aggregate}$	0.46	0.46	0.46	0.46
R (conductivity)	0.1	0.1	0.1	0.1

''Thermohydraulic spalling mechanisms in concretes with different binders with and without PP-fibers under fire exposure: An experimental and numerical analysis'' (Project Nr. 491928256). We also express our sincere appreciation to our colleagues, specifically acknowledging the collaborative efforts of BAM divisions 6.3: Structure Analysis, 7.1: Building Materials, and 7.4: Technology of Construction Materials. Their expertise and resources have significantly enriched the scope and depth of our study.

Funding Open Access funding enabled and organized by Projekt DEAL.

Data availability All data will be accessible upon request.

Declarations

Conflict of interest The authors declare that they have no known competing financial interests, personal relationships or any other affairs that could have appeared to influence the work reported in this paper.

Appendix A Estimation of surface relaxivity

Surface relaxivity was estimated by determining the best fit between MIP and ^{1}H-NMR results of pressure saturated samples. This method has already been used in the past in various studies dealing with the determination of fluid content in rocks, concrete or other building materials. Before comparing the samples, an equal sampling density for measurements is necessary. Therefore, the MIP pore size distribution was resampled to fit the NMR T_2-time distribution with a frequency of 30 points per decade. Subsequently, the surface relaxivity p_2 was chosen as the number providing the best match between the MIP and NMR curves displayed in Fig. 10.

Appendix B Simulation parameters and boundary conditions

For the simulation of the blended concretes the simulation parameters and initial conditions in Table 6 are conducted. For a detailed formulation of the constitutive laws, parametric relationships, and material parameter evolution, see [25, 26].

The boundary conditions are defined in accordance with the approach presented in Sect. 3.6 and remain consistent across all investigated cement types.

$$\left(\rho_{gw} v_g + \rho_w v_w + \rho_g v_{gw}\right)\boldsymbol{n} = \beta_c\left(\rho_{gw} - \rho_{gw,\infty}\right) \text{ on } \Gamma_c \tag{11}$$

$$\left(\rho_w v_l \Delta h_{\text{phase}} - \lambda_{eff} \nabla T\right) n = \alpha_c\left(T - T_\infty\right) + e\sigma_0 (T^4 - T_\infty^4) \tag{12}$$

Equation 11 is defined with capillary pressure parameters of β_c= 0.028 (ms^{-1}) on the heated side and β_c= 0.009 (ms^{-1}) on the rear side, with a gas–water equilibrium density of $\rho_{gw,\infty}$= 0.0031 (kg/

m^3) at both boundaries. Equation 12 governs the heat transfer on the rear side of the specimen, with convective heat transfer coefficient $\alpha_c = 8$ ($Wm^{-2}K$) and radiation term $e\sigma_0 = 5.1e^{-8}$ ($Wm^{-2}K$). In addition to the Cauchy boundary conditions applied in Eqs. 11 and 12, Dirichlet boundary conditions are imposed for the pressure equation, setting the gas pressure to $p_g = 101365$ (Pa) on both sides. Furthermore, the temperature profile at depths of 5 mm, 10 mm, 20 mm, 30 mm, 50 mm, and 70 mm from the heated side is prescribed based on the data measured by the calibrated heater.

Open Access This article is licensed under a Creative Commons Attribution 4.0 International License, which permits use, sharing, adaptation, distribution and reproduction in any medium or format, as long as you give appropriate credit to the original author(s) and the source, provide a link to the Creative Commons licence, and indicate if changes were made. The images or other third party material in this article are included in the article's Creative Commons licence, unless indicated otherwise in a credit line to the material. If material is not included in the article's Creative Commons licence and your intended use is not permitted by statutory regulation or exceeds the permitted use, you will need to obtain permission directly from the copyright holder. To view a copy of this licence, visit http://creativecommons.org/licenses/by/4.0/.

References

1. Pittrich T, Weise F, Stelzner L (2025) The impact of blended cements on the spalling behavior of concrete at elevated temperatures: a review. Mater Struct. https://doi.org/10.1617/s11527-025-02713-x
2. Bažant Z P (1997) Analysis of Pore Pressure, thermal Stredd and Fracture in Rapidly Heated Concrete. International Workshop on fire Performance of High-Strength Concrete. Gaithersburg
3. Ulm FJ, Coussy O, Bazant ZP (1999) The "'Chunnel"' fire I: chemoplastic softening in rapidly heated concrete. J Eng Mech 125:272–282. https://doi.org/10.1061/(ASCE)0733-9399(1999)125:3(272)
4. Schneider U (1982) Behaviour of Concrete at High Temperatures Deutscher Ausschuss für Stahlbeton, pp 1–110
5. McNamee R (2019) Fire Spalling Theories—Realistic and More Exotic Ones. In: Proceedings of the 6th International Workshop on Concrete Spalling due to Fire Exposure. Sheffield
6. Peters S, Vu G, Meschke G (2025) A multiscale model for predicting the Young's modulus and the thermal-expansion coefficient of concrete at high temperatures. Constr Build Mater. https://doi.org/10.1016/j.conbuildmat.2025.141259
7. Shorter GW, Harmathy TZ (1961) Discussion on the Fire-resistance of prestressed concrete beams, pp 313–315
8. Pistol K, Weise F, Meng B et al (2011) The mode of action of polypropylene fibres in high performance concrete at high temperatures. In: 2nd International RILEM Workshop on Concrete Spalling due to Fire Exposure. Delft, pp 289–296
9. Weber B, Wyrzykowski M, Griffa M et al (2013) Neutron radiography of heated high-performance mortar. MATEC Web of Conferences vol 6
10. Toropovs N, Lo Monte F, Wyrzykowski M et al (2015) Real-time measurements of temperature, pressure and moisture profiles in high-performance concrete exposed to high temperatures during neutron radiography imaging. Cem Concr Res 68:166–173. https://doi.org/10.1016/j.cemconres.2014.11.003
11. Dauti D, Tengattini A, Dal Pont S et al (2018) Analysis of moisture migration in concrete at high temperature through in situ neutron tomography. Cem Concr Res 111:41–55. https://doi.org/10.1016/j.cemconres.2018.06.010
12. Powierza B, Stelzner L, Oesch TS et al (2019) Water migration in one-side heated concrete: 4D in-situ CT monitoring of the moisture-clog-effect. J Nondestruct Eval 38:66
13. Van der Heijden GHA, Pel L, Adan OCG (2012) Fire spalling of concrete, as studied by NMR. Cem Concr Res 42:265–271. https://doi.org/10.1016/j.cemconres.2011.09.014
14. Stelzner L, Powierza B, Oesch T et al (2019) Thermally-induced moisture transport in high-performance concrete studied by X-ray-CT and ^{1}H-NMR. Constr Build Mater 224:600–609. https://doi.org/10.1016/j.conbuildmat.2019.07.065
15. Guo J, Tian W, Cheng X et al (2024) Study on the evolution of concrete pore structure and moisture transfer mechanism after high temperature based on different sequence NMR technology. Constr Build Mater. https://doi.org/10.1016/j.conbuildmat.2024.135739
16. Chen X-T, Rougelot T, Davy CA et al (2009) Experimental evidence of a moisture clog effect in cement-based materials under temperature. Cem Concr Res 39:1139–1148. https://doi.org/10.1016/j.cemconres.2009.07.015
17. Pittrich T, Stelzner L, Weise F (2024) Fire-induced spalling of normal strength concrete with different types of blended Portland cement. In: The 13th International Conference on Structures in Fire. Coimbra, pp 451–461
18. Wu K, Shi H, Xu L et al (2016) Microstructural characterization of ITZ in blended cement concretes and its relation to transport properties. Cem Concr Res 79:243–256. https://doi.org/10.1016/j.cemconres.2015.09.018
19. Berodier E, Scrivener K (2015) Evolution of pore structure in blended systems. Cem Concr Res 73:25–35. https://doi.org/10.1016/j.cemconres.2015.02.025
20. Deschner F, Winnefeld F, Lothenbach B et al (2012) Hydration of Portland cement with high replacement by siliceous fly ash. Cem Concr Res 42:1389–1400. https://doi.org/10.1016/j.cemconres.2012.06.009

21. Mendes A, Sanjayan J, Collins F (2008) Phase transformations and mechanical strength of OPC/Slag pastes submitted to high temperatures. Mater Struct 41:345–350. https://doi.org/10.1617/s11527-007-9247-8
22. DIN EN 197-1 (2011) Cement-Part 1: Composition specifications and conformity for common cements, Beuth Verlag GmbH, Berlin
23. DIN EN 12390-2 (2019) Testing hardened concrete—Part 2: Making and curing specimens for strength tests, Beuth Verlag GmbH, Berlin
24. Pimienta P, McNamee R, Hager I et al (2023) Recommendation of RILEM TC 256-SPF on the method of testing concrete spalling due to fire: material screening test. Mater Struct. https://doi.org/10.1617/s11527-023-02202-z
25. RILEM TC 116-PCD (1999) RILEM TC 116-PCD: Permeability of Concrete as a Criterion of its Durability. Materials ans Structures 32:174–179
26. Klinkenberg LJ (1941) The Permeability of Porous Media to Liquids and Gases. Production Practice, pp 200–213
27. International Organization for Standardization (2016) Evaluation of pore size distribution and porosity of solid materials by mercury porosimetry and gas adsorption—Part 1: Mercury Porosimetry (ISO Standard No. 15901-1)
28. Bunke N (1991) Prüfung von Beton—Empfehlungen und Hinweise als Ergänzung zu DIN 1048. Deutscher Ausschuss für Stahlbeton. https://doi.org/10.2366/3708068
29. Kruschwitz S, Munsch S, Telong M et al (2023) The NMR core analyzing tomograph: a multi-functional tool for non-destructive testing of building materials. Magn Reson Lett 3:207–219. https://doi.org/10.1016/j.mrl.2023.03.004
30. Fordham EJ, Enkataramanan L, Mitchell J et al (2017) What are, and what are not, Inverse Laplace Transforms. J Basic Princ Diffus Theory, Exp Appl. https://doi.org/10.62721/diffusion-fundamentals.29.952
31. Schulte Holthausen R, Raupach M (2018) Determination of porosity and pore size distribution in concrete by single-sided ^{1}H NMR—From white cement pastes to grey cement mortars. IBAUSIL: Weimar, pp 595–603
32. Muller ACA, Scrivener KL (2017) A reassessment of mercury intrusion porosimetry by comparison with 1H NMR relaxometry. Cem Concr Res. https://doi.org/10.1016/j.cemconres.2017.05.024
33. Zhao P, Wang L, Xu C et al (2020) Nuclear magnetic resonance surface relaxivity and its advanced application in calculating pore size distributions. Mar Pet Geol 111:66–74. https://doi.org/10.1016/j.marpetgeo.2019.08.002
34. She AM, Yao W, Yuan WC (2012) Evolution of various states of water in blended cementitious materials. Appl Mech Mater 193:389–392. https://doi.org/10.4028/www.scientific.net/AMM.193-194.389
35. Lewis R, Schrefler BA (1998) The Finite Element Method in the Static and Dynamic Deformation and Consolidation in Porous Media. John Wiley and Sons, Hoboken
36. Hassanizadeh M, Gray WG (1979) General conservation equations for multi-phase systems: 1. Averaging procedure. Adv Water Resour 2:131–144
37. Peters S, Pittrich T, Stelzner L et al (2025) Model based evaluation of effects of the composition of CO2 -reduced blended concrete on the chemo-thermo-hygral behavior at elevated temperatures. Cement Concr Compos. https://doi.org/10.1016/j.cemconcomp.2025.106163
38. Gawin D, Majorana B, Schrefler B (1999) Numerical analysis of hygro-thermic behavior and damage of concrete at high temperature. Mech Cohesive-Frict Mater 4:37–74
39. Gawin D, Pesavento F (2012) An overview of modeling cement based materials at elevated temperatures with mechanics of multi-phase porous media. Fire Technol 48:753–793. https://doi.org/10.1007/s10694-011-0216-y
40. Gawin D, Pesavento F, Schrefler BA (2003) Modelling of hygro-thermal behaviour of concrete at high temperature with thermo-chemical and mechanical material degradation. Comput Methods Appl Mech Eng 192:1731–1771. https://doi.org/10.1016/S0045-7825(03)00200-7
41. Peters S, Meschke G (2024) Computational multiscale modelling of thermallyinduced dehydration of blended hardened cement paste. Cem Concr Res. https://doi.org/10.1016/j.cemconres.2024.107485
42. Sugrañez R, Álvarez JI, Cruz-Yusta M et al (2013) Controlling microstructure in cement based mortars by adjusting the particle size distribution of the raw materials. Constr Build Mater 41:139–145. https://doi.org/10.1016/j.conbuildmat.2012.11.090
43. Bentz DP, Garboczi EJ, Haecker CJ et al (1999) Effects of cement particle size distribution on performance properties of Portland cement-based materials. Cem Concr Res. https://doi.org/10.1016/S0008-8846(99)00163-5
44. Richardson IG, Groves GW (1992) Microstructure and microanalysis of hardened cement pastes involving ground granulated blast-furnace slag. J Mater Sci 27:6204–6212
45. Richardson IG (1999) The nature of C-S-H in hardened cements. Cem Concr Res 29:1131–1147
46. Ranger M, Tange Hasholt M (2023) Relationship between chloride migration, bulk electrical conductivity and formation factor of blended cement pastes. Nord Concr Res 69:33–53. https://doi.org/10.2478/ncr-2023-0009
47. Higuera-Flórez C, Cárdenas-Pulido J, Lizarazo-Marriaga J et al (2023) Implementation of the formation factor (F) to evaluate properties of cement-based materials from electrochemical techniques. 2023 Congreso Internacional de Innovación y Tendencias en Ingeniería (CONIITI). Bogotá, pp 1–6. https://doi.org/10.1109/CONIITI61170.2023.10324013
48. Yio MHN, Wong HS, Buen NR (2019) 3D pore structure and mass transport properties of blended cementitious materials. Cem Concr Res 117:23–37. https://doi.org/10.1016/j.cemconres.2018.12.007
49. López M, Castro JT (2010) Effect of natural pozzolans on porosity and pore connectivity of concrete with time. Rev Ing Constr 25:419–431
50. Jiang W, Zhang D, Zheng X et al (2023) Development of pore pressure in cementitious materials under low thermal effects: evidence from optimization of pore structure by incorporation of fly ash. Materials. https://doi.org/10.3390/ma16124214
51. Saillio M, Baroghel-Bouny V, Bertin M et al (2019) Phase assemblage of cement pastes with SCM at different ages.

Constr Build Mater 244:144–157. https://doi.org/10.1016/j.conbuildmat.2019.07.059
52. Kapeluszna E, Kotwica Ł, Rózycka A et al (2017) Incorporation of Al in C-A-S-H gels with various Ca/Si and Al/Si ratio: microstructural and structural characteristics with DTA/TG, XRD, FTIR and TEM analysis. Constr Build Mater 155:643–653. https://doi.org/10.1016/j.conbuildmat.2017.08.091
53. Myers RJ, L'Hôpital E, Provis JL et al (2015) Effect of temperature and aluminium on calcium (alumino)silicate hydrate chemistry under equilibrium conditions. Cem Concr Res 68:83–93
54. Matschei T, Lothenbach B, Glasser FP (2007) The AFm phase in Portland cement. Cem Concr Res 37:118–130. https://doi.org/10.1016/j.cemconres.2006.10.010

Publisher's Note Springer Nature remains neutral with regard to jurisdictional claims in published maps and institutional affiliations.

Paper 3

Thermal Decomposition in Blended Cement Systems and its Effect on Fire-induced Concrete Spalling: Insights from XRD and TGA

Publisher's version

Published in *Case Studies in Construction Materials*

Volume 24, 2026

DOI: https://doi.org/10.1016/j.cscm.2026.e05784

Authors: Tim Pittrich, Daniel Jansen, Frank Weise, Ludwig Stelzner, Frank Dehn

Case Studies in Construction Materials 24 (2026) e05784

Contents lists available at ScienceDirect

Case Studies in Construction Materials

journal homepage: www.elsevier.com/locate/cscm

Thermal decomposition in blended cement systems and its effect on fire-induced concrete spalling: Insights from XRD and TGA

Tim Pittrich [a,*], Daniel Jansen [b], Frank Weise [a], Ludwig Stelzner [a], Frank Dehn [c]

[a] Federal Institute for Materials Research and Testing, Unter den Eichen 87, Berlin 12205, Germany
[b] University of Erlangen-Nuremberg, Schloßgarten 5a, Erlangen 91054, Germany
[c] Karlsruhe Institute of Technology, Gotthard, Franz Straße 3, Karlsruhe 76131, Germany

ARTICLE INFO

Keywords:
Fire concrete spalling
High temperatures
Blended cements
Dehydration
XRD
TGA

ABSTRACT

Blended cements are gaining increasing popularity due to their lower CO_2-footprint in comparison to ordinary Portland cement (OPC). However, this growing use raises the potential risk of buildings made with blended cement concrete being exposed to fire, which can lead to heavy damages caused by explosive concrete spalling. It has already been shown that the cement type strongly influences the fire-induced concrete spalling and the thermally induced moisture transport, however, to understand the mechanisms behind these findings the thermal decomposition behavior of the cementitious matrix must be investigated more systematically. Therefore, the phase content of three blended cement pastes (CEM II/A-LL, CEM III/A and CEM II/B-Q) was studied in comparison with a Portland cement paste (CEM I) after temperature exposure to 20 °C, 105 °C, 300 °C and 500 °C. Clear differences in the initial phase composition and their dehydration behavior between the individual cement types were recognized. In conclusion, blended cements showed lower amounts of AFt and AFm phases and additionally lower amounts of portlandite and C-(A)-S-H were found in CEM III/A and CEM II/B-Q pastes. The results suggest that higher AFt and AFm contents in CEM I, which are associated with greater water release at relatively low temperatures may ultimately reduce the spalling risk. Furthermore, C-(A)-S-H in CEM III/A and CEM II/B-Q showed increased thermal stability and large amounts of non-hydrated phases were found in every blended cement paste. Both of those aspects might contribute to thermomechanical spalling and the overall increased spalling susceptibility observed in blended cement concrete.

1. Introduction

Nowadays, blended cements gain attention as their utilization is an effective way to reduce the CO_2-emssions caused by the ordinary Portland cement (OPC) production. In blended cements part of the Portland cement clinker is replaced by fillers and/or supplementary cementitious material (SCM). These materials can be of natural origin (e.g. limestone) or man-made materials such as by products from the steel or power industry. Therefore, there is a wide range of usable materials that influence concrete properties on the mineralogical level. The mineralogical composition of non-hydrated and hydrated OPC and blended cements is already well known.

* Corresponding author.
E-mail addresses: tim.pittrich@bam.de (T. Pittrich), daniel.jansen@fau.de (D. Jansen), frank.weise@bam.de (F. Weise), ludwig.stelzner@bam.de (L. Stelzner), frank.dehn@kit.edu (F. Dehn).

https://doi.org/10.1016/j.cscm.2026.e05784
Received 17 October 2025; Received in revised form 12 December 2025; Accepted 8 January 2026
Available online 13 January 2026
2214-5095/© 2026 The Author(s). Published by Elsevier Ltd. This is an open access article under the CC BY license (http://creativecommons.org/licenses/by/4.0/).

OPC mainly consists of the clinker phases C_3S, C_2S, C_3A and C_4AF[1] and minor amounts of free lime (CaO). In addition, it contains sulfate carriers in the form of gypsum, anhydrite or bassanite as well as secondary components such as limestone. Blended cements contain the same clinker minerals but fillers and/or SCMs are used to replace fractions of the Portland cement clinker. Up to now most commonly used fillers and SCMs are limestone (LS), fly ash (FA) and blast furnace slag (BFS). However, the long-term availability of FA and BFS is questionable and therefore the interest in alternatives such as calcined clays (CC) rise as their raw material is globally available and they provide good pozzolanic properties after activation [1]. During hydration clinker minerals mainly form C-S-H and portlandite as well as sulfoaluminate phases in the form of ettringite (AFt) which in later hydration stages partly converts into AFm phases. In addition to the regular hydration process blended cements experience further pozzolanic or latent hydraulic reactions. The pozzolanic reaction describes the consumption of portlandite during the presence of water and a reactive silicate bearing SCM leading to the formation of additional C-S-H or C-(A)-S-H respectively. Therefore, blended cements in general show lower amounts of portlandite [2].

Due to the increasing popularity of blended cements the probability of buildings made with blended cement concrete being exposed to fire rises. When exposed to fire, concrete undergoes various chemical and physical changes, which cause an overall decrease in strength and in the worst-case explosive spalling. Responsible for spalling are thermohydraulic and thermomechanical mechanisms. While neither is yet fully understood, several contributing factors have been identified. The thermohydraulic spalling mechanism is often associated with an increase in pore pressure and/or the sudden evaporation of superheated water within the concrete matrix. These processes generate internal stresses that can exceed the tensile strength of the material, leading to explosive spalling. The thermomechanical mechanisms are linked to restrained thermal expansion and thermal incompatibility between cement paste and the aggregates. These mismatches can induce significant internal stresses, which may also result in spalling. A comprehensive overview of various theories and mechanisms related to concrete spalling can be found in [3]. Many studies showed that the cement type used influences fire induced concrete spalling, however, the reasons behind those findings remain rather unclear [4]. During a fire event, it can be assumed that the point of time and amount of water release, which depends heavily on the dehydration of the different mineral phases found in different types of hardened cement paste, has a decisive influence on thermohydraulic processes. Of particular interest is the temperature range between 250 °C and 450 °C, as fire-induced spalling typically occurs within this range. To understand those differences, further understanding of the decomposition of blended cement pastes at elevated temperatures is necessary. The general dehydration and decomposition behavior of hardened cement paste can be described as follows (Fig. 1): Initially, free and physical bound water within the capillary pores begins to evaporate at temperatures up to approximately 200 °C. Between 80 and 150 °C, ettringite starts to dehydrate accompanied by the gradual loss of chemically bound water from the C-S-H, which ultimately decomposes into β-C_2S between 600 and 800 °C. The AFm phases release their water in the range of 130–180 °C. Portlandite ($Ca(OH)_2$) dehydrates between 460 and 540 °C, forming CaO. From around 600 °C, calcium carbonate ($CaCO_3$) also begins to decompose into CO_2 and CaO [5,6].

Even though the basic principle of thermal decomposition remains very similar in all cementitious systems, there can be significant differences in water release and decomposition of the cement matrix depending on the phase type and content. Investigations by Zhang and Ye [7] as well as Saillio et al. [8] looked at the quantitative phase development of OPC cement paste exposed to elevated temperatures. Zhang and Ye analyzed hardened Portland cement paste with a water to cement ratio (w/c) of 0.5 cured for 28 d by X-ray diffraction (XRD) with subsequent Rietveld analysis. In total, the samples were exposed to ten different temperatures starting at 105 °C up to 1000 °C. It was observed that the phase composition barely changes between 105 and 400 °C. At 500 °C, the crystallinity decreases and the dehydration of portlandite was noticed accompanied with the formation of amorphous lime. At temperatures above 600 °C the crystallinity increased again which was caused by the decomposition of amorphous C-S-H into β-C_2S. In addition, the formed lime started to become more and more crystalline with higher applied temperatures. It should be noted that the content of all amorphous phases was summarized in this study and therefore no precise information concerning the amounts of C-S-H, ettringite, AFm etc. was given. The group of Saillio et al. [8] took a closer look into the phase assemblage of a 5-year-old Portland cement paste submitted to various high temperature and cooling regimes, including air and water quenching. The pastes, prepared with a w/c of 0.272, were subjected to temperatures between 100 °C and 1000 °C. Subsequently, the samples were subjected to either air cooling or water quenching in a freshwater tank, simulating the thermal shock that may occur during real-life fire extinguishing scenarios. The quantification of the phase assemblage before and after heating was conducted by a method combining XRD, nuclear magnetic resonance (NMR) spectroscopy, inductively coupled plasma atomic emission spectroscopy (ICP-AES) and thermal gravimetric analysis (TGA) stated in [9]. Due to the allowance of air- and water-cooling rehydration happened which led to the presence of hydrated phases also after heating especially in the water-cooled samples. Standing out was once again the dehydration of portlandite at 500 °C as well as the gradual decomposition of C-S-H which finally resulted in the formation of anhydrous phases mostly C_2S and C_3S. Research conducted by Song et al. [6] analyzed the phase transformation of Portland cement blended with slag qualitatively by means of High-Temperature X-ray diffraction (HT-XRD). The OPC reference and the OPC-BFS (74 wt% BFS, 6 wt% gypsum) were made with a water to binder ratio of 0.4 and cured for 3 d, 28 d and 56 d. Upon the respective day of testing, the samples were placed in the diffractometer and simultaneously heated with 1 K/min until the specific temperature was reached. Finally, the XRD patterns were recorded. Next to the composition differences caused by the raw materials, slight differences of the mineral phase composition in the initial state appeared. Minor traces of hydro garnet were only found in the hardened OPC paste as well as much lower contents of portlandite in the OPC-GBFS sample. After exposure to high temperatures the first phase to decompose was ettringite at 75 °C followed

[1] Cement chemistry notation will be used in this paper: C = CaO; S = SiO_2; A = Al_2O_3; F = Fe_2O_3; $ = SO_3; H = H_2O

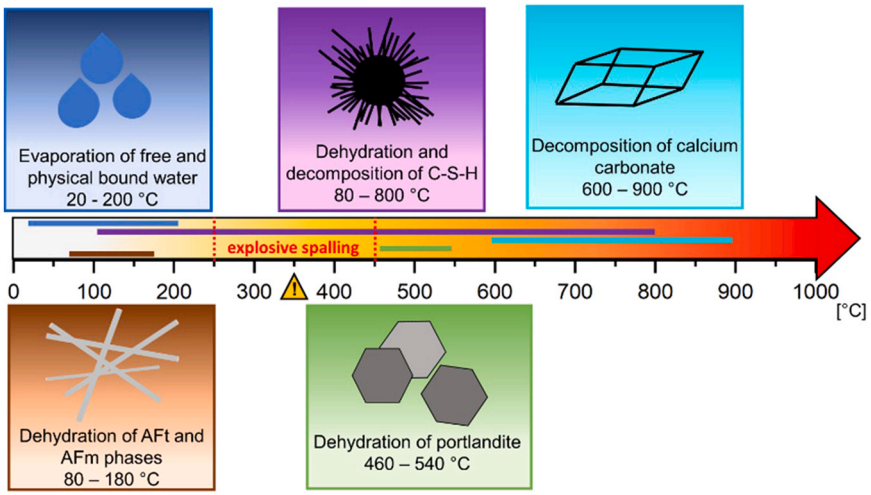


Fig. 1. Schematic representation of the dehydration and decomposition of the main phases in hardened cement paste in concrete.

by the AFm phases which disappeared at 160 °C in both pastes. Thereupon, hydrogarnet decomposed between 200 and 380 °C in the hardened OPC paste. The decomposition of the main binder phase C-S-H was firstly noted after exposure to 400 °C where the CaO layers got destroyed. However, the actual dehydration already starts at temperatures around 80 °C. This early stage of dehydration is not detectable in XRD patterns, as moderate temperatures primarily affect the interlayer spacing of hydration products without altering their crystalline structure. Beyond 600 °C the dehydration of portlandite and decomposition of CaO_3 was reported. Furthermore, the formation of α_1-C_2S, and lime was observed during the high temperature exposure. Lin et al. [10] studied the thermal decomposition behavior of OPC, as well as binary and ternary blends of OPC with LS and CC after 180 d of curing, over a temperature range of 20 – 900 °C. Key findings included the formation of monocarboaluminate in limestone-containing blends, and both monocarboaluminate and hemicarboaluminate in limestone calcined clay cement (LC^3) systems. The peak intensity increased with higher proportions of limestone and calcined clay. Upon exposure to 300 °C, the AFt and AFm phases were no longer detectable. Instead, katoite was observed, which was reported to positively influence strength development. At higher temperatures of 550 °C, katoite and portlandite decomposed and a further increase up to 900 °C led to the decomposition of calcium carbonate and eventually C-S-H. Cao et al. [11] investigated the thermal stability of LC^3 between 100 and 400 °C. An OPC reference mix was compared to a LC^3 mix consisting of 53 wt.-% OPC, 30 wt.-% CC 15 wt.-% LS and 2 wt.-% gypsum prepared with a w/b of 0.325. The samples were measured after 150 d of hydration. Due to the use of calcined clay and limestone, significant quartz and calcite peaks were present. After exposure to 50 °C, both ettringite and monocarboaluminate were still present in the two pastes. However, it was stated that due to the synergetic reaction between CC, LS and portlandite increased contents of monocarboaluminate phases were detected in LC^3 samples. Further temperature increases up to 100 °C led to the decomposition of ettringite and a partial conversion of monocarboaluminate into hemicarboaluminate. Both AFm type phases dehydrated and disappeared completely at 200 °C. The pattern's crystallinity between 2θ angles of 25 – 35 ° decreased which was attributed to the dehydroxylation of the C-(A)-S-H. Lower amounts of portlandite were recorded in the LC^3 specimens due to its pozzolanic character, the total amount in both mixes decreased noticeably at 400 °C. Additionally, the phases katoite and strätlingite formed after an exposure to 100 °C. Studies by Donatello et al. [12] analyzed the phase evolution of a high-volume FA blended cement paste in comparison to a Portland-composite cement CEM II/A-M paste with a w/b of 0.32 and 0.36, respectively, after 70 d of curing. In the initial state due to the large amount of pozzolans, the high-volume FA paste showed no portlandite. In addition, C-S-H was recorded as well as the typical FA phases quartz, anorthite, maghemite and hematite. After 800 °C, the appearance of laihunite was noted. The CEM II/A-M sample showed the typical hydration phases of a cementitious binder in the form of C-S-H, portlandite and ettringite. Based on the raw material's composition, calcite and slag could also be

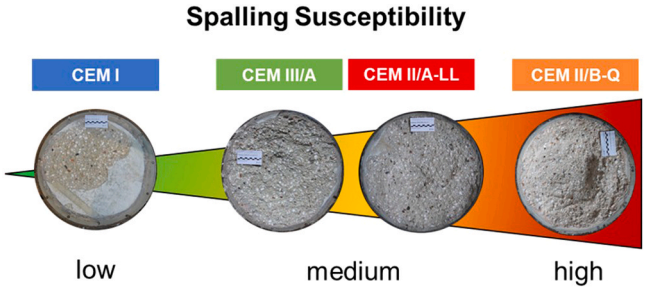


Fig. 2. Spalling susceptibility of normal strength concrete with different types of cement after HC fire exposure.

identified.

Although numerous studies have investigated the thermal decomposition and dehydration behavior of cementitious materials [13–15], their impact on concrete's spalling behavior has often been overlooked. However, with the growing adoption of low-carbon blended cements in sustainable construction, interest in understanding the spalling behavior of blended cement concrete has increased significantly in recent years [4]. In-depth spalling studies on concretes with standardized blended cements, such as, CEM II/A-L(L), CEM II/B-V, and CEM III/A, conducted by various research groups have produced both consistent findings but also contradictions [16–19]. However, phase assemblage and phase transformations at high temperatures, which strongly influence concrete properties, have never been included in these investigations. In our previous research we showed that blended cements increase the spalling susceptibility of normal strength concrete used for tunnel construction when exposed to hydrocarbon (HC) fire (Fig. 2) [20]. We also demonstrated that the cement type significantly influences the thermally induced moisture transport during one-sided heating [21]. As mentioned above, there is only very limited information available on the quantitative phase transformation of blended cement pastes due to high-temperature exposure with regards to explosive spalling, in particular for cement mixes containing calcined clays. Especially the type and number of hydrated phases with their corresponding dehydration behavior are of interest to evaluate their impact on thermohydraulic effects. Thus, in-depth studies were carried out regarding the phase development in four different cement pastes (CEM I, CEM II/A-LL, CEM II/A and CEM II/B-Q) after exposure to high temperatures (105 – 500 °C). XRD with subsequent Rietveld analysis was used to quantify the phase composition before and after heating. In addition, the dehydration behavior was analyzed by TGA.

2. Raw materials and sample preparation

Four different cements from the same manufacturer with the same cement clinker classified after DIN EN-197–1 [22], CEM I 42.5 N (96 % clinker, 4 % LS), CEM II/A-LL 42.5 N (86 % clinker, 14 % LS), CEM III/A 42.5 N (56 % clinker, 4 % LS, 40 % BFS) and CEM II/B-Q 42.5 N (72 % clinker, 3 % LS, 25 % CC) were investigated throughout this work. The chemical composition determined by X-ray fluorescence (XRF) analysis and loss of ignition (LOI) provided by the manufacturer compared to the XRF data from measurements carried out independently both according to DIN EN 196–1–2 [23] are shown in Table 1. The XRF measurements at our institution were carried out using a Zetium PANalytical device with a Rh tube anode working in the range of 24–60 kV. For each cement two fused tablets prepared at 1065 °C were used. The $Na_2O_{equiv.}$ corresponds to $Na_2O_{equiv.} = Na_2O + 0.658 \times K_2O$. Table 2 provides an overview of the specific surface area according to Blaine. The cement pastes were prepared with a w/c of 0.47 and cast into prismatic molds (4 ×4 x 16 cm) (Fig. 3a)). After 1 day of curing, the samples were demolded and kept in a water bath for 6 more days and then stored in a climate chamber at (20 ± 2) °C and (65 ± 5) % RH until they reached an age of > 180 days. The conditioning time meets the duration recommended by RILEM TC 256-SPF for fire testing [24], consistent with the procedure applied in our previously conducted spalling experiments [20]. In this study, particular attention was given to ensure that the hydration conditions of the cement paste closely matched those of the concrete fire-test specimens. This approach aimed to achieve a comparable degree of hydration, albeit at the expense of potentially increased carbonation, since previous research has shown that saturated or sealed curing conditions significantly affect both the degree of hydration and the associated moisture distribution [25–27], factors considered critical for explosive concrete spalling.

For the XRD analysis with Rietveld refinement, samples of the four cements and the cement pastes were prepared both before and after high temperature treatment. Before the high-temperature treatment, four sub-samples of almost equal size were obtained by splitting the prisms with a hydraulic stone press (Fig. 3b)). Thereafter, the cubic samples were gradually heated at 2 K/min in a drying cabinet from Memmert under atmospheric conditions to target temperatures of 105 °C and 300 °C. The exposure to 500 °C at 2 K/min was carried out in a Carbolite muffle furnace, Type CWF 11/23/E301, also under atmospheric conditions. Once the respective target

Table 1
Chemical composition determined by XRF of the cements provided by the manufacturer (man.) and the chemical composition determined by XRF independently (lab.).

Oxide [wt.-%]	CEM I		CEM II/A-LL		CEM III/A		CEM II/B-Q	
	man.	lab.	man.	lab.	man.	lab.	man.	lab.
SiO_2	18.73	19.84	16.98	18.38	24.85	26.44	32.35	33.99
Al_2O_3	5.01	5.11	4.44	4.81	7.02	7.29	8.31	8.38
Fe_2O_3	3.22	2.99	2.74	2.67	2.38	1.91	3.14	3.00
CaO	61.65	61.88	59.68	60.67	52.39	52.47	46.29	45.58
MgO	3.10	2.89	3.08	3.19	5.01	4.94	2.42	2.50
SO_3	3.06	3.27	3.11	3.34	3.08	3.93	2.31	2.48
K_2O	1.04	1.01	0.91	0.96	0.84	0.94	1.33	1.26
Na_2O	0.21	0.25	0.17	0.22	0.25	0.30	0.21	0.21
Cl	0.05	-	0.06	-	0.06	-	0.04	-
P_2O_5	0.27	0.21	0.28	0.21	0.21	0.16	0.21	0.22
CO_2	1.90	-	6.30	-	1.69	-	1.44	-
H_2O	0.71	-	0.70	-	0.62	-	0.82	-
LOI	**2.61**	**2.07**	**7.0**	**4.60**	**2.31**	**0.93**	**2.26**	**0.94**
Na_2O equiv.	0.89	0.91	0.77	0.85	0.80	0.92	1.08	1.03

Table 2
Specific surface area according to Blaine.

Cement	CEM I	CEM II/A-LL	CEM III/A	CEM II/B-Q
Blaine value [cm^2/g]	2900	4650	4890	6050

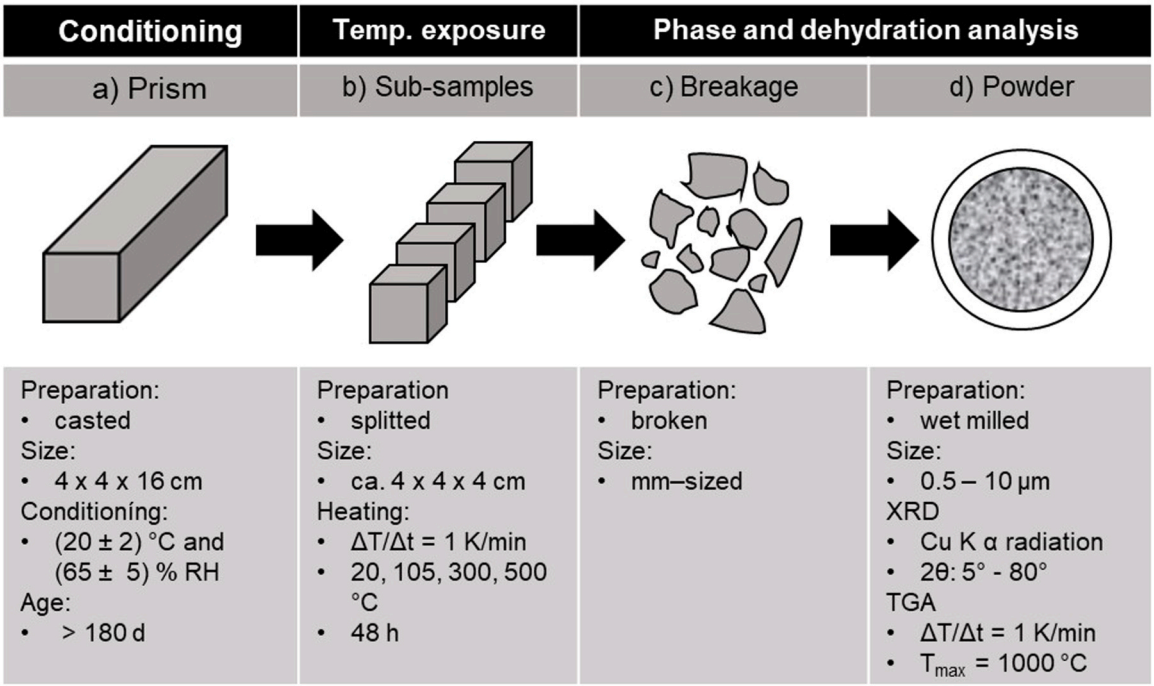


Fig. 3. Sample preparation steps of the hardened cement paste samples.

temperature was reached, it was maintained for 48 h. Even tough tunnel fires can last for such long periods of time (e.g. Mont Blanc Tunnel fire 1999) [28], spalling is usually only expected in the first 20 min. However, the extended heating period was selected to ensure a uniform temperature distribution and complete phase transformation throughout the relatively thick specimen, as hardened cement paste exhibits very low thermal diffusivity which decreases further as temperature rises [29,30]. This approach guarantees that the subsequent XRD analyses are performed on samples that are as homogeneous as possible and free from inhomogeneities caused by incomplete phase transformations due to insufficient temperature equilibration. The temperature gradient that occurs during a real fire and the associated phase composition gradient can thus be analyzed in single steps to understand the cement type specific transformations and their impact on spalling. Further carbonation is not expected, since the rate of carbonation decreases rapidly above 100 °C as with continuous temperature exposure necessary water becomes unavailable [31]. Thereupon, the samples were sealed in plastic wrap and stored in a desiccator to minimize the effects of rehydration. In the next step, the samples were first coarsely crushed (Fig. 3c)) and then finely ground using a McCrone Micronizing Mill (Fig. 3d)). Anhydrous isopropanol was used as the milling medium and was subsequently removed by drying. The milling process lasted 6 min, resulting in a powder with a particle size range between 0.5 – 10 µm [32]. An overview of the sample matrix is given in Table 3. The TGA analysis of the four hardened cement pastes was conducted using residual material from the samples prepared for XRD, prior to any high-temperature exposure.

Table 3
Overview of the sample matrix including the non-hydrated cements and hardened cement pastes exposed to different temperatures.

Material	Sample			
Cement	CEM I	CEM II/A-LL	CEM III/A	CEM II/B-Q
Hardened cement paste	CEM I_20C	CEM II/A-LL_20C	CEM III/A_20C	CEM II/B-Q_20C
	CEM I_105C	CEM II/A-LL_105C	CEM III/A_105C	CEM II/B-Q_105C
	CEM I_300C	CEM II/A-LL_300C	CEM III/A_300C	CEM II/B-Q_300C
	CEM I_500C	CEM II/A-LL_500C	CEM III/A_500C	CEM II/B-Q_500C

3. Methodology

3.1. XRD

The XRD measurements for quantitative analysis of the mineral phases were performed on a Bruker D8 DaVinci diffractometer equipped with an energy dispersive LynxEye detector. The X-ray generator was operated at 40 kV and 25 mA using Cu Kα radiation. Data were collected over a 2θ range of 5° to 80°, with a step size of 0.011° and a counting time of 0.5 s per step. One measurement per sample was performed and deemed sufficient, as repeat measurements of random samples from the same batch showed very good agreement. Rietveld refinement was carried out using **TOPAS V7.0**. The crystal structures used are listed in Table 4 along with their corresponding Inorganic Crystal Structure Database (ICSD) codes. Where no ICSD code is available, the corresponding original literature reference is provided. In anhydrous cement, the typical accuracy is 0.6 – 2 wt% for clinker minerals, 2 wt% for amorphous phases and 0.3 wt% for the residual constituents [33,34]. In the hydrated state, the error for C-S-H content is assumed to be ± 4 wt% [35]

3.2. TGA

Thermogravimetric analysis to investigate the dehydration behavior of the cement paste was also performed twice on ground samples from the same batch used for the XRD samples of each cement type. Roughly 10 mg per sample was measured in a TGA/DSC 3 from Mettler Toledo and heated under a nitrogen (N_2) atmosphere at a heating rate of 10 K/min from 25 °C to 1000 °C.

4. Results

4.1. XRD

The measured XRD patterns of the raw cement are shown in Fig. 4 with the corresponding quantitative phase content displayed in Table 5. The amount of clinker phases decreases with increasing substitution rates of SCMs in the different cement types. Anhydrite and Basanite were identified as sulfate carriers in every cement with slightly different amounts. Moreover, calcite was also found in every sample. For CEM I, CEM III/A and CEM II/B-Q calcite only functioned as a secondary component and therefore appeared in low amounts between 2.5 and 5 wt%. In CEM II/A-LL calcite functioned as the main replacement material for the cement clinker and therefore higher contents of 14 wt% were measured. Additional differences can be seen in the contents of amorphous phases. CEM III/A shows the largest amount of amorphous phase which comes from the replacement of clinker with blast furnace slag. In CEM II/B-Q comparably high fractions of amorphous phases can be seen, caused by the addition of calcined ilitic-kaolinitic clay, which also accounts for the large amounts of quartz present and traces of mica.

The results of the XRD analysis of the hardened cement pastes are presented in Fig. 5. Table 6 provides an overview of the phase composition of all hardened cement pastes analyzed in the initial state (20 °C) and after exposure to 105, 300 and 500 °C. As expected, large residual amounts of the clinker minerals C_3S, C_2S, C_3A and C_4AF were found in the CEM I_20C due to the highest proportion of cement clinker and the coarse grain size distribution associated with the smallest specific surface area according to Blaine. CEM II/A-LL_20C paste showed the second most amount of those phases as it has the second highest amount of clinker and the second smallest Blaine value. In CEM III/A_20C and CEM II/B-Q_20C barely any clinker minerals were left, indicating a near complete hydration. In addition, calcite was detected in all samples as it was a secondary component of the cements. However, increasing amounts of calcium carbonate with the appearance of vaterite was caused by carbonation of the samples. The tendency of increasing calcite contents in comparison to the non-hydrated cement are caused by the transition of metastable vaterite into calcite [36]. Especially hardened

Table 4
Crystal structures and their corresponding ICSD codes.

Phase	ICSD Code
C_3S	94742
C_2S	963
C_3A cubic	1841
C_3A orthorhombic	100220
C_4AF	9197
Anhydrite	16382
Bassanite	79529
Ettringite	155395
Hemicarbonate	263
Monocarbonate	59237
Monosulfate	100138
C-S-H	Bergold et al. [35]
Portlandite	34241
Calcite	80869
Vaterite	15879
Quartz	174

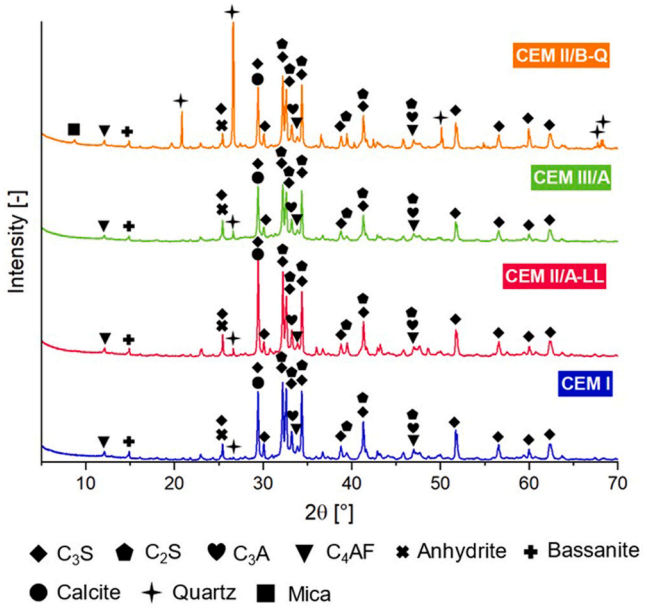


Fig. 4. XRD patterns of the different cements.

Table 5
Phase composition of the cements used [wt%].

Mineral phase	CEM I	CEM II/A-LL	CEM III/A	CEM II/B-Q
C_3S	50.0	47.0	32.0	40.0
C_2S	13.0	10.0	7.0	4.0
C_3A	9.8	7.5	5.4	6.7
C_4AF	6.2	5.8	3.9	1.2
Anhydrite	2.0	1.8	1.2	1.1
Bassanite	1.2	1.4	1.1	1.5
Calcite	5.0	14.0	3.8	2.5
Quartz	0.3	0.7	0.8	16.0
Amorphous	7.8	6.2	42.0	14.5
Others	4.5	4.8	2.7	8.2

cement pastes of CEM III/A and CEM II/B-Q showed high contents of carbonate phases suggesting a stronger degree of carbonation, which is often observed in slag or calcined clay cement blends [37,38]. After exposure to 500 °C, parts of the vaterite tend to decompose, while calcite remains stable which is consistent with previous findings of Li et al. [39]. This phenomenon occurs due to the lower lattice packing density of vaterite in comparison to calcite [40]. Another noticeable point is the significant amounts of quartz (at least 12 wt%) found in the CEM II/B-Q cement paste samples which is a byproduct from the calcined clay.

Lower amounts of AFt and AFm phases (hemicarboaluminate, monocarboaluminate and monosulfoaluminate) were identified in the blended cement pastes (CEM II/A-LL_20C, CEM III/A_20C and CEM II/B-Q_20C) ranging between 8.5 and 9.0 wt%, compared to 11.6 wt% in CEM I_20C. After an exposure to 105 °C, ettringite dehydrated and is no longer visible in the XRD patterns. A further temperature increase to 300 °C led to the dehydration and decomposition of all AFm phases in every sample.

Lower amounts of C-(A)-S-H were identified in CEM III/A and CEM II/B-Q hardened pastes, with values of 22 and 23 wt%, respectively, compared to approximately 30 wt% in CEM I and CEM II/A-LL hardened pastes. However, the thermal stability of the C-(A)-S-H phases varied among the different cement types. While the C-(A)-S-H in CEM I_300C and CEM II/A-LL_300C underwent significant dehydration between 105 °C and 300 °C and was almost completely decomposed after exposure to 500 °C, the C-(A)-S-H in CEM II/B-Q_300C and particularly in CEM III/A_300C remained stable up to 300 °C. Near-complete dehydration and decomposition were only observed after exposure to 500 °C in CEM III/A_500C and CEM II/B-Q_500C. The increased thermal stability of slag cement paste was also reported by Jia et al. [41] and might be associated with the formation of more tightly packed C-(A)-S-H gels. Beside the C-S-H content the amount of portlandite also varied between the single cement pastes. Lower portlandite contents of around 5 wt% were observed throughout the CEM III/A and CEM II/B-Q hardened cement paste samples, while higher amounts of approximately 10 and 8 wt% were recorded in CEM I and CEM II/A-LL samples respectively. These differences are caused by the lower amounts of available clinker minerals and the pozzolanic reaction of the slag and calcined clay containing binders. Even after exposure to 500 °C, portlandite always appeared in the XRD patterns. However, the detected peaks decreased in height, but increased in width with rising temperature exposure, which indicates a decline in crystallinity but no complete degradation of the structure. Hence, despite the

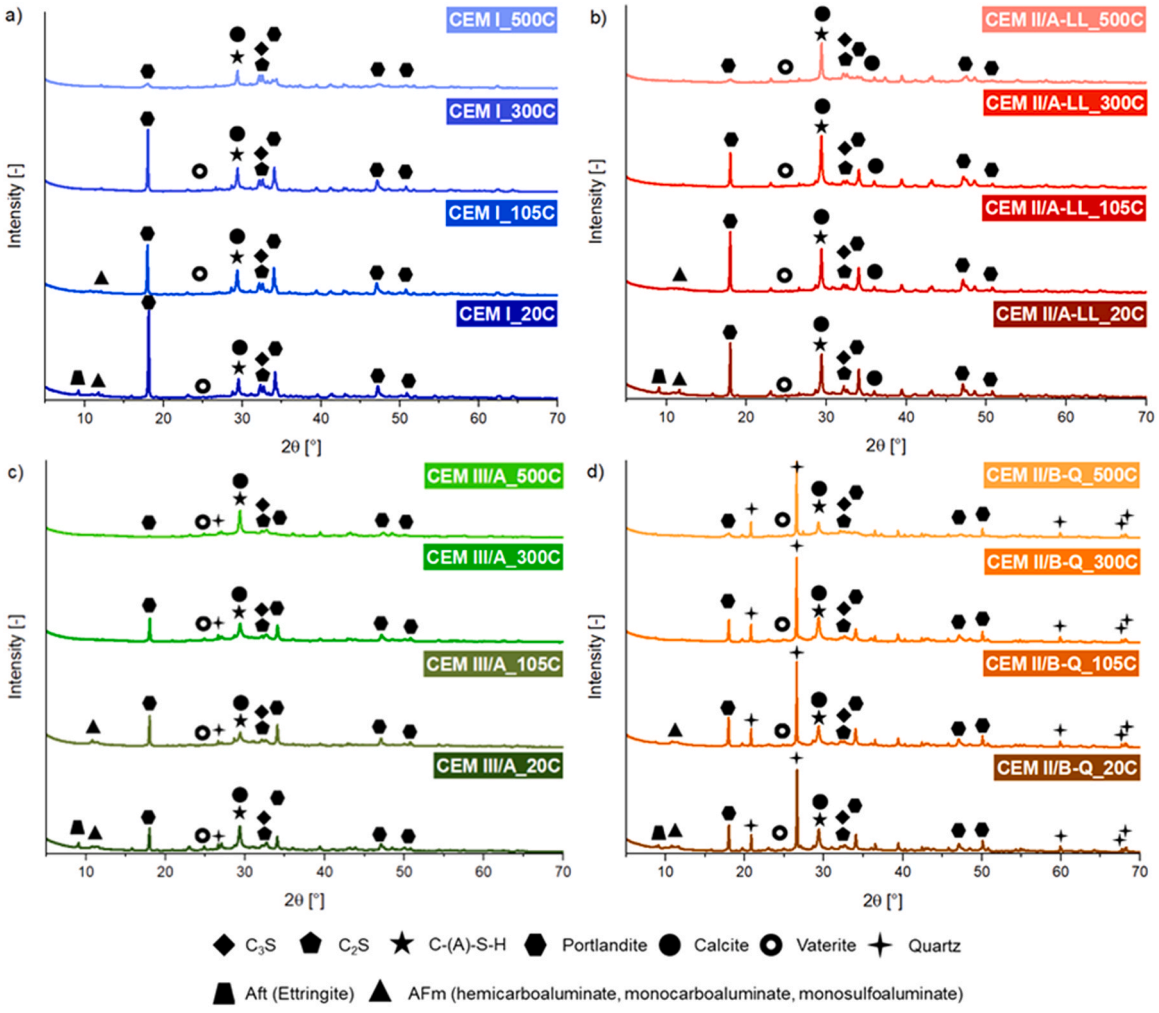


Fig. 5. XRD patterns of the different hardened cement pastes after exposure to 20 °C, 105 °C, 300 °C and 500 °C.

occurring dehydration the crystal structure remains detectable, similar findings were reported by Song et al. [6]. Interestingly, CEM III/A_500 C exhibited a more pronounced decomposition of portlandite. The underlying cause remains uncertain; however, previous studies have shown that the phase assemblage of the non-hydrated cement and chemical environment during hydration can influence its size and morphology [42,43], which may also affect the thermal stability of portlandite. Overall, crystallinity decreased after temperature exposure to 500 °C, caused mainly by the dehydroxylation of C-(A)-S-H leading to an increase of the amorphous phase content. The high content of amorphous phases in hardened CEM III/A paste is based on the residual content of blast furnace slag, which generally reacts to only about 40 % after a hydration period of 6 months [44].

4.2. TGA

Fig. 6 shows the results of the TGA for the different hardened cement pastes. Because of the solvent exchange during the sample preparation with isopropanol no free evaporable water remained. The water loss up to 200 °C can be mainly attributed to the dehydration of AFt and AFm phases. Here, the largest mass loss was recorded in the CEM I_20C sample, which corresponds to the XRD measurements where the most amounts of AFt and AFm phases were found. For CEM II/B-Q_20C a noticeable increase in water loss was displayed between 140 and 200 °C, which can be attributed to AFm phases (most likely monocarboaluminate). Furthermore, CEM III/A_20C cement paste shows the lowest mass loss over the temperature increase up to 500 °C, which would support the idea of a thermally more stable C-(A)-S-H phase in the slag cement also seen in the XRD results. Between 400 °C and 500 °C the dehydration of portlandite was observed, resulting in a comparatively lower mass loss in the latent hydraulic and pozzolanic cementitious systems. The relatively low temperature onset of dehydration suggests low crystallinity of the portlandite phase. Lastly, the decomposition of calcium carbonate was detected already between 500 and 760 °C. A closer look into the differential thermal gravimetry (DTG) showed a two stage mass loss associated with the decomposition of calcium carbonate, whereas the first is coming from low crystalline vaterite

Table 6
Phase composition in wt% of the hardened cement pastes before and after exposure to temperatures of 105, 300 and 500 °C determined by XRD.

Sample		C_3S	C_2S	C_3A	C_4AF	Ettringite	Hemicarb.	Monocarb.	Monsulf.	C-(A)-S-H	Portlandite	Calcite	Vaterite	Quartz	Amorphous	Others
CEM I	20 C	5.8	7.0	2.0	3.6	4.0	1.6	5.7	0.3	30.0	9.0	4.7	4.4	0.3	20.8	0.8
	105 C	6.0	8.0	2.0	3.6	0.0	1.5	3.2	0.4	35.0	10.0	8.8	5.8	0.3	14.4	1.0
	300 C	6.8	8.0	2.0	4.0	0.0	0.0	0.3	0.0	21.0	11.0	8.8	4.9	0.5	31.7	1.0
	500 C	7.0	9.0	2.0	3.3	0.0	0.0	0.0	0.0	10.0	9.0	7.0	0.5	0.4	50.8	1.0
CEM II/A-LL	20 C	2.0	3.8	1.0	2.3	2.7	1.0	4.8	0.0	30.0	8.5	12.6	4.6	0.4	25.1	1.2
	105 C	2.0	4.0	1.0	2.9	0.0	0.9	3.0	0.4	34.0	9.4	14.0	3.5	0.5	23.2	1.2
	300 C	2.0	4.0	1.1	1.7	0.0	0.0	0.0	0.0	21.0	7.6	25.0	6.0	0.4	29.7	1.5
	500 C	2.0	5.0	1.0	1.5	0.0	0.0	0.0	0.0	5.0	7.0	18.0	1.0	0.4	57.7	1.4
CEM III/A	20 C	0.7	1.2	0.2	1.0	3.5	1.0	4.0	0.0	22.0	4.0	7.1	11.0	0.7	43.0	0.6
	105 C	0.8	2.0	0.2	1.2	0.0	1.6	3.2	0.0	21.0	5.0	2.5	3.0	0.5	58.5	0.5
	300 C	0.5	2.0	0.2	1.3	0.0	0.0	0.0	0.0	22.0	6.0	5.0	8.0	0.7	53.6	0.7
	500 C	0.8	2.4	0.2	1.4	0.0	0.0	0.0	0.0	7.0	0.1	14.0	9.0	0.5	63.9	0.7
CEM II/B-Q	20 C	0.4	2.0	0.5	1.2	1.3	1.5	5.2	1.0	23.0	4.5	8.0	10.0	12.0	24.8	4.0
	105 C	0.8	2.0	0.0	1.7	0.0	1.2	5.2	0.0	28.0	5.7	8.0	7.5	13.0	21.8	5.1
	300 C	0.9	2.0	0.0	1.5	0.0	0.0	0.0	0.0	21.0	4.7	12.0	10.0	14.0	29.0	4.9
	500 C	1.0	2.0	0.2	0.4	0.0	0.0	0.0	0.0	7.0	4.8	6.0	2.5	14.0	56.4	5.7

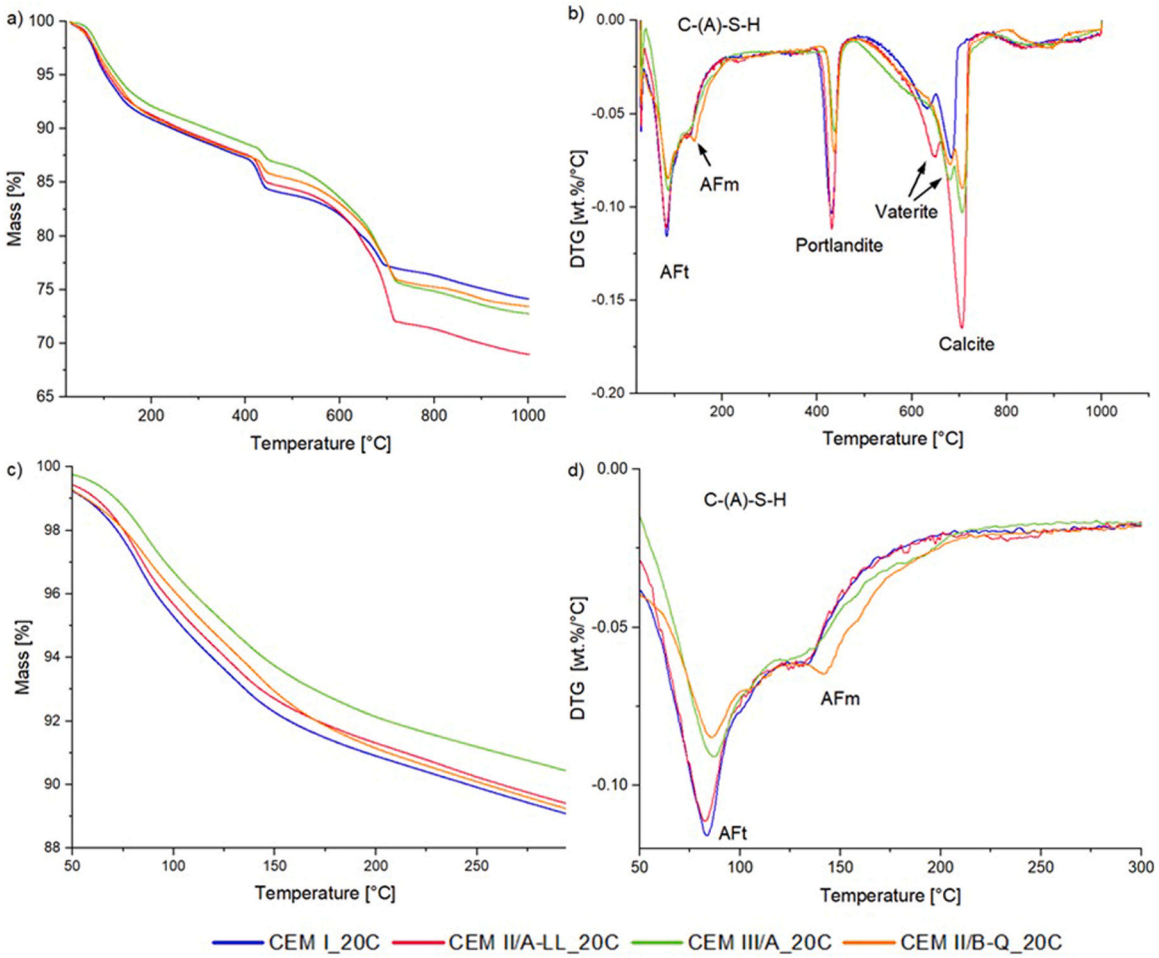


Fig. 6. Thermal analysis of the hardened cement pastes a) TGA 20–1000 °C; b) DTG 20–1000 °C; c) TGA 50–300 °C; d) DTG 50–300 °C.

and amorphous calcium carbonate present due to carbonation [39]. This also explains why the decomposition started at comparably low temperatures, where it would be not expected for pure and well crystalline calcite [39]. The overall mass loss associated with calcium carbonate was obviously the most pronounced for CEM II/A-LL_20C. However, both CEM III/A_20C and CEM II/B-Q_20C exhibit a higher mass loss than the CEM I paste, despite having similar initial calcium carbonate contents. This was attributed to more pronounced carbonation in the blended cement paste samples. This observation is consistent with the XRD results, which showed the highest amounts of vaterite in the CEM III/A_20C and CEM II/B-Q_20C samples. Up to 500 °C, the CEM I paste showed the relative highest mass loss (which was solely attributed to dehydration) of 16.2 wt% followed by CEM II/A-LL_20C, CEM II/B-Q_20C and CEM III/A_20C with 15.64, 14.76, and 13.60 wt% respectively. The final relative mass loss after thermal exposure to 1000 °C was highest in the CEM II/A-LL_20C at 31.08 wt% followed by CEM II/B-Q_20C (26.60 wt%), CEM III/A_20C (27.28 wt%) and CEM I_20C (25.91 wt %). This trend is attributed to the decomposition of carbonate phases.

5. Discussion

The analysis of the phase composition and dehydration behavior of the cement pastes was carried out to gain deeper insight into the increased spalling susceptibility observed for blended cement concretes. This study revealed clear differences in both phase content and decomposition behavior. The behavior of the hydrate phases up to around 300 °C plays a particular role, as this temperature range is typically associated with explosive spalling. It was observed that CEM I cement pastes tend to have higher amounts of combined AFt and AFm phases, which already dehydrate between 70 and 200 °C. This might have a positive impact, lowering the spalling susceptibility in OPC concrete since more water can be released at comparable moderate temperatures before spalling occurs. All cement pastes exhibit carbonation, with more pronounced carbonation observed in CEM III/A and CEM II/B-Q samples. This is occurs more rapidly in C-(A)-S-H due to reduced portlandite contents [41]. Furthermore, CEM I and CEM II/A-LL showed higher contents of C-(A)-S-H in comparison to CEM III/A and CEM II/B-Q. The XRD results recorded after high temperature exposure showed that C-(A)-S-H in CEM II/B-Q and particularly in CEM III/A paste is thermally more stable, which was also confirmed by the TGA

measurements retaining more water and structural stability at higher temperatures. This is also in alignment with observations reported by Xu et al. [45] who concluded that the 'dreierketten'-like structure of C-(A)-S-H in slag blended cement systems remains stable up to 450 °C. Responsible for this increased thermal stability might be the more tightly packed structure of C-(A)-S-H gels [41] which incorporate higher amounts of non-evaporable water [46]. In addition, the increased carbonation of the C-(A)-S-H phases due to less portlandite contents [47] can lead to the formation of calcium-carbonate modified silica gel, which shows increased high-temperature resistance [39]. However, this effect would only affect the first few centimeters in large concrete structures and therefore is less relevant for explosive spalling. The improved thermal stability of C-(A)-S-H in slag- or pozzolan-containing systems may contribute to enhanced mechanical performance at elevated temperatures, as reported in literature [48,49]. However, our observations indicate a more pronounced increase in permeability after exposure to 150 °C in concrete samples produced with the same cements (Table 7) [21]. This suggests that the increase is not due to more severe degradation of the cementitious matrix. Instead, other factors, such as pore pressure and the associated development of microcracks, may be responsible for this phenomenon. Currently, no experimental data on pore pressure in concretes with these cements are available; however, numerical simulations by Peters et al. [50] based on the same cements indicate a slight increase in pore pressure for CEM III/A and CEM II/B-Q concrete in comparison to CEM I concrete. Additionally, simulations by Jia et al. [51] concluded that the incorporation of fly ash influences pore pressure and crack development in cementitious materials. Furthermore, Reiners et al. [19] reported that concrete made with blended cements exhibits a less distinct interfacial transition zone (ITZ). As a result, there is no effective "cushion" to accommodate the expansion of aggregates, leading to more severe cracking in slag and pozzolan containing concretes. Both aspects may explain the observed competing effects: increased thermal stability of the cementitious matrix coupled with a steeper rise in permeability at elevated temperatures.

In our previous study, we showed that the development of the drying front and permeability in concrete changes with the cement type used [21]. The detected moisture profiles after heating correlate very well with the dehydration behavior of the hardened cement pastes, meaning that the sequence of drying from the least progressed in CEM III/A to the most progressed in CEM I matches with the sequence of mass loss determined by TGA up to 216 °C (Fig. 7). At higher temperatures, it appears as if the drying behavior shown in the ^{1}H NMR relaxometry measurements is the same in all types of concrete. This is because the NMR tomograph cannot fully detect chemically bound water, thus, further differences only appear in the mass loss obtained by TGA. The comparison indicates that the thermally induced moisture transport is consistent with dehydration behavior of the cementitious matrix. Furthermore, this explains why CEM III/A and CEM II/B-Q concrete exhibit very different drying behaviors despite having the same initial moisture content and permeability development as described in [21] (see Table 7). In this regard, it should also be added that the increase in permeability at higher temperatures has probably only minor impact on the drying behavior, as most of the water is already released up to 200 °C. It must be noted that the correlation between cement mass loss and the progression of the drying front can only be considered indirect. In concrete, additional factors, such as the quantity and type of aggregates, the ITZ, and the resulting crack formation also play a significant role. Furthermore, in a real concrete component, constraints and applied loads must be taken into account, as they can influence the structural behavior and thermomechanical response.

In summary, the results lead to the hypothesis that stronger water retention during heating in blended cement concrete, caused by thermally more stable hydrate phases, increases the risk of spalling, as more moisture remains available before the onset of the moisture clog. Although the observed moisture differences appear minor, previous research has demonstrated that even slight increases in moisture content can significantly raise spalling susceptibility, even when permeability is constant [52].

6. Conclusion

The analysis of the thermally induced phase decomposition in blended cement pastes showed clear differences between the individual cement pastes. Regarding explosive spalling of concrete, the following conclusions were drawn:

- All blended cement pastes tend to show lower amounts of early dehydrating AFt and AFm phases in comparison to CEM I paste observed in the XRD results. The TGA showed similar tendencies, with a slightly higher water loss for CEM I paste. In blended cement concrete lower permeabilities further inhibit water release leading to more available moisture in a temperature range critical for explosive spalling.
- The C-(A)-S-H in blended cements with latent hydraulic or pozzolanic properties showed better thermal stability especially in CEM III/A paste, since less decomposition was recorded over increasing temperatures. The increased thermal stability might be caused by the denser structure of C-(A)-S-H gels as well as their enhanced carbonation which may lead to the formation of calcium-modified silica gels with improved thermal properties.
- The drying behavior and associated moisture transport in blended cement concrete is strongly determined by the dehydration behavior of the cementitious matrix up to 200 °C. The development, particularly the different increase of permeability with increasing temperatures seems to play a less significant role as most of the water is already released below 200 °C. Therefore, the initial permeability is more decisive for evaluating the spalling risk of concrete.
- The increased thermal stability of hardened cement pastes containing slag and calcined clays is often considered beneficial for concrete strength at high temperatures, however, the opposite is true for fire-induced spalling. Therefore, its use in practice must be carefully considered if fire resistance is required.

7. Outlook

Besides the impact on the thermohydraulic mechanism, the cement type might also influence the thermomechanical behavior of

Table 7
Intrinsic gas permeability of the different concretes after exposure to 20 °C, 105 °C, 150 °C, 170 °C and 300 °C [21].

Intrinsic permeability		CEM I	CEM II/A-LL	CEM III/A	CEM II/B-Q
Permeability $K_{gas(20\ °C)}$		2.13×10^{-17}	5.86×10^{-18}	2.19×10^{-18}	5.47×10^{-18}
Permeability $K_{gas(105\ °C)}$		1.55×10^{-16}	3.49×10^{-17}	3.10×10^{-17}	3.31×10^{-17}
Permeability $K_{gas(150\ °C)}$	[m^2]	2.36×10^{-16}	7.69×10^{-17}	1.04×10^{-16}	1.43×10^{-16}
Permeability $K_{gas(170\ °C)}$		3.20×10^{-16}	1.20×10^{-16}	1.65×10^{-16}	2.05×10^{-16}
Permeability $K_{gas(300\ °C)}$		1.16×10^{-15}	4.88×10^{-16}	1.17×10^{-15}	9.99×10^{-16}

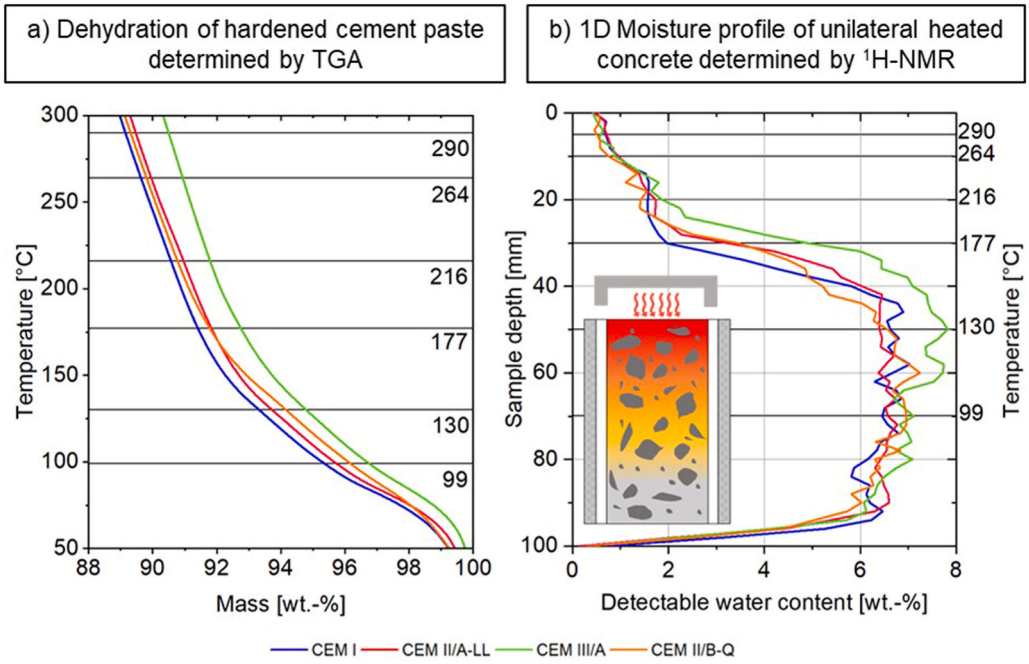


Fig. 7. Comparison between a) the dehydration behavior of the hardened cement pastes (TGA) and b) the moisture profiles in concrete made with the corresponding cement after one sided heating (^{1}H NMR) described in [21] shows the same sequence of water loss.

concrete.

The increased thermal stability of C-(A)-S-H in CEM II/B-Q and CEM III/A might lead to different thermomechanical behaviors particularly with regard to load-induced thermal strains (LITS). In concrete structures where thermal deformations are usually partially or completely restrained, LITS have a positive influence. LITS act in the direction of the applied load and therefore reduce compressive stresses caused by the restrained thermal expansion [53] potentially lowering the risk of explosive spalling. Key mechanisms behind the formation of LITS are thermal transient creep and drying creep, which are both strongly dependent on the decomposition of the hydrate phases and the associated water transport [54,55]. Peters et al. [56] observed that the evolution of the degree of C-S-H dehydration is in close agreement with experimentally determined evolution of LITS caused by creep-like C-S-H sliding under compressive load. Thermally stable C-(A)-S-H found in CEM II/B-Q and CEM III/A paste might inhibit this effect, leading to lower LITS and lower relaxation rates of thermally induced stresses. Hence, increasing the spalling susceptibility in blended cement concrete made with those types of cement.

Furthermore, the thermal mismatch between the shrinking cement matrix and the expanding aggregates at elevated temperatures (around 150 °C) is considered to be a key factor for explosive concrete spalling. The mismatch generates internal stresses that tend to promote spalling. The shrinkage behavior of pure cement paste progresses through four distinct stages according to Koyama et al. [57]: Initially, between 20 °C and 140 °C, shrinkage begins due to the evaporation of free water and the dehydration of AFt phases. This is followed by a steady shrinkage phase from 140 °C to 300 °C, driven by the loss of interlayer water from the C-S-H gel. Between 300 °C and 490 °C, shrinkage accelerates significantly due to further water loss. Finally, in the stabilization stage beyond 490 °C, C-S-H begins to recrystallize, which reduces further contraction. In blended cement pastes, however, the composition of residual non-hydrated phases varies considerably and should not be neglected. For example, the CEM II/B-Q cement examined in this study contains a high proportion of quartz, which can be considered micro-aggregates. This introduces thermal incompatibility even at the binder level. Quartz aggregates exhibit a particularly pronounced thermal mismatch, but similar effects are also observed with limestone and slag aggregates [58]. The impact of these factors should not be overlooked when assessing the influence of cement type on explosive spalling, especially when aiming for a comprehensive and holistic understanding.

In the future, investigations based on the present results should take a closer look at the thermo-mechanical behavior of blended cement concrete in order to verify or reject the hypotheses regarding the differences in LITS and the thermal mismatch between the cement constituents mentioned above.

CRediT authorship contribution statement

Frank Dehn: Writing – review & editing, Supervision. **Frank Weise:** Writing – review & editing, Supervision, Resources, Project administration, Funding acquisition, Conceptualization. **Ludwig Stelzner:** Writing – review & editing, Supervision, Resources, Project administration, Funding acquisition, Conceptualization. **Tim Pittrich:** Writing – review & editing, Writing – original draft, Visualization, Investigation, Formal analysis, Conceptualization. **Daniel Jansen:** Writing – review & editing, Resources, Investigation, Formal analysis.

Declaration of Competing Interest

The authors declare the following financial interests/personal relationships which may be considered as potential competing interests: Tim Pittrich reports financial support was provided by German Research Foundation. If there are other authors, they declare that they have no known competing financial interests or personal relationships that could have appeared to influence the work reported in this paper.

Acknowledgements

We gratefully acknowledge the support of the German Research Foundation (DFG) and extend our gratitude for their financial support throughout the project ‘‘Thermohydraulic spalling mechanisms in concretes with different binders with and without PP fibers under fire exposure: An experimental and numerical analysis’’ (Project Nr. 491928256). We also express our sincere appreciation to our colleagues, specifically acknowledging the collaborative efforts of BAM divisions 6.3: Structure Analysis, 7.1: Building Materials, and 7.4: Technology of Construction Materials. Their expertise and resources have significantly enriched the scope and depth of our study.

Data availability

Data will be made available on request.

References

[1] K.L. Scrivener, J.M. Vanderley, E.M. Gartner, Eco-efficient cements: Potential economically viable solutions for a low-CO2 cement-based materials industry, Cem. Concr. Res 114 (2018) 2–26, https://doi.org/10.1016/j.cemconres.2018.03.015.
[2] B. Lothenbach, K. Scrivener, R.D. Hooton, Supplementary cementitious materials, Cem. Concr. Res 41 (2011) 1244–1256, https://doi.org/10.1016/j.cemconres.2010.12.001.
[3] McNamee R. (2019) Fire Spalling Theories - Realistic and More Exotic Ones. Proceedings of the 6th International Workshop on Concrete Spalling due to Fire Exposure: Sheffield, England.
[4] T. Pittrich, F. Weise, L. Stelzner, The impact of blended cements on the spalling behavior of concrete at elevated temperatures: a review, Mater. Struct. 58 (2025), https://doi.org/10.1617/s11527-025-02713-x.
[5] I. Hager, Behaviour of cement concrete at high temperature (Technical Sciences), Bull. Pol. Acad. Sci. 61 (2013), https://doi.org/10.2478/bpasts-2013-0013.
[6] H. Song, Y. Jeong, S. Bae, et al., A study of thermal decomposition of phases in cementitious systems using HT-XRD and TG, Constr. Build. Mater. 169 (2018), https://doi.org/10.1016/j.conbuildmat.2018.03.001.
[7] Q. Zhang, G. Ye, Quantitative analysis of phase transition of heated Portland cement paste, J. Therm. Anal. Calor. 112 (2013) 629–636.
[8] Saillio M., Sabeur H., Vincent J. et al (2021) Phase assemblage of a 5 year-old cement paste after submission to various high temperature and cooling regime. https://doi.org/10.1016/j.conbuildmat.2021.122440.
[9] M. Saillio, V. Baroghel-Bouny, M. Bertin, et al., Phase assemblage of cement pastes with SCM at different ages, Constr. Build. Mater. 244 (2019) 144–157, https://doi.org/10.1016/j.conbuildmat.2019.07.059.
[10] R.-S. Lin, Y. Han, X.-Y. Wang, Macro–meso–micro experimental studies of calcined clay limestone cement (LC3) paste subjected to elevated temperature, Cem. Concr. Compos 116 (2021), https://doi.org/10.1016/j.cemconcomp.2020.103871.
[11] Y. Cao, Y. Wang, Z. Zhang, et al., Thermal stability of limestone calcined clay cement (LC3) at moderate temperatures 100–400 °C, Cem. Concr. Compos. (2023), https://doi.org/10.1016/j.cemconcomp.2022.104832.
[12] S. Donatello, C. Kuenzel, A. Palomo, et al., High temperature resistance of a very high volume fly ash cement paste, Cem. Concr. Compos 45 (2014), https://doi.org/10.1016/j.cemconcomp.2013.09.010.
[13] L. Xu, J. Wang, K. Li, et al., A systematic review of factors affecting properties of thermal-activated recycled cement, Resour. Conserv. Recycl. 185 (2022), https://doi.org/10.1016/j.resconrec.2022.106432.
[14] N.C. Collier, Transition and Decomposition Temperatures of Cement Phases - A Collection of Thermal Analysis Data, Ceram. -Silik. áty 60 (2016) 338–343, https://doi.org/10.13168/cs.2016.0050.
[15] M. Sundin, H. Hedlund, A. Cwirzen, Eco-Concrete in High Temperatures, Mater 16 (2023), https://doi.org/10.3390/ma16124212.
[16] Kirnbauer J. and Schneider U. (2011) Influence of cement type and aggregate shape on explosive concrete spalling. 2nd International RILEM Workshop on Concrete Spalling due to Fire Exposure: Delft, The Netherlands 432-439.
[17] I. Hager, K. Mróz, T. Tracz, Concrete propensity to fire spalling: Testing and observations, MATEC Web Conf. 163 (2018), https://doi.org/10.1051/matecconf/201816302004.
[18] M.J. Miah, F. Lo Monte, R. Felicetti, et al., Impact of external biaxial compressive loading on the fire spalling behavior of normal-strength concrete, Constr. Build. Mater. 366 (2023), https://doi.org/10.1016/j.conbuildmat.2022.130264.
[19] J. Reiners, J. Zehfuß, F. Dehn, et al., The influence of the physical and chemical properties of hardened cement paste on the heat-induced explosive spalling of concrete, Civ. Eng. Des. 6 (2024) 4–21, https://doi.org/10.1002/cend.202300020.

[20] Pittrich T., Stelzner L. and Weise F. (2024) Fire-induced spalling of normal strength concrete with different types of blended Portland cement. The 13th International Conference on Structures in Fire: Coimbra, Portugal 451-461.
[21] Pittrich T., Peters S., Meschke G. et al (2025) Thermally induced moisture transport in concrete with different types of blended Portland cement studied by ^{1}H NMR relaxometry. https://doi.org/10.21203/rs.3.rs-7913874/v1.
[22] DIN EN 197-1, Cement - Part 1: Composition specifications and conformity for common cements, Beuth Verlag GmbH, Berlin, Germany, 2011.
[23] DIN EN 196-2, Methods of testing cement – Part 2: Chemical analysis of cement, Beuth Verlag GmbH, Berlin, Germany, 2013.
[24] P. Pimienta, R. McNamee, I. Hager, et al., Recommendation of RILEM TC 256-SPF on the method of testing concrete spalling due to fire: material screening test, Mater. Struct. 56 (2023), https://doi.org/10.1617/s11527-023-02202-z.
[25] Bentz D.P., Snyder K.A. and Stutzman P.E. (1997) Hydration of Portland Cement: The Effects of Curing Conditions. Proceedings of the 10th International Congress on the Chemistry: Sweden.
[26] D.P. Bentz, P.E. Stutzman, Curing, Hydration, and Microstructure of Cement Paste, Acids Mater. J. (2006) 348–356.
[27] M. Nematollahzade, A. Tajadini, A. Iman, et al., Influence of different curing conditions and water to cement ratio on properties of self-compacting concretes, Constr. Build. Mater. 237 (2020), https://doi.org/10.1016/j.conbuildmat.2019.117570.
[28] Catmur J., King K., Parsons M. et al (2023) A Service Analysis of the Mont Blanc Tunnel Fire. Safety Critical Systems Symposium:113-145.
[29] K.Y. Shin, S.B. Kim, J.H. Kim, et al., Thermo-physical properties and transient heat transferof concrete at elevated temperatures, Nucl. Eng. Des. 212 (2002) 233–241.
[30] Q. Zhang, D. Yan, Temperature dependence ofthermal diffusivity of OPCand CAC cement paste, Adv. Cem. Res. 28 (2016) 576–582, https://doi.org/10.1680/jadcr.15.00146.
[31] D. Wang, T. Noguchi, T. Nozaki, et al., Investigation of the carbonation performance of cement-based materials under high temperatures, Constr. Build. Mater. 272 (2021), https://doi.org/10.1016/j.conbuildmat.2020.121634.
[32] A.J. Locock, D. Chesterman, D. Caird, et al., Miniaturization of mechanical milling for powder X-ray diffraction, Powder Diffr. 27 (2012) 189–193, https://doi.org/10.1017/S0885715612000516.
[33] G. Walenta, T. Füllmann, M. Gimenez, Quantitative Rietveld analysis of cement and clinker, Int. Cem. Rev. (2001) 51–54.
[34] T. Westphal, G. Walenta, T. Füllmann, et al., Characterisation of cementitious materials— Part III, Int. Cem. Rev. (2002) 47–51.
[35] S.T. Bergold, F. Goetz-Neunhoffer, J. Neubauer, Quantitative analysis of C-S-H in hydrating alite pastes by in-situ XRD, Cem. Concr. Res 53 (2013) 119–126, https://doi.org/10.1016/j.cemconres.2013.06.001.
[36] T. Ogino, T. Suzuki, K. Sawada, The rate and mechanism of polymorphic transformation of clacium carbonate in water, J. Cryst. Growth 100 (1990) 159–167, https://doi.org/10.1016/0022-0248(90)90618-U.
[37] F. Lollini, E. Redaelli, Carbonation of blended cement concretes after 12 years of natural exposure, Constr. Build. Mater. 276 (2021), https://doi.org/10.1016/j.conbuildmat.2020.122122.
[38] R. Bucher, P. Diedrich, G. Escadeillas, et al., Service life of metakaolin-based concrete exposed to carbonation Comparison with blended cement containing fly ash, blast furnace slag and limestone filler, Cem. Concr. Res 99 (2017) 18–29, https://doi.org/10.1016/j.cemconres.2017.04.013.
[39] Y. Li, T. Mi, W. Liu, et al., Chemical and mineralogical characteristics of carbonated and uncarbonated cement pastes subjected to high temperatures, Compos. Part B 216 (2021), https://doi.org/10.1016/j.compositesb.2021.108861.
[40] G. Sun, X. Liu, B. Lian, et al., Research Progress on Vaterite Mineral and Its Synthetic Analogs, Mater 15 (2025), https://doi.org/10.3390/min15080796.
[41] Z. Jia, C. Chen, J. Shi, et al., The microstructural change of C-S-H at elevated temperature in Portland cement/GGBFS blended system, Cem. Concr. Res (2019), https://doi.org/10.1016/j.cemconres.2019.05.018.
[42] E. Gallucci, K. Scrivener, Crystallisation of calcium hydroxide in early age model and ordinary cementitious systems, Cem. Concr. Res 37 (2007) 492–501, https://doi.org/10.1016/j.cemconres.2007.01.001.
[43] S. Galmarini, A. Aimable, N. Ruffray, et al., Changes in portlandite morphology with solvent composition: Atomistic simulations and experiment, Cem. Concr. Res 41 (2011) 1330–1338, https://doi.org/10.1016/j.cemconres.2011.04.009.
[44] V.K. Singh, 17 - Developments in Portland slag cements. Woodhead Publishing Series in Civil and Structural Engineering, The Science and Technology of Cement and Other Hydraulic Binders, Woodhead Publishing, 2023, pp. 625–651.
[45] L. Xu, J. Wang, K. Li, et al., New insights on dehydration at elevated temperature and rehydration of GGBS blended cement, Cem. Concr. Compos. 139 (2023), https://doi.org/10.1016/j.cemconcomp.2023.105068.
[46] E. Kapeluszna, Ł. Kotwica, A. Rózycka, et al., Incorporation of Al in C-A-S-H gels with various Ca/Si and Al/Si ratio: Microstructural and structural characteristics with DTA/TG, XRD, FTIR and TEM analysis, Constr. Build. Mater. 155 (2017) 643–653, https://doi.org/10.1016/j.conbuildmat.2017.08.091.
[47] S. von Greve-Dierfeld, B. Lothenbach, A. Vollpracht, et al., Understanding the carbonation of concrete with supplementary cementitious materials: a critical review by RILEM TC 281-CCC, Mater. Struct. 53 (2020), https://doi.org/10.1617/s11527-020-01558-w.
[48] H. Seleem, A.M. Rashad, T. Elsokary, Effect of elevated temperature on physico-mechanical properties of blended cement concrete, Constr. Build. Mater. 25 (2011) 1009–1017, https://doi.org/10.1016/j.conbuildmat.2010.06.078.
[49] A. Savva, P. Manita, K.K. Sideris, Influence of elevated temperatures on the mechanical properties of blended cement concretes prepared with limestone and siliceous aggregates, Cem. Concr. Compos 27 (2005) 239–248, https://doi.org/10.1016/j.cemconcomp.2004.02.013.
[50] S. Peters, T. Pittrich, L. Stelzner, et al., Model based evaluation of effects of the composition of CO2 -reduced blended concrete on the chemo-thermo-hygral behavior at elevated temperatures, Cem. Concr. Compos. 163 (2025), https://doi.org/10.1016/j.cemconcomp.2025.106163.
[51] W. Jiang, D. Zhang, X. Zheng, et al., Development of Pore Pressure in Cementitious Materials under Low Thermal Effects: Evidence from Optimization of Pore Structure by Incorporation of Fly Ash, Mater 16 (2023), https://doi.org/10.3390/ma16124214.
[52] M. Maier, M. Zeiml, R. Lackner, On the effect of pore-space properties and water saturation on explosive spalling of fire-loaded concrete, Constr. Build. Mater. (2020), https://doi.org/10.1016/j.conbuildmat.2019.117150.
[53] G. Torelli, P. Mandal, M. Gillie, et al., Concrete strains under transient thermal conditions: A state-of-the-art review, Eng. Struct. 127 (2016) 172–188, https://doi.org/10.1016/j.engstruct.2016.08.021.
[54] U. Schneider, Concrete at High Temperatures – A General Review, Fire Saf. J. 13 (1988) 55–68, https://doi.org/10.1016/0379-7112(88)90033-1.
[55] Z.P. Bazant, Y. Xi, Drying creep of concrete: constitutive model and new experiments separating its mechanisms, Mater. Struct. 27 (1994) 3–14.
[56] S. Peters, G. Vu, G. Meschke, A multiscale model for predicting the Young's modulus and the thermal-expansion coefficient of concrete at high temperatures, Constr. Build. Mater. 479 (2025), https://doi.org/10.1016/j.conbuildmat.2025.141259.
[57] T. Koyama, M. Ozawa, M. Kanematsu, Study on the thermal shrinkage behavior of cement paste under high temperature envirnoment, Cem. Sci. Concr. Technol. 78 (2024) 128–136, https://doi.org/10.14250/cement.78.128.
[58] U. Schneider, Behav. Concr. High. Temp. Dtsch. Aussch. F. üR. Stahlbeton (1982) 1–110.

Paper 4

Analysis of thermohydraulic spalling in blended cement concrete

Publisher's version

Published in Fire Technology

Volume 62, 2026

https://doi.org/10.1007/s10694-026-01989-x

Authors: Tim Pittrich, Frank Dehn, Frank Weise, Ludwig Stelzner

Fire Technology (2026) 62:158
https://doi.org/10.1007/s10694-026-01989-x

Analysis of Thermohydraulic Spalling in Blended Cement Concrete

Tim Pittrich[1,2] · **Frank Dehn**[2] · **Frank Weise**[1] · **Ludwig Stelzner**[1]

Received: 30 November 2025 / Revised: 17 July 2026 / Accepted: 9 August 2026
© The Author(s) 2026

Abstract
Recently, the construction industry has increasingly focused on the development of more sustainable transport infrastructure, such as tunnels, driven by the growing use of clinker-reduced cements. One major challenge in this context is fire exposure, which can lead to severe structural damage through concrete spalling, thereby compromising the integrity of the structure. To date, the fire-induced spalling behavior of blended cement concrete remains insufficiently understood. This is particularly concerning, given the increasing adoption of blended cements with reduced clinker content, which are expected to see widespread use in the future. Consequently, a deeper understanding of how different cement types influence spalling susceptibility is of great importance. A comprehensive study was conducted to investigate spalling behavior and analyze the associated thermo-hydraulic effects in concretes made with CEM I, CEM II/A-LL, CEM III/A, and CEM II/B-Q. The findings revealed that the use of blended cements generally led to increased spalling susceptibility, even in normal-strength concrete. Additional analysis indicated that blended cement concretes exhibited lower permeability and higher moisture content, both of which are likely contributors to the elevated spalling risk. Furthermore, the study showed that moisture transport during heating closely follows the dehydration behavior of the cementitious matrix. Blended cement pastes were found to contain lower quantities of early-dehydrating AFt and AFm phases, as well as more thermally stable C-(A)-S-H phases. Moreover, the incorporation of polypropylene fibers into the concrete mix effectively mitigated spalling across all cement types. Therefore, demonstrating the continued effectiveness of polypropylene fibers as a spalling prevention strategy.

Keywords Fire induced spalling · Blended cement · SCM · Moisture transport · Dehydration · PP fibers

1 Introduction

The maintenance and expansion of transport infrastructure form the backbone of any economy. This applies not only to various types of transport routes and bridge structures but also to tunnel systems. However, the rise in traffic volume, vehicle speeds, and the expanding

Extended author information available on the last page of the article

Published online: 22 August 2026

size of tunnels also heightens the risk of tunnel fires [1]. These fires can have devastating consequences due to the rapid heat development in such confined environments. Beyond the threat to human life, tunnel fires can cause severe structural damage, primarily due to the loss of reinforced concrete strength at elevated temperatures and the occurrence of spalling. The latter results in the loss of the concrete cover, thereby exposing the steel reinforcement directly to high temperatures. This exposure causes further significant strength degradation and ultimately compromises the structural integrity of the tunnel. This not only leads to high repair costs but also results in significant economic losses due to prolonged tunnel closures.

At the same time, the concrete industry is already responsible for approximately 6–7% of global CO_2 emissions, with around 5% attributed to Portland cement production alone [2]. As the demand for infrastructure continues to grow, more sustainable alternatives are urgently needed to reduce the environmental impact of the construction sector. Roughly two-thirds of the CO_2 emissions from Portland cement production stem from the decomposition of limestone, a process that remains unavoidable, even in technologically optimized cement plants. Consequently, reducing the clinker factor is considered one of the most effective strategies for producing greener cement [2]. This can be achieved by partially replacing cement clinker with supplementary cementitious materials (SCMs) such as fly ash, blast furnace slag, or limestone to create blended cements. However, the long-term availability of fly ash and slag is uncertain, highlighting the need for viable alternatives. Calcined clays show great promise in this regard due to their global abundance, excellent pozzolanic properties, and significantly lower CO_2 emissions during production [3].

With the increasing variety of SCMs and the growing use of blended cements in practice, understanding their behavior under fire exposure is of great importance to ensure the continued safety and resilience of infrastructure. Against this background a comprehensive study regarding the spalling behavior with subsequent analysis of the thermohydraulic influences was carried out (see Fig. 1). The work of this project included a detailed literature review, in-depth fire spalling tests, investigations of the thermally induced moisture trans-

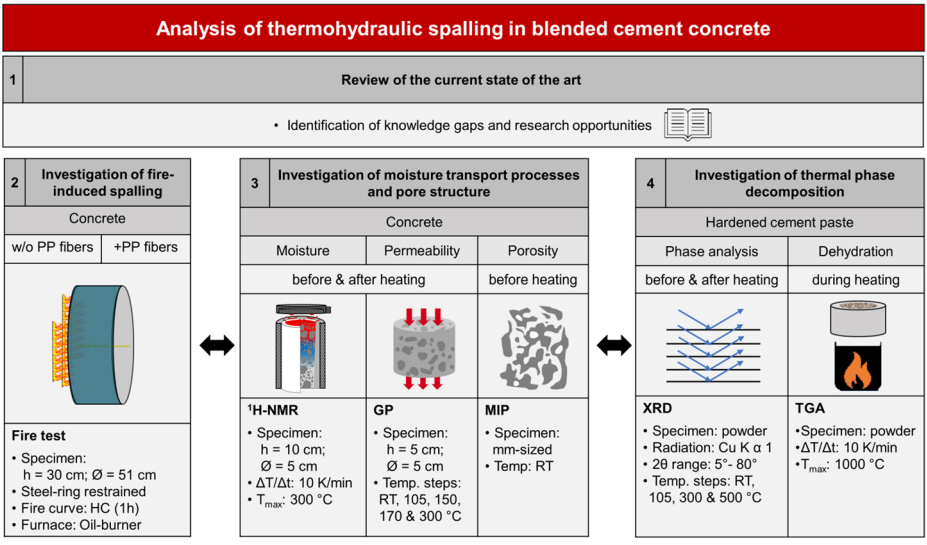


Fig. 1 Research program

port processes by hydrogen proton nuclear magnetic resonance (^{1}H-NMR) relaxometry, determination of gas permeability (GP) as well as the analysis of the pore structure by mercury intrusion porosimeter (MIP). Moreover, decomposition and dehydration behavior of hardened blended cement pastes were studied by X-ray diffraction (XRD) and thermal gravimetric analysis (TGA).

2 State of the Art

The concept of a thermohydraulic spalling mechanism in concrete was first introduced by Shorter and Harmathy in 1961 [4]. The authors stated that during fire exposure, the water within the concrete begins to evaporate, initiating pressure-driven moisture migration both towards the surface and deeper into the concrete element. Due to the temperature gradient established across the cross-section, water vapor condenses in the cooler interior, forming a saturated zone. As saturation increases, a so-called moisture clog develops, which impedes further moisture transport and leads to a buildup of pore pressure. If this pressure exceeds the tensile strength of the concrete, spalling occurs. However, the direct relationship between pore pressure and spalling has not been conclusively verified, as accurate pore pressure measurements during fire tests remain technically challenging. More recent studies suggest that the acceleration of concrete fragments may primarily influenced by initial microcracking and the associated adiabatic expansion of superheated water [5].

In addition to the thermohydraulic mechanism, which according to Bažant may act primarily as a trigger [6], thermomechanical mechanisms have also been identified as contributing factors to explosive spalling. Two primary sources of thermomechanical stress have been recognized. The first one deals with thermal mismatch between cement paste and aggregates. At approximately 150 °C, cement paste tends to shrink, while aggregates continue to expand [7]. This mismatch in thermal deformation induces internal stresses that can lead to microcracking, thereby promoting explosive spalling. The second one is based on restraint thermal dilations as the temperature gradient during fire exposure causes differential thermal expansion within the concrete cross-section. When this expansion is restrained by surrounding structural elements, compressive stresses develop parallel to the heated surface. These, in turn, generate transverse tensile stresses. If these stresses exceed the tensile strength of the concrete, spalling may occur [8, 9].

A commonly used mitigation strategy against spalling is the addition of Polypropylene fibers (PP fibers) to the concrete mixture. During a fire scenario the PP fibers melt around 160 °C which allows water vapor to escape through empty fiber channels and the developed microcrack network caused by the thermal expansion forces [10].

To understand the impact of blended cements on the fire-induced spalling behavior of concrete, the current state of the art was thoroughly reviewed in our previous paper [11]. It can be briefly concluded that the type of cement can significantly influence spalling behavior under fire exposure. Notably, the use of silica fume (SF) and metakaolin (MK) increases spalling susceptibility, primarily due to the formation of a very dense microstructure. Conversely, high amounts of FA (> 25%) tend to reduce the risk of spalling, while lower amounts show no consistent trend. For other supplementary cementitious materials and cement types, no definitive conclusions could be drawn, as existing results are marked by considerable uncertainty and contradiction. This is largely due to the limited number of

Table 1 Concrete composition

Component [kg/m³]	CEM I		CEM II/A-LL		CEM III/A		CEM II/B-Q	
	w/o PP	with PP	w/o PP	with PP	w/o PP	with PP	w/o PP	with PP
cement	420		420		420		420	
water (w/c)	197 (0.47)		197 (0.47)		197 (0.47)		197 (0.47)	
superplasticiser	0	1.5	0	3.4	0	2.1	2.5	5.0
PP fibers	0	2	0	2	0	2	0	2
quarzitic agg								
0/2 mm	646	640	646	634	640	637	634	628
2/4 mm	153	152	153	150	152	151	150	149
4/8 mm	221	219	221	217	219	218	217	215
8/16 mm	679	675	679	668	679	669	666	661

Table 2 Slump flow of the fresh concrete

	CEM I		CEM II/A-LL		CEM III/A		CEM II/B-Q	
	w/o PP	with PP	w/o PP	with PP	w/o PP	with PP	w/o PP	with PP
slump flow [mm]	445	395	395	500	418	455	390	465

studies that employed well-defined spalling experiments with suitable testing and evaluation protocols. Comparisons between different research groups were challenging due to variations in experimental setups and evaluation criteria. Moreover, no particular results regarding the influence of cement containing calcined clay existed up to this date even though they are forecast to be the leading SCM of the future.

3 Experimental Investigations

3.1 Fire-Induced Spalling

In the next phase of the study, in-depth spalling tests were conducted to gain further insight into the influence of blended cements on the spalling behavior of concrete. These tests and evaluation methods followed the RILEM Recommendations of RILEM TC 256-SPF [12, 13]. The key findings are summarized below the complete description of the testing set up and results can be found in [14].

Tunnel-grade normal strength concrete (NSC) was prepared using four different cement types in accordance with DIN EN197-1 [15]: Ordinary Portland cement CEM I 42.5 N as the reference, limestone cement CEM II/A-LL 42.5 N and slag cement CEM III/A 42.5 N representing current practice, and calcined clay cement CEM II/B-Q 42.5 N reflecting future trends. The exact chemical and mineralogical phase composition is reported in Pittrich et al. [16]. The concrete mix had a water-to-cement ratio (w/c) of 0.47 and included quarzitic aggregates. Although Eurocode 2 [17] does not prescribe specific measures against spalling for NSC, an additional mix was prepared for each concrete composition containing 2 kg/m³ of PP fibers (l = 6 mm; Ø = 15.4 µm) to evaluate their effectiveness in blended cement systems. All concrete compositions are given in Table 1. Because the inclusion of PP fibers significantly reduces concrete workability, higher amounts of superplasticizer were required to maintain consistency comparable to the fiber-free mixes (see Table 2). The specimens

were demolded one day after casting and subsequently placed under water for 6 more days, afterwards the specimens were conditioned at (20 ± 2) °C and (65 ± 5) % RH until the day of testing (> 90 d). A steel-ring restrained test setup, similar to that used by Klimek et al. [18] based on the work of Ozawa et al. [19], was employed to simulate the behavior of a large-scale concrete element under fire exposure. During the fire tests, the 8 mm thick steel ring and the outer edge region of the specimen were kept thermally insulated. Thereby, the steel ring restrains the thermal expansion of the heated concrete core. As a result, compressive stresses developed perpendicular to the direction of fire exposure. The final test specimens had a diameter of 51 cm and a height of 30 cm.

Fire testing was carried out using a 1 m³-furnace with two oil burners, applying the Hydrocarbon (HC) fire curve for a duration of one hour. For each concrete composition two tests were performed. During the experiment, video and audio recordings were made to count the spalling events. Temperature measurements were taken using embedded Type K thermocouples positioned at depths of 10, 20, 30, 50, and 100 mm in the center of the specimen. The specimen's topography was analyzed before and after the fire test with a 3D Laser scanner after all loose debris were removed. The scanners accuracy is specified as 20 µm + 35 µm/m, comprising a fixed base accuracy of 20 µm and an additional error of 35 µm per meter of measured length. Furthermore, the moisture content on the day of testing was determined by drying two cylindrical specimens (h = 30 cm; d = 10 cm) from the same production batch at 105 °C to constant mass. Constant mass was defined as a change in mass of ± 0.1 wt.-% within 24 h.

The results presented in Fig. 2 indicate a significant increase in spalling susceptibility across all types of blended cement concrete. In contrast, CEM I concrete exhibited minimal damage, with only five recorded spalling events and an average spalled volume of 1.5 vol.-%. CEM II/A-LL and CEM III/A showed notably higher levels of deterioration, each with an average of 83 and 111 spalling events and average spalled volumes of around 7 vol.-%. The most severe damage was observed in CEM II/B-Q concrete, which on average experienced 176 spalling events with a spalled volume exceeding 9 vol.-%. Of particular interest was the temperature development at a depth of 50 mm, where reinforcement layers are typically located (see Fig. 3). While CEM I concrete maintained temperatures around 400 °C, significantly higher temperatures were recorded for the blended cements: ca. 600 °C for CEM III/A, 700 °C for CEM II/A-LL, and above 1000 °C for CEM II/B-Q. These elevated temperatures are attributed to the absence of adequate concrete cover. Since temperatures above 500 °C can lead to a substantial reduction in the strength of reinforcing steel, this finding underscores the increased vulnerability of blended cement concretes under fire exposure. The most likely cause of this occurrence is the increased moisture content in blended cement concrete (see Fig. 2). Although these differences may seem minor, it was demonstrated by Maier et al. [20] that even slight increases in moisture can significantly raise spalling susceptibility. This critical finding must be carefully considered in the development of more sustainable concrete formulations in future construction.

However, with the addition of PP fibers no spalling was recorded in any specimen, concluding that the PP fibers are equally effective regardless of the cement type used. However, Fig. 3 shows local surface uplifts of up to 5 mm occurred, which can be attributed to crack formation within the specimens. Furthermore, it should be highlighted that the temperatures in 50 mm depth were similar for every concrete type with a maximum temperature after 60 min of fire exposure of around 200 °C (see Fig. 3), protecting a potential reinforcement

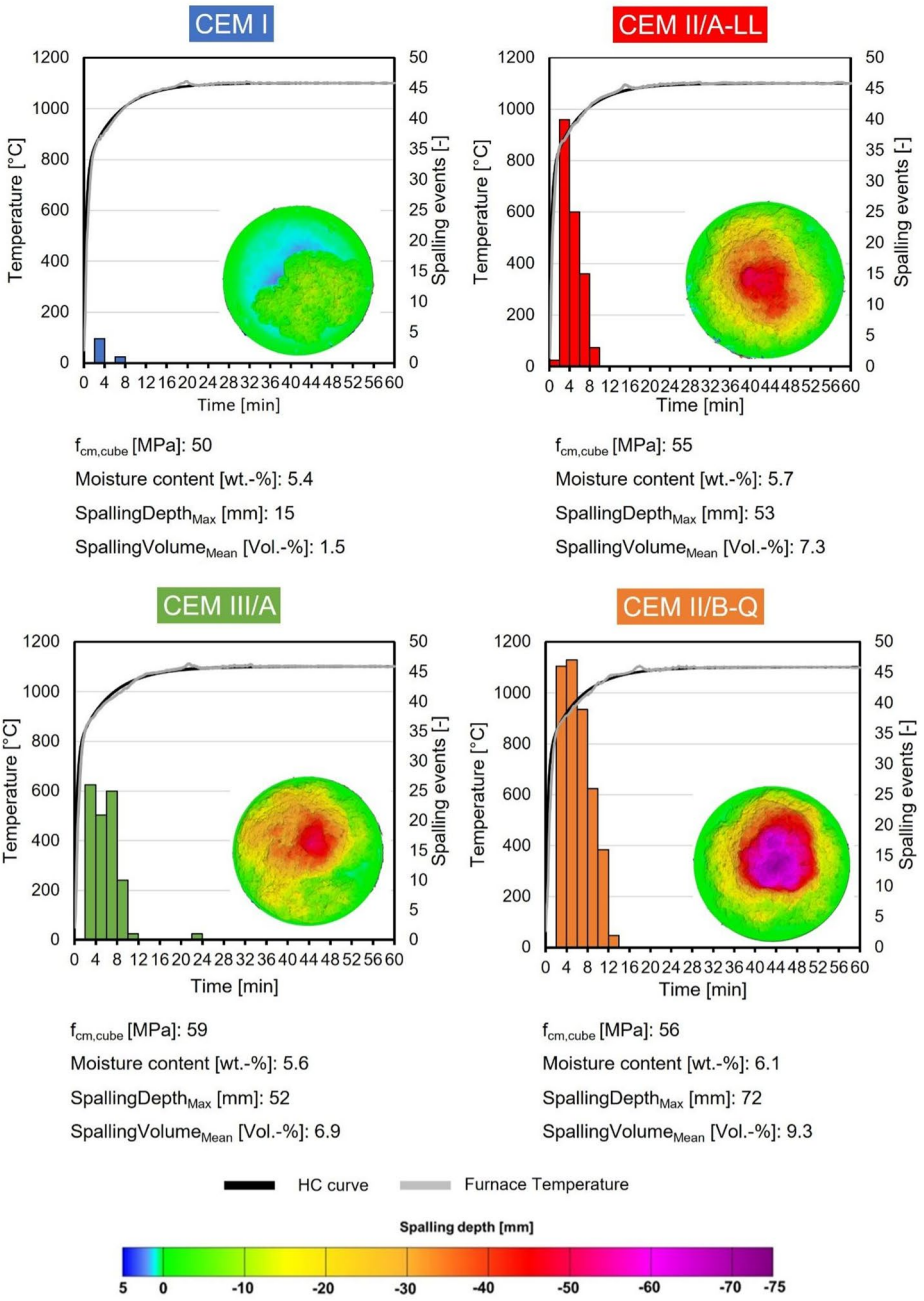


Fig. 2 Summary of the fire tests, showing the furnace temperature, the number of spalling events and the concrete properties in relation to the spalling volume and maximum spalling depth as mean values of two specimens. The 3D-scan represents one exemplary sample of each concrete type

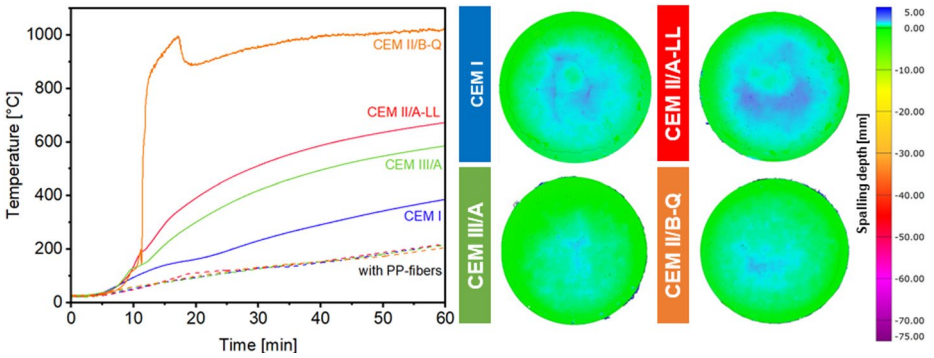


Fig. 3 Temperature development in 50 mm depth in the different concretes with and without PP fibers during fire exposure (left) and difference of the surface height distribution of the PP fiber-reinforced concrete specimens after fire exposure (right)

layer from direct flame exposure and consequent strength loss. Therefore, PP fibers remain a successful mitigation strategy.

3.2 Moisture Transport Processes and Pore Structure

The thermally induced moisture transport was analyzed to understand the reasons behind the different spalling behaviors found in the different types of blended cement concrete. ^{1}H-NMR relaxometry measurements were carried out before and after heating to obtain information about the pore size specific moisture distribution and the corresponding development of the moisture clog. The NMR-tomograph worked with a vertical resolution of 2 mm and was equipped with a 52 mm diameter radio-frequency coil. To enhance the decay of the transverse relaxation time (T_2), a Carr–Purcell–Meiboom–Gill (CPMG) pulse sequence was employed. The sequence used an echo time of 70 µs, generated 1429 echoes, and included 200 scans for each slice (for further details about the device see [21]). The inversion of the recorded signal was conducted with NUCLEUS a Matlab tool developed by Hiller and Costabel [22]. Additionally, supportive analysis in the form of GP and MIP measurements were conducted to receive further knowledge on the pore structure and transport properties. The main findings are presented below; further information and results can be found in [23].

The ^{1}H-NMR relaxometry measurements were conducted on small scale concrete cylinders cast in a Macor ceramic following the methodology of Stelzner et al. [24] for two samples of each concrete. First, pore size specific moisture distribution was determined before heating. Thereafter, the samples were exposed to one sided heating (10 K/min) until a surface temperature of 300 °C was reached and held constant for 40 more mins. Then, the samples were allowed to cool freely for 120 min and the pore size specific moisture distribution was determined again. It should be noted that measuring the moisture distribution in the cooled state may not fully reflect its distribution during heating. This discrepancy can result in deeper penetration of the drying front and less pronounced moisture clogging. Based on the numerical analysis reported in [23] it can be estimated that the shift in depth and moisture content between the end of heating and the measurement in the cooled state is within 10 mm and 1 vol.-%, respectively, for every concrete type. Nevertheless, the relative differences in drying behavior are still sufficiently accurately reflected in the measurements after

cooling for the interpretation of the results. The temperature was recorded in accompanying specimens of the same kind in depths of 5 mm, 10 mm, 20 mm, 30 mm, 50 mm and 70 mm. In addition, the initial porosity was measured by means of MIP on small concrete fragments after [25]. The gas permeability measurements were carried out with Ar gas following pressure steps of 3,4 and 5 bar on accompanying cylindric samples (h = 5 cm; Ø = 5 cm) after exposure to 20, 105, 150, 170 and 300 °C according to [26]. Thereafter, the intrinsic gas permeability was determined after Klinkenberg [27].

The results in Fig. 4 clearly show a less pronounced initial drying gradient on the top and bottom in CEM III/A and CEM II/B-Q accompanied with a higher average moisture content of 13.4 and 13.2 vol.-% equal to 6.5 and 6.4 wt.-%. In comparison to 11.7 and 11.0 vol.-% equal to 5.7 and 5.3 wt.-% in CEM I and CEM II/A-LL concrete. In general, all samples have most of their water stored as gel pore water ($d_{Pore} \leq 10$ nm) and only minor fractions in capillary pore water ($d_{Pore} > 10$ nm). While CEM I and CEM II/A-LL show a quite equal moisture distribution, CEM III/A is exhibiting the most amount of capillary water and CEM II/B-Q the most amount of gel pore water. After high-temperature exposure the drying front and the subsequent appearance of the moisture clog were confirmed in every specimen. The onset of the moisture clog was defined here as the intersection between the initial water content prior to heating and the water content measured after heating. In particular, CEM II/B-Q showed the overall deepest sitting moisture clog. In addition, reconfiguration of the pore water from gel to capillary pores was recognized in all the samples leading to an overall increase in capillary pore water. In the area of the moisture clog the capillary pore water was now even the dominate fraction, except for CEM II-B-Q sample where the capillary pore water content never exceeds the gel pore water content. The effect of the PP fibers was noticeably detectable during the NMR measurements shown in Fig. 4. The results showed a slightly decreased moisture content in the PP fibers mixes in the initial state. After one-sided

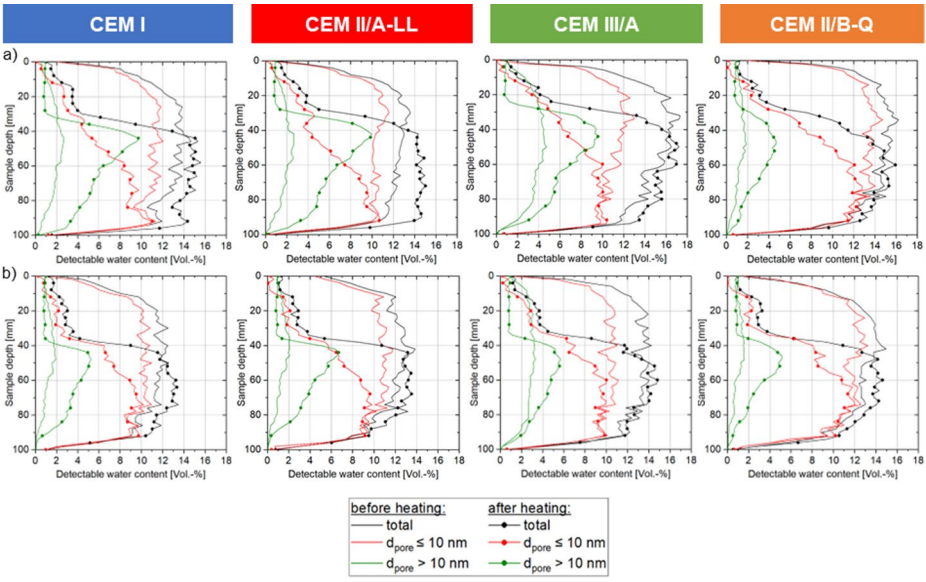


Fig. 4 1D moisture profiles with average pore size specific moisture distribution before and after one-sided heating **a** without PP fibers; **b** with PP fibers

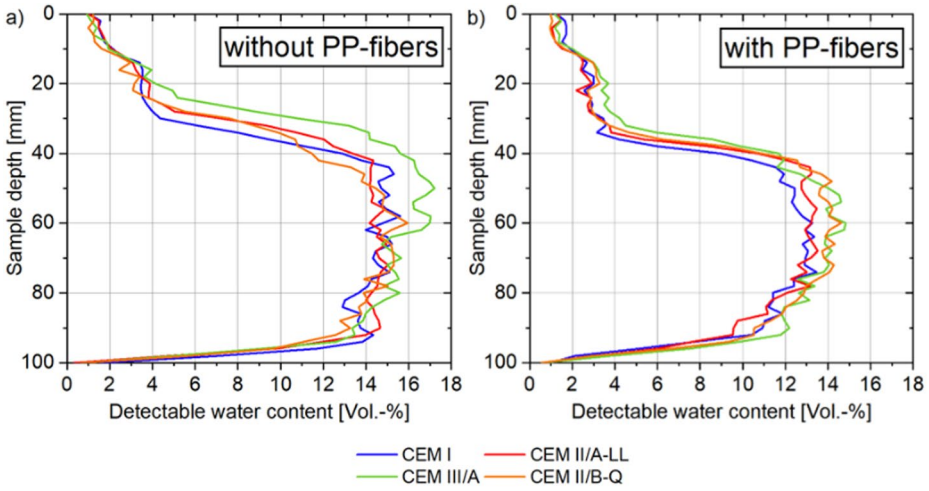


Fig. 5 1D moisture profile after heating **a** without PP fibers; **b** with PP fibers

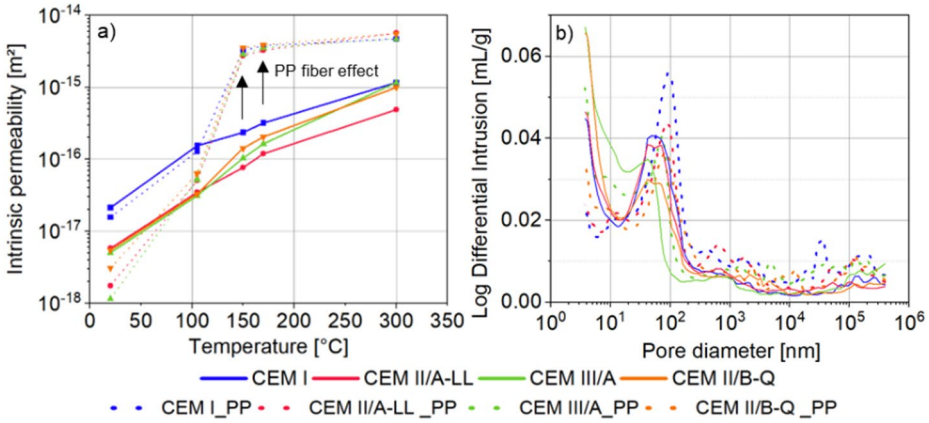


Fig. 6 **a** Average intrinsic gas permeability after exposure to 20, 105, 150, 170 and 300 °C showing the effect of the PP fibers on permeability development; **b** Average initial differential porosity

heating, all concretes showed a more advanced drying front with comparable drying gradients. Despite the fibers, the moisture clog was still detected within every sample at similar depths. This indicates that the transport properties in every type of concrete became equal with fiber addition at elevated temperatures and the cement type specific differences almost disappeared completely. A direct comparison between the 1D moisture profiles after heating for concrete with and without PP fibers is provided in Fig. 5.

The gas permeability measurements (see Fig. 6a) showed a higher initial permeability for CEM I concrete in comparison to blended cement concrete, with increasing temperature the permeability in all samples increased. However, at temperatures above 105 °C CEM III/A and CEM II/B-Q experienced a steeper permeability increase in comparison to CEM I and CEM II/A-LL. Therefore, the initial differences between CEM I and CEM III/A or CEM

II/B-Q concrete became less pronounced and ultimately vanished at 300 °C. This indicates that the permeability differences at elevated temperatures between these types of concrete are much smaller than in the initial state and therefore suggesting that the permeability alone might not be the only driving force responsible for the thermally induced moisture transport. The effectiveness of PP fibers is also visible in the development of permeability, where after exceeding temperatures of 105 °C the permeability suddenly increases to the same level in every type of concrete. Interestingly, the main permeability increase occurs at temperatures below the fiber melt starting at 150 °C, which has also been observed in other studies [28, 29].

The MIP results (Fig. 6b) showed a similar picture for CEM I and CEM II/A-LL concrete with equal pore size distributions. The CEM II/B-Q sample showed a similar course but more gel pores and less capillary pores. CEM III/A sample exhibited the lowest number of capillary pores over 30 nm but the highest number of small capillary and gel pores below this size. No major differences in the pore size distribution above 200 nm were recognized. The MIP measurements in PP fiber mixtures showed a slight increase in porosity and an overall pore coarsening effect in the initial state, however, the pore coarsening seemingly did not increase the initial permeability of PP fiber concrete.

3.3 Thermal Phase Decomposition

The ^{1}H-NMR measurements revealed that differences in moisture distribution cannot be attributed solely to variations in permeability. This is particularly evident in CEM III/A and CEM II/B-Q concretes, which, despite having similar initial moisture contents and permeabilities, exhibit markedly different moisture profiles after heating. These findings suggest that moisture distribution is strongly influenced by the decomposition and dehydration behavior of the respective cementitious pastes.

To investigate this further, the mineral phase composition and dehydration behavior were analyzed using XRD and TGA on hardened cement paste samples published in [16]. For the XRD analysis, nearly cubic specimens (ca. 4 × 4 × 4 cm³) were heated with 2 K/min to 105 °C, 300 °C, and 500 °C and held for 48 h. After heating, the samples were sealed in plastic foil and stored in a desiccator to prevent rehydration. Subsequently, the samples were broken, immersed in isopropanol, and ground into a fine powder using a McCrone mill. The measurements were performed using a Bruker D8 DaVinci device using Cu Kα radiation and a step width of 0.05° per second, covering a range from 5° to 80°. The obtained data was quantitatively evaluated by Rietveld refinement using TOPAS V7.0 software.

Figure 7 presents the phase composition before and after thermal exposure. Significant initial differences were observed. CEM I exhibited the highest content of AFt (Ettringite) and AFm phases (hemicarboaluminate, monocarboaluminate and monosulfoaluminate), approximately 11.6 wt.-%, whereas CEM II/A-LL, CEM III/A, and CEM II/B-Q showed contents between 8.5 and 9.0 wt.-%, respectively. Additionally, CEM I and CEM II/A-LL contained higher amounts of C-(A)-S-H and portlandite compared to CEM III/A and CEM II/B-Q. These differences are attributed to the lower Portland cement clinker content in the latter cements, resulting in reduced hydrate formation. Moreover, the pozzolanic reaction leads to the formation of C-(A)-S-H at the expense of portlandite. Calcium carbonate was detected in all samples, with particularly high quantities in CEM II/A-LL as expected. However, comparable amounts were also found in the other specimens. The presence of

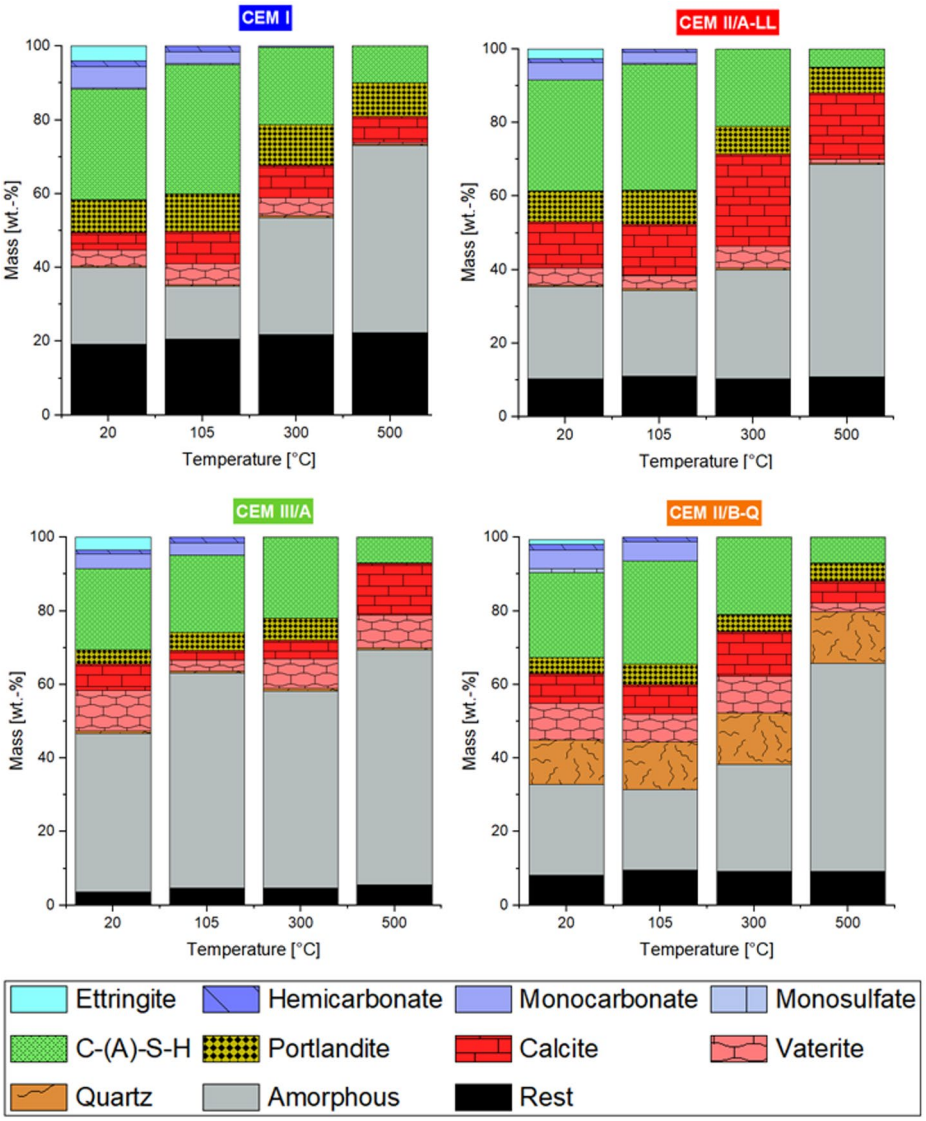


Fig. 7 Phase composition of the different hardened cement pastes after exposure to 20, 105, 300 and 500 °C determined by XRD Rietveld Analysis

significant quantities of vaterite suggests carbonation, especially in CEM III/A and CEM II/B-Q pastes, likely due to their lower portlandite contents [30, 31]. Furthermore, larger fractions of quartz were identified in the CEM II/B-Q sample which are a byproduct of calcined clay. Upon heating to 105 °C, decomposition of AFt phases was observed in all samples. Increasing the temperature to 300 °C led to further decomposition of AFm phases. In CEM I and CEM II/A-LL, C-(A)-S-H underwent significant decomposition at 300 °C and was nearly completely decomposed at 500 °C. In contrast, the C-(A)-S-H phases in CEM III/A and CEM II/B-Q remained largely stable up to 300 °C, with substantial decomposi-

tion only occurring at 500 °C. This indicates a higher thermal stability of the main hydrate phases in these cements. The dihydroxylation of C-(A)-S-H is primarily responsible for the increased amorphous content observed after exposure to 500 °C. Portlandite was still detectable even after heating to 500 °C, although its characteristic peaks in the XRD patterns showed reduced intensity and increased width, indicating a loss of crystallinity due to dehydration rather than complete structural degradation. This observation aligns with findings reported in the literature [32].

The TGA results presented in Fig. 8 were obtained using a Mettler Toledo instrument under nitrogen atmosphere, with a heating rate of 10 K/min up to 1000 °C. Due to the solvent exchange during sample preparation, no free evaporable water remained in the specimens.

The results indicate that CEM I exhibited the most pronounced mass loss associated with the decomposition of AFt and AFm phases within the temperature range of 70 to 200 °C, which is consistent with the XRD findings. In the case of CEM II/B-Q, a significant mass loss was attributed to the decomposition of AFm phases, most likely monocarboaluminate. CEM III/A showed the least mass loss overall, supporting the hypothesis that its main hydrate phase, C-(A)-S-H, is thermally more stable. Up to 300 °C, the highest mass loss was observed in CEM I, followed by CEM II/A-LL, CEM II/B-Q, and finally CEM III/A. Beyond 300 °C, the decomposition of portlandite was detected, with the highest contents found in CEM I and CEM II/A-LL, again in agreement with the XRD results. Starting at approximately 500 °C, the decomposition of calcium carbonate was observed, continuing up to around 760 °C. Notably, a two-stage decomposition process was identified: the first peak corresponds to the breakdown of amorphous and poorly crystalline vaterite, while the second peak represents the decomposition of calcite. The highest relative mass loss in this temperature range was recorded for CEM II/A-LL, due to its initially high calcite content. Pozzolanic and latent hydraulic binders also exhibited significant mass loss, attributed to carbonation and subsequent decomposition of calcium carbonate phases.

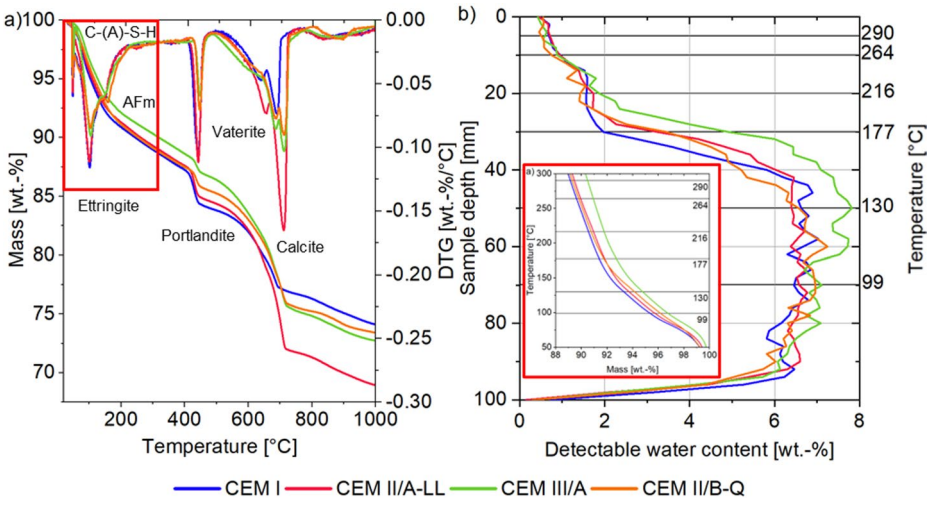


Fig. 8 **a** Dehydration behavior of the different cement pastes **b** comparison between mass loss in cement paste (TGA) and the drying behavior after one sided heating (^{1}H-NMR) showing the same sequence of mass loss up to 300 °C (10 K/min)

A comparison between the TGA and ^{1}H-NMR moisture profiles recorded after heating show the same sequence of mass loss and drying, respectively (see Fig. 8). This shows that the thermally induced moisture distribution and the development of the drying front plus moisture clog is highly dependent from the dehydration behavior of the cementitious matrix. Concluding that the permeability alone is not sufficient to describe the moisture transport in concrete.

4 Discussion

The results of this study clearly demonstrate that the type of cement significantly influences the spalling behavior of concrete. The lowest spalling susceptibility was observed in CEM I concrete, which can be attributed to its high permeability, low moisture content, and efficient water release during high-temperature exposure. This combination results in a reduced amount of energy stored in the form of hot water, allowing much of it to escape early during a fire event. Although CEM III/A and CEM II/B-Q concretes exhibit similar permeability to CEM I at elevated temperatures, this factor appears to play a minor role. TGA indicates that the majority of water is released between 50 °C and 170 °C, suggesting that permeability at lower temperatures is more critical for effective water release. In CEM III/A and CEM II/B-Q concretes, higher initial moisture content and restricted evaporation lead to greater energy availability, thereby increasing the risk of spalling. CEM II/A-LL concrete, which shows the lowest permeability across the entire temperature range, also presents a potential spalling risk. However, its moisture distribution and dehydration behavior closely resemble those of CEM I, indicating that transport properties may be more influential than moisture content alone.

Nevertheless, the results are consistent with current findings regarding spalling mechanisms proposed by Yarmohammadian and Felicetti [33], which emphasize the importance of sufficient thermal energy and water during crack initiation for the severity of spalling. A coherent representation of the conducted investigations normalized over the sample depth of the one-sided heated cylinders is given in Fig. 9. Here it can be distinguished between a dry, moist and saturated zone (''moisture clog''). The dry zone refers to the region up to the point where moisture content begins to rise sharply, marking the start of the moist zone. This moist zone extends until the onset of the moisture clog, which is defined as the intersection between the water content after heating with the initial state before heating. The measured temperature distribution within the specimens is consistent across all cement types. Therefore, it can be stated that there are no significant differences in thermal conductivity or heat capacity among the different concrete types, which may influence spalling. Nevertheless, due to reduced dehydration and lower permeability, blended cement concrete retains higher water content in the moist zone prior to the beginning of the moisture clog developed at temperatures between 150 and 230 °C. This fits well with the fire tests in which spalling began to occur at concrete temperatures between 170 and 240 °C [14]. Therefore, it can be concluded that the greater amount of available thermal energy in the form of hot water in concrete made with blended cements, significantly increases the risk of explosive spalling. In concretes containing PP fibers, the drying zone extends deeper due to increased permeability. As a result, the moist zone becomes thinner and shifts further inward, where lower temperatures prevail. Due to the uniformly increased permeability across all con-

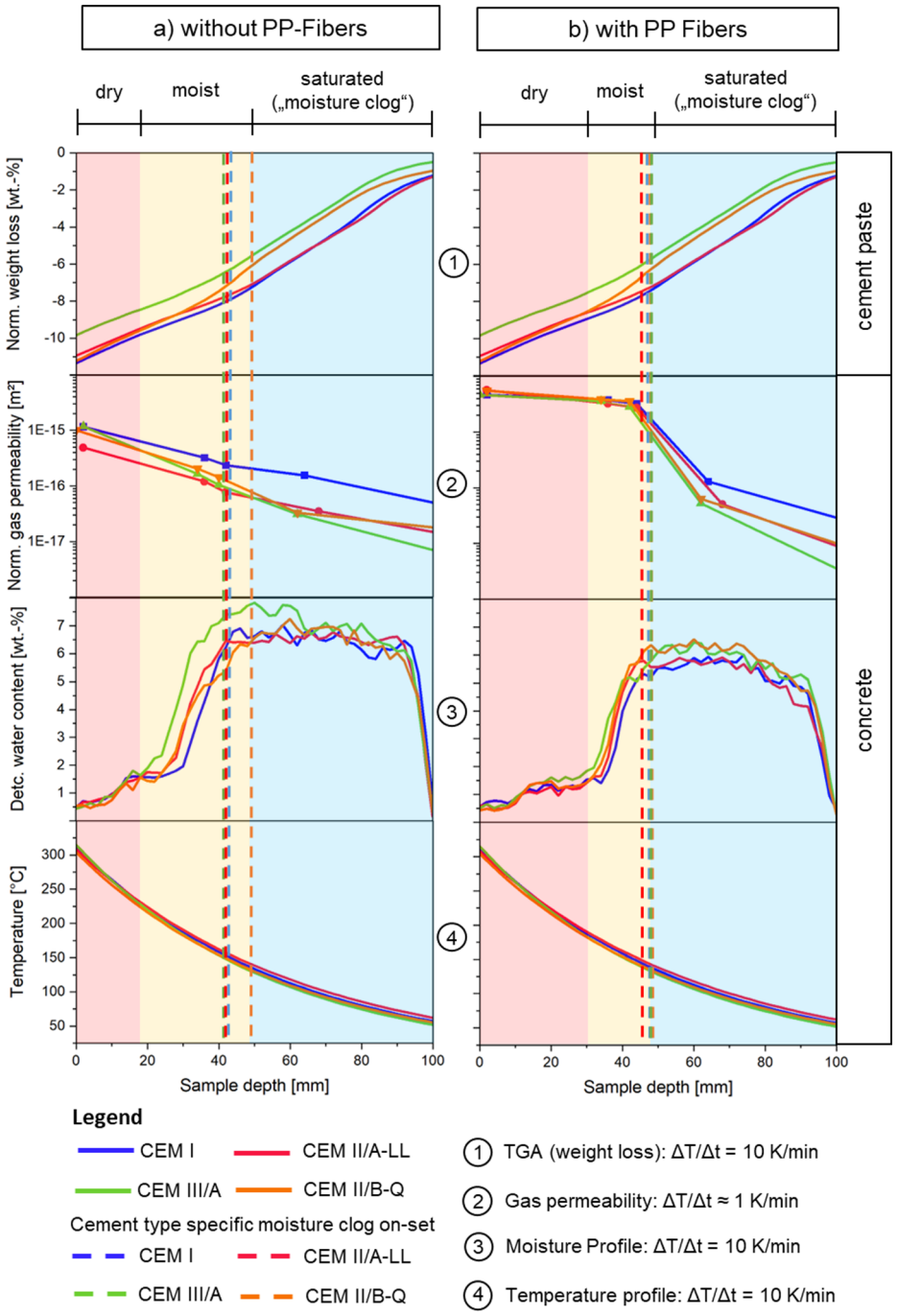


Fig. 9 Coherent representation of the investigations carried out with regard to dehydration behavior, gas permeability, moisture distribution, and temperature distribution after 70 min normalized over the sample length in different types of concrete **a** without PP fibers; **b** with PP fibers

crete types, moisture differences become much smaller and almost disappear. Although the drying sequence is influenced by permeability, it still matches the sequence of weight loss in the cement paste, as phase decomposition occurs independently of permeability. Because moisture availability is now significantly reduced in areas with lower temperatures (approximately 125–175 °C), spalling no longer occurs, as insufficient thermal energy can accumulate to cause damage. It should be noted that the temperature profiles presented in Fig. 9 were only measured in concrete without PP fibers but previous investigations with the same test set-up showed that the influence of PP fibers on the temperature development is neglectable [34].

The presented results show clearly why blended cement concrete is more prone to spalling than conventional concrete. However, the differences in spalling susceptibility between the single blended cement concrete types are still not fully understood.

Interestingly, CEM II/B-Q concrete exhibited the most severe spalling, despite behaving similarly to CEM III/A in many respects. The temperature measurements showed no significant differences, indicating that the thermal conductivity and heat capacity of the investigated materials are comparable. With similar temperature evolution and distribution during heating, no significant differences in dehydration kinetics are expected as shown by the TGA and XRD data. This suggests that additional thermohydraulic or thermomechanical factors must be contributing. Notably, CEM II/B-Q concrete contained significantly more gel pore water compared to the other mixes. This raises the question of whether pore size distribution influences pore pressure. First indications in this direction are given by Jiang et al. [35] who found that pore pressure increases with decreasing porosity and pore radius in unsaturated pores, potentially explaining the heightened spalling in CEM II/B-Q concrete.

In addition to thermohydraulic effects, potential thermomechanical contributions may also be responsible for the observed differences in spalling behavior. Since the majority of the concrete volume consists of aggregates, it can be assumed that no significant differences arise in terms of the stresses caused by restrained thermal expansion for the tested concretes with different cements. Furthermore, as the stiffness of concrete is largely governed by the aggregates too, the effects of the cement paste dehydration can be considered minor as described by Peters et al. [36]. Nevertheless, mineralogical differences may also contribute to the observed behavior through other underlying mechanisms. The enhanced thermal stability of C-(A)-S-H phases in CEM II/B-Q and CEM III/A could alter thermomechanical responses, particularly regarding load-induced thermal strains (LITS). In restrained concrete structures, LITS can be beneficial, as they develop in the direction of the applied load and help reduce compressive stresses caused by restrained thermal expansion [37], potentially lowering the risk of spalling. LITS primarily result from thermal transient creep and drying creep, both of which are closely linked to the decomposition of hydrate phases and associated water transport [38, 39]. Peters et al. [36] observed that the progression of C-S-H dehydration closely aligns with the development of LITS, attributed to creep-like sliding of C-S-H under compressive stress. However, the thermally stable C-(A)-S-H phases in CEM II/B-Q and CEM III/A may inhibit this sliding, leading to reduced LITS and lower stress relaxation, ultimately increasing spalling susceptibility. In addition to LITS, the differing dehydration behavior of the cement types may influence the thermal mismatch between the shrinking hardened cement paste and the expanding aggregates during heating. Koyama et al. [40] describe the shrinkage behavior of pure cement paste as a sequence of four characteristic stages. In the initial stage (20 °C to 140 °C), shrinkage is triggered by

the evaporation of free water and the decomposition of AFt phases. This is followed by a more moderate shrinkage regime between 140 °C and 300 °C, mainly governed by the release of interlayer water from the C–S–H structure. Beyond this range, from 300 °C to 490 °C, shrinkage intensifies markedly due to continued dehydration of C-S-H and especially portlandite. Based on the presented TGA and XRD results, it can be assumed that hardened cement paste of CEM I exhibits more pronounced shrinkage than the blended cements, as it contains higher amounts of AFt and AFm phases as well as portlandite, all of which significantly contribute to shrinkage. However, spalling was least pronounced for CEM I, indicating that, in this case, the effect of shrinkage and thermal mismatch does not appear to be a dominant factor. Nonetheless, in addition to the hydration phases, the residual mineralogical composition of the cementitious matrix should not be disregarded, as it may lead to thermal mismatch between hydrate and non-hydrate phases at the binder scale. XRD analysis revealed high quartz content in CEM II/B-Q concrete, which acts in a further sense as very fine aggregate. The thermal mismatch between the cement paste and quartz can generate internal stresses that promote spalling. This mismatch is particularly pronounced for quartz but also applies to limestone and unreacted slag, which are present in significant quantities in CEM II/A-LL and CEM III/A, potentially further increasing the risk of explosive spalling in comparison to CEM I concrete.

The addition of 2 kg/m³ of PP fibers effectively prevented spalling in all concrete types, primarily due to the uniform increase in permeability at elevated temperatures. This demonstrates that a viable solution to the heightened spalling risk in blended cement concretes already exists, albeit at the expense of reduced workability in the fresh concrete state. For concrete with CEM I, omitting PP fibers may be considered to preserve workability. This is supported by the apparently sufficient permeability, which results in only minimal spalling and moderate temperature increases within the structural member due to adequate concrete cover. Due to the low permeability of blended cement concretes, severe spalling occurs, resulting in significant temperature increases endangering the structural integrity of the component. Consequently, the incorporation of PP fibers is necessary to provide sufficient permeability and enable reliable moisture release to avoid spalling during fire exposure. However, further investigations are required to assess whether the same fiber dosage with larger diameters (e.g., d = 32 µm), resulting in a lower number of fibers at the same volumetric content, or reduced fiber dosages, can provide sufficient protection while minimizing the negative impact on workability. If this is not the case with conventional fibers, the next step could be the introduction of altered PP fibers, which are known to be much more effective [41]. As these aspects were not investigated in this study, no definitive recommendations regarding fiber size, dosage and type can be provided at this stage. However, these considerations are particularly relevant for the use of calcined clay cement, which further compromise workability. Therefore, combining PP fibers with calcined clays may present significant practical challenges for concrete technology.

The findings of this study highlight that the use of blended cements in applications where fire protection is of paramount importance should be carefully evaluated, even in NSC. At present, Eurocode 2 does not provide provisions addressing the use of blended cements in relation to fire-induced spalling. However, further comprehensive and in-depth research is required to fully understand the influence of cement type and to establish well-founded regulations.

5 Conclusion

This research project investigated the impact of blended cements on the spalling behavior of normal strength concrete. The study included a comprehensive literature review, spalling experiments, and the characterization of moisture distribution, transport mechanisms, and dehydration behavior of various cement pastes. The following conclusions were drawn:

- **State of the art**: The literature review of the current state of the art revealed that cement type significantly influences the spalling susceptibility of concrete. However, the number of studies featuring well-defined testing procedures and comprehensive material characterization still remains limited. Moreover, comparisons between different research groups proved to be challenging due to the lack of standardized testing protocols. As a result, clear trends could only be identified for SF, MK, and high volumes of FA (>25%). While SF and MK tend to increase spalling susceptibility, high-volume FA appears to reduce it.
- **Spalling Susceptibility**: The use of CEM II/A-LL, CEM III/A, and particularly CEM II/B-Q increased the spalling susceptibility. This is attributed to higher water retention at elevated temperatures, resulting from high initial moisture contents, reduced permeability and a more thermally stable cementitious matrix in blended cement concretes. Thus, the amount of available energy in the form of hot water increases in the area ahead of the moisture clog at temperatures where spalling occurred (170–240 °C). The differences in spalling behavior among the individual blended cements are not yet fully understood. Potential influencing factors include pore-size-specific moisture distribution and the specific mineral phase composition, which may affect thermomechanical properties. The increased tendency for spalling in concretes with lower clinker content, despite their environmental benefits, must be carefully considered in future construction practices, especially in tunnel construction.
- **Effectiveness of PP Fibers**: The incorporation of 2 kg/m³ of PP fibers effectively prevented explosive spalling across all cement types. Therefore, sufficient concrete cover remained to protect a potential reinforcement layer from direct flame exposure and consequent strength loss. PP fibers thus remain a reliable mitigation strategy. However, further research is needed to determine whether lower fiber dosages could be sufficient, especially in systems containing calcined clay, where higher fiber content adversely affects workability.

Acknowledgements We gratefully acknowledge the support of the German Research Foundation (DFG) and extend our sincere thanks for their financial support throughout the joint project "Thermohydraulic spalling mechanisms in concretes with different binders with and without PP fibers under fire exposure: An experimental and numerical analysis" (Project No. 491928256). We also express our deep appreciation to our project partner, Ruhr University Bochum, for their outstanding collaboration. Special thanks are extended to our colleagues at BAM, in particular the teams from divisions 6.3: Structure Analysis, 7.1: Building Materials, and 7.4: Technology of Construction Materials. Their expertise and resources have significantly enriched the scope and depth of this study.

Author Contributions T: P.: Conceptualization, Investigation, Formal analysis, Visualization, Writing – original draft, Writing – review & editing. F.D.: Supervision, Writing – review & editing. F.W.: Conceptualization, Resources, Funding acquisition, Project administration, Supervision, Writing – review & editing. L.S.: Conceptualization, Resources, Funding acquisition, Project administration, Supervision, Writing – review & editing.

Funding Open Access funding enabled and organized by Projekt DEAL.

Data Availability Data will be made available on request.

Declarations

Conflict of interest The authors declare that they have no known competing financial interests, personal relationships or any other affairs that could have appeared to influence the work reported in this paper.

Open Access This article is licensed under a Creative Commons Attribution 4.0 International License, which permits use, sharing, adaptation, distribution and reproduction in any medium or format, as long as you give appropriate credit to the original author(s) and the source, provide a link to the Creative Commons licence, and indicate if changes were made. The images or other third party material in this article are included in the article's Creative Commons licence, unless indicated otherwise in a credit line to the material. If material is not included in the article's Creative Commons licence and your intended use is not permitted by statutory regulation or exceeds the permitted use, you will need to obtain permission directly from the copyright holder. To view a copy of this licence, visit http://creativecommons.org/licenses/by/4.0/.

References

1. Fehérvári S (2008) Characteristics of Tunnel fires. Concr Struct 56–60
2. Schneider M (2019) The cement industry on the way to a low-carbon future. Cem Concr Res. https://doi.org/10.1016/j.cemconres.2019.105792
3. Scrivener KL, Vanderley JM, Gartner EM (2018) Eco-efficient cements: Potential economically viable solutions for a low-CO2 cement-based materials industry. Cem Concr Res 114:2–26. https://doi.org/10.1016/j.cemconres.2018.03.015
4. Shorter GW, Harmathy TZ (1961) Discussion on the Fire-resistance of prestressed concrete beams. 313–315
5. Felicetti R, Yarmohammadian R, Dal Pont S et al (2024) Fast vapour migration next to a depressurizing interface: a possible driving mechanism of explosive spalling revealed by neutron imaging. Cem Concr Res. https://doi.org/10.1016/j.cemconres.2024.107508
6. Bažant ZP, Cusatis G (2005) Concrete creep at high temperature and its interaction with fracture: Recent progress. CONCREEP 7: Nantes 449–460
7. Schneider U (1982) Behaviour of Concrete at High Temperatures. Deutscher Ausschuss für Stahlbeton, pp 1–110
8. Bažant ZP (1997) Analysis of Pore Pressure, thermal Stredd and Fracture in Rapidly Heated Concrete. International Workshop on fire Performance of High-Strength Concrete: Gaithersburg
9. Ulm FJ, Coussy O, Bazant ZP (1999) The "Chunnel" fire I: chemoplastic softening in rapidly heated concrete. J Eng Mech 125:272–282. https://doi.org/10.1061/(ASCE)0733-9399(1999)125:3(272)
10. Pistol K, Weise F, Meng B et al (2011) The mode of action of polypropylene fibres in high performance concrete at high temperatures. 2nd International RILEM Workshop on Concrete Spalling due to Fire Exposure: Delft, The Netherlands 289–296
11. Pittrich T, Weise F, Stelzner L (2025) The impact of blended cements on the spalling behavior of concrete at elevated temperatures: a review. Mater Struct. https://doi.org/10.1617/s11527-025-02713-x
12. Pimienta P, McNamee R, Hager I et al (2023) Recommendation of RILEM TC 256-SPF on the method of testing concrete spalling due to fire: material screening test. Mater Struct. https://doi.org/10.1617/s11527-023-02202-z
13. Pimienta P, McNamee R, Hager I et al (2024) Recommendation of RILEM TC 256-SPF on fire spalling assessment during standardised fire resistance tests: complementary guidance and requirements. Mater Struct. https://doi.org/10.1617/s11527-023-02248-z
14. Pittrich T, Stelzner L, Weise F (2024) Fire-induced spalling of normal strength concrete with different types of blended Portland cement. The 13th International Conference on Structures in Fire: Coimbra, Portugal 451–461
15. DIN EN 197-1 (2011) Cement-Part 1: Composition specifications and conformity for common cements. Beuth Ver lag GmbH, Berlin

16. Pittrich T, Jansen D, Weise F et al (2026) Thermal decomposition in blended cement systems and its effect on fire-induced concrete spalling: insights from XRD and TGA. Case Stud Constr Mater. https://doi.org/10.1016/j.cscm.2026.e05784
17. Eurocode 2 (2010) Design of concrete structures - Part 1–2: General rules - Structural fire design; German version EN 1992-1-2:2004+AC:2008. Beuth Verlag GmbH, Berlin
18. Klimek A, Stelzner L, Hothan S et al (2024) Influence of thermal strain on concrete spalling. Mater Struct. https://doi.org/10.1617/s11527-023-02274-x
19. Ozawa M, Tanibe T, Kamata R et al (2018) Behavior of ring-restrained high-performance concrete under extreme heating and development of screening test. Constr Build Mater 162:215–228. https://doi.org/10.1016/j.conbuildmat.2017.11.144
20. Maier M, Zeiml M, Lackner R (2020) On the effect of pore-space properties and water saturation on explosive spalling of fire-loaded concrete. Constr Build Mater. https://doi.org/10.1016/j.conbuildmat.2019.117150
21. Kruschwitz S, Munsch S, Telong M et al (2023) The NMR core analyzing tomograph: a multi-functional tool for non-destructive testing of building materials. Magn Reson Lett 3:207–219. https://doi.org/10.1016/j.mrl.2023.03.004
22. Hiller T, Costabel S (2025) NUCLEUS – a Matlab-based graphical user interface for forward and inverse modelling of NMR relaxometry data. SoftwareX. https://doi.org/10.1016/j.softx.2025.102447
23. Pittrich T, Peters S, Meschke G et al (2026) Thermally induced moisture transport in concrete with different types of blended Portland cement studied by 1H-NMR relaxometry. Mater Struct. https://doi.org/10.1617/s11527-026-03025-4
24. Stelzner L, Powierza B, Oesch T et al (2019) Thermally-induced moisture transport in High-Performance Concrete studied by X-ray-CT and ^{1}H-NMR. Constr Build Mater 224:600–609. https://doi.org/10.1016/j.conbuildmat.2019.07.065
25. International Organization for Standardization (2016) Evaluation of pore size distribution and porosity of solid materials by mercury porosimetry and gas adsorption - Part 1: Mercury Porosimetry (ISO Standard No. 15901-1)
26. RILEM TC 116-PCD (1999) RILEM TC 116-PCD: Permeability of Concrete as a Criterion of its Durability. Mater Struct 32:174–179
27. Klinkenberg LJ (1941) The Permeability of Porous Media to Liquids and Gases. Production Practice: 200–213
28. Muhammed A, Carre H, La Borderie C et al (2025) Influence of Polypropylene Fibers on Thermal-Induced Permability Changes in Concrete. 12th Int Conf Fract Mech Concrete Concrete Struct Vienna Austria. https://doi.org/10.21012/FC12.1244
29. Bošnjak J, Ožbolt J, Hahn R (2013) Permeability measurement on high strength concrete without and with polypropylene fibers at elevated temperatures using a new test setup. Cem Concr Res 53:104–111. https://doi.org/10.1016/j.cemconres.2013.06.005
30. Lollini F, Redaelli E (2021) Carbonation of blended cement concretes after 12 years of natural exposure. Constr Build Mater 276. https://doi.org/10.1016/j.conbuildmat.2020.122122
31. Bucher R, Diedrich P, Escadeillas G et al (2017) Service life of metakaolin-based concrete exposed to carbonation Comparison with blended cement containing fly ash, blast furnace slag and limestone filler. Cem Concr Res 99:18–29. https://doi.org/10.1016/j.cemconres.2017.04.013
32. Song H, Jeong Y, Bae S et al (2018) A study of thermal decomposition of phases in cementitious systems using HT-XRD and TG. Constr Build Mater. https://doi.org/10.1016/j.conbuildmat.2018.03.001
33. Yarmohammadian R, Felicetti R (2025) From Crack Initation To Instability At High Temperature: A Two Stage Mechanism For Fire-Induced Spalling in Concrete. 12th International Conference on Fracture Mechanics of Concrete and Concrete Structures: Vienna, Austria
34. Stelzner L (2021) Analyse des thermisch induzierten Feuchtetransports in gefügedichten Beton. Dissertation. University of Stuttgart
35. Jiang W, Zhang D, Zheng X et al (2023) Development of pore pressure in cementitious materials under low thermal effects: evidence from optimization of pore structure by incorporation of fly ash. Materials (Basel). https://doi.org/10.3390/ma16124214
36. Peters S, Vu G, Meschke G (2025) A multiscale model for predicting the Young's modulus and the thermal-expansion coefficient of concrete at high temperatures. Constr Build Mater 479. https://doi.org/10.1016/j.conbuildmat.2025.141259
37. Torelli G, Mandal P, Gillie M et al (2016) Concrete strains under transient thermal conditions: A state-of-the-art review. Eng Struct 127:172–188. https://doi.org/10.1016/j.engstruct.2016.08.021
38. Schneider U (1988) Concrete at High Temperatures -- A General Review. Fire Saf J 13:55–68. https://doi.org/10.1016/0379-7112(88)90033-1
39. Bazant ZP, Xi Y (1994) Drying creep of concrete: constitutive model and new experiments separating its. Mech Mater Struct 27:3–14

40. Koyama T, Ozawa M, Kanematsu M (2024) Study on the thermal shrinkage behavior of cement paste under high temperature envirnoment. Cem Sci Concrete Technol 78:128–136. https://doi.org/10.14250/cement.78.128
41. Weise F, Stelzner L, Weinberger J et al (2017) Influence of the pre-treatment of PP-fibres by means of electron irradiation on the spalling behaviour of High-Strength Concrete. 5th International Workshop on Concrete Spalling: Boras, Sweden 345–358

Publisher's Note Springer Nature remains neutral with regard to jurisdictional claims in published maps and institutional affiliations.

Authors and Affiliations

Tim Pittrich[1,2] · Frank Dehn[2] · Frank Weise[1] · Ludwig Stelzner[1]

✉ Tim Pittrich
tim.pittrich@bam.de

✉ Ludwig Stelzner
ludwig.stelzner@bam.de

Frank Dehn
frank.dehn@kit.edu

Frank Weise
frank.weise@bam.de

[1] Federal Institute For Materials Research and Testing, Berlin, Germany

[2] Karlsruhe Institute of Technology, Karlsruhe, Germany